



**UNIVERSITÀ  
DEGLI STUDI  
DI PADOVA**

Sede Amministrativa

**UNIVERSITÀ DEGLI STUDI DI PADOVA**

Sede Consorziata

**UNIVERSITÀ DEGLI STUDI DI BOLOGNA**

Dipartimento di tecnica e gestione dei sistemi industriali

Scuola di dottorato di ricerca in ingegneria mecatronica e innovazione meccanica del  
prodotto – Indirizzo in impianti industriali e logistica XXVII Ciclo

## **"Methods and tools for the optimization of renewable technologies and hybrid energy systems"**

*"Metodi e strumenti per l'ottimizzazione di tecnologie rinnovabili e sistemi energetici ibridi"*

**Direttore della Scuola:** Chiar.mo Prof. Alessandro Persona

**Supervisore:** Chiar.mo Prof. Mauro Gamberi

**Dottorando:** Alessandro Graziani



# Methods and tools for the optimization of renewable technologies and hybrid energy systems

*Alessandro Graziani*



*Doctoral school in*  
**MECHATRONICS AND PRODUCT INNOVATION ENGINEERING**  
**UNIVERSITY OF PADUA**  
*(XXVII Cycle)*

January, 2015



# Abstract

The United Nations (UN) project “Sustainable energy for all” sets three ambitious objectives to favor a sustainable development and to limit climate change:

- Universal access to modern energy services. Electricity is currently not available for 1.3 billion people and the global energy demand is expected to grow of about 35% within 2040, due to the increasing world population and the expanding economies
- Double the global rate of improvement in energy efficiency
- Double the share of renewable energy sources (RESs) in the global energy mix

In addition, according to the climate scenario assessed in the fifth assessment report (AR5) of the International Panel on Climate Change (IPCC), the prevention of undesirable climate effects requires a 40-70% reduction of greenhouse gas (GHG) emissions, compared with 2010 levels, by mid-century, and to near-zero by the end of this century (IPCC, 2014).

The achievement of such objectives requires and encourages the spread of RESs in the global energy mix, gradually replacing depleting and polluting energy sources based on fossil fuels, which still have the main incidence on the energy sector. RESs already play a major role in several countries, due to the technological development and the increasing market competitiveness, and the world renewable power capacity reached 22.1% in 2013, showing an increasing trend in 2014 (REN, 2014). However, supporting policies, robust investments from the private sector and efforts from the scientific community are still crucial to demonstrate the technical and economic sustainability and effectiveness of RESs, helping their large-scale diffusion.

Starting from such a background, this Ph.D dissertation focuses on the study, design and development of methods and tools for the optimization and enhancement of renewable energy technologies and their effective integration with energy storage solutions and traditional energy sources powered by fossil fuels (hybrid energy systems).

The analysis of the major literature and the different scenarios and perspectives of RESs in the national and international contexts have shown that their economic sustainability, and then their diffusion, is closely connected to a number of technical, economic/financial and geographical parameters. Such parameters are the input of the analytic models developed for the techno-economic design of photovoltaic (PV) plants and small wind turbines (SWTs) and applied to the economic feasibility study, through multi-scenario analysis, of such systems in some of the main European Union (EU) Countries. Among the obtained results, the self-consumption of the produced energy plays a crucial role in the economic viability of SWTs and PV plants and, particularly, after the partial or total cut of incentives and uncertainties related to supporting policies within the EU context. The study of the energy demand profile of a specific user and the adoption of battery energy storage (BES) systems have been identified as effective strategies to increase the energy self-consumption contribution. Such aspects have led to the development of an analytic model for the techno-

## II

*economic design of a grid connected hybrid energy system (HES), integrating a PV plant and a BES system (grid connected PV-BES HES). The economic profitability of the grid connected PV-BES HES, evaluated for a real case study, is comparable with PV plants without storage in case of a significant gap between the cost of energy purchased from the grid and the price of energy sold to the grid, but high BES system costs due to the initial investment and the maintenance activities and the eventual presence of incentives for the energy sold to the grid can make the investment not particularly attractive. Thus, the focus has shifted to the techno-economic analysis of off-grid HES to meet the energy demand of users in remote areas. In this context, BES systems have a significant role in the operation and management of the system, in addition to the storage of exceeding energy produced by the intermittent and variable RESs. The analysis has also been strengthened by an industrial application with the aim to configure, test and install two off-grid HESs to meet the energy demand of a remote village and a telecommunication system.*

*In parallel, two experimental activities in the context of solar concentrating technology, a promising and not fully developed technology, have been carried out. The former activity deals with the design, development and field test of a Fresnel lens pilot-scale solar concentrating prototype for the PV energy distributed generation, through multi-junction solar cells, and the parallel low temperature heat recovery (micro-cogeneration CPV/T system). The latter activity deals with the development of a low cost thermal energy (TES) storage prototype for concentrating solar power (CSP) plants. TES systems show a great potential in the CSP plants profitability since they can overcome the intermittent nature of sunlight and increase the capacity factor of the solar thermal power plant.*

*Concluding, the present Ph.D dissertation describes effective methods and tools for the optimization and enhancement of RESs. The obtained results, showing their critical issues and potential, aim to contribute to their diffusion and favor a sustainable development.*

# Sommario

*Il progetto delle Nazioni Unite “Sustainable energy for all” ha fissato tre obiettivi ambiziosi per favorire uno sviluppo sostenibile e limitare l’impatto del cambiamento climatico:*

- Accesso universale a moderni servizi elettrici. Tali servizi sono attualmente indisponibili per circa 1.3 miliardi di persone ed è previsto un aumento del 40% della domanda globale di energia elettrica entro il 2040, a causa dell’incremento della popolazione mondiale e delle economie in crescita nei paesi in via di sviluppo*
- Raddoppio del tasso globale di miglioramento dell’efficienza energetica*
- Raddoppio del contributo di fonti di tipo rinnovabile nel mix energetico globale*

*Inoltre, lo scenario climatico proposto nel “fifth assessment report (AR5)” redatto da “International Panel on Climate Change (IPCC)” stabilisce la necessità di ridurre l’emissione di gas ad effetto serra del 40-70%, rispetto ai valori registrati nel 2010, entro il 2050 ed eliminarli in modo quasi definitivo entro la fine del secolo con lo scopo di evitare effetti climatici indesiderati. Il raggiungimento di tali obiettivi richiede e incoraggia la diffusione di fonti energetiche rinnovabili (FER) all’interno del mix energetico globale, rimpiazzando gradualmente le fonti di energia convenzionali basate su combustibili fossili, inquinanti e in via di esaurimento, che hanno ancora l’incidenza principale nel settore energetico. A seguito nel loro sviluppo tecnologico e la crescente competitività nel mercato, le FER rivestono già un ruolo fondamentale nel mix energetico di numerose Nazioni ricoprendo il 22.1% del fabbisogno globale di energia nel 2013 e mostrando un andamento in rialzo nel 2014 (REN, 2014). Tuttavia, sono ancora cruciali politiche di supporto, ingenti investimenti privati e contributi della comunità scientifica per dimostrare l’efficacia e la sostenibilità tecnica ed economica delle FER e favorire, quindi, una loro diffusione in larga scala.*

*In questo contesto, la seguente tesi di dottorato è rivolta allo studio, progettazione e sviluppo di metodi e strumenti per l’ottimizzazione e la valorizzazione di tecnologie energetiche rinnovabili e la loro integrazione efficace con fonti di produzione di energia convenzionali alimentate da combustibili fossili e sistemi di accumulo di energia (Sistemi energetici di tipo ibrido). I contributi scientifici disponibili in letteratura e l’analisi dei diversi scenari e delle prospettive delle FER nei vari contesti nazionali ed internazionali hanno dimostrato che la loro sostenibilità economica, e quindi la loro diffusione, è strettamente legata ad una serie di parametri tecnici, economico / finanziari e geografici. Tali parametri sono stati impiegati come input in due modelli analitici sviluppati per la progettazione tecnico-economica di impianti fotovoltaici (FV) e micro turbine eoliche e applicati per lo studio della loro fattibilità economica, attraverso analisi multi-scenario, in alcuni dei maggiori Paesi Europei. I risultati ottenuti hanno mostrato come l’autoconsumo dell’energia prodotta rivesta un ruolo fondamentale nella redditività economica dei citati impianti ed, in particolare, a seguito del taglio parziale o totale dei sistemi di incentivazione e l’incertezza attorno alle politiche di supporto all’interno del panorama Europeo. Lo studio specifico del profilo di domanda*

*elettrica delle utenze e l'impiego di sistemi di accumulo di energia sono stati identificati come strategie efficaci al fine di incrementare la quota di autoconsumo. Tali considerazioni hanno portato allo sviluppo di un modello analitico utile alla progettazione tecnico-economica un sistema energetico ibrido connesso alla rete Nazionale integrante un impianto FV e un sistema di accumulo a batterie. La redditività del sistema, valutata su un caso reale, risulta comparabile a un impianto fotovoltaico privo di batterie in caso di un gap significativo tra il costo dell'energia elettrica acquistata dalla rete e il prezzo di vendita dell'energia elettrica ceduta in rete. Tuttavia, gli elevati costi dovuti all'acquisto iniziale e alle attività di manutenzione, e l'eventuale incentivazione sulla vendita dell'energia in rete, non rendono l'investimento particolarmente attrattivo per impianti connessi alla rete. L'attenzione si è quindi rivolta all'analisi tecnico-economica di sistemi energetici ibridi non connessi alla rete, comunemente definiti in isola o off-grid, per soddisfare il fabbisogno energetico di utenti in area remote e quindi prive di allaccio a una rete elettrica. In tali sistemi, i sistemi di accumulo a batterie, oltre alla capacità di accumulo dell'energia prodotta in eccesso variabili e intermittenti FER, hanno funzioni fondamentali nella gestione del sistema stesso. L'attività è stata anche rafforzata da un'applicazione industriale per la configurazione, test e installazione di due sistemi energetici ibridi in isola impiegati per soddisfare il fabbisogno energetico di un villaggio e di un sistema di telecomunicazione situati in aree remote.*

*In parallelo, sono state svolte due attività sperimentali applicate alla promettente, ma non ancora completamente sviluppata a livello industriale, tecnologia solare a concentrazione. La prima attività riguarda la progettazione, sviluppo e test sperimentali di un prototipo in scala ridotta di concentratore solare a lenti di Fresnel per la produzione distribuita di energia elettrica, mediante l'uso di celle fotovoltaiche multi giunzione, ed energia termica a bassa temperatura, tramite un sistema di recupero termico. La seconda attività concerne lo sviluppo e test sperimentali di un prototipo di sistema di accumulo termico per impianti termodinamici alimentati da sistemi a concentrazione solare. Il sistema di accumulo consente di compensare la natura intermittente e variabile della fonte solare incrementando le ore di funzionamento dell'impianto termodinamico con i conseguenti benefici economici.*

*Concludendo, la presente tesi di dottorato include la descrizione di metodi e strumenti per l'ottimizzazione e valorizzazione delle FER. I risultati evidenziano le criticità e potenzialità dei sistemi studiati con lo scopo di contribuire a una loro diffusione e favorire uno sviluppo sostenibile.*



# Acknowledgements

*Before addressing the content of this Ph.D dissertation, I would like to dedicate this page to express my sincere gratitude to all the people who have contributed to my personal and professional growth during the three years of my doctoral experience.*

*First of all, a special thanks and appreciation to my supervisor Professor Mauro Gamberi. His expertise, knowledge and the continuous support throughout my research path have been fundamental to achieve all the outlined objectives. I would like to extend this appreciation to my colleague, and friend, Marco Bortolini, whose support and help has been crucial, especially in the first period of the doctorate.*

*In the same way, I would like to thank all the group of the Department of Industrial Engineering - Alma Mater Studiorum University of Bologna, with whom I worked in different research activities and I shared moments of work and leisure. I would like to express my gratitude to Professor Emilio Ferrari, Professor Riccardo Manzini, Professor Cristina Mora, Professor Arrigo Pareschi and Professor Alberto Regattieri, to the colleagues and friends Riccardo Accorsi, Lucia Botti, Alessandro Cascini, Luca Crocetta, Francesco Fabri, Stefano Penazzi, Francesco Piana, Chiara Pini, Francesco Pilati, Giulia Santarelli, Lorenzo Versari and to all the graduating students / research fellows.*

*Special thanks to the all the Professors and Ph.D students of the doctoral school in Mechatronics and production innovation engineering – University of Padua.*

*I am also grateful to the Professor Y. Goswami and all the members of the Clean Energy Research Center – University of South Florida, for the opportunity to spend a magnificent period abroad and to increase my knowledge and expertise in the field of renewable energy.*

*A great thanks to all my friends, my football and futsal teammates, too many to be mentioned. The funny and relaxing moments with you all helped me to better deal with the stressful and difficult periods of the Ph.D experience.*

*Finally, I would like to express my heartfelt gratitude to my Family and in particular my Parents, Graziella & Paolo, and my Brother Davide..For Everything..*

Alessandro



# Table of contents

<b>Abstract .....</b>	<b>I</b>
<b>Sommario.....</b>	<b>III</b>
<b>Acknowledgements .....</b>	<b>V</b>
<b>Table of contents .....</b>	<b>VII</b>
<b>List of Figures .....</b>	<b>XIII</b>
<b>List of Tables .....</b>	<b>XIX</b>
<b>Abbreviations .....</b>	<b>XXI</b>
<b>1. Introduction .....</b>	<b>1</b>
<i>References.....</i>	6
<i>Web - References .....</i>	6
1.1 Research overview.....	7
1.2 Dissertation outline.....	9
<b>2. Renewable Energy Plant Design.....</b>	<b>13</b>
2.1 Techno-Economic design of photovoltaic (PV) plants .....	13
2.1.1 PV sector historical overview for the main EU countries .....	14
2.1.2 Performance Cost Model.....	15
2.1.3 PV sector elements for the eight EU countries: the 2012 scenario	19
2.1.4 Multi-country and multi-parameter analysis.....	22
2.1.5 Results and discussions.....	24
2.1.5.1 Incentive Vs No-Incentive Scenario.....	24
2.1.5.2 Sensitivity analysis of the cash outflows.....	25
2.1.5.3 Energy self-consumption role .....	26
2.1.5.4 Impact of irradiation level .....	27
2.1.5.5 Impact of financial parameters .....	28
2.1.6 Conclusions.....	29
2.1.7 Final remarks and future research .....	30
<i>References.....</i>	32
<i>Legislations .....</i>	36

<i>Web - References</i> .....	36
2.2 Techno-Economic design of small wind turbines (SWTs).....	38
2.2.1 <i>Literature review</i> .....	39
2.2.2 <i>Analyzed SWTs</i> .....	40
2.2.3 <i>Economic performance parametric model</i> .....	41
2.2.4 <i>SWT installation investment and operative outflows</i> .....	42
2.2.5 <i>SWT income flows</i> .....	46
2.2.6 <i>SWT economic analysis for the EU</i> .....	48
2.2.6.1 <i>SWT installation investment distribution</i> .....	48
2.2.6.2 <i>Country analysis</i> .....	49
2.2.6.3 <i>Economic wind speed threshold</i> .....	51
2.2.7 <i>Conclusions and further research</i> .....	53
2.2.8 <i>Final remarks</i> .....	53
<i>References</i> .....	55
<i>Legislations</i> .....	57
<b>3. Energy Storage Technology</b> .....	<b>59</b>
3.1 <i>Energy storage system overview</i> .....	60
3.2 <i>Battery energy storage (BES) system overview</i> .....	62
3.2.1 <i>BES definitions and terms</i> .....	63
3.2.2 <i>Charge/Discharge process</i> .....	65
3.2.3 <i>Impact of the temperature on the performance of BES systems</i> ...	67
<i>References</i> .....	68
<b>4. Hybrid Energy System Design</b> .....	<b>71</b>
4.1 <i>Grid-connected hybrid energy system (HES): overview</i> .....	73
4.2 <i>Grid-connected PV-BES HES design</i> .....	74
4.2.1 <i>PV-BES HES architecture</i> .....	74
4.2.2 <i>PV-BES analytic model</i> .....	76
4.2.2.1 <i>PV plant analytic model</i> .....	77
4.2.2.2 <i>BES system analytic model</i> .....	78
4.2.2.3 <i>Economical model</i> .....	79
4.2.2.4 <i>Lifetime PV-BES cost analysis</i> .....	80
4.2.3 <i>Case study</i> .....	81

4.2.3.1 Temperature and irradiation profiles.....	81
4.2.3.2 Load profile.....	82
4.2.3.3 Input Data.....	84
4.2.4 Results and discussions.....	85
4.2.5 Conclusions.....	91
4.3 Off-grid HES design: overview .....	92
4.4 Off-grid PV-BES-Diesel generator HES design .....	93
4.4.1 PV-BES-Diesel generator HES architecture.....	94
4.4.2 Analytic model.....	96
4.4.2.1 PV plant analytic model .....	96
4.4.2.2 BES system analytic model .....	97
4.4.2.3 Economical model .....	99
4.4.2.4 Lifetime hybrid energy system cost analysis .....	100
4.4.3 Case study .....	101
4.4.3.1 Temperature and irradiation profiles.....	101
4.4.3.2 Load profile.....	103
4.4.3.3 Off-grid HES detailed architecture.....	103
4.4.3.4 PV-BES system parameters.....	105
4.4.3.5 Diesel generator and other parameters .....	106
4.4.4 Results and discussions.....	108
4.4.5 Conclusions and further research .....	111
4.4.6 Final remarks .....	112
4.4.7 Acknowledgements .....	114
Appendix A-4.4.....	115
4.5 Off-grid PV-BES-SWT-Diesel generator HES design.....	116
4.5.1 PV-BES-SWT-Diesel generator HES architecture .....	116
4.5.2 Further developments .....	117
4.5.3 Acknowledgements .....	117
Appendix A-4.5.....	118
References.....	119
Legislations .....	124
Web references.....	124

<b>5. Solar Concentrating Technology .....</b>	<b>125</b>
5.1 Solar concentration background.....	125
5.2 Concentrating solar power (CSP) technology.....	128
5.2.1 Parabolic trough collector (PTC) technology.....	130
5.2.2 Tower solar power (TSP) technology.....	131
5.2.3 Stirling dish collector (SDC) technology.....	132
5.2.4 Linear Fresnel collector (LFC) technology.....	133
5.3 Concentrating photovoltaics (CPV) technology.....	134
5.3.1 CPV solar cells.....	135
5.3.2 Cell cooling and heat recovery.....	137
5.3.3 CPV plant technologies.....	138
5.3.4 Fresnel lens refraction optic.....	139
References.....	141
<b>6. Concentrating PV/T Prototype .....</b>	<b>143</b>
6.1 CPV technology overview and prototype objectives.....	143
6.2 CPV/T Prototype description.....	145
6.2.1 Support steel structure.....	146
6.2.2 Solar collectors.....	147
6.2.3 Solar receivers.....	149
6.2.3.1 Triple-junction photovoltaic (TJPV) Cells.....	149
6.2.3.2 Water heat exchangers (WHEs).....	150
6.2.4 Solar biaxial tracking system.....	151
6.2.4.1 Motion control strategy.....	154
6.2.5 Electronic variable load.....	158
6.2.6 Real-time motion control and monitoring system.....	159
6.2.6.1 Power supply unit.....	160
6.2.6.2 Motion control unit.....	160
6.2.7 Hydraulic circuit for cell cooling and thermal recovery.....	161
6.2.8 Auxiliary weather station.....	163
6.3 Manufacturing cost analysis.....	164
6.4 Field-tests and experimental campaign.....	165
6.4.1 Accuracy in solar tracking.....	166
6.4.2 Single TJPV cell electric conversion efficiency analysis.....	167

6.4.3 <i>Prototype electric and thermal conversion efficiency analysis</i> .....	168
6.4.3.1 Secondary optics development and field tests .....	170
6.5 Conclusions and final remarks .....	171
<i>Acknowledgements</i> .....	173
<i>References</i> .....	173
<b>7. TES Prototype for CSP plants</b> .....	<b>177</b>
7.1 Thermal energy storage (TES) solutions for CSP Plants .....	177
7.2 TES prototype .....	181
7.2.1 <i>TES prototype overview and experimental test set-up</i> .....	181
7.2.2 <i>Pressure drop model and experimental validation</i> .....	186
7.2.2.1 Introduction.....	186
7.2.2.2 Experimental test set-up.....	189
7.2.2.3 Experimental test results: pressure drop .....	191
7.2.3 <i>Preliminary experimental tests: charging and discharging cycles</i>	195
7.2.4 <i>Acknowledgements</i> .....	196
<i>References</i> .....	196
<b>8. Conclusions</b> .....	<b>199</b>
8.1 Future developments.....	201





# List of Figures

Figure 1.1 Total annual anthropogenic GHG emissions by group of gases 1970-2010 (IPCC, 2014) .....	1
Figure 1.2 RESs share in the global energy mix, 2013 (REN, 2014) .....	2
Figure 1.3 Average Annual Growth Rates of RES capacity in the power sector, from 2008 to 2013 (REN, 2014) .....	3
Figure 1.4 Solar PV total global capacity, 1995-2013 (REN 2013; REN, 2014) .....	4
Figure 1.5 Wind power Total Global Capacity, 2000-2013 (REN, 2014) .....	5
Figure 1.6 Research framework .....	8
Figure 1.7 Dissertation outline framework .....	12
Figure 2.1 Historical trend of PV sector in the main EU countries (Photovoltaic energy barometer 2007, 2009, 2010, 2011, 2012; IEA, 2010) .....	15
Figure 2.2 Flow chart of the proposed PV system analysis .....	16
Figure 2.3 Incentive vs. no-incentive scenarios for the eight countries and residential rooftop plants ( $c_{module}$ according to Eq.2.7, $HI, y = 1400\text{kWh/m}^2\cdot\text{year}$ , $OCC = 3\%$ , $\varphi = 0\%$ , $\chi_{sold} = 50\%$ ) .....	24
Figure 2.4 Incentive vs. no-incentive scenarios for the eight countries and industrial rooftop plants ( $c_{module}$ according to Eq.2.7, $HI, y = 1400\text{kWh/m}^2\cdot\text{year}$ , $OCC = 3\%$ , $\varphi = 0\%$ , $\chi_{sold} = 50\%$ ) .....	24
Figure 2.5 Sensitivity analysis of cash outflows .....	25
Figure 2.6 Impact of $\chi_{sold}$ on NPV residential rooftop plants ( $c_{module}$ according to Eq.2.7, $P_o = 3\text{kWp}$ , $HI, y = 1400\text{kWh/m}^2\cdot\text{year}$ , $OCC = 3\%$ , $\varphi = 0\%$ ) .....	26
Figure 2.7 Impact of $\chi_{sold}$ on NPV, industrial rooftop plants ( $c_{module}$ according to Eq.2.7, $P_o = 100\text{kWp}$ , $HI, y = 1400\text{kWh/m}^2\cdot\text{year}$ , $OCC = 3\%$ , $\varphi = 0\%$ ) .....	26
Figure 2.8 Impact of the irradiance levels, $HI, y$ , on NPV and country typical ranges ( $c_{module}$ according to Eq.2.7, $OCC = 3\%$ , $\varphi = 0\%$ , $\chi_{sold} = 50\%$ ) .....	27
Figure 2.9 Impact of financial parameters on PV plant profitability ( $c_{module}$ according to Eq.2.7, $HI, y = 1400\text{kWh/m}^2\cdot\text{year}$ , $r = 4\%$ , $\chi_{sold} = 50\%$ ) .....	28
Figure 2.10 PV module cost trend from 2001 to 2012 (Mints, 2012) .....	30
Figure 2.11 Wind power installed in the EU27 area at the end of 2012 (EWEA, 2012) .....	38
Figure 2.12 Flow chart of the proposed economic performance parametric model .....	42
Figure 2.13 Purchase cost (Price list ex works) referred to each turbine model .....	43
Figure 2.14 Europe Wind Atlats at 50m above ground level (Risø National Laboratory, 1989) .....	47
Figure 2.15 SWT average cost distribution .....	48
Figure 2.16 NPV for France varying the SWT turbine model, $v$ and the financial leverage .....	49

Figure 2.17 <i>NPV</i> for Germany varying the SWT turbine model, $\nu$ and the financial leverage .....	49
Figure 2.18 <i>NPV</i> for Italy varying the SWT turbine model, $\nu$ and the financial leverage....	50
Figure 2.19 <i>NPV</i> for Spain varying the SWT turbine model, $\nu$ and the financial leverage .	50
Figure 2.20 <i>NPV</i> for The Netherlands varying the SWT turbine model, $\nu$ and the financial leverage .....	51
Figure 2.21 Economic wind speed thresholds for each country varying the <i>OCC</i> (from 2% to 10%). 100% financed scenario .....	52
Figure 2.22 Economic wind speed thresholds for each country varying the <i>OCC</i> (from 2% to 10%). 0% financed scenario .....	52
Figure 3.1 Lead-acid and lithium-ion batteries comparison (Battke et al., 2013) .....	63
Figure 3.2 Schematic of the voltage during a constant current discharge and charge .....	65
Figure 3.3 Schematic of the discharge curve of a battery with different voltage losses.....	66
Figure 3.4 Schematic of discharge curves for a battery with a strong impact of current rate on the available capacity (e.g. lead-acid batteries) and a battery with lower impact of current rates (e.g. lithium-ion batteries) .....	67
Figure 4.1 Reference diagram for a generic HES .....	72
Figure 4.2 Reference diagram for the grid-connected PV-BES HES .....	75
Figure 4.3 Energy flow control chart for each studied hour, $h$ .....	76
Figure 4.4 Irradiance and temperature influence on the PV module performance .....	77
Figure 4.5 Trend for turnkey PV system costs (2012-2013).....	80
Figure 4.6 Monthly average irradiation profile for Bologna, Italy .....	82
Figure 4.7 Monthly average temperature profile for Bologna, Italy .....	82
Figure 4.8 Hourly load profile for the considered case study .....	83
Figure 4.9 Hourly load profile, detail of July .....	83
Figure 4.10 <i>LCOE</i> values for different PV rated powers (2013 extra EU c-Si technology)	85
Figure 4.11 <i>LCOE</i> values for different PV rated powers and BES system capacities .....	86
Figure 4.12 Monthly average energy produced by PV system.....	87
Figure 4.13 Hourly detail of the battery state of charge for the month of April .....	87
Figure 4.14 Average monthly BES system state of charge, <i>SOCB</i> , $h$ .....	88
Figure 4.15 Average monthly energy surplus and energy purchased from the grid .....	88
Figure 4.16 Battery Charge/Discharge currents .....	89
Figure 4.17 PV-BES system cost distribution for the best economic scenario .....	89
Figure 4.18 University complex layout and available rooftop area .....	90
Figure 4.19 Reference diagram for the off grid HES .....	95
Figure 4.20 Electric energy flow control chart for each studied hour, $h$ .....	96
Figure 4.21 Yakutsk - Remote village location .....	101
Figure 4.22 Irradiation profile for Yakutsk (Russia) .....	102
Figure 4.23 Russian irradiation map.....	102
Figure 4.24 Temperature profile for Yakutsk (Pogodaiklimat, 2014) .....	103

Figure 4.25 Hourly load profile for the remote village in Yakutsk (Russia) .....	103
Figure 4.26 Case study - HES architecture .....	104
Figure 4.27 Generator fuel consumption as a function of power supplied .....	107
Figure 4.28 <i>LCOE</i> values for different PV rated powers (2014 EU c-Si technology) .....	108
Figure 4.29 <i>LCOE</i> values for different PV rated power and BES system capacity .....	109
Figure 4.30 HES cost distribution for the best scenario .....	111
Figure 4.31 <i>LCOE</i> as-is and to be scenarios .....	113
Figure 4.32 Installed 20kWp PV Plant – Yakutsk .....	114
Figure 4.33 HES: 2 x Diesel generators, 20kWp PV plant, 100kWh BES system .....	114
Figure 4.34 PV-BES-Diesel generator HES single-line diagram .....	115
Figure 4.35 PV-BES-WT-Diesel generator HES architecture .....	116
Figure 4.36 PV-BES-WT-Diesel generator HES single-line diagram .....	118
Figure 5.1 Different components of solar radiation .....	125
Figure 5.2 Acceptance angle examples in an ideal concentrator .....	126
Figure 5.3 CSP plant schematic .....	128
Figure 5.4 Reflection of solar radiation through parabolic mirror .....	130
Figure 5.5 PTC-based CSP plant .....	130
Figure 5.6 TSP-based CSP plant (Pavlović, 2012) .....	131
Figure 5.7 TSP-based CSP plant adopting molten salts as HTF and superheated steam as working fluid designed with IPSE Pro Software .....	132
Figure 5.8 SDC-based CSP plant (Pavlović, 2012) .....	132
Figure 5.9 LFC-based CSP plant (Pavlović, 2012) .....	133
Figure 5.10 Solar PV cell classification .....	135
Figure 5.11 TJPV solar cell layout, example .....	136
Figure 5.12 Active and passive cooling (Vivar et al., 2012) .....	137
Figure 5.13 Point-Focus Dish and Linear-Focus Trough (Muñoz et al., 2010) .....	138
Figure 5.14 Point-Focus and Linear-Focus Fresnel Lenses (Muñoz et al., 2010) .....	139
Figure 5.15 Heliostat CPV (Muñoz et al., 2010) .....	139
Figure 5.16 Biconvex converging lens .....	140
Figure 5.17 Equivalent Fresnel of a plano-convex lens .....	140
Figure 6.1 CPV/T prototype, front and back views .....	146
Figure 6.2 CPV/T prototype, support steel structure .....	147
Figure 6.3 Support steel structure: the vertical pillar and the horizontal shaft .....	147
Figure 6.4 Solar collector aluminum frame and integration in the prototype .....	148
Figure 6.5 TJPV cell layout and spectral response .....	149
Figure 6.6 TJPV cell connected in a ceramic 80x80mm squared plate .....	150
Figure 6.7 Polyvinylchloride WHE 3D render .....	150
Figure 6.8 WHE integrating TJPV cell .....	151
Figure 6.9 Solar azimuth and solar altitude angles .....	151
Figure 6.10 Zenithal tracking mechanism .....	152

Figure 6.11 Azimuthal tracking mechanism.....	152
Figure 6.12 Solar collimator integrated to the solar collector .....	153
Figure 6.13 Light sensors, picture and polar characteristic curve .....	153
Figure 6.14 Light sensor electrical acquisition circuit .....	154
Figure 6.15 On-off control of the implemented solar tracking system .....	155
Figure 6.16 Astronomic solar equations .....	155
Figure 6.17 Light sensors feedback loop control strategy .....	156
Figure 6.18 Hybrid control strategy, flow-chart of the switching procedure.....	157
Figure 6.19 Best tracking strategy as a function of $M_s$ .....	157
Figure 6.20 I-V and P-V curves, example.....	158
Figure 6.21 Electronic variable load for MPP tracking.....	159
Figure 6.22 Hardware control board .....	159
Figure 6.23 Motion control unit circuit.....	161
Figure 6.24 Hydraulic cooling circuit scheme .....	162
Figure 6.25 Hydraulic cooling circuit, key elements inside the protection box .....	162
Figure 6.26 Weather station integrating the pyranometer, the air temperature thermometer and the anemometer.....	163
Figure 6.27 Pyrheliometer for direct solar irradiation measurement .....	164
Figure 6.28 Functional cost analysis, percentages refer to the full manufacturing cost...	165
Figure 6.29 Accuracy in solar collimation, shadow related to the angular misalignment .	166
Figure 6.30 Shadow before and after the system realignment.....	167
Figure 6.31 Global radiation and direct fraction profiles on July 23, 2012 .....	167
Figure 6.32 Experimental I-V and P-V curves for a single TJPV cell .....	168
Figure 6.33 High dispersion of concentrated solar radiation around the focus point .....	169
Figure 6.34 Secondary optic element concept .....	169
Figure 6.35 Developed aluminum truncated pyramid SOE .....	170
Figure 6.36 Different sun rays distribution with the adoption of the developed SOE .....	170
Figure 6.37 Test of 4 TJPV cells with SOE .....	171
Figure 6.38 Global CV system installations and forecast (IHS, 2013) .....	173
Figure 7.1 CSP plant and TES system main components .....	179
Figure 7.2 TES system selection criteria .....	179
Figure 7.3 TES system available technologies.....	180
Figure 7.4 TES system architecture .....	181
Figure 7.5 Architecture of the developed packed bed TES system .....	182
Figure 7.6 Schematic of the packed bed system.....	182
Figure 7.7 Flanged steel storage tank components .....	183
Figure 7.8 a) Shielded thermocouple for air measurements. b) Exposed tip thermocouple for iron ore temperature measurements .....	184
Figure 7.9 Thermocouple locations .....	184
Figure 7.10 Thermocouple row in the packed bed .....	185

Figure 7.11 Schematic of the packed bed system .....	190
Figure 7.12 Measured pressure gradient versus air mass flux .....	191
Figure 7.13 Pressure gradient as a function of particle Reynolds number. Shape factor of 0.495 is used in the pressure correlations .....	192
Figure 7.14 Correlation between pressure gradient and particle Reynolds number for lower Reynolds number range. Particle shape factor of 0.495 is considered. ....	193
Figure 7.15 Pressure gradient as a function of particle Reynolds number. Shape factor of 0.70 is used in the pressure drop correlations.....	194
Figure 7.16 Packed bed temperature during charging and discharging mode .....	195
Figure 7.17 Packed bed charging air temperature along bed height .....	196
Figure 8.1 Average Annual Growth Rates of RES capacity in the power sector, from 2008 to 2013 (REN, 2014).....	199



## List of Tables

Table 2.1 FiT for France [€/kWh].....	20
Table 2.2 FiT for Germany [€/kWh] .....	20
Table 2.3 FiT for Italy [€/kWh] .....	21
Table 2.4 UK PV system incentives [€/kWh].....	21
Table 2.5 Country economic and financial data: electricity price, tax level and inflation ...	22
Table 2.6 Values for the PCM input parameters. ....	23
Table 2.7 SWT Technical data (Market survey) .....	40
Table 2.8 SWT power curves derived from wind turbine datasheets.....	41
Table 2.9 Cost for different truck models.....	43
Table 2.10 Average costs for SWT transportation to EU countries.....	44
Table 2.11 Installation costs by factor .....	44
Table 2.12 EU tax rates on the corporate gross income (KPMG, 2011).....	45
Table 2.13 Incentives and energy market prices for the considered EU countries (2012)	47
Table 2.14 “Turnkey” investments .....	48
Table 2.15 2011 and 2012 wind power installations and total capacity in the five considered EU countries (EWEA, 2013; WWEA, 2014).....	54
Table 2.16 2013 and half-year 2014 wind power installations and total capacity in the five considered EU countries (EWEA, 2013; WWEA, 2014).....	54
Table 3.1 Summary of the main ESS technologies (Kouskou et al., 2014) .....	61
Table 3.2 ESSs characteristics (Kouskou et al., 2014; Castillo et al. 2014) .....	62
Table 3.3 Cycle life for a lead-acid battery as a function of <i>DOD</i> and temperature .....	65
Table 4.1 Standard electric conversion efficiencies for PV-BES systems .....	72
Table 4.2 Case study adopted values and ranges: PV plant .....	84
Table 4.3 Case study adopted values and ranges: BES system .....	84
Table 4.4 Case study adopted values and ranges: financial and environmental param....	85
Table 4.5 PV-BES HES and traditional system best scenarios.....	86
Table 4.6 Design parameters for the PV-BES system .....	90
Table 4.7 Multisource energy production system review. ....	92
Table 4.8 PV plant main parameters .....	105
Table 4.9 PV Plant Installation Costs (2014).....	105
Table 4.10 BES system parameters.....	106
Table 4.11 PV-BES system electric conversion device parameters .....	106
Table 4.12 Diesel generator maintenance program .....	107
Table 4.13 Diesel generator and environmental/economic parameters.....	108
Table 4.14 <i>LCOE</i> results for different HES scenarios .....	110
Table 4.15 Economic profitability of the different HES scenarios .....	110
Table 5.1 CSP plants installed worldwide and ongoing projects (Baharoon et al., 2015)	128

Table 5.2 Main features of the described CSP plant technologies (Baharoon et al., 2015)	133
Table 5.3 Energy band gap of the most commonly adopted semi-conductors	135
Table 6.1 Features of the adopted Fresnel lenses	148
Table 6.2 TJPV cell electrical features	149
Table 6.3 Features of the four adopted environmental condition sensors	164
Table 6.4 Prototype manufacturing costs	165
Table 6.5 Prototype power and thermal performances	168
Table 6.6 Prototype power and thermal performances with SOE integration	171
Table 7.1 Iron ore prototype system components	185
Table 7.2 Coefficient for Reichlet's Equation, Equation 7.2 (Eisfeld and Schnitzlein, 2001)	188
Table 7.3 System components	190
Table 7.4 Bed parameters	191
Table 7.5 Percent average relative absolute error (ARAE) for the 3 pressure correlations in which sphericity is considered	193



# *Abbreviations*

AC	Alternate current	LFC	Linear Fresnel collector
AH	Autonomy hour	MCPV	Medium concentrating photovoltaics
a-Si	Amorphous silicon	MJPV	Multi junction photovoltaic
BES	Battery energy storage	MPPT	Maximum power point tracking
CHP	Combined heat and power	NOCT	Normal operating cell temperature
CLFC	Compact linear Fresnel collector	NPV	Net present value
COP	Continuous power	OCC	Opportunity cost of capital
CPV	Concentrating photovoltaics	OCV	Open circuit voltage
CPV/T	Concentrating photovoltaics/Thermal	PB	Payback
CR	Concentration ratio	PCM	Performance cost model
c-Si	Crystalline silicon	PTC	Parabolic trough collector
CSP	Concentrated solar power	PV	Photovoltaic
DC	Direct current	RES	Renewable energy source
DOD	Depth of discharge	SDC	Stirling dish collector
EC	European Commission	SOC	State of charge
EBT	Earnings before taxes	SOE	Secondary optic element
ESS	Energy storage system	SOH	State of health
EU	European Union	SWT	Small wind turbine
FIT	Feed in tariff	TES	Thermal energy storage
GHG	Greenhouse gas	TJPV	Triple junction photovoltaic
HAWT	Horizontal axis wind turbine	TSP	Tower solar power
HCPV	High concentrating photovoltaics	UPS	Uninterruptible power source
HES	Hybrid energy system	VAT	Value added tax
HTF	Heat transfer fluid	VAWT	Vertical axis wind turbine
LCOE	Levelized cost of electricity	VRLA	Valve regulated lead acid
LCPV	Low concentrating photovoltaics	WHE	Water heat exchanger



# 1. Introduction

The United Nations (UN) project “Sustainable energy for all” sets three ambitious objectives to favor a sustainable development and to limit climate change:

- Universal access to modern access services. Electricity is currently not available for 1.3 billion people and the global energy demand is expected to grow of about 35% within 2040, due to the increasing world population and the growing prosperity and expanding economies of developing countries
- Double the global rate of improvement in energy efficiency
- Double the share of renewable energy sources (RESs) in the global energy mix

In addition, according to the fifth assessment report (AR5) of the International Panel on Climate Change (IPCC), the global emissions of greenhouse gases (GHGs) are at unprecedented level despite the rising attention to policies limiting the climate change. As in Figure 1, the total GHG emissions reach 49(±4.5) GtCO<sub>2</sub>eq/year in 2010, while the average annual GHG emission growth from 2000 to 2010 is of about 1.0 GtCO<sub>2</sub>eq/year (+2.2%), compared to the 0.4 GtCO<sub>2</sub>eq/year (+1.3%) measured from 1970 to 2000, showing an exponential trend.

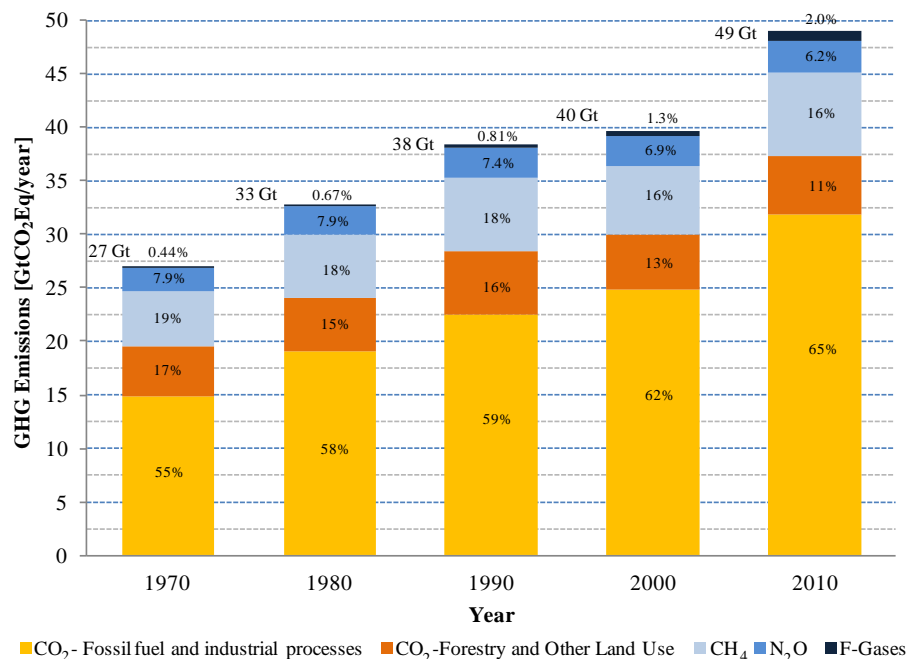


Figure 1.1 Total annual anthropogenic GHG emissions by group of gases 1970-2010 (IPCC, 2014)

However, the climate change scenarios assessed in the AR5 of the IPCC show that to have a likely chance of limiting the increase in global mean temperature to 2°C, and thus prevent undesirable climate effects, means lowering GHG emissions by 40 to 70 percent compared with 2010 by mid-century, and to near-zero by the end of this century (IPCC, 2014).

The guidelines, provided by the most influent international institutions, e.g. the United Nations and the World Bank, emphasize the need to mark a turning point to the energy mix composition increasing the incidence of the RESs, gradually replacing depleting and polluting energy sources based on fossil fuels (UN, 2011; World Bank, 2011). RESs already play a major role in several countries, due to the technological development and the increasing market competitiveness, and the world renewable power capacity reached 22.1% in 2013, showing an increasing trend in 2014. Figures 1.2 provide the RESs share in the global energy mix, together with the contribution of the different sources, at the end of 2013.

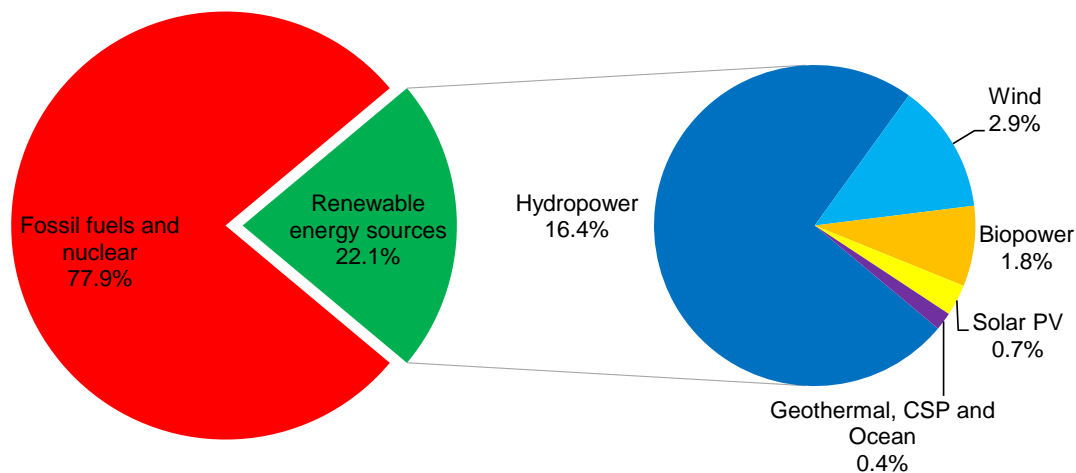


Figure 1.2 RESs share in the global energy mix, 2013 (REN, 2014)

The RESs global capacity exceeds 1,560GW in 2013 with an increase of more than 8% over 2012. Hydropower reached 1,000GW, with a 4% increase, while other RESs experienced a 17% increase reaching a total capacity of 560GW. RESs contributed to more than 56% of net additions to the global power capacity with hydropower and solar photovoltaic (PV) accounting for about one-third of renewable power capacity added in 2013, followed closely by wind power (29%). Driven by the set ambitious environmental targets, e.g. the European Directive (29/2009/EC), known as "20/20/20 climate and energy package", the European countries contribute for 235GW of non-hydro RES power capacity, representing almost the 42% of the global non-hydro RES power capacity.

Concerning the power sector, the annual growth rates of the different RESs in 2013, presented in Figure 1.3, show a relevant development of solar energy, i.e. 55% and 48% average annual increase of solar PV and concentrated solar power (CSP) installed capacity, respectively, from 2008 to 2013, and wind power, i.e. 21.0% average annual increase from 2008 to 2013. The present dissertation focuses on such renewable

technologies, whose continuous development, potential and the growth margin compared to hydropower and geothermal power allows increasing significantly the RES contribution in the global energy mix. In the following, the current status of solar and wind power technologies, together with the dissertation content and outline, are presented.

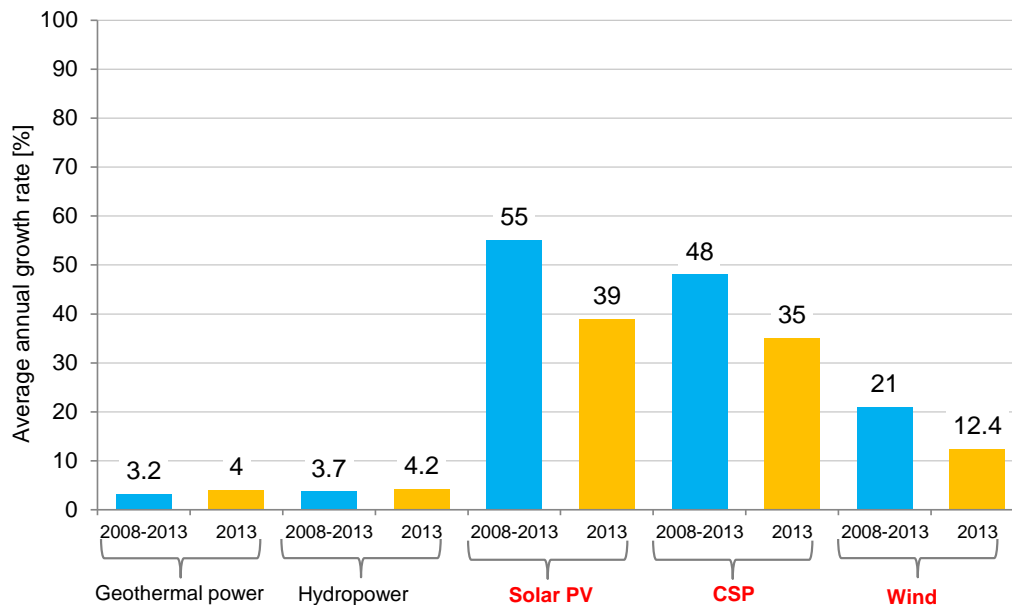


Figure 1.3 Average Annual Growth Rates of RES capacity in the power sector, from 2008 to 2013 (REN, 2014)

Solar PV and CSP show a great potential due to the enormous theoretic potential of the solar source, equal to 3.9 trillion PJ per year (Quaschnig, 2005). PV technology is one of the most suitable RES to switch the electricity generation from few large centralized facilities to a wide set of small decentralized and distributed systems reducing the environmental impact and increasing the energy fruition in the remote areas.

Such strengths have pushed several countries, worldwide, to promote massive investments in technologies to convert solar radiation into electric power energy through the introduction of specific strategies and customized national supporting policies. The prices for the PV components, e.g. module and conversion devices, have rapidly decreased, making the PV systems competitive compared to the other energy sources. The grid parity is already reached in several countries, worldwide (Branker *et al.*, 2011; Bazilian *et al.*, 2013). As a result, the solar PV market experienced an exponential growth from 2004 to 2013 (See Figure 1.4), with 98% of total PV capacity installed since the beginning of 2004 and almost 50% in the 2012 and 2013.

The global solar PV market had a record year, after a brief slowdown, installing more capacity than any other non-hydro RESs, *i.e.* more than 39GW, reaching a total capacity of approximately 139 GW. After a pioneering role played since 2001 with several promoting measure and supporting policies, Europe has lost his leadership in PV installations, *i.e.* resulting in 75% of the global generation capacity in 2010, due to the total or partial cut and uncertainties related to such policies and the increasing PV market outside the European area. Asia has become the largest regional market with 22.7GW of

PV installations in 2013 (China 12.9GW, Japan 6.9GW), followed by Europe (10.4GW) and North America (5.4GW).

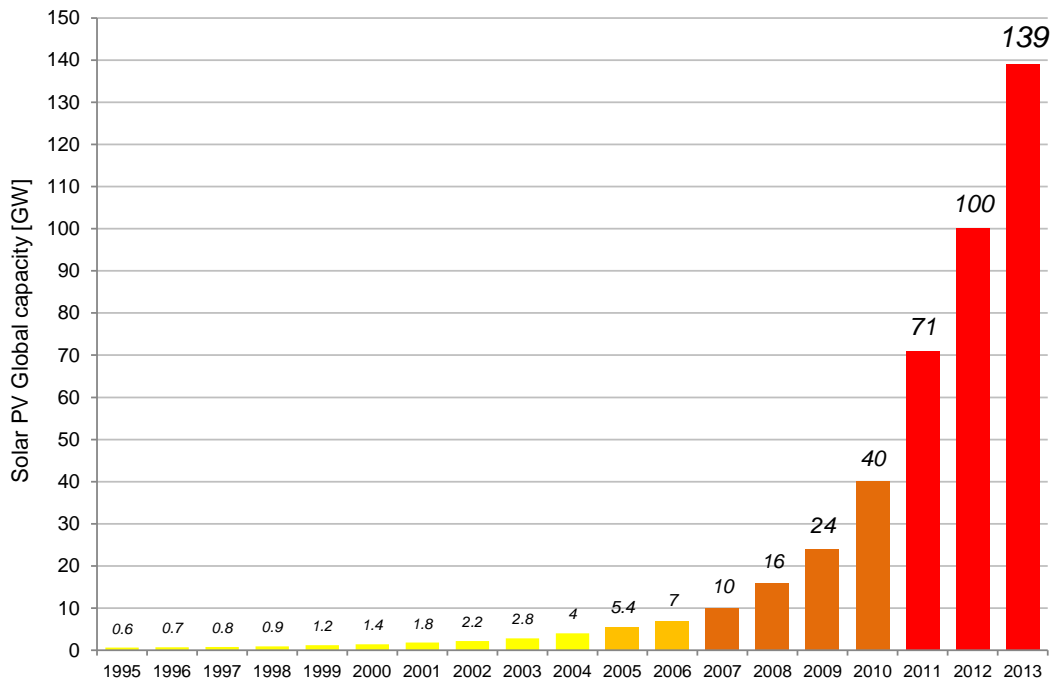


Figure 1.4 Solar PV total global capacity, 1995-2013 (REN 2013; REN, 2014)

Among solar PV technologies, concentrating photovoltaics (CPV) market remains small, *i.e.* 165MW installed capacity at the end of 2013, but the interest is increasing to high efficiency achievable in locations with significant values of the direct fraction of solar radiation.

CSP market has confirmed its growth in 2013, after record growth in 2012. The total global capacity reached 3.4GW (0.9GW installed in 2013). Global installed capacity of CSP has increased about ten times since 2004 and from the end of 2008 to the end of 2013, total global capacity have grown at an average annual rate approaching 50%, showing the increasing interest on such a technology. The United States became the leading market in 2013, adding 375 MW to end the year with almost 0.9 GW in operation, and about 1 GW under construction. Spain sustained its global leadership in existing CSP capacity, adding 350 MW in 2013 to increase operating capacity by 18%, for a total of 2.3 GW at the end of 2013. In other markets, capacity reached 250MW, increasing three times the annual installed capacity.

Concerning wind power, such technology achieved its maturity in the 90s. In those years, several countries adopted significant incentive legislations with the aim of stimulating and promoting the installation and use of wind power systems connected to the national electric grid. Consequently, the capital costs of wind power have declined, while technological advances, including taller towers, longer blades, and smaller generators in low wind speed areas, have increased capacity factors. Such aspects have lowered the costs of wind generated electricity, improving the competitiveness with fossil fuel based power sources. There are several countries where the energy market and wind power

generation is so developed that the old incentive policies are mitigated or even abrogated showing that wind farms are competitive if compared to traditional fossil fuels. Despite these largely positive trends, during 2013 the industry continued to be challenged by downward pressure on prices, increased competition among turbine manufacturers, competition with low-cost gas in some markets, reductions in policy support driven by economic austerity, and declines in key markets. The market development in the last two decades resulted in a total installed capacity of 318GW in 2013 (See Figure 1.5).

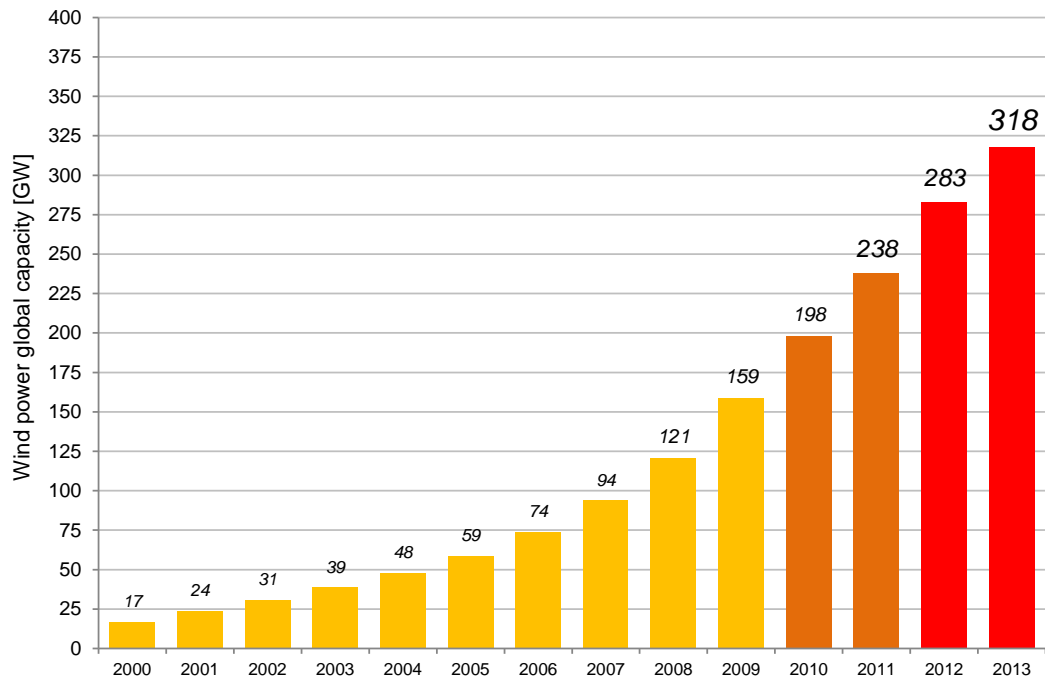


Figure 1.5 Wind power Total Global Capacity, 2000-2013 (REN, 2014)

More than 35 GW of wind power capacity was added in 2013, increasing the global total above 318 GW. However, following several record years, the wind power market experienced a 10 GW reduction compared with 2012. Asia has represented the largest market (sixth consecutive year) accounting for almost 52% of added capacity, followed by the EU (about 32%) and North America (less than 8%). The EU has remained the top region for cumulative wind capacity, *i.e.* 37%, although Asia is rapidly closing the gap, *i.e.* more than 36%. Wind accounted for the largest share (32%) of new EU power capacity in 2013 with more than 11 GW of wind capacity was added for a total exceeding 117 GW.

While renewable capacity continues to rise at a rapid rate from year to year, the share of renewable electricity on the global generation is increasing more slowly, about 3% from 2012 to 2013 due to the rapid increase of the overall energy demand.

For this reason and to reach UN and international institutions aforementioned social, economic and environmental objectives, supporting policies, robust investments from the private sector and efforts from the scientific community are still crucial to demonstrate the technical and economic sustainability and effectiveness of RESs, helping their large-scale diffusion.

Starting from such a background, this Ph.D dissertation focuses on the study, design and development of methods and tools for the optimization and enhancement of renewable energy technologies and their effective integration with traditional energy sources powered by fossil fuel and energy storage systems (hybrid energy systems).

In the next *Paragraph 1.1* an overview of the research is presented, while *Paragraph 1.2* explains more in detail the content of each *Chapter* of this Ph.D dissertation.

## References

Bazilian, M., Onyeji, I., Liebreich, M., MacGill, I., Chase, J., Shah, J., Gielen, D., Arent, D., Landfear, D., S. Zhengrong, S., 2013. Re-considering the economics of photovoltaic power, *Renewable Energy* 53, 329-338.

Branker, K., Patha, M.J.M., Pearce, J.M., 2011. A review of solar photovoltaic levelized cost of electricity. *Renewable and Sustainable Energy Reviews* 15, 4470-4482.

International Panel on Climate Change (IPCC), 2014. Summary for policymakers of the 5th Assessment Report (AR5) 1–33

Quaschnig, V., 2005. Understanding renewable energy systems, Earthscan, London.

Renewable energy policy network for the 21st century (REN21), 2013. *Renewables 2013 Global Status Report*, 2013.

Renewable energy policy network for the 21st century (REN21), 2014. *Renewables 2014 Global Status Report*, 2014.

World Bank, 2011. Promotion of new clean energy technologies and the world bank group (2011).

## Web - References

United Nations (UN), 2011. "Sustainable energy for all" Project. <http://www.se4all.org/>.



## 1.1 Research overview

The research path framework and logic is depicted in Figure 1.6. The reference literature and the analysis of different scenarios and perspectives of RESs in the national and international contexts have shown that their economic sustainability, and then their spread, is closely connected to a number of technical, economic/financial, geographical and political parameters. Such parameters are the input of the analytic models developed for the techno-economic design of PV plants and small wind turbines (SWTs) and applied to the economic feasibility study, through multi-scenario analysis, of such systems in some of the main EU Countries. Among the obtained results, the self-consumption of the produced energy plays a crucial role in the economic viability of SWTs and PV plants and, in particular, after the partial or total cut of incentives and uncertainties related to supporting policies within the EU context. The study of the energy demand profile of a specific user and the adoption of battery energy storage (BES) systems have been identified as effective strategies to increase the energy self-consumption contribution. Such aspects have led to the development of an analytic model for the techno-economic design of a grid connected hybrid energy system (HES), integrating a PV plant and a BES system (PV-BES HES). The PV-BES HES, evaluated for a real case study, is comparable with PV plants without storage in case of a significant gap between the cost of energy purchased from the grid and the price of energy sold to the grid, but high BES system costs due to the initial investment and the maintenance activities can make the investment not particularly attractive. Thus, the focus has shifted to the techno-economic analysis of off-grid HESs to meet the energy demand of users in remote areas. In this context, BES systems have an important role in the operation and management of the HES, in addition to the storage of exceeding energy produced by the RESs. The activity has also been carried out in collaboration with the Company Margen S.p.A. with the aim to configure, test and install two off-grid HES to meet the energy demand of a remote villages and a telecommunication system in Yakutsk (Russia).

In parallel, two experimental activities in the context of solar concentrating technology have been carried out. The former activity deals with the design, development and field test of a Fresnel lens pilot-scale solar concentrating prototype for the PV energy distributed generation, through multi-junction solar cells, and the parallel low temperature heat recovery (micro-cogeneration CPV/T system). The latter activity has been developed during the permanence at the Clean Energy Research Center - University of South Florida (Tamp, FL - United States). The research activity has focused on the development and tests of a low cost thermal energy storage (TES) prototype for CSP plants able to overcome the intermittent and random nature of the solar radiation increasing the power plant working hours, and therefore, its economic profitability.

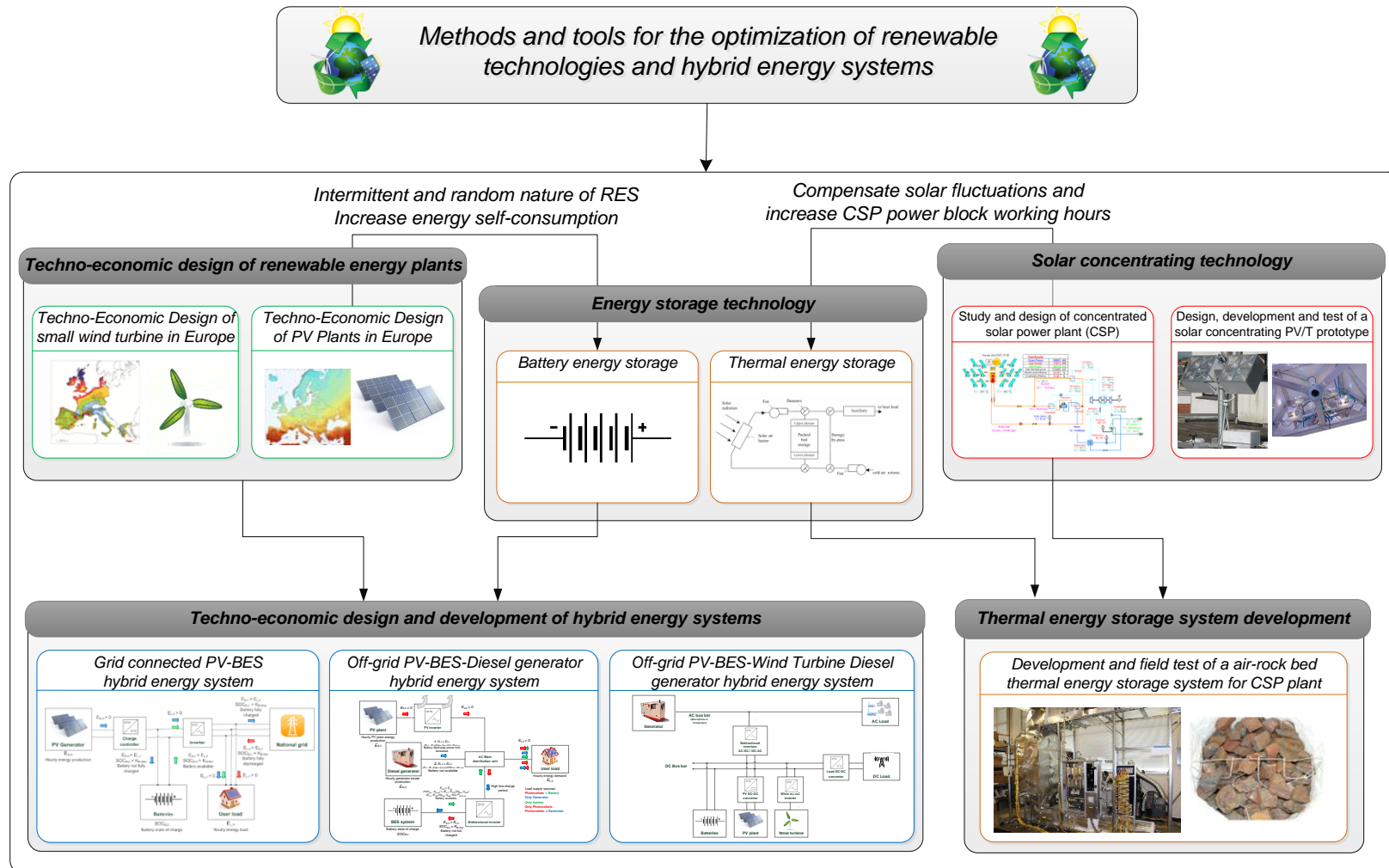


Figure 1.6 Research framework

## 1.2 Dissertation outline

In accordance with the introduced research overview, this *Paragraph* presents the reminder of the Ph.D. dissertation (See Figure 1.7) including the description of the content of each *Chapter* and the main obtained results. *Chapter 1* and *Chapter 8* discuss, respectively, the current scenario for RESs and the main conclusions of the dissertation together with indications and perspectives for further research.

- *Chapter #2 - Renewable Energy Plant Design:* This *Chapter* deals with the analytic models developed for the techno-economic design of PV plants (*Paragraph 2.1*) and SWTs (*Paragraph 2.2*) and applied to the economic feasibility study, through multi-scenario analysis, of such systems in some of the main EU Countries. Concerning the SWTs, the model takes into account technical, economic/financial, geographic parameters and country peculiarities, e.g. incentives and supporting policies, evaluating the SWT turnkey costs, annual costs/revenues and calculating common economic evaluation indices, such as net present value and payback time, for each considered scenario. The analysis, referred to the year 2012, has considered ten different SWTs with rated power up to 200kW from both European and extra European countries. The SWT economic and technical parameters have been obtained through a market survey. The results show the economic profitability and competitiveness, for the reference year, of the most cost-effective SWTs in five European countries, *i.e.* France, Germany, Italy, Spain and The Netherlands, in accordance with the respective anemological conditions.

Similarly to the study of SWTs, a multi-scenario analysis has been performed to determine the economic feasibility of PV plants in eight of the main European Countries, *i.e.* France, Germany, Greece, Italy, The United Kingdom, The Netherlands, and Turkey. The developed analytic model takes into account technical, economic/financial, geographical parameters and country peculiarities. Among the technical parameters, a deep attention is addressed on the role of self-consumption, the type of installation, *i.e.* residential vs industrial, and the comparison between incentive and no-incentive scenarios. Self-consumption introduces economic benefits due to the gap between costs and selling price of electricity to the National grid. The results, referred to the year 2012, show that the PV supporting policies were still crucial in the economic profitability of PV plants. In addition, the achievement of self-sustainability, *i.e.* no incentives provided, of PV plants is strongly linked to the role of self-consumption, as well as to the decrease in the costs of installation and operation of PV plants.

- *Chapter #3 – Energy Storage Technology:* This *Chapter* presents a brief review of energy storage systems, identified as an effective strategy to overcome the intermittent and random nature of RESs and to increase the energy self-

consumption rate. Particularly, BES systems are suitable for PV plants and SWTs and this *Chapter* also includes their technical features and properties providing the right framework for the analysis on HESs described in the *Chapter 4*.

- *Chapter #4 – Hybrid Energy System Design:* the adoption of BES and the study of the user energy demand profile have been identified as effective strategies to increase energy self-consumption rate and to increase RESs profitability and competitiveness. This *Chapter* focuses on the techno-economic design of a grid connected HES integrating a PV plants and a BES system and a similar analysis extended to off-grid HESs, integrating RESs, fossil fuel based generators and BES systems. In the grid connected HES the electricity demand is satisfied through the PV-BES system and the national grid, used as the backup power source. The aim is to present the PV-BES system design and management strategy and to discuss an analytical model to determine the PV plant rated power and the BES system capacity able to minimize the levelized cost of the electricity (*LCOE*). The amount of energy purchased from the grid introduces an additional cost proportional to the grid electricity tariff, while the energy sold to the grid, proportional to the electricity market price, is computed as an opportunity cost. As a consequence, the obtained *LCOE* values can be directly compared with the grid electricity tariff, showing immediately the competitiveness and profitability of the PV-BES system configuration. The proposed model considers the hourly energy demand profile for a reference year relating the analysis to the hourly irradiation and the temperature trend for the installation site. Furthermore, the proposed model has been applied to design the grid connected PV-BES system installed at the new buildings of the Engineering and Architecture School of the Bologna University, Italy. A multi-scenario analysis is assessed varying the PV-BES system rated power and capacity. The results, referred to the year 2013, show the economic profitability of PV plant aimed to meet the energy demand of the user, and therefore oriented to self-consumption, while the competitiveness of storage systems is connected to the gap between the purchase cost and selling price of electricity from the grid.

Such analysis has been extended to off-grid energy HESs integrating a PV plant, a diesel generators and BES system designed the meet the energy demand of users in remote areas. In this type of configuration, BES system plays a fundamental role storing the exceeding energy produced by the RESs, optimizing the diesel generator management, *e.g.* management of pre-heating, cooling times and transient conditions, and guaranteeing the energy supply during generator failure or low irradiation periods, *i.e.* emergency power source. The diesel generator, which costs are a linked to the fuel consumption, function of the supplied power, and the maintenance activities, function of the generator working hours, works as back-up power source. The developed analytic model is able to determine the PV system rated power and the BES system capacity able to

minimize the *LCOE*. The model has been applied to the design of a HES installed in a remote village in Yakutsk (Russia) and developed in collaboration with the company Margen S.p.A. The model takes into account the hourly energy demand, the irradiation and the temperature profiles for the installation site calculating the hourly PV plant yield, the battery charge-discharge processes and the generator energy request. A multi-scenario analysis is carried out varying the PV plant and BES system capacity. The results, referred to the year 2014, highlight the technical feasibility and the moderate economic profitability of such a system for a context with a medium irradiation level and a relatively low fuel cost. The *Chapter 4* also includes the technical features of a second HES developed in collaboration with Margen S.p.A. integrating PV plant, SWT, BES system and diesel generators designed to supply a telecommunication system installed in Russia.

- *Chapter #5 - Solar Concentrating Technology*: This *Chapter* provides a conceptual background of solar concentration principles and a review of the available technical plant engineering solutions. The topics discussed are the basis and provide the right framework for the two experimental activities conducted to develop a CPV prototype and the thermal energy storage (TES) system described, respectively, in the following *Chapter 6* and *Chapter 7*.
- *Chapter #6 – Concentrating PV/T prototype*: This *Chapter* presents a research activity concerning about the design, development and tests of a Fresnel lens pilot-scale solar concentrating prototype for the PV energy distributed generation, through multi-junction solar cells, and the parallel low temperature heat recovery (micro-cogeneration CPV/T system). The whole research activity is part of the co-financed Mi.S.T.I.Co. project (Micro-systems and innovative technologies for the solar energy cogeneration) - Partners: Bruno Kessler Foundation (Trento, Italy), Universities of Padova, Bologna and Trento. The experimental results point out the complexity and critical issues of the CPV/T technology, which efficiency depends upon the accurate integration of different expensive components, *i.e.* the solar collectors and receivers, tracking system, *etc.* Research activities and industrial developments are focused on the efficiency and cost reduction to make such a technology competitive with traditional PV plants and other RESs.
- *Chapter #7 -TES prototype for CSP plants*: The *Chapter 7* describes the research activity focused on the development of a low cost storage solution for solar central receiver technology developed during the permanence at the Clean Energy Research Center - University of South Florida (Florida - United States). The system consists of a packed bed of pellets as the storage media and uses air as the heat transfer fluid. This TES system may overcome the intermittent nature of sunlight and increase the capacity factor of solar thermal power plant and it is promising TES concept due to its single tank design and employment of cheap and abundant storage media such as sand and rock. The TES system is charged

with a high temperature air flow coming from the central receiver and it is discharged with a lower temperature air flow coming from the turbine outlet or the external ambient. Consequently, this charging-discharging process allows supplying the thermodynamic cycle for a certain number of hours when the solar radiation is not available. The research activity has focused on the development and implementation of a pilot-scale prototype system adopting iron rocks as the storage media to test its performance and behavior.

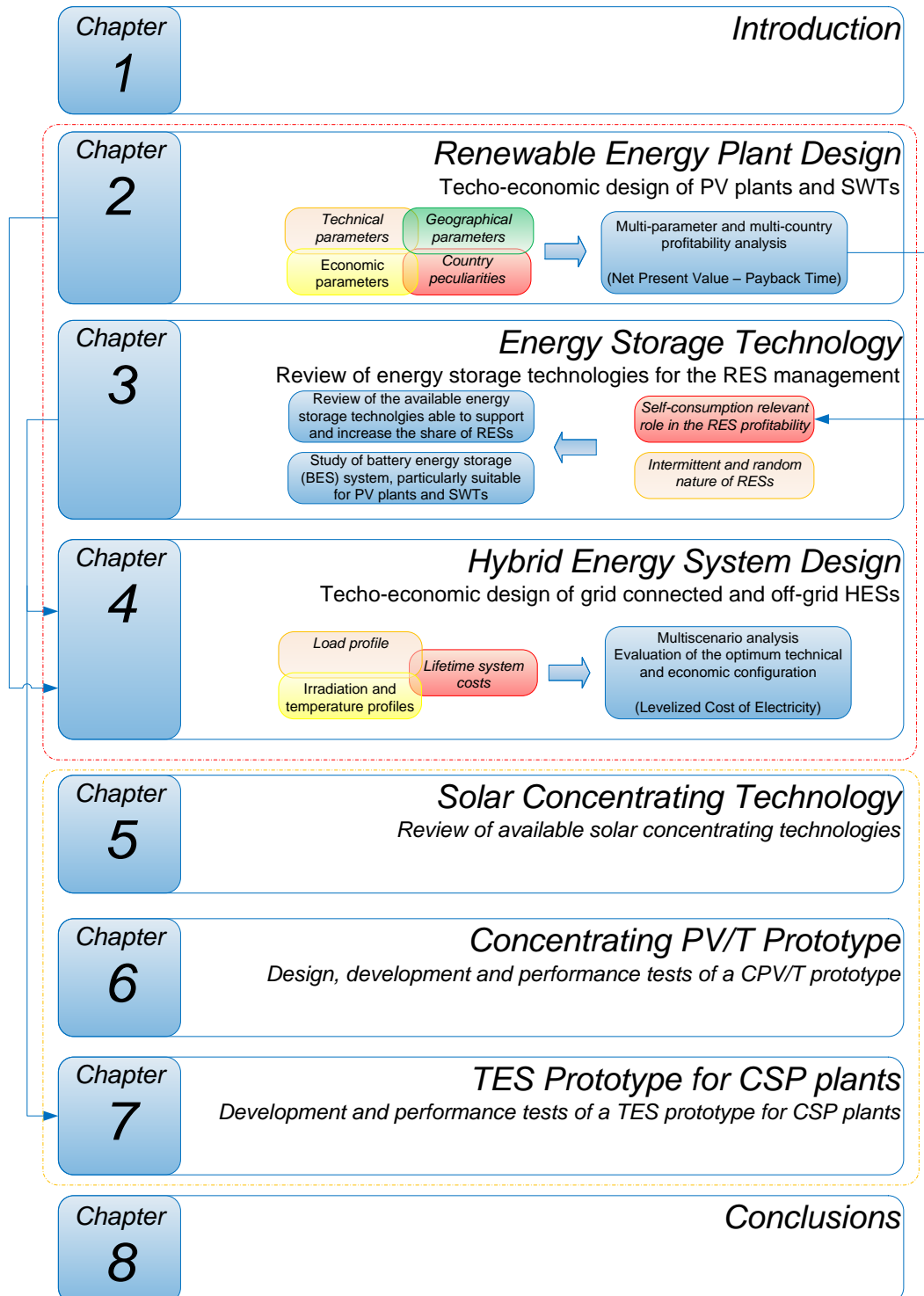


Figure 1.7 Dissertation outline framework

## 2. Renewable Energy Plant Design

### *Techno-economic design of PV plants and SWTs*

This *Chapter 2* deals with the analytic models developed for the techno-economic design of photovoltaic (PV) plants (*Paragraph 2.1*) and small wind turbines (SWTs) (*Paragraph 2.2*) and applied to the economic feasibility study, through a multi-scenario analysis, of such systems in some of the main European Union (EU) Countries (Year 2012).

### *2.1 Techno-Economic design of photovoltaic (PV) plants*

This *Paragraph* focuses on the economic assessment of PV plants, introducing a performance cost model (PCM), based on the net present value (NPV) and payback (PB) capital budget indices, to quantify the net cash flows through the plant lifetime and evaluate their economic sustainability. The analysis is based on Bortolini *et al.* (2013) and take into account a set of parameters affecting the plant performances, *i.e.* technical, environmental, economic and financial parameters, with the purpose to highlight those which are the most critical.

The proposed model overcomes the wide set of existing literature studies including, in a unique model, a multi-country and multi-parameter analysis considering both the country peculiarities and the technical, environmental and economic conditions of several PV plant configurations. In the literature, a wide set of contributions provides single country analyses of the current PV sector status. As example, Bernal-Augustin and Dufo-Lopez (2006), Fernandez-Infantes *et al.* (2006) and Hernández *et al.* (2008) present detailed economic studies on PV systems for Spain, while Hammond *et al.* (2012) focus on the United Kingdom context. Furthermore, Focacci (2009) reviews the PV sector for Italy, Audenaert *et al.* (2010) propose an economic evaluation of grid connected PV systems in Flanders, Belgium, and Šály *et al.* (2006) review the status and conditions of PVs in Slovakia. Outside the EU area, several contributions refer to the US, China and other developed countries, *e.g.* Fthenakis *et al.* (2009), Zhang *et al.* (2012), Becerra-López and Golding (2008), or, even, to developing countries belonging to the sun belt area where the potential of the solar energy is higher than elsewhere. Diarra and Akuffo (2002) focus on Mali, Al-Salaymeh *et al.* (2010) consider PV systems located in Jordan, Ghoneim *et al.* (2002) investigate the scenario for Kuwait, Mitscher and Rüter (2012) focus on the Brazilian region, while Nässén *et al.* (2002) propose an assessment of solar PVs in northern Ghana.

A parallel research field focuses on the comparison among countries considering single aspects of the PV energy sector. Several works discuss the national incentive policies highlighting similarities and differences among current legislations (Reiche *et al.* (2004), Rowlands (2005), Campoccia *et al.* (2007), Di Dio *et al.* (2007), Barbose *et al.* (2008), Campoccia *et al.* (2009)), while other studies evaluate the trend of the PV cell costs with a long-term horizon correlating the past trend of the PV system costs to the current state of the art of the PV cell manufacturing technologies in different countries (Photovoltaic energy barometer 2007, 2009, 2010, 2011, 2012).

Starting from a survey of the current status of the national legislations and the incentive schemes for supporting the PV sector and the current market conditions, referred to the year 2012, in eight relevant countries of the EU area, *i.e.* France, Germany, Greece, Italy, Spain, The Netherlands, Turkey and United Kingdom, this multi-parameter analysis investigates the technical and economic features making PV investments potentially profitable.

According to the defined purpose, the remainder of this Paragraph is organized as follows: *sub-Paragraph 2.1.1* briefly provides the historical overview of PV sector in the European area, while *sub-Paragraph 2.1.2* presents the adopted PCM for the economic assessment of each considered scenario and it provides a full description of the model parameters. The PV sector status and the key differences among the eight considered countries, with reference to the year 2012, are included in *sub-Paragraph 2.1.3*. The multi-country analysis is introduced in *sub-Paragraph 2.1.4* and the obtained results are extensively discussed in *sub-Paragraph 2.1.5*. The last *sub-Paragraphs 2.1.6 and 2.1.7* concludes the paper providing final remarks and suggestions for further research.

### *2.1.1 PV sector historical overview for the main EU countries*

The historical trend from 2005 to 2011, which is the period of the great expansion of the PV sector in the EU area, of the PV installed capacity for the eight considered countries clearly highlights three major phenomena about the status of the PV sector in the EU area (Figure 2.1). The first is the significant increase of the installed capacity through the years for all countries, *i.e.* from 2170MWp operating in 2005 to 46454MWp operating in 2011, with an increase higher than twenty times the 2005 level. The second phenomenon is the unequal distribution of the installed capacity among countries. Germany, itself, has the 53.5% of the total amount of the installed capacity followed by Italy (27.5%), Spain (9.0%) and France (6.1%). The other countries present lower percentages and, together, have the last 3.9% of the total capacity. Finally, the third phenomenon deals with the different gradient of the waveforms of Figure 2.1. Particularly, Germany presents a constant annual increase of the installed capacity, *i.e.* an increase of about 35% over the previous year, while, other countries, like Italy, Spain and United Kingdom, present an erratic behaviour. The main cause for such differences lies in the national supporting policies each country actuates and their evolution through the years, *e.g.* a systematic



support to the PV sector with the progressive decrease of the national incentive strategies vs. spot actions followed by the partial or total cut off of such supports.

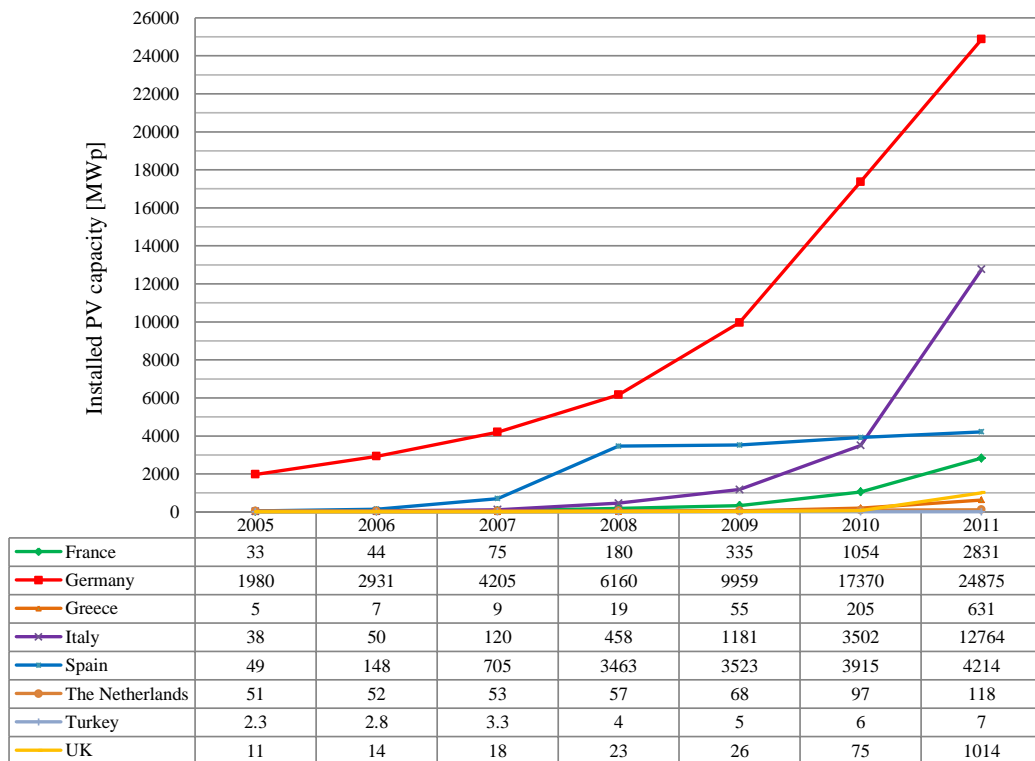


Figure 2.1 Historical trend of PV sector in the main EU countries (Photovoltaic energy barometer 2007, 2009, 2010, 2011, 2012; IEA, 2010)

These phenomena further justify the following review, referred to year 2012, of the incentive schemes, the market conditions and the tax levels for each of the eight considered countries. Such parameters are the key inputs of the PCM described in the following *sub-Paragraph*.

### 2.1.2 Performance Cost Model

Figure 2.2 presents the flow chart of the proposed approach for the PV system analysis highlighting the technical, geographical, economic/financial data and country peculiarities included in the model together with the analysis steps. Starting from the input data, the PCM calculates the entity of the initial investment and the annual revenues and costs. Such data allow computing the *NPV* and *PB* justifying the economic feasibility of the analyzed configuration. PCM results are, further, compared through a multi-parameter analysis to highlight the technical, geographical, economic/financial parameters and country peculiarities most affecting the PV system profitability.

Focusing on the PCM, *Equation 2.1* defines the analytic expression for the *NPV*, while *Equation 2.2* considers the *PB*, i.e. the minimum number of years necessary to return on the investment (Feibel, 2003).

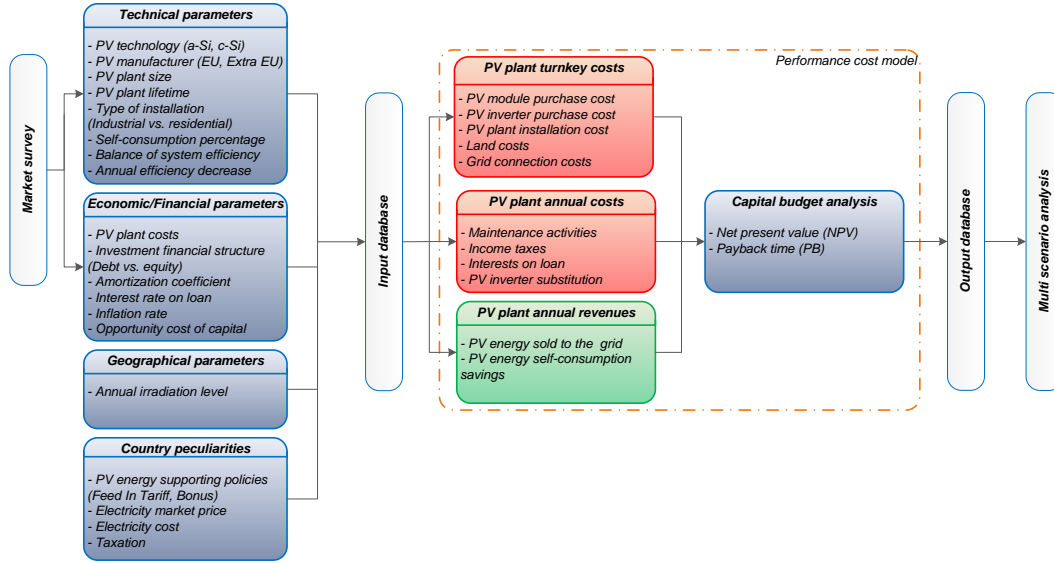


Figure 2.2 Flow chart of the proposed PV system analysis

$$NPV = -C_0 + \sum_{j=1}^{Lt} \frac{R_j - C_j}{(1+OCC)^j} \quad (2.1)$$

$$-C_0 + \sum_{j=1}^{PB} \frac{R_j - C_j}{(1+OCC)^j} = 0 \quad (2.2)$$

Where:

- $C_0$  is the outflow for the initial investment. For residential plants the VAT is, already, included [€]
- $R_j$  is the revenue for year  $j = 1..Lt$  [€/year]
- $C_j$  is the operative outflow for year  $j = 1..Lt$  [€/year]
- $OCC$  is the opportunity cost of capital [%]
- $Lt$  is the estimated plant lifetime [year]

The initial investment,  $C_0$ , includes all the plant installation costs and the land purchase if the PV system is non-integrated.

$$C_0 = P_o \cdot c_{module} + \left( \psi \cdot \frac{P_o}{\eta_{module} \cdot H_{I,r}} \right) \cdot c_{land} = P_o \cdot c_{module} + S \cdot c_{land} \quad (2.3)$$

Where:

- $P_o$  is the nominal plant size measured at standard test conditions, *i.e.* irradiance of  $1000 \text{ W/m}^2$ , solar spectrum of AM 1.5 and module temperature of  $25^\circ\text{C}$  [kWp] (IEC 61724:1998)
- $H_{I,r}$  is the yearly module reference in-plane irradiance, usually assumed equal to  $1 \text{ kW/m}^2$  [kW/m<sup>2</sup>] (IEC 61724:1998)
- $\eta_{module}$  is the PV module efficiency [%]

- $S$  is the required ground area for non-integrated PV systems, necessary for service facilities and to limit module shading effects [ $m^2$ ]
- $\psi$  is the “spacing factor” defined as the ratio between the necessary ground area,  $S$ , and the PV module area,  $\left(\frac{P_o}{\eta_{module} \cdot H_{1,r}}\right)$  (Breckl and Topič, 2011)
- $c_{land}$  is the land cost ( $c_{land} = 0$  for integrated PV systems) [ $€/m^2$ ]
- $c_{module}$  is the specific installation cost of the PV system [ $€/kWp$ ] obtained through a market research for both EU and extra EU manufactures and considering the two most frequently adopted silicon cell technologies, *i.e.* amorphous (a-Si) and crystalline (c-Si) solar cells

The following correlation functions between PV installation cost and its rated power express the aforementioned market research outcomes.

$$c_{module}^{EU\ cSi} = 2828.7 \cdot P_o^{-0.128} \quad (2.4)$$

$$c_{module}^{Extra\ EU\ cSi} = 2539.9 \cdot P_o^{-0.139} \quad (2.5)$$

$$c_{module}^{EU\ aSi} = 2356.4 \cdot P_o^{-0.114} \quad (2.6)$$

$$c_{module}^{Extra\ EU\ aSi} = 2115.8 \cdot P_o^{-0.126} \quad (2.7)$$

The operative outflow for the generic year  $j = 1..Lt$ , is as follows:

$$C_j = C^{OM\&I} \cdot (1 + g)^{j-1} + C_j^D + C_j^I + C_j^T \quad (2.8)$$

Where:

- $C^{OM\&I}$  is the annual operation and maintenance outflow [ $€/year$ ]
- $g$  is the inflation rate [%]
- $C_j^D$  is the annual outflow for the interest paid to finance the investment [ $€/year$ ]
- $C_j^I$  is the outflow due to the inverter substitution. For residential plants VAT is, already, included [ $€/year$ ]
- $C_j^T$  is the annual tax cost, ( $C_j^T = 0$  if the net cash flow is negative and for all the residential installations) [ $€/year$ ]

The interest paid to finance the investment,  $C_j^D$ , occurs for non-totally private equity financed investments and it is calculated through the straight line depreciation approach as in *Equation 2.9* (Feibel, 2003).

$$C_j^D = r \cdot \left[ \varphi \cdot C_0 - \sum_{z=1}^{j-1} \left( \frac{(1+r)^{Lt \cdot r}}{(1+r)^{Lt \cdot z - 1}} \cdot \varphi \cdot C_0 - C_z^D \right) \right] \quad (2.9)$$

Where:

- $r$  is the money interest rate on loan [%]
- $\varphi$  is the loan percentage [%]

Furthermore, the inverter substitution cost,  $C_j^I$ , is a common expenditure during the PV plant lifetime. In the present model, a market research drives the computation of such a cost. *Equation 2.10* expresses the inverter substitution cost as a function of its plant size, while *Equation 2.11* is the best fit curve correlating the inverter specific cost, i.e.  $c_{inverter}$ , to its rated power.

$$C_j^I = c_{inverter} \cdot P_o \quad (2.10)$$

$$c_{inverter} = 0.0325 \cdot P_o^2 + 196.25 \cdot P_o + 350.95 \quad (2.11)$$

The amount of the annual tax cost,  $C_j^T$ , is expressed in *Equation 2.12* adopting the Earning Before Tax (EBT) approach (Feibel, 2003).

$$C_j^T = [R_j - C^{OM\&I} \cdot (1+g)^{j-1} - C_j^D - C_j^I - A] \cdot t \quad (2.12)$$

Where:

- $A = \frac{(1+OCC)^a \cdot OCC}{(1+OCC)^a - 1} \cdot c_{module} \cdot P_o$  is the plant amortization rate, supposed constant [€/year]
- $a$  is the plant amortization period [year]
- $t$  is the corporate tax level [%]

The revenue,  $R_j$ , which increases the plant *NPV*, comes from both the energy self-consumption and the national grid sell of the produced energy. In the former case, the users do not buy electricity from the grid, while in the latter the benefits come both from the incentives, if provided, and from the energy selling.

The following *Equation 2.13* introduces the annual revenue expression for year  $j = 1..Lt$ , while the following *Equations 2.14 - 2.16* define the annual cost saving due to the energy self-consumption, i.e.  $R_j^c$  [€/year], and the revenue from the energy sale, i.e.  $R_j^s$  [€/year].

$$R_j = R_j^s \cdot \chi_{sold} + R_j^c \cdot (1 - \chi_{sold}) \quad (2.13)$$

$$R_j^c = E_c \cdot (1+g)^{j-1} \cdot E_{A,y} \cdot [1 - (j-1) \cdot \eta_{d,y}] \quad (2.14)$$

$$R_j^s = i \cdot E_{A,y} \cdot [1 - (j - 1) \cdot \eta_{d,y}] \text{ if the national FiT is provided} \quad (2.15)$$

$$R_j^s = E_{mp} \cdot (1 + g)^{j-1} \cdot E_{A,y} \cdot [1 - (j - 1) \cdot \eta_{d,y}] \text{ otherwise, i.e. no FiT} \quad (2.16)$$

Where:

- $\chi_{sold}$  is the percentage of the produced energy sold to the grid [%]
- $E_c$  is the electricity price for the energy bought from the grid [€/kWh]
- $i$  is the feed in tariff (FiT) [€/kWh]
- $E_{mp}$  is the electricity price for the energy sold to the grid [€/kWh]
- $\eta_{d,y}$  is the yearly efficiency system decrease [%](IEC 61724:1998)
- $E_{A,y}$  is the annual yield calculated through the following Equation 2.17 [kWh/year] (IEC 61724:1998)

$$E_{A,y} = H_{I,y} \cdot A_a \cdot \eta_{module} \cdot \eta_{bos} \quad (2.17)$$

Where:

- $H_{I,y}$  is the total yearly in-plane irradiation [kWh/(m<sup>2</sup>·year)] (IEC 61724:1998)
- $A_a = \frac{P_o}{\eta_{module} \cdot H_{I,r}}$  is the PV module area [m<sup>2</sup>] (IEC 61724:1998)
- $\eta_{bos}$  is the Balance of System (BOS) efficiency [%](IEC 61724:1998)

### 2.1.3 PV sector elements for the eight EU countries: the 2012 scenario

An effective strategy for the national institutions and governments to support the spread of the PV technology and to encourage the investors is the adoption of incentive schemes to contribute to the creation of profitable economic conditions to the energy production from the solar source. Such an energy policy strategy has been adopted in almost all the main EU countries, even if differences exist. Dusonchet and Telaretti (2010a, 2010b) and Avril *et al.* (2012) review this issue in depth comparing country strategies and legislations. In the following, details about the incentive schemes for the eight considered countries are proposed. Data refers to year 2012.

**France** - The French government supports PV sector through the FiT scheme of Table 2.1. Incentives are for 20 years and residential plants benefit of a, further, 7% value added tax (VAT) reduction calculated on the PV installation turnkey cost (French legislation, Arrêté du 4 mars 2011; Jäger-Waldau *et al.*, 2011; RES-Legal, 2012).

Table 2.1 FiT for France [€/kWh]

Plant type	Residential	Industrial
Integrated systems < 9kWp	0.3539	0.2136
Integrated systems 9kWp-36kWp	0.3096	-
Simplified integrated systems 0-36kWp	-	0.1842
Simplified integrated 36kWp-100kWp	-	0.1750
Non integrated systems	0.1051	0.1051

**Germany** - German government applies a FiT to PV systems for 20 years. The FiT decreases every year due to a fixed reduction rate function of the previous year installed capacity. For PV systems installed in 2012, the decrease rate is of 15% (Jäger-Waldau *et al.*, 2011; RES-Legal, 2012; JRC European Commission, 2011; German Government, EGG 2009).

Table 2.2 FiT for Germany [€/kWh]

Plant type	FiT	Additional FiT based on self-consumption ratio	
Integrated systems < 30kWp	0.244	< 30%	0.105
		> 30%	0.142
Integrated systems 30 kWp-100kWp	0.232	< 30%	0.094
		> 30%	0.130
Integrated systems 100kWp-1MWp	0.220	< 30%	0.081
		> 30%	0.118
Integrated systems > 1MWp	0.184	-	-
Non integrated systems	0.179	-	-

**Greece** - Greece applies a FiT to energy from PV systems with installed electrical capacity lower than 1MWp. The FiT is for 20 years for non-integrated and building integrated systems over 10kWp and of 25 years for building integrated systems up to 10kWp. FiT grants 0.250€/kWh for building integrated systems up to 10kWp. For non-integrated and building integrated systems with rated power lower than 100kWp the FiT is of 0.225€/kWh, while it decreases to 0.180€/kWh for higher power plants (res-legal.de, 2012, Greece Legislation, Law 3581/2010; HELAPCO, 2012).

**Italy** - Since August 2012, a new incentive scheme is in force in Italy. As in Table 2.3, an overall FiT for production and sale of PV energy and a premium tariff for self-consumption are introduced. Furthermore, a FiT increase of 10% is applicable if more than 60% of the investment is from EU producers, excluding the labor cost. Italian legislation, also, provides a 10% VAT reduction to any PV installation (Jäger-Waldau *et al.*, 2011; RES-Legal, 2012; JRC European Commission, 2011; Italian Legislation, Decreto Ministeriale 05/05/2011, Italian Legislation, Decreto Ministeriale, 05/07/2012, GSE, 2012).

**Spain** - In Spain, the FiT for PV systems is of 0.289€/kWh for building integrated systems with rated power lower than 20kWp, 0.204€/kWh for building integrated systems with rated power between 20kWp and 2MWp and 0.135€/kWh for non-integrated systems (Jäger-Waldau *et al.*, 2011; RES-Legal, 2012; JRC European Commission, 2011; Spanish Legislation, R.D. 1565 19/11/2010; Spanish Legislation, R.D. 14 23/12/2010).

*Table 2.3 FiT for Italy [€/kWh]*

Plant size	Integrated systems		Non-integrated systems	
	FiT	Premium tariff	FiT	Premium tariff
1kWp-3kWp	0.208	0.126	0.201	0.119
3kWp -20kWp	0.196	0.114	0.189	0.107
20kWp-200kWp	0.175	0.093	0.168	0.086
200kWp-1000kWp	0.142	0.060	0.135	0.053
1000kWp-5000kWp	0.126	0.044	0.120	0.038
> 5000kWp	0.119	0.037	0.113	0.031

**The Netherlands** - During 2011, the Dutch government promoted the production of renewable energy through the Sustainable Energy Incentive Scheme Plus (SDE+) providing a 15 years FiT of 0.120€/kWh. From 2012, Dutch government cuts all incentives to energy production from PV systems (RES-Legal, 2012; JRC European Commission, 2011; Dutch Ministry of Economic Affairs, Agriculture and Innovation, Energy Report 2011, Solarplaza, The Global Energy (PV) Platform, 2012).

**Turkey** - FiT in Turkey are for 20 years and equals to 0.100€/kWh for PV systems commissioned before the end of 2015. A FiT increase of 0.052€/kWh is applicable if plant components are manufactured in Turkey (Turkish Legislation 5436 10/05/2005; Turkish Legislation, Law 6094 29/12/2010; Dinçer, 2011).

**United Kingdom** - FiT scheme to support PV systems with rated power lower than 50MWp is in Table 2.4. FiT is granted for 25 years (RES-Legal, 2012; JRC European Commission, 2011).

*Table 2.4 UK PV system incentives [€/kWh]*

Plant size	FiT
< 4kWp	0.260
4kWp-10kWp	0.210
10kWp-50kWp	0.188
50kWp-200kWp	0.160
> 250kWp	0.105

Finally, Table 2.5 provides further economic and financial data about the current values of the electricity prices, the tax levels and the annual inflation ratios. Such parameters are

included in the PCM model described in the previous *sub-Paragraph 2.1.2* (Europe's Energy Portal, 2011; EC Eurostat, Energy price statistics 2011; EC Eurostat, Annual inflation rate 2011; Mercato Elettrico, 2012, EC Energy, Quarterly Reports 2011; APX ENDEX, 2012; USAID-HIPP, 2011; EC Taxation and Customs Union, 2012; Worldwidetax, 2012).

*Table 2.5 Country economic and financial data: electricity price, tax level and inflation*

Country	Electricity prices [€/kWh]			Tax levels		
	Energy sold to the market	Energy bought from the grid (industry)	Energy bought from the grid (residential)	Corporate tax	VAT	Annual inflation rate
France	0.0449	0.1340	0.2781	33.33%	19.60%	2.30%
Germany	0.0623	0.1188	0.1403	29.51%	19.00%	2.50%
Greece	0.0774	0.1565	0.2164	25.00%	23.00%	3.10%
Italy	0.0483	0.1261	0.2154	31.40%	21.00%	2.90%
Spain	0.0535	0.0763	0.1478	30.00%	18.00%	3.10%
The Netherlands	0.0448	0.1149	0.1676	25.00%	19.00%	2.50%
Turkey	0.0472	0.1181	0.2202	20.00%	18.00%	6.50%
United Kingdom	0.0740	0.0790	0.1220	24.00%	20.00%	2.40%

### 2.1.4 Multi-country and multi-parameter analysis

The introduced PCM is adopted to develop a multi-country and multi-parameter analysis to study the conditions most affecting the profitability of PV systems in the considered EU countries. Several scenarios are assessed. Each of them comes from a specific setting of the PCM input parameters (Figure 2.2), while varying such parameters the comparison among different scenarios becomes possible. Particularly, nineteen independent parameters need to be defined to fix each scenario. In Table 2.6, the boundary conditions for such parameters are presented adopting plausible values or ranges of variation (Campoccia *et al.*, 2009; PVGIS, 2012; Quintana *et al.*, 2002; Šúri *et al.*, 2007; Danchev *et al.*, 2010; Branker *et al.*, 2011; Harvey, 1996; Reis *et al.*, 2002).

For each combination of the aforementioned parameters, *i.e.* the previously called scenarios, the PCM is applied computing both the *NPV* and the *PB*. A parametric Microsoft Excel© datasheet, developed with Visual Basic for Applications programming language, allows to speed the computation process. The following *sub-Paragraph 2.1.5*, presents the key outcomes of the analysis.



Table 2.6 Values for the PCM input parameters.

Parameter	Adopted values
<i>Technical data</i>	
$P_o$	3, 20, 50, 100, 1000kWp for industrial PV plants 3-6-9-12-15kWp for residential PV plants
$L_t$	20 years
$\chi_{sold}$	0%, 50%, 100%
$\eta_{module}$	8% (a-Si), 14% (c-Si)
$\eta_{bos}$	85%
$\eta_{a,y}$	1%
$\psi$	3
<i>Geographical/Environmental data</i>	
$H_{l,y}$	from 800 to 1800kWh/m <sup>2</sup> ·year, step 50kWh/m <sup>2</sup> ·year
$H_{l,r}$	1kW/m <sup>2</sup>
<i>Economic/Financial data</i>	
$a$	10 years
$c_{land}$	9€/m <sup>2</sup> for non-integrated PV plants, 0€/m <sup>2</sup> for integrated PV plants
$c_{module}$	according to Equations 2.4-2.7
$c^{OM\&I}$	equal to 1% of $C_0$
$c_{inverter}$	according to Eq. 11, $c_{inverter} = 0$ for $j \neq 7, 14$ (inverter replacement occurs two times during the plant lifetime)
$g$	according to Table 2.5, column 7
$OCC$	3%, 6%
$r$	3%, 4%, 5%, 6%, 7%, 8%, 9%, 10%
$\varphi$	0%, 50%, 100%
<i>Country peculiarities</i>	
$E_c$	according to Table 2.5, columns 3 and 4
$E_{mp}$	according to Table 2.5, column 2
$i$	according to the national schemes reviewed in <i>sub-Paragraph 2.1.3</i>
$t$	according to Table 2.5, column 5

2.1.5 Results and discussions

2.1.5.1 Incentive Vs No-Incentive Scenario

Firstly, the impact of the national support schemes and FiT to promote the PV sector are investigated. Residential and industrial plants are studied separately due to the differences in the legislations in force. Figure 2.3 and Figure 2.4 propose a relevant subset of the obtained results. In the figure captions the values of the input parameters assumed to be constant are provided in brackets.

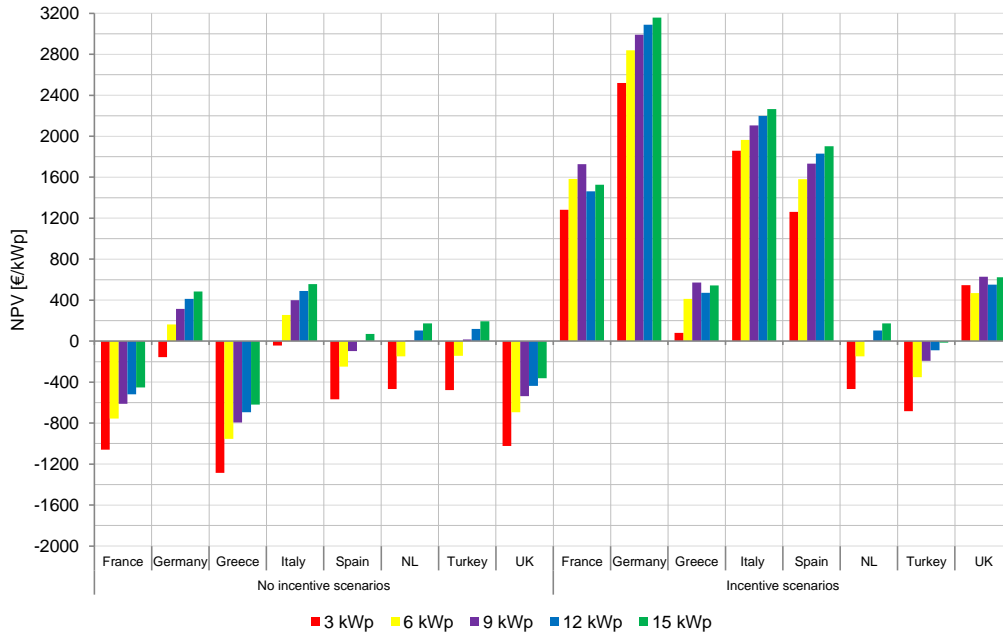


Figure 2.3 Incentive vs. no-incentive scenarios for the eight countries and residential rooftop plants ( $c_{module}$  according to Eq.2.7,  $H_{I,y} = 1400\text{kWh/m}^2\cdot\text{year}$ ,  $OCC = 3\%$ ,  $\varphi = 0\%$ ,  $\chi_{sold} = 50\%$ )

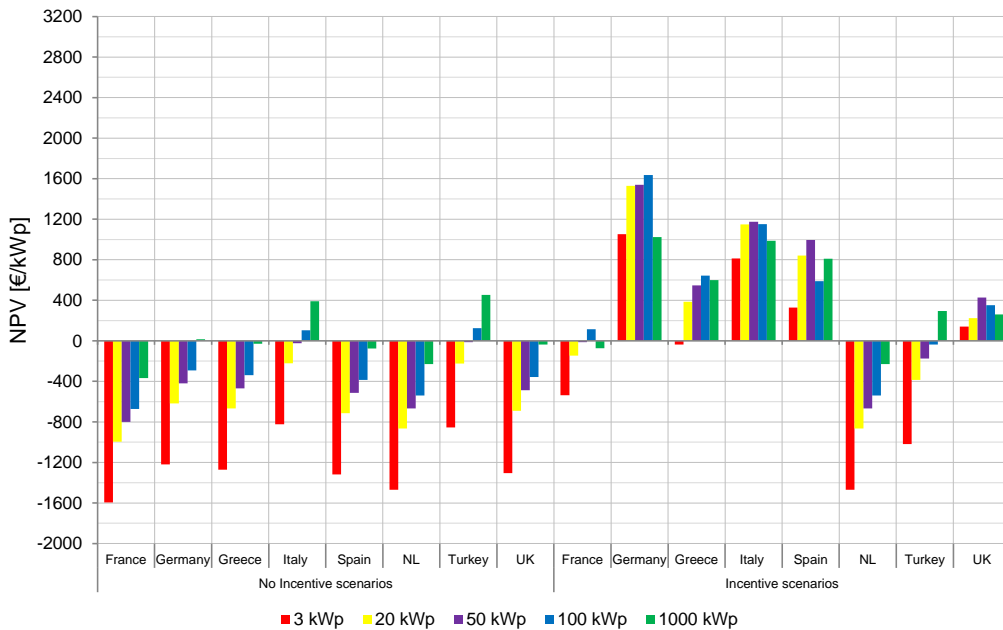


Figure 2.4 Incentive vs. no-incentive scenarios for the eight countries and industrial rooftop plants ( $c_{module}$  according to Eq.2.7,  $H_{I,y} = 1400\text{kWh/m}^2\cdot\text{year}$ ,  $OCC = 3\%$ ,  $\varphi = 0\%$ ,  $\chi_{sold} = 50\%$ )

Results highlight the key role still played by the national support policies. The incentive scenarios outperform no-incentive scenarios for all the plant sizes and countries, except for The Netherlands, in which the results are the same due to the absence of national FiT, and Turkey due to the concurrent low level of the FiT and the high inflation rate raising the electric energy cost through the years. For several of the presented scenarios the benefit introduced by the FiT marks the difference between convenient, *i.e.*  $NPV > 0$ , and non-convenient, *i.e.*  $NPV < 0$ , investments. Furthermore, a positive correlation between the  $NPV$  and the plant size is registered for all no-incentive scenarios, while, if incentives are provided, such a trend is not always experienced due to the progressive reduction of the FiT with the plant size increase. Figure 2.4 clearly justifies this evidence. Finally, the comparison between the two graphs points out the higher support introduced by the national incentive schemes to the residential plants toward the industrial applications. As example, for Germany, Italy and Spain the  $NPVs$  for the former plant group are higher than 50% respect to the industrial plants, even if the PV plant sizes are lower and relevant scale phenomena exist. Although the annual revenues depend on few parameters, *i.e.* the electricity prices,  $E_{mp}$  and  $E_c$ , and the self-consumption ratio,  $(1 - \chi_{sold})$ , the negative cash flows are a function of several cost drivers. Consequently, a sensitivity analysis is of interest for such outflows.

### 2.1.5.2 Sensitivity analysis of the cash outflows

The average results, among all scenarios, are summarized in Figures 2.5.

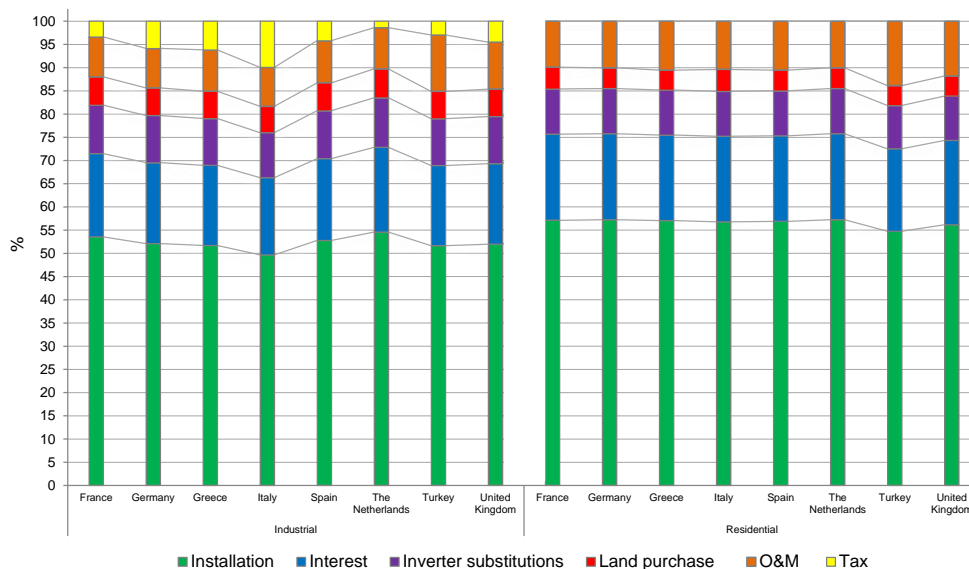


Figure 2.5 Sensitivity analysis of cash outflows

The installation, interest on debt and land purchase drivers are all related to outcomes directly connected to the initial investment, necessary to install and start up the plant, even if the cash flows occur during the whole system lifetime. The percentage impact of such drivers on the total outcomes is between 75% and 80% and few differences exist among the eight countries. Consequently, the most of the outflows required to install and manage a PV system are during the early periods of the investment lifetime. Furthermore,

for the industrial plants, four out of six drivers present the same values because of the hypothesis, behind the proposed analysis, of adopting the same PV technologies for all the countries. Differences, in the residential scenario outflows, are due to the VAT levels, specific to each country.

### 2.1.5.3 Energy self-consumption role

A third relevant outcome of the analysis is the impact of the ratio between the self-consumed and the market sold electricity, *i.e.* the previously introduced  $\chi_{sold}$  parameter. A comparison among the eight countries is in Figure 2.6 and Figure 2.7 for residential and industrial installations, respectively.

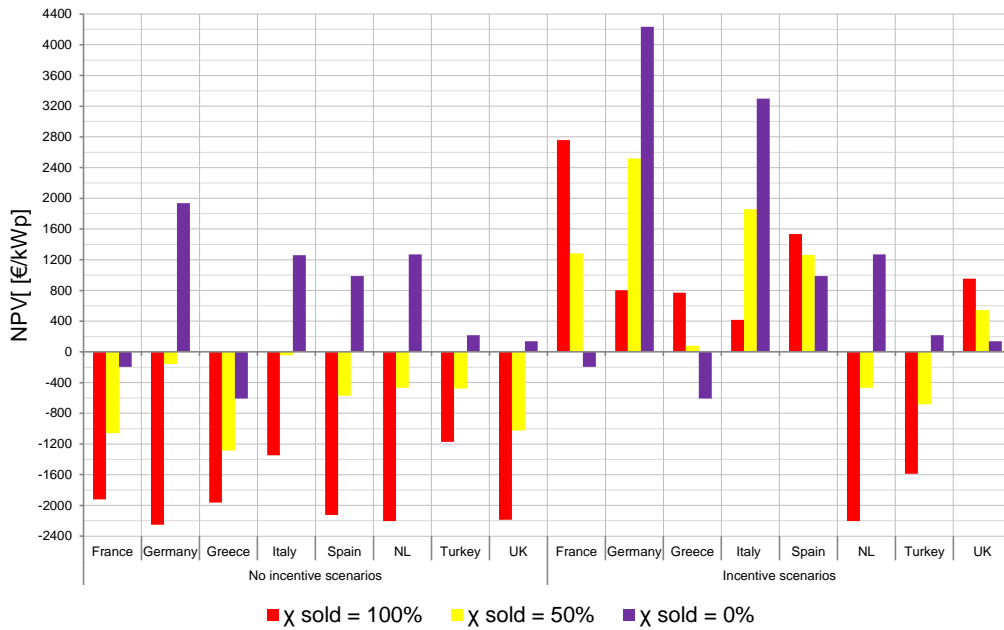


Figure 2.6 Impact of  $\chi_{sold}$  on NPV residential rooftop plants ( $c_{module}$  according to Eq.2.7,  $P_o = 3kWh$ ,  $H_{1,y} = 1400kWh/m^2 \cdot year$ ,  $OCC = 3\%$ ,  $\varphi = 0\%$ )

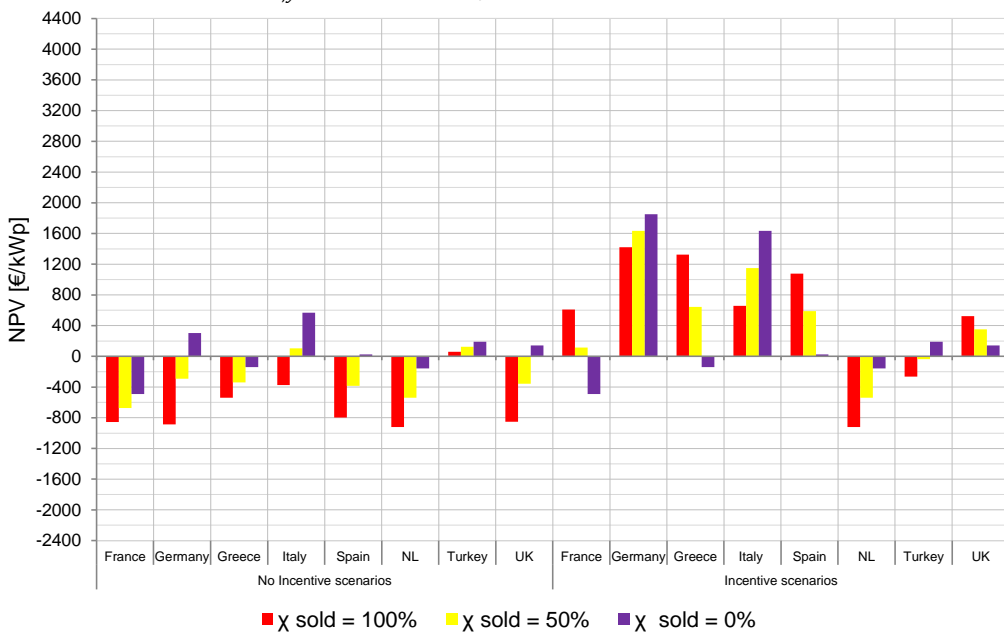


Figure 2.7 Impact of  $\chi_{sold}$  on NPV, industrial rooftop plants ( $c_{module}$  according to Eq.2.7,  $P_o = 100kWh$ ,  $H_{1,y} = 1400kWh/m^2 \cdot year$ ,  $OCC = 3\%$ ,  $\varphi = 0\%$ )

For no incentive scenarios,  $\chi_{sold} = 0\%$  is a necessary condition to generate positive  $NPVs$ , *i.e.* convenient investments. On the other side, in presence of the national supports to the PV sector, results vary among the countries mainly due to the peculiarities in the legislations currently in force. Two sets of countries, presenting opposite trends, are identified. On one side, Germany, Italy and Turkey encourage the self-consumption of the produced energy, *i.e.*  $\chi_{sold} = 0\%$  scenarios outperform  $\chi_{sold} = 50\%$  and  $\chi_{sold} = 100\%$  scenarios, while, on the other side, France, Greece, Spain and United Kingdom, spread the exchange of the PV energy to the electricity market through favorable tariffs and/or tax breaks. Such evidences are coherent to the review proposed in previous *sub-Paragraph 2.1.3*. Finally, the described trend is more evident for the residential scenarios (Figure 2.6).

#### 2.1.5.4 Impact of irradiation level

Considering the incidence of the environmental conditions on the  $NPV$  and  $PB$ , the irradiation level significantly impacts on the plant profitability. For each country, power size and system installation type, *i.e.* residential and industrial, a lower economic limit to  $H_{I,y}$  exists to mark the difference between convenient and non-convenient investments. Figure 2.8 presents such results for typical scenarios together with the range of the measured irradiance levels for the country locations in which the 90% of the built-up areas are situated (PVGIS, 2012; Šuri *et al.*, 2007). The red dashed line marks the convenient and non-convenient regions.

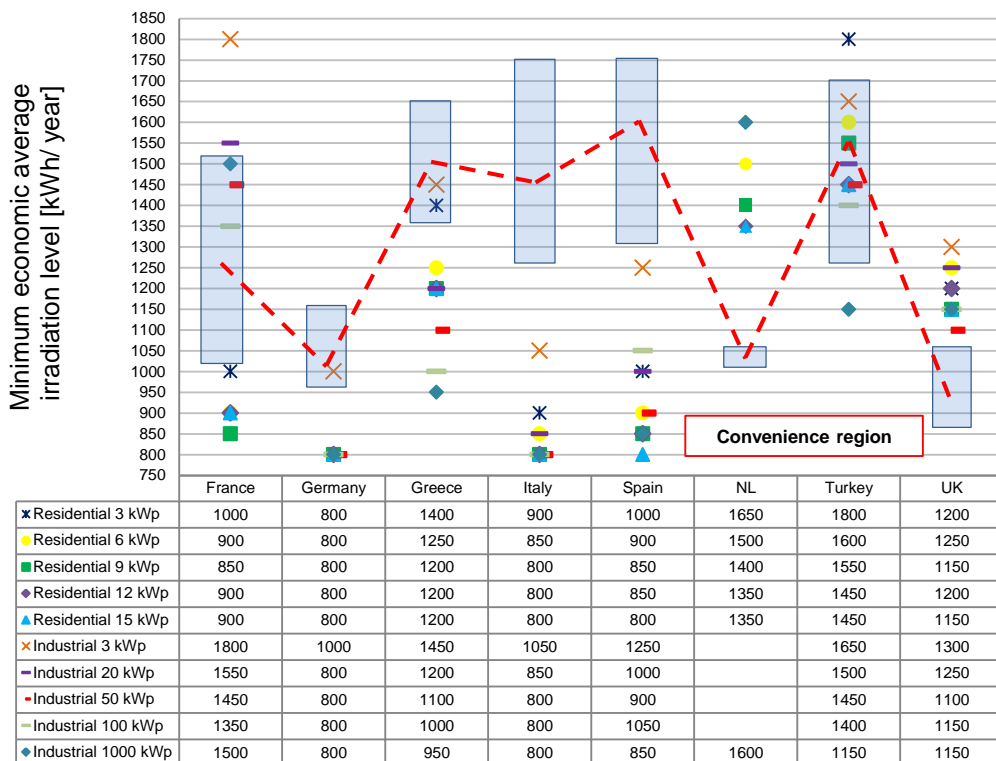


Figure 2.8 Impact of the irradiance levels,  $H_{I,y}$ , on  $NPV$  and country typical ranges ( $c_{module}$  according to Eq.2.7,  $OCC = 3\%$ ,  $\phi = 0\%$ ,  $\chi_{sold} = 50\%$ )

The most of the economic lower limits for all the eight countries, except for The Netherlands and United Kingdom, fall in the convenience region, *i.e.* the correspondent investments present  $NPV > 0$ . About the two exceptions: for The Netherlands by replacing  $\chi_{sold} = 50\%$  to  $\chi_{sold} = 0\%$ , *i.e.* totally self-consumed electric energy, the economic limits, for all scenarios, decrease and they fall in the convenience region. For United Kingdom, favorable results are for  $\chi_{sold} = 100\%$  due to the current FiT level promoting the market exchange of energy, as shown in previous Figure 2.6 and Figure 2.7.

### 2.1.5.5 Impact of financial parameters

A further group of parameters potentially affecting the PV plant profitability is related to the financial structure of the investment to build and run the PV system. Particularly, two major parameters, belonging to such a group, are the loan percentage,  $\varphi$ , *i.e.* the percentage of the investment financed through debt, and the opportunity cost of capital,  $OCC$ , adopted to discount the net cash flows. A sensitivity analysis for these two parameters belongs to the proposed analysis. The key results are in Figure 2.9.

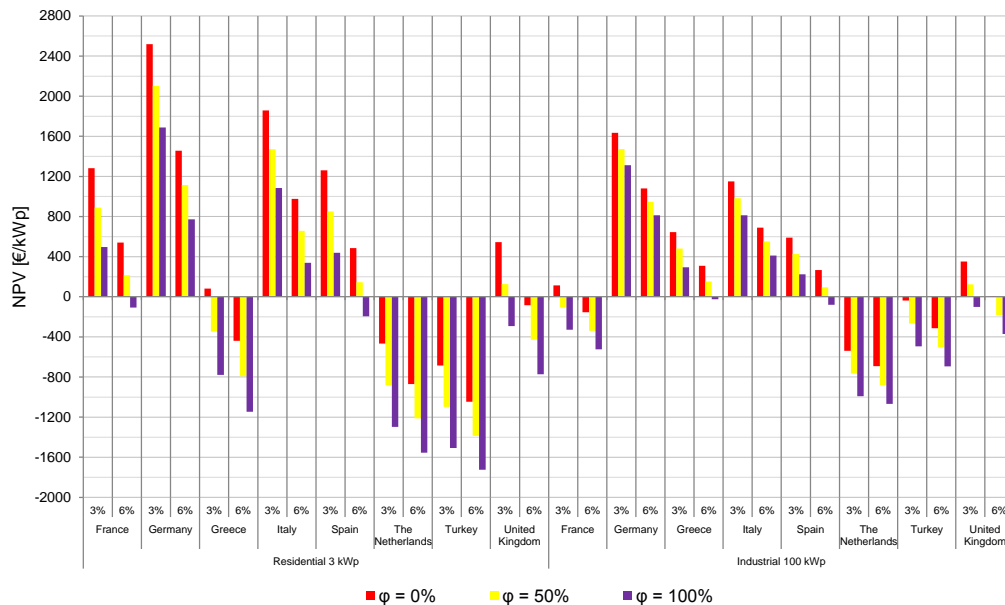


Figure 2.9 Impact of financial parameters on PV plant profitability ( $c_{module}$  according to Eq.2.7,  $H_{1,y} = 1400 \text{ kWh/m}^2 \cdot \text{year}$ ,  $r = 4\%$ ,  $\chi_{sold} = 50\%$ )

A negative correlation between  $\varphi$ ,  $OCC$  and the  $NPV$  exist. The higher such parameters, the lower the  $NPV$  is. This trend is experienced for all countries, plant sizes and installation features so that, a relevant conclusion is the independence of the financial structure of the investment from the country peculiarities and plant features, *i.e.* total equity investments and low values of the opportunity cost of capital are, always, preferable. For some scenarios, *e.g.* United Kingdom, the increase of the  $OCC$  from 3% to 6% generates the switch from positive to negative values of the  $NPV$ . Furthermore, the  $PB$  is, also, affected by the financial structure of the investment. Focusing on the convenient scenarios, only,  $\varphi = 0\%$  configurations present an average  $PB$  of 9.3 years for residential plants and 7.7 years for industrial plants, while for no private equity

financed investments the  $PB$  rises to 13.8 years for residential installations and 11.0 years for industrial plants. Furthermore, given the same investment financial structure, the lower  $PB$  values for industrial plants toward residential installations are due to the lower initial investment (see previous Figure 2.5) and the fiscal benefit introduced by the plant amortization during the first years of the plant lifetime, *i.e.*  $C_j^T$  is low due to the high values of the amortization rate  $A$ .

Furthermore, the impact on the  $NPV$  of the cell technologies, *i.e.* a-Si vs. c-Si, and module manufacturers, *i.e.* EU vs. extra EU, is, also, investigated. The results proposed in the previous *sub-Paragraphs* refer to a-Si cells produced by extra EU manufacturers, *i.e.* Equation 2.7. Considering the other alternatives, *i.e.* Equations 2.4-2.6, the costs generally rise of an approximately constant value generating a consequent  $NPV$  decrease between 200 and 400€/kWp, while the differentials among the scenarios do not significantly change. At last, the gap between rooftop, *i.e.* integrated, and ground PV plants, *i.e.* non-integrated, is positive. The land purchase costs and the lower support offered by national schemes to non-integrated systems generate worse performances for the last plant group. Several non-integrated scenarios are not convenient at all, while, if  $NPV > 0$ , the average gap between the two installation configurations is close to 25.9%.

### 2.1.6 Conclusions

This analysis investigates the technical and economic feasibility of PV plants for eight relevant countries in the EU area, *i.e.* France, Germany, Greece, Italy, Spain, The Netherlands, Turkey and United Kingdom. A multi-country and multi-parameter analysis, based on a PCM computing the  $NPV$  and  $PB$  capital budget indices, allows to assess the profitability of the investments in the PV plants under several configurations. The proposed analysis includes the main technical, geographical, economic/financial parameters, together with the current support schemes and legislations currently in force to spread the PV plants in the EU area. A large set of scenarios are studied and the results compared to highlight useful trends that can drive future investments in the PV sector. For all countries, the results, referred to the year 2012, point out the key role still played by the incentive strategies to support the investments in the PV plants for the reference year. Particularly, the German, Italian and Spanish scenarios are the most favourable, outperforming all the other countries for the most of the investigated plant sizes and installation features. On the contrary, Turkey presents weak support conditions, while The Netherlands recently cuts off all the incentives, so that, for several of their scenarios, the  $NPV$  is negative. Considering no-incentive scenarios, the role of energy self-consumption is relevant due to the gap between the cost of energy purchased from the grid and the price of energy sold to the grid. Positive  $NPV$ s are obtained for high level of self-consumption rates for residential installations, while the lower electricity cost in the industrial case make the investment less profitable.

The PV plant cost structure forces relevant investments and cash outflows in the early years of the plant lifetime, *i.e.* the 75÷80% of the full outflow, while the revenues are,

substantially, uniformly distributed through the years. National incentives and tax breaks, provided by country legislations, allow to partially compensating such a misalignment between positive and negative flows, contributing to the reduction of the *PB* and the increase of the plant economic feasibility. Furthermore, results highlight a direct dependence of the plant profitability on the plant size, while negative correlations are experienced considering low equity financed investments and high opportunity costs of capital. Finally, the environmental conditions and, particularly, the country average irradiation level, should fit to the economic irradiation level, *i.e.* the minimum value of the solar irradiation making the *NPV* positive. Results highlight an excellent fit for the French, German, Greek, Italian and Spanish areas, while criticalities occur in The Netherlands and United Kingdom in which gaps of 350 kWh/ m<sup>2</sup>-year and 100 kWh/ m<sup>2</sup>-year exist.

### 2.1.7 Final remarks and future research

Final remarks deal with the future perspective of the PV sector. First of all, in the 2012, the spread of the PV systems was still linked to the energy policies adopted by the national governments and institutions even if the increase of the electricity cost, associated to the energy self-consumption, the module efficiency and the parallel decrease of the PV system installation costs are leading the PV systems to the grid parity. The decreasing trend of the PV system installation costs (Figure 2.10), represents a favorable condition to ensure the future feasibility of the systems based on the solar source in the EU area (Mints, 2012; GreenTechMedia, 2012).

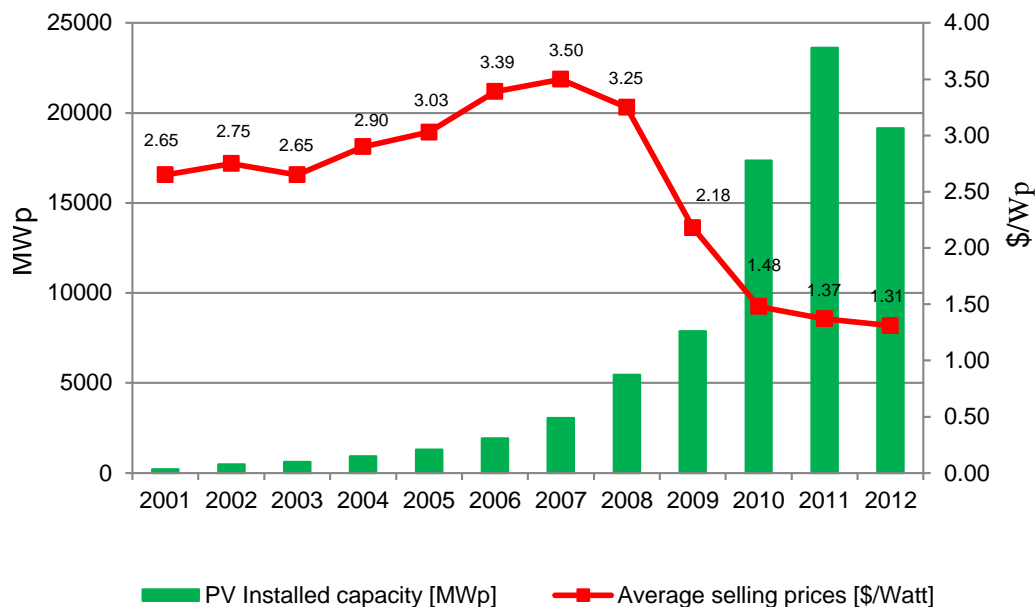


Figure 2.10 PV module cost trend from 2001 to 2012 (Mints, 2012)

Among the obtained results, the self-consumption of the produced energy plays a crucial role in the economic viability of PV plants and, in particular, after the partial or total cut of incentives and uncertainties related to supporting policies within the European context. In this case the grid parity concept is extended to a comparison of PV energy generation costs toward the grid electricity tariff. Chiaroni *et al.* (2014) deeply evaluates the role of



energy self-consumption for the PV plant profitability in a mature market characterised by the absence of public policy incentives (Italy), after four year of uncapped and uncontrolled FiT (Antonelli & Desideri, 2014), concluding that an increase in self-consumption share is a key strategy for the future of PV in mature and developed market without supporting policies, *i.e.* the Italian and more in general the European market.

In this context, the study of the energy demand profile of a specific user and the adoption of battery energy storage (BES) systems are identified as effective strategies to increase the energy self-consumption contribution. Such aspects have led to the analysis presented in the *Chapter 4* about the development of an analytic model for the techno-economic design of a grid connected hybrid energy system, integrating a PV plant and a BES system (PV-BES hybrid energy system). The model takes into account the hourly energy demand profile with the aim to study the role of self-consumption and to evaluate the economic competitiveness of BES system integrated in a PV plant.

Further research deals also with the application of the proposed analysis to other geographical areas, *e.g.* the Far East and the African region, presenting different features, constraints and local conditions. The continuous update of the parameters included in both the PCM and the multi-country and multi-parameter analysis, with particular reference to the constant monitoring of the national support schemes and the electricity market prices and conditions, is, also, of interest to study new scenarios, perspectives and opportunities of evolution for the PV renewable energy sector.

## References

- Al-Salaymeh, A., Al-Hamamre, Z., Sharaf, F., Abdelkader, M.R., 2010. Technical and economical assessment of the utilization of photovoltaic systems in residential buildings: The case of Jordan. *Energy Convers. Manag.* 51, 1719–1726.
- Antonelli, M., Desideri, U., 2014. The doping effect of Italian feed-in tariffs on the PV market. *Energy Policy* 67, 583–594.
- Audenaert, A., De Boeck, L., De Cleyn, S., Lizin, S., Adam, J.-F., 2010. An economic evaluation of photovoltaic grid connected systems (PVGCS) in Flanders for companies: A generic model. *Renew. Energy* 35, 2674–2682.
- Avril, S., Mansilla, C., Busson, M., Lemaire, T., 2012. Photovoltaic energy policy: Financial estimation and performance comparison of the public support in five representative countries. *Energy Policy* 51, 244–258.
- Barbose, G., Wiser, R., Bolinger, M., 2008. Designing PV incentive programs to promote performance: A review of current practice in the US. *Renew. Sustain. Energy Rev.* 12, 960–998.
- Becerra-López, H.R., Golding, P., 2008. Multi-objective optimization for capacity expansion of regional power-generation systems: Case study of far west Texas. *Energy Convers. Manag.* 49, 1433–1445.
- Bernal-Agustín, J.L., Dufo-López, R., 2006. Economical and environmental analysis of grid connected photovoltaic systems in Spain. *Renew. Energy* 31, 1107–1128.
- Bortolini, M., Gamberi, M., Graziani, A., Mora, C., Regattieri, A., 2013. Multi-parameter analysis for the technical and economic assessment of photovoltaic systems in the main European Union countries. *Energy Convers. Manag.* 74, 117–128.
- Branker, K., Pathak, M.J.M., Pearce, J.M., 2011. A review of solar photovoltaic levelized cost of electricity. *Renew. Sustain. Energy Rev.* 15, 4470–4482.
- Brecl, K., Topič, M., 2011. Self-shading losses of fixed free-standing PV arrays. *Renew. Energy* 36, 3211–3216.
- Campoccia, A., Dusonchet, L., Telaretti, E., Zizzo, G., 2007. Feed-in tariffs for grid-connected PV systems: The situation in the European community, in: *Proceedings of 2007 IEEE Lausanne Powertech*. pp. 1981–1986.

- Campoccia, A., Dusonchet, L., Telaretti, E., Zizzo, G., 2009. Comparative analysis of different supporting measures for the production of electrical energy by solar PV and Wind systems: Four representative European Cases. *Sol. Energy* 83, 287–297.
- Chiaroni, D., Chiesa, V., Colasanti, L., Cucchiella, F., D'Adamo, I., Frattini, F., 2014. Evaluating solar energy profitability: A focus on the role of self-consumption. *Energy Convers. Manag.* 88, 317–331.
- Danchev, S., Maniatis, G., Tsakanikas, A., 2010. Returns on investment in electricity producing photovoltaic systems under de-escalating feed-in tariffs: The case of Greece. *Renew. Sustain. Energy Rev.* 14, 500–505.
- Di Dio, V., Favuzza, S., La Caseia, D., Miceli, R., 2007. Economical incentives and systems of certification for the production of electrical energy from renewable energy resources, in: 2007 International Conference on Clean Electrical Power, ICCEP '07, 277–282.
- Diarra, D., Akuffo, F.O., 2002. Solar photovoltaic in Mali: potential and constraints. *Energy Convers. Manag.* 43, 151–163.
- Dinçer, F., 2011. Overview of the photovoltaic technology status and perspective in Turkey. *Renew. Sustain. Energy Rev.* 15, 3768–3779.
- Dusonchet, L., Telaretti, E., 2010a. Economic analysis of different supporting policies for the production of electrical energy by solar photovoltaics in western European Union countries. *Energy Policy* 38, 3297–3308.
- Dusonchet, L., Telaretti, E., 2010b. Economic analysis of different supporting policies for the production of electrical energy by solar photovoltaics in eastern European Union countries. *Energy Policy* 38, 4011–4020.
- EurObserv'ER Systèmes solaire, 2011. Photovoltaic energy barometer 2011. *Le J. des énergies renouvelables* 202, 144–171.
- EurObserv'ER Systèmes solaires, 2009. Photovoltaic energy barometer 2009. *Le J. des énergies renouvelables* 190, 72–102.
- EurObserv'ER Systèmes solaires, 2010. Photovoltaic energy barometer 2010. *Le J. des énergies renouvelables* 196, 128–160.
- EurObserv'ER Systèmes solaires, 2012. Photovoltaic energy barometer 2012. *Le J. des énergies renouvelables* 7, 108–131.

- European Commission, 2011a. Quarterly Report on Electricity Market, DG Energy Vol. 4, Issue 2: April 2011 – June 2011.
- European Commission, 2011b. Quarterly Report on Electricity Market, DG Energy Vol. 4, Issue 3: July 2011 – September 2011.
- Feibel, B.J., 2003. Investment Performance Measurement. Wiley Interscience, New York.
- Fernandez-Infantes, A., Contreras, J., Bernal-Agustín, J.L., 2006. Design of grid connected PV system considering electrical, economical and environmental aspect: a practical case. *Renew. Energy* 31, 2042–2062.
- Focacci, A., 2009. Residential plants investment appraisal subsequent to the new supporting photovoltaic economic mechanism in Italy. *Renew. Sustain. Energy Rev.* 13, 2710–2715.
- Fthenakis, V., Mason, J.E., Zweibel, K., 2009. The technical, geographical, and economic feasibility for solar energy to supply the energy needs of the US. *Energy Policy* 37, 387–399.
- Ghoneim, A. a., Al-Hasan, A.Y., Abdullah, A.H., 2002. Economic analysis of photovoltaic-powered solar domestic hot water systems in Kuwait. *Renew. Energy* 25, 81–100.
- Hammond, G.P., Harajli, H. a., Jones, C.I., Winnett, A.B., 2012. Whole systems appraisal of a UK Building Integrated Photovoltaic (BIPV) system: Energy, environmental, and economic evaluations. *Energy Policy* 40, 219–230.
- Harvey, L.D.D., 1996. Solar-hydrogen electricity generation and global CO<sub>2</sub> emission reduction. *Int. J. Hydrogen Energy* 21, 583–595.
- Hernández, J.C., Medina, A., Jurado, F., 2008. Impact comparison of PV system integration into rural and urban feeders. *Energy Convers. Manag.* 49, 1747–1765.
- International Energy Agency (IEA), 2010. Key world energy statistics (2010).
- International Standard IEC 61724:1998, Photovoltaic system performance monitoring - Guidelines for measurement, data exchange and analysis, 1998.
- Jäger-Waldau, A., Szabó, M., Scarlat, N., Monforti-Ferrario, F., 2011. Renewable electricity in Europe. *Renew. Sustain. Energy Rev.* 15, 3703–3716.
- JRC European Commission, 2011. Scientific and Technical Reports: PV Status Report 2011.

- Market, S., 2012. Bumpy ride for PV Paula Mints looks at the outlook for.
- Ministry of Economic Affairs, Agriculture and Innovation, 2011. Energy report 2011.
- Mints, P., 2012. PV in prices – the hard sell. *Renew. energy Focus* 13, 34–36.
- Mitscher, M., Rüther, R., 2012. Economic performance and policies for grid-connected residential solar photovoltaic systems in Brazil. *Energy Policy* 49, 688–694.
- Nässén, J., Evertsson, J., Andersson, B. a., 2002. Distributed power generation versus grid extension: an assessment of solar photovoltaics for rural electrification in Northern Ghana. *Prog. Photovoltaics Res. Appl.* 10, 495–510.
- Quintana, M.A, King, D.L., McMahon, T.J., Osterwald, C.R., 2002. Commonly observed degradation in field-aged photovoltaic modules, in: *Proceedings 29th IEEE Photovoltaic Specialists Conference, New Orleans, Louisiana.* pp. 1436 – 1439.
- Reiche, D., Bechberger, M., 2004. Policy differences in the promotion of renewable energies in the EU member states. *Energy Policy* 32, 843–849.
- Reis, A.M. , Coleman, N.T., Marshall, M.W., Lehman, P.A., Chamberlin, C.E., 2002. Comparison of PV module performance before and after 11-years of field exposure, in: *Proceedings 29th IEEE Photovoltaic Specialists Conference, New Orleans, Louisiana,* 1432–1435.
- Rowlands, I.H., 2005. Envisaging feed-in tariffs for solar photovoltaic electricity: European lessons for Canada. *Renew. Sustain. Energy Rev.* 9, 51–68.
- Šály, V., Ružinský, M., Baratka, S., 2006. Photovoltaics in Slovakia—status and conditions for development within integrating Europe. *Renew. Energy* 31, 865–875.
- Šúri, M., Huld, T.A., Dunlop, E.D., Ossenbrink, H.A., 2007. Potential of solar electricity generation in the European Union member states and candidate countries. *Sol. Energy* 81, 1295–1305.
- USAID Hydropower Investment Promotion Project (USAID-HIPP), 2011. *Turkish Power Market Monthly Report (2011).*
- Zhang, D., Chai, Q., Zhang, X., He, J., Yue, L., Dong, X., Wu, S., 2012. Economical assessment of large-scale photovoltaic power development in China. *Energy* 40, 370–375.

### *Legislations*

French legislation, Arrêté du 4 mars 2011 fixant les conditions d'achat de l'électricité produite par les installations utilisant l'énergie radiative du soleil telles que visées au 3° de l'article 2 du décret 2000-1196 du 6 décembre 2000.

German Government 2009, EEG Gesetz für den Vorrang Erneuerbarer Energien (Erneuerbare-Energien-Gesetz), 2009 (last amended on 01/01/12).

Greece Legislation, Renewable Energy Legislation, Law 3581/2010 amending the law 3468/2006, Generation of Electricity using Renewable Energy Sources and High-Efficiency Cogeneration of Electricity and Heat and Miscellaneous Provisions.

Italian Legislation, Incentivation of electricity production from solar photovoltaic plants, Decreto Ministeriale 05/05/2011.

Italian Legislation, Incentivation of electricity production from solar photovoltaic plants, Decreto Ministeriale 05/07/2012.

Spanish legislation, Real Decreto 1565/2010, de 19 de noviembre, por el que se regulan y modifican determinados aspectos relativos a la actividad de producción de energía eléctrica en régimen especial, R.D. 1565 19/11/2010.

Spanish legislation, C 14/2010, de 23 de diciembre, por el que se establecen medidas urgentes para la corrección del déficit tarifario del sector eléctrico, R.D. 14 23/12/2010.

Turkish legislation, Law on utilization of renewable energy sources for the purpose of generating electrical energy, Law n. 5436, 10/05/2005, Amended by Law 6094, 29/12/2010.

Turkish legislation, Law 6094/2010 amending the Law 5436/2005, Law on utilization of renewable energy sources for the purpose of generating electrical energy.

### **Web - References**

APX Endex (AE), United Kingdom and The Netherlands Electricity market price, <ftp://ftp.apxgroup.com/>, Last access: August, 2012.

Europe's Energy Portal, 2011. Electricity prices for EU households and industrial consumers on November 2011, <http://www.energy.eu/>, Last access: August, 2012.

European Commission, Eurostat Annual Inflation Rate 2011. <http://epp.eurostat.ec.europa.eu/>. Last access: August, 2012.

European Commission, Eurostat Energy Price Statistics 2011. Half-yearly electricity and gas prices, first half of 2011, <http://epp.eurostat.ec.europa.eu/>, Last access: August, 2012.

European Commission, Taxation and Customs Union 2012. Taxation trends in the European Union, <http://ec.europa.eu/>, Last access: August, 2012.

Gestore Servizi Energetici (GSE), <http://www.gse.it/it/Pages/default.aspx>, Last access: August, 2012.

Green Tech Media, PV technology, Production and cost outlook: 2012-2016, <http://www.greentechmedia.com>, Last access: December, 2012.

Hellenic Association of Photovoltaic Companies (HELAPCO), <http://www.helapco.gr/>, Last access: August, 2012.

Legal sources on renewable energy (Res-Legal), <http://www.res-legal.de/>, Last access: August, 2012.

Mercato Elettrico, 2012. Comparison of European exchanges, <http://www.mercatoelettrico.org/>, Last access: August, 2012.

Photovoltaic Geographical Information System (PVGIS), <http://re.jrc.ec.europa.eu/pvgis/index.htm>, Last access: August, 2012.

Worldwidetax, 2012. Turkey V.A.T. and Other Taxes, <http://www.worldwidetax.com/>, Last access: August, 2012.

## 2.2 Techno-Economic design of small wind turbines (SWTs)

Wind energy represents an effective RES due to its low carbon footprint and its high level of producible power. Nowadays, wind power plants reach a relative maturity due to economic scale factors, while SWT still demonstrate uncertainties especially from the profitability point of view. The recent literature presents a wide set of studies about the economic feasibility of SWTs but most of them are, generally, oriented to a specific country or geographical area. In this context, this *Paragraph* presents a complete technical and economic analysis, based on Bortolini *et al.* (2014), of SWTs extended to five of the major EU countries, *i.e.* France, Germany, Italy, Spain and The Netherlands, representing at the end of 2012, approximately, the 70% of the total installed EU wind power, *i.e.* 106GW, (see Figure 2.11). The analysis considers ten commercial turbines, including eight horizontal axis wind turbines (HAWT, with sizes of 2.5, 6, 10, 20, 30, 50, 80 and 200 kWp) and two vertical axis wind turbines (VAWT, with sizes of 3 and 4 kWp).

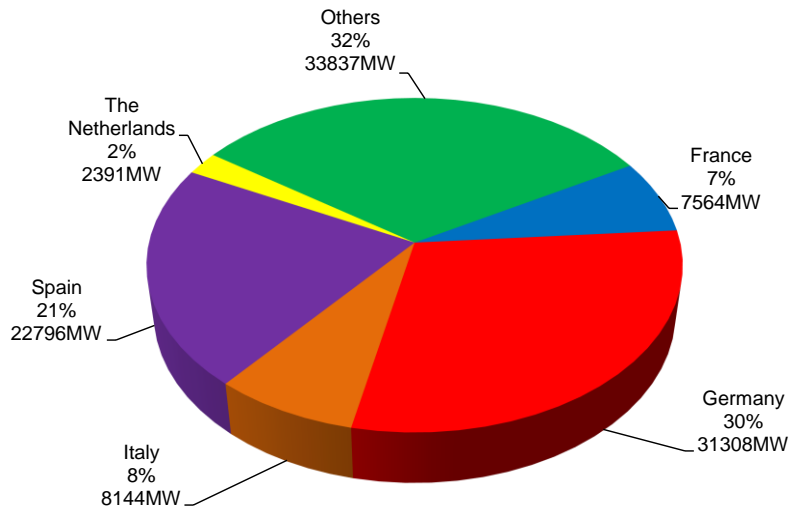


Figure 2.11 Wind power installed in the EU27 area at the end of 2012 (EWEA, 2012)

The aim is to assess the profitability of such systems studying the anemological, technical and financial conditions making these installations cost-effective. To meet this purpose, an economic performance parametric model is developed to point out the profitability conditions of SWTs. The parameters included in the analysis belong to four main categories: technical (power curve, system maintenance, *etc.*), economic/financial (system cost, loan cost, *etc.*), geographical (anemological conditions) parameters and country peculiarities (incentive scheme, inflation, tax, and grid energy price). Moreover, the adopted approach is tailored to each considered country. According to such purposes, the next *sub-Paragraph 2.2.1* presents an overview of the recent literature state of the art, while the *sub-Paragraph 2.2.2* reports the technical data of the analyzed SWTs. *Sub-Paragraph 2.2.3* introduces the developed economic performance model, while the next *sub-Paragraphs 2.2.4 and 2.2.5* describe, in detail, the costs and incomes of SWT systems and the incentive/taxation scenario for the year 2012 for the different EU countries. The consequent results are summarized in *sub-Paragraph 2.2.6* highlighting



the parameters that mainly affect the economic profitability of a SWT. Finally, the last *sub-Paragraphs 2.2.7 and 2.2.8* ends the paper, drawing final remarks about the analysis and providing suggestions for further research.

### 2.2.1 Literature review

The attention of wind power has significantly increased since the early 70s, after the first oil price shock. Among the RESs, wind already achieved its maturity for the energy market and met the first relevant growth, worldwide, in the 90s (Yue *et al.*, 2001; EWEA, 2012). In those years, several countries adopted significant incentive legislations with the aim of stimulating and promoting the installation and use of wind power systems connected to the national electric grid. Actually, there are several countries, like The Netherlands, where the energy market and wind power generation are so developed that the old incentive policies are mitigated or even abrogated (WWEA, 2009; WWEA, 2010) showing that wind power plants can compete against the traditional fossil fuels. Nevertheless, relevant difficulties remain making difficult a widespread diffusion of this technology, *e.g.* the availability and choice of the most suitable installation sites and the system power sizes. An effective evaluation of the environmental impact for these power plants is presented in the literature (Wizelius, 2007; Valentine, 2010). Furthermore, as the efficiencies and performances of new WTs are continuously rising, the choice of a suitable and worthwhile location becomes essential in terms of wind quality (Lu *et al.*, 2009; Walters & Walsh, 2011). Krohn *et al.* (2009) identify three crucial characteristics affecting the wind quality: the overall wind speed, the consistency of the wind speed and the consistency of the wind speed direction. Thus, feasibility studies based on the “average” speed for a given area should be improved introducing a wind speed probability distribution function, *e.g.* Weibull statistic distribution, to properly model wind fluctuations. About SWTs, several contributions are developed to evaluate their technical performances and applicability to the consumer market. In 2008, the U.S. Department of Energy’s (DOE) National Renewable Energy Laboratory (NREL) began testing SWTs through an independent project. Four SWTs (from 1.2kW to 11kW) are selected for testing at the NREL’s National Wind Technology Center (Bowen *et al.*, 2009). In the same year, a new methodology to select a wind turbine generator, including both performance and economic considerations, was presented (Doddamani & Jangamshetti, 2008). Weibull probability density function is used to analyze the wind data and to predict the SWT performances. Furthermore, Šimi *et al.* (2009) present a paper focused on SWTs potential estimation. They study seven SWTs with rated power from 3.0kW to 3.5kW using an experimental wind speed dataset, while Elmore & Gallagher (2009) propose an approach to predict the wind power performances using regional climate dataset. Moreover an analysis of SWTs with less than 10kW of power for the installation in Croatia is presented in Ref. (Simic *et al.*, 2013) from a techno-economical point of view. From an economic point of view, SWTs require significant initial investments in relation to their size and are less profitable than large turbine plants because all system components

have decreasing costs in relation to their size (Valentine, 2011). For this reason several surveys on the economic feasibility of SWTs are drawn up to provide a reference for the decision making phase (Villanueva & Feijóo, 2010; Carta, Ramírez, & Velázquez, 2009; Ardente *et al.*, 2008). In this direction, a wide set of economic studies show the profitability of SWTs in specific geographical areas. Mostafaeipour *et al.* (2011) evaluate the economic profitability of SWTs up to 10kW in Iran, showing that these systems are, generally, feasible in such area, while Stockton studies the feasibility of an “opportunity-scale” wind power plant in the Hawaii islands (Stockton, 2004). Kelleher & Ringwood (2009) and Li *et al.* (2012) consider the economic viability of micro WT’s for domestic applications in Ireland concluding that such systems look promising when they are installed in locations with relatively high wind speed, *e.g.* higher than 6m/s. This circumstance, together with the long payback period of the investment, constitutes a significant barrier to the diffusion of domestic micro wind applications. Furthermore, an interesting study tailored on the Barbados Islands is presented by Bishop and Amaratunga (2008). They propose a 10MW distributed wind energy scheme using micro wind turbines with horizontal and vertical axis configurations. The study illustrates the great potential of SWTs to be competitive with conventional wind power plants. Walters *et al.* (2011) and Peacock *et al.* (2008) investigate the diffusion of micro-scale WT’s, from 0.4kW to 2.5kW, in the UK and Mithraratne (2009) presents roof-top WT’s like a feasible system in New Zealand to supply a fraction of the power needed by a domestic consumer.

### 2.2.2 Analyzed SWTs

Ten SWT models, coming from both European and extra- European suppliers, are considered in this study. The following Table 2.7 collects their main technical data obtained through a market survey, while Table 2.8 reports the rated power curves, *i.e.* the power rate for increasing values of the wind speed.

Table 2.7 SWT Technical data (Market survey)

Model	Producer	Type	Blades	Rated power [kWp]	Diameter [m]	Height [m]	Turbine weight [kg]	Structure weight [kg]	Cut in speed [m/s]	Rated speed [m/s]	Cut out speed [m/s]	Swept area [m <sup>2</sup> ]	Operating life [Years]
Are110	Cascade Wind co. (U.S.A.)	HAWT	3	2.5	3.60	13.0	143	1,408	2.50	11.0	15.5	10.10	20
Skyline sl-30	En-Eco (Italy)	VAWT	3	3	3.00	8.0	85	360	3.00	12.0	18.0	9.00	20
Uge-4k	Urban Green Energy (U.K.)	VAWT	3	4	2.75	7.5	200	360	3.00	12.0	25.0	5.95	20
Ampair 6000 x 5,5	Ampair (U.K.)	HAWT	3	6	5.50	15.0	190	2,051	3.50	15.0	17.0	23.74	20
Fortis Alize	Fortis (NL)	HAWT	3	10	7.00	30.0	310	2,815	4.00	12.0	15.0	38.50	20
Jacobs 31-20	Jacobs Wind Systems (U.S.A.)	HAWT	3	20	9.50	36.0	1133	3,860	3.50	11.6	17.8	70.88	20
H30k	Ge shandong (China)	HAWT	3	30	12.00	18.0	2000	3,500	3.00	12.0	20.0	113.10	20
Redriven 50kw	Redriven (Canada)	HAWT	3	50	14.30	36.0	2835	3,378	2.00	11.0	18.0	624.42	20
Wes18	Windenergy Solutions (NL)	HAWT	2	80	18.00	30.0	3986	8,200	2.70	12.5	25.0	254.00	20
WES30	Windenergy Solutions (NL)	HAWT	2	200	30.00	40.0	10330	18,850	2.70	12.5	25.0	707.00	20

Table 2.8 SWT power curves derived from wind turbine datasheets

Wind speed [m/s]	Power curve [kW]									
	Are110	Skyline sl-30	Uge-4k	Ampair 6000 x 5.5	Fortis Alize	Jacobs 31-20	Hz30k	Redriven 50kw	Wes18	WES30
1.00	-	-	-	-	-	-	-	-	-	-
2.00	-	-	-	-	-	-	-	-	-	-
3.00	0.15	-	-	-	-	-	-	1.50	-	-
4.00	0.15	0.10	0.15	0.25	0.50	1.00	1.00	3.00	2.90	4.40
5.00	0.30	0.20	0.30	0.60	0.50	1.00	2.50	5.00	6.00	14.90
6.00	0.50	0.30	0.50	1.00	1.00	2.00	4.00	7.50	11.00	29.30
7.00	0.70	0.50	0.65	1.50	1.90	3.80	6.00	11.00	17.70	56.30
8.00	1.20	0.80	0.90	2.30	2.80	5.80	9.00	16.00	27.70	77.20
9.00	1.60	1.10	1.25	3.30	4.00	8.00	13.00	23.00	39.20	116.00
10.00	2.00	1.50	1.75	4.50	5.20	11.00	17.50	32.00	51.40	145.00
11.00	2.30	2.00	2.75	6.00	6.80	14.50	23.00	40.00	63.80	179.00
12.00	2.50	2.50	3.65	6.00	8.50	18.00	31.00	52.00	74.20	200.00
13.00	2.50	3.25	4.15	6.00	9.80	20.00	34.00	55.00	79.90	200.00
14.00	2.50	3.60	4.30	6.00	10.00	20.00	29.00	55.00	82.20	200.00
15.00	2.30	3.60	4.25	6.00	10.00	20.00	30.00	55.00	83.00	200.00
16.00	2.30	3.60	4.20	6.00	10.00	20.00	30.00	55.00	83.00	200.00
17.00	-	3.60	4.15	6.00	4.00	20.00	30.00	55.00	83.00	200.00
18.00	-	3.60	4.13	6.00	3.20	20.00	30.00	55.00	83.00	200.00
19.00	-	-	4.10	6.00	3.30	-	30.00	-	83.00	200.00
20.00	-	-	4.10	6.00	3.40	-	30.00	-	83.00	200.00
21.00	-	-	4.10	6.00	3.50	-	30.00	-	83.00	200.00
22.00	-	-	4.10	6.00	3.60	-	-	-	83.00	200.00
23.00	-	-	4.10	6.00	4.00	-	-	-	83.00	200.00
24.00	-	-	4.10	-	4.20	-	-	-	83.00	200.00
25.00	-	-	4.10	-	4.60	-	-	-	83.00	200.00
26.00	-	-	-	-	-	-	-	-	-	-
27.00	-	-	-	-	-	-	-	-	-	-

### 2.2.3 Economic performance parametric model

An economic analytic model is developed and applied to study the economic feasibility, through a multi-scenario analysis, of SWTs in some of the main European Union countries. The model, which flow chart is in Figure 2.12, takes into account technical, economic/financial, geographic parameters and country peculiarities, e.g. incentives and supporting policies, evaluating the SWT turnkey costs, annual costs/revenues and calculating common economic evaluation indices, such as *NPV* and *PB*, for each considered scenario.

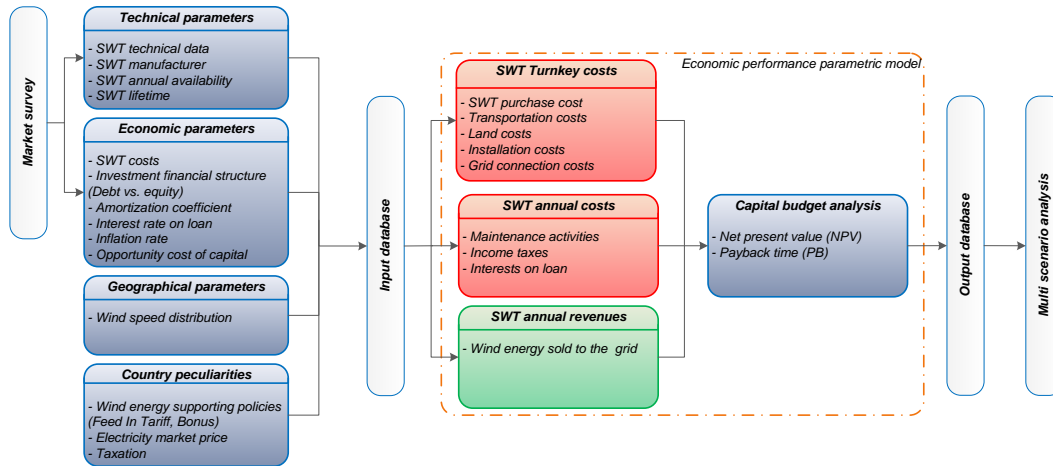


Figure 2.12 Flow chart of the proposed economic performance parametric model

The *NPV* is determined as follows:

$$NPV = -C_0 + \sum_{j=1}^n \frac{R_j - C_j}{(1+OCC)^j} \quad (2.18)$$

Where:

- $C_0$  is the initial investment to install the SWT [€]
- $R_j$  and  $C_j$  represent, respectively, the cash inflows (incomes) and outflows for the generic  $j$ th year,  $j = 1, \dots, n$  [€/year]
- $OCC$  is the opportunity cost of capital [%]
- $n$  is the expected system lifetime [years]

The initial investment,  $C_0$ , generally represents the 70–80% of the total cost for a wind energy project (Dunlop, 2006; Bolinger & Wiser, 2009), and consequently its accurate estimation is crucial to make the whole analysis effective. The incomes,  $R_j$ , derived from the installation of a SWT, are function of the wind energy production ratio, used either for local consumption or for sale to the electric grid. The term  $C_j$  represents the operative annual outflows and it is due to three relevant drivers: Operation & Maintenance, interests paid for financing the investment and the tax level.

#### 2.2.4 SWT installation investment and operative outflows

The investment for SWT installation,  $C_0$ , is expressed as:

$$C_0 = C_P + C_T + C_I \quad (2.19)$$

Where:

- $C_P$  is the purchase cost [€]
- $C_T$  is the transportation cost [€]
- $C_I$  is the installation cost [€]

The purchase cost,  $C_p$ , for each considered SWT, is determined through a market survey considering several producers worldwide located. The survey results are summarized in the following Figure 2.13 reporting the price for each turbine expressed in €/kWp. The SWTs are ordered according to the turbine size. The graph shows that the purchasing costs have not an evident connection to the plant sizes due to the producer peculiarities, e.g. producer country, producer cost structure, market policies, etc.

The transportation cost,  $C_T$ , is quantified assuming that all the turbines are shipped from the suppliers to each considered installation country. Such a cost is evaluated considering that the total transportation cost of a turbine is due to two different types of trips: a transport by sea to reach the EU mainland (necessary only for extra-EU turbine suppliers) and a land transport by truck. The cost of the transport by sea is assumed independent from the destination country because all the five EU countries (France, Italy, Germany, Spain and The Netherlands) are quite close to each other if compared to the extra-EU departure ports (USA, Canada and China). This cost ranges from 1700€ to 2700€ as a function of the SWT model. With regard to the land transport by truck, the following Table 2.9 reports the average fix and variable costs for different types of vehicle.

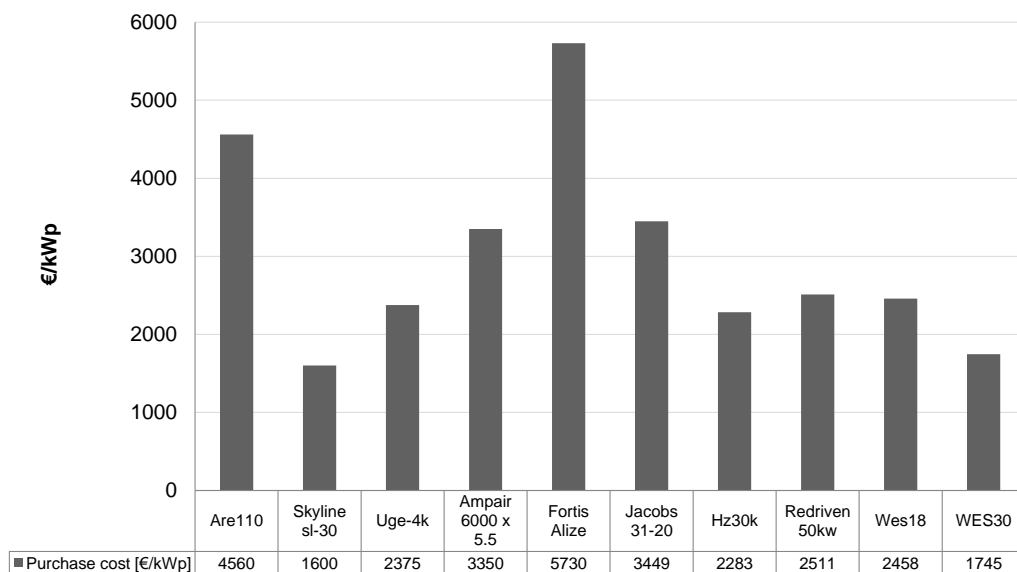


Figure 2.13 Purchase cost (Price list ex works) referred to each turbine model

Table 2.9 Cost for different truck models

Vehicle type	Fixed carry cost [€]	Variable carry cost [€/km]
Truck	90	0.95
Articulated-truck	105	1.05
B-train truck	120	1.15

For each SWT, the following Table 2.10 proposes the average values of the transportation costs for the five countries. For the sake of brevity, details for each country are omitted even if they are included to the analytic model to represent the country

peculiarities. Nevertheless, small variations among countries occur. The range of oscillation around the average values of Table 2.10 is  $\pm 3\%$  for all countries.

Table 2.10 Average costs for SWT transportation to EU countries

Are110	Skyline sl-30	Uge-4k	Ampair 6000 x 5.5	Fortis Alize	Jacobs 31-20	Hz30k	Redriven 50kw	Wes18	WES30
€3,331	€1,331	€1,619	1,619€	€947	€3,352	€2,489	€3,189	€1,086	€4,136

The installation cost,  $C_I$ , is probably the most critic parameter to be evaluated. It should consider five relevant factors:

- Building material cost, *i.e.* expenditures to purchase the materials required for the turbine installation as well as to lay the foundation. All these elements are correlated to the power plant weight and height and to the rotor diameter
- Installation labor cost, *i.e.* worker salary, crane rental, purchase of the equipment used by the installation team
- Engineering cost, *i.e.* expenditures for the preliminary and executive projects, feasibility study and engineering
- Land purchase cost, *i.e.* cost for the required ground surface. Considering the tower height, a circular area of the same radius is assumed necessary
- Grid connection cost, *i.e.* cables, power unit and control system, including license fees

These factors are quite different for each turbine. Table 2.11 shows such costs expressed in [€/kWp]. Data are from a market survey focused on the Italian context and then extended to the other countries. Results match with the installation costs per kWp proposed by the literature. Considering the aggregate total costs, the presence of economic scale factors is evident: the smallest SWT, *i.e.* Are110 (2.5kWp), has a total installation cost per kWp about 10 times higher than the biggest SWT, *i.e.* Wes30 (200kW).

Table 2.11 Installation costs by factor

Model	Turbine size [kW]	Building material [€/kWp]	Labor [€/kWp]	Engineering [€/kWp]	Land purchase [€/kWp]	Grid connection [€/kWp]	Total [€/kWp]	Total [€]
Are110	2.5	1,040	288	133	832	389	2,682	6,704
Skyline sl-30	3	676	92	92	286	324	1,618	4,854
Uge-4k	4	507	69	69	187	243	1,186	4,744
Ampair 6000 x 5.5	6	453	57	57	499	162	1,291	7,748
Fortis Alize	10	488	70	70	1,066	97	1,937	19,373
Jacobs 31-20	20	244	39	39	812	97	1,336	26,718
Hz30k	30	155	21	21	182	67	481	14,440
Redriven 50kw	50	264	32	32	354	40	748	37,386
Wes18	80	172	21	21	181	25	435	34,828
WES30	200	91	11	11	144	10	270	54,070

The operative outflow for each  $j$ th year of the SWT lifetime,  $C_j$ , is determined as:

$$C_j = C_{O\&M_j} + C_{D_j} + C_{T_j} \quad (2.20)$$

Where:

- $C_{O\&M_j}$  is the annual operation and maintenance outflow [€/year]
- $C_{D_j}$  is the outflow due to interest paid for financing the initial investment, at year 0 ( $C_{D_j} = 0$  if the whole investment is paid through equity) [€/year]
- $C_{T_j}$  is the annual tax outflow [€/year]

According to standard literature (Pantaleo et al., 2005; Sinisuka & Nugraha, 2013), for the developed analysis,  $C_{O\&M_j}$  is assumed to be equal to the 2% of the turbine purchasing cost, while  $C_{D_j}$ , expresses the interest that each year the investors have to pay for the loan obtained to finance, entirely or partially, the investment. The following Equation 2.21 allows calculating the annual value for  $C_{D_j}$ .

$$C_{D_j} = r \cdot [\varphi \cdot C_0 - \sum_{k=1}^{k < j} (s \cdot \varphi \cdot C_0 - C_{D_k})] \quad (2.21)$$

Where:

- $r$  is the interest rate on debts, assumed constant and equal to 6%
- $\varphi$  is the percentage of  $C_0$  financed through load, i.e. financial leverage. In the analysis, two scenarios are considered:  $\varphi = 100\%$  and  $\varphi = 0\%$ . i.e. unlevered scenario
- $s$  is the amortization coefficient

The third term in Equation 2.20 is the annual tax outflow,  $C_T$ . It is evaluated adopting the Earning Before Tax (EBT) approach and considering the specific tax rates imposed to the corporate gross income in France, Germany, Italy, Spain and The Netherlands (See Table 2.12).

Table 2.12 EU tax rates on the corporate gross income (KPMG, 2011)

Country	Average tax level
France	33.33%
Germany	29.37%
Italy	31.40%
Spain	30.00%
The Netherlands	25.00%

### 2.2.5 SWT income flows

The incomes generated by the SWTs are expressed, for each  $j$ th year, as:

$$R_j = E_j \cdot P_E \quad (2.22)$$

Where:

- $E_j$  is the electricity produced in the generic  $j$ th year [kWh]
- $P_E$  is the energy sale price or the incentive price, if present, for the wind energy sold to the grid [€/kWh]

$E_j$  is computed considering the annual plant availability,  $T_j$ , expressed in [h/year], the turbine operative power curve  $P(v)$  [W] (See Table 2.8), and the wind speed probability density function  $W(v)$  for the installation region.

$$E_j = \int_0^{\infty} T_j \cdot W(v) \cdot P(v) \cdot dv \quad (2.23)$$

The function  $W(v)$ , defined accordingly to the following *Equation 2.24* represents the Weibull probability wind speed distribution and it is a frequently adopted statistic distribution to estimate the wind speed for a particular location. It relates the probability of occurrence of a specific wind speed,  $v$ , to the scale parameter,  $s$ , and the shape parameter,  $k$ .

$$W(v) = k/s \cdot (v/s)^{k-1} \cdot \exp[-(v/s)^k] \quad (2.24)$$

Where:

- $v$  is the wind speed [m/s]
- $k$  is the shape parameter [m/s]
- $s$  is the scale parameter [m/s]

These anemological factor, together with the average speed level,  $\bar{v}$ , are specific data for each wind site. The following *Equation 2.25* expresses the analytic relation between them. This Equation allows defining the wind speed distribution for a generic installation site by means of the only two of such three parameters.

$$\bar{v} = s \cdot \Gamma\left(\frac{k+1}{k}\right) \quad (2.25)$$

Where  $\Gamma(\dots)$  is the well-known Gamma function.



Adopting *Equations 2.22-2.25* the incoming flows for the generic  $j$ th year,  $R_j$ , can be determined. In particular, for each geographical area, it is necessary to know the wind distribution, *i.e.* the shape parameter and the average wind speed, the performances of the SWT and the energy price. With regard to the wind conditions, each country, usually, records the most common environmental parameters, measured by its meteorological stations. Reliable wind speed dataset are almost available and the main parameters, average wind speed,  $\bar{v}$ , and shape factor,  $k$ , are easily accessible data (see, as example, Figure 2.14, from the European Wind atlas, for the EU average wind speed).

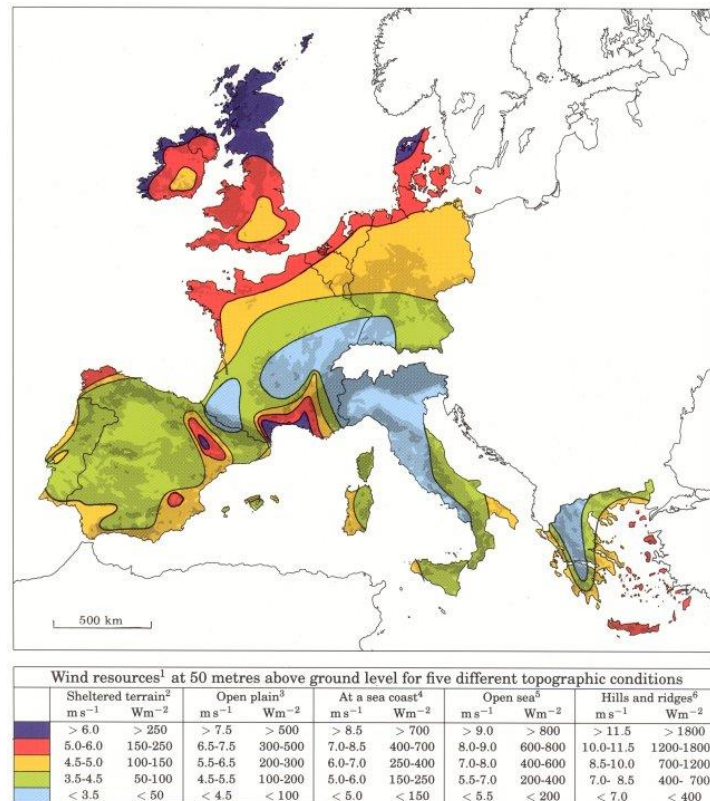


Figure 2.14 Europe Wind Atlats at 50m above ground level (Risø National Laboratory, 1989)

About the energy price, another important aspect to consider is the national legislations, which promote RESs through different supporting schemes. The following Table 2.13 summarizes, for each of the five considered countries, the incentive schemes and amounts that constitute the energy price,  $P_E$ , in *Equation 2.22*.

Table 2.13 Incentives and energy market prices for the considered EU countries (2012)

EU Country	Incentive				Electricity market		
	Legal reference	Support system	Amount [c€/kWh]	Notes	Duration [year]	Name	Price [c€/kWh]
France	French Government (2008)	FiT	8.20		15	Power next	4.35
Germany	German Government (2009)	FiT	5.02	9.2 for the first 5 years	20	EXX	5.21
Italy	Italian Government (2007)	FiT	30.00		15	GME	7.32
Spain	Spanish Government (2007)	FiT	7.91		20	OPEL	5.62
The Netherlands	Dutch Government (2008)	Bonus	6.05	Bonus added to the market price	15	APX	5.25

### 2.2.6 SWT economic analysis for the EU

The results presented in this *sub-Paragraph* are obtained considering an inflation rate of 1.5%, an opportunity cost of capital  $OCC = 4\%$ , a wind shape factor  $k = 1.3$  and a system availability of 90%.

#### 2.2.6.1 SWT installation investment distribution

The initial installation investment distribution, *i.e.* the turnkey cost, for the considered SWTs is a first outcome of the economic model analysis. The obtained values, averaged on the five considered EU countries, ranges from 7600€/kWp, for the smallest Are110 turbine, to 1700€/kWp, for the greatest Wes30 turbine. Table 2.14 presents the results, expressed in €/kWp, for each turbine model and shows a moderately evident decreasing trend with size increase, except for the Fortis Alize turbine (10kWp) that presents a high purchase cost if compared to the other plants.

Table 2.14 “Turnkey” investments

Model	Turbine size [kW]	Building material [€/kWp]	Labor [€/kWp]	Engineering [€/kWp]	Land purchase [€/kWp]	Grid connection [€/kWp]	Transportation [€/kWp]	Total [€/kWp]	Total [€]
Are110	2.5	1,040	288	133	832	389	1,332	3,648	7,662
Skyline	3	676	92	92	286	324	444	1,280	3,342
Uge-4k	4	507	69	69	187	243	405	1,900	3,491
Ampair	6	453	57	57	499	162	270	2,680	4,241
Fortis Alize	10	488	70	70	1,066	97	95	4,584	6,616
Jacobs	20	244	39	39	812	97	168	2,759	4,262
Hz30k	30	155	21	21	182	67	83	1,826	2,391
Redriven	50	264	32	32	354	40	64	2,009	2,280
Wes18	80	172	21	21	181	25	14	1,967	2,416
WES30	200	91	11	11	144	10	21	1,396	1,687

Considering aggregate data, the following Figure 2.15 reports the distribution of the investment cost drivers for installing a SWT in EU.

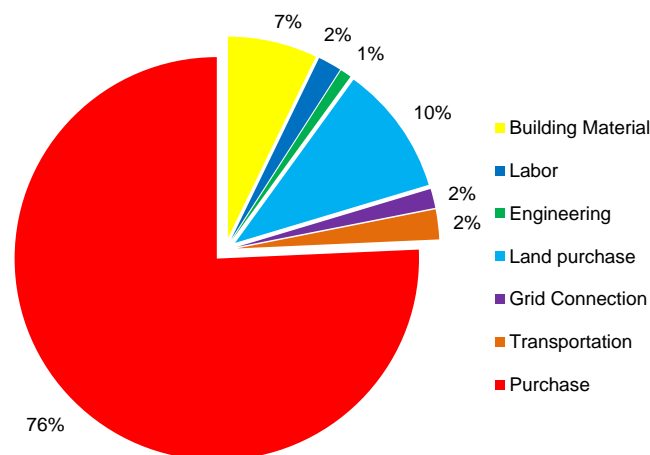


Figure 2.15 SWT average cost distribution

The purchase cost represents the main investment factor, followed by construction costs (building material, labor, engineering and land purchase), transportation cost and the grid connection cost.

### 2.2.6.2 Country analysis

The five EU countries considered in this analysis (France, Germany, Italy, Spain and The Netherlands) are supposed to be possible geographical locations for SWT installations. The previously presented model is adopted to study the convenience of such installations collecting and comparing the results. The following figures summarize the *NPV* trends varying the SWT type and the average wind speed,  $\bar{v}$ , (from 2 to 14m/s). The aim is evaluating the profitability conditions for each turbine. Both the *NPV* trend for the unlevered and 100% financed scenarios (with an interest rate of 3%) are represented.

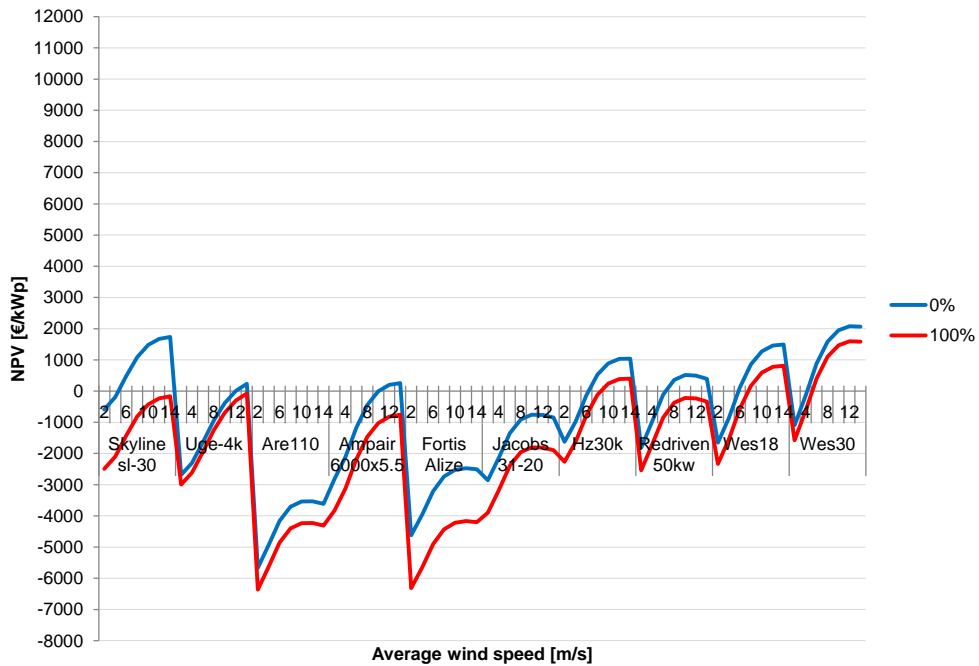


Figure 2.16 *NPV* for France varying the SWT turbine model,  $\bar{v}$  and the financial leverage

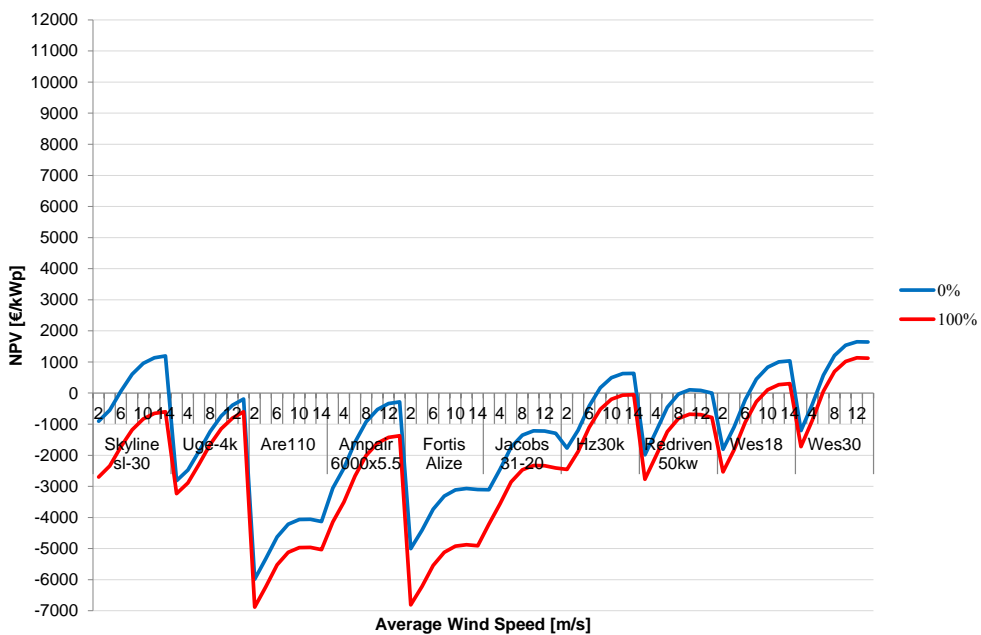


Figure 2.17 *NPV* for Germany varying the SWT turbine model,  $\bar{v}$  and the financial leverage

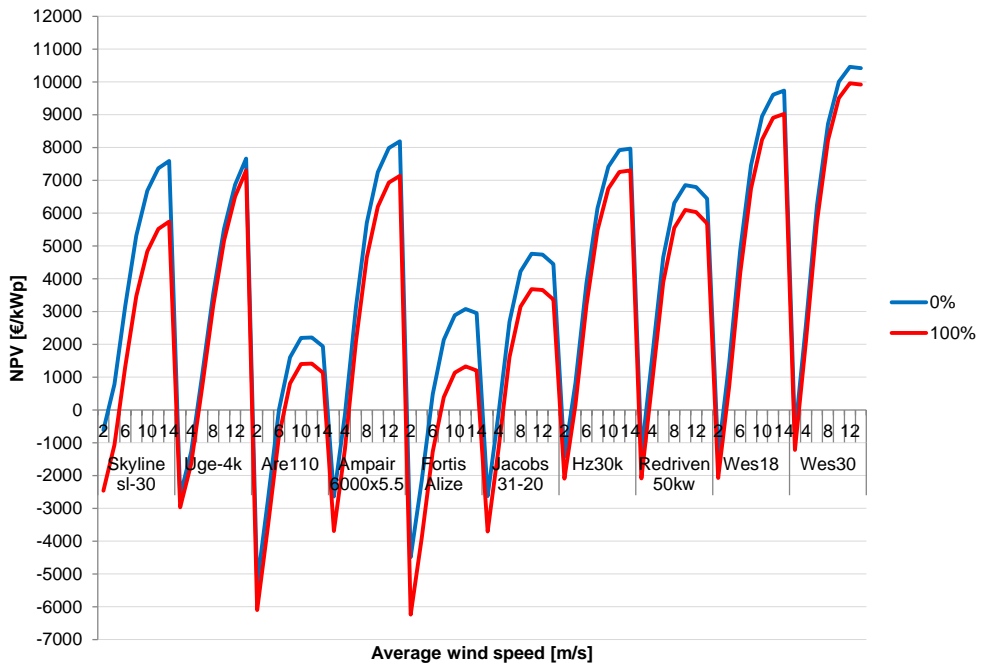


Figure 2.18 NPV for Italy varying the SWT turbine model,  $\bar{v}$  and the financial leverage

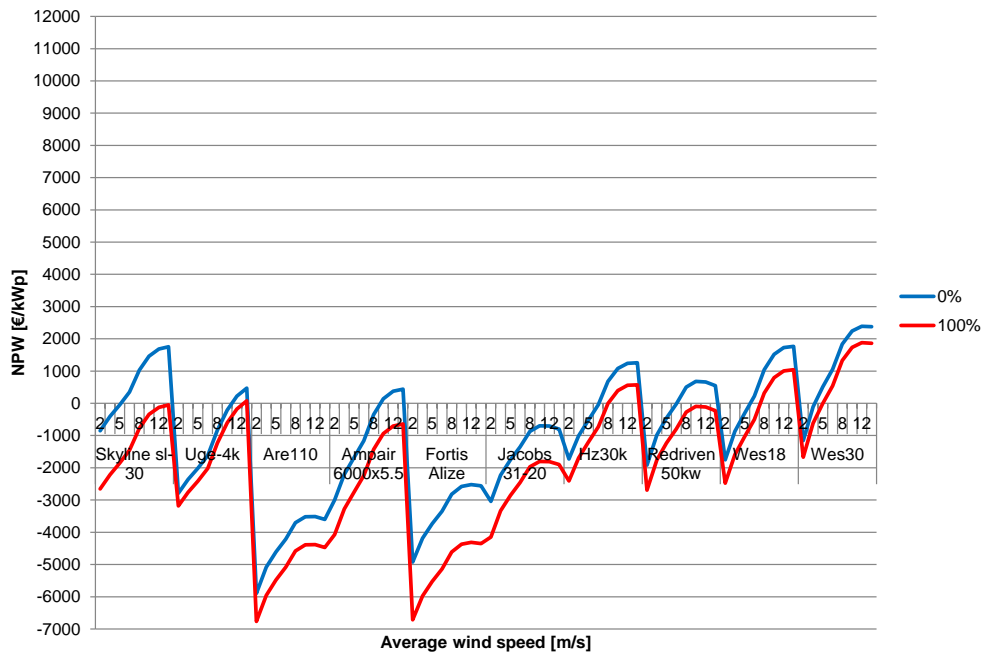


Figure 2.19 NPV for Spain varying the SWT turbine model,  $\bar{v}$  and the financial leverage

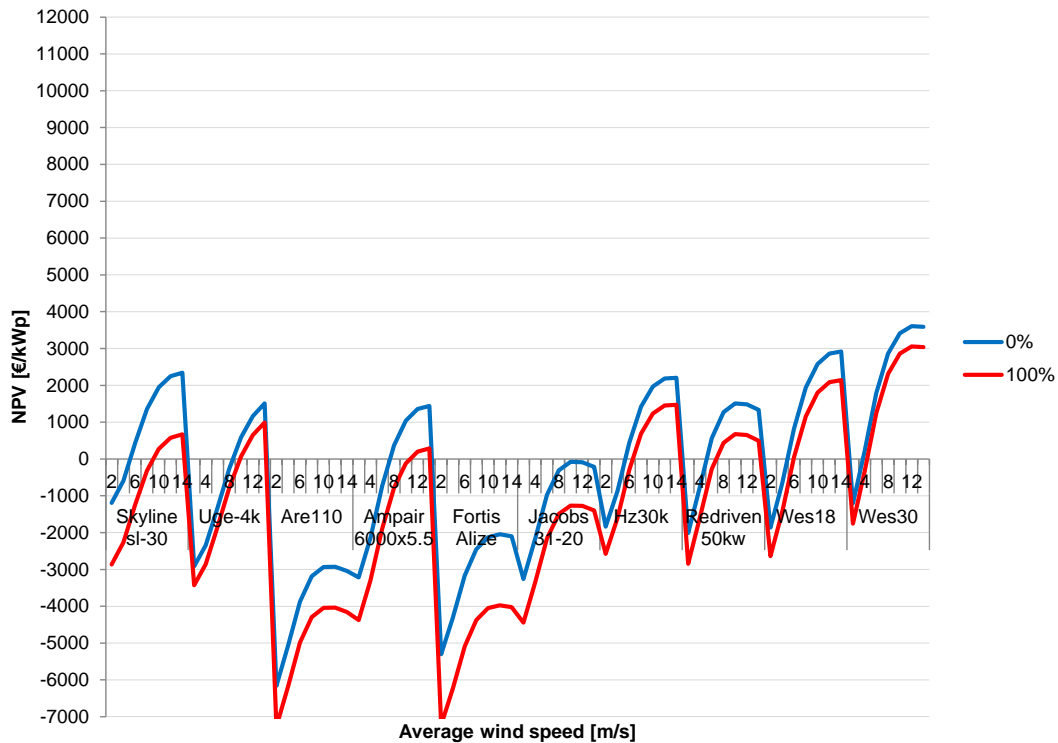


Figure 2.20 NPV for The Netherlands varying the SWT turbine model,  $\bar{v}$  and the financial leverage

France and Germany (see Figures 2.16 and Fig. 2.17) moderately show the same curve profiles with maximum profits ranging from 1000 to 2000€/kWp. Several turbines are not economically feasible even in presence of high wind speed values. The presence of an external financial support is a relevant circumstance to be considered: a significant economic difference, from 5% to 10% on the final *NPV*, between the financial levered and unlevered scenarios can be deduced from the curves for all countries. The Italian case (see Figure 2.18) appears different from all the others mainly because Italy presents the highest feed-in-tariff (30c€/kWh) compared to the other countries. In Italy, every SWT is profitable in presence of moderate and high wind speeds, with *NPV* that ranges from 2000 to 10000€/kWp. Spain (see Fig. 2.19) presents positive *NPV* values for almost any SWT with values comparable to the French and German cases, while The Netherlands (see Fig. 2.20) has better *NPV*. For some turbines the performance indicator is higher than 2000€/kWp and it reaches 3000€/kWp for Wes turbines.

### 2.2.6.3 Economic wind speed threshold

The following Figure 2.21 and Figure 2.22 depict the average wind values making the investment profitable, *i.e.*  $NPV > 0$  and payback period lower than 15 years. Figure 2.21 refers to 100% financed scenario, while Figure 2.22 considers a financial unlevered investment. The smaller the wind speed, the higher the *NPV* is. Figures 2.21 and 2.22 highlight that some SWTs (Are110, Fortis Alize and Jacobs 31-20) are not profitable in many countries (France, Germany, Spain and The Netherlands) because they have a minimum economic wind speed threshold greater than 14m/s. Furthermore, for the financial unlevered scenarios, the most part of economic wind speed values, if present,

are around 5÷7m/s. These values coincide to the threshold wind speeds making wind power plants profitable. On the contrary, in the 100% financing scenario, the economic average wind speed increases and the majority of them ranges between 7 and 9m/s, representing a wind speed not frequently experienced within the considered countries. On the contrary, Italy has low economic average wind speed values that start from 2.5m/s, for all the turbine models. This circumstance makes the SWT installation almost always profitable in this country both for the financial levered and unlevered scenarios.

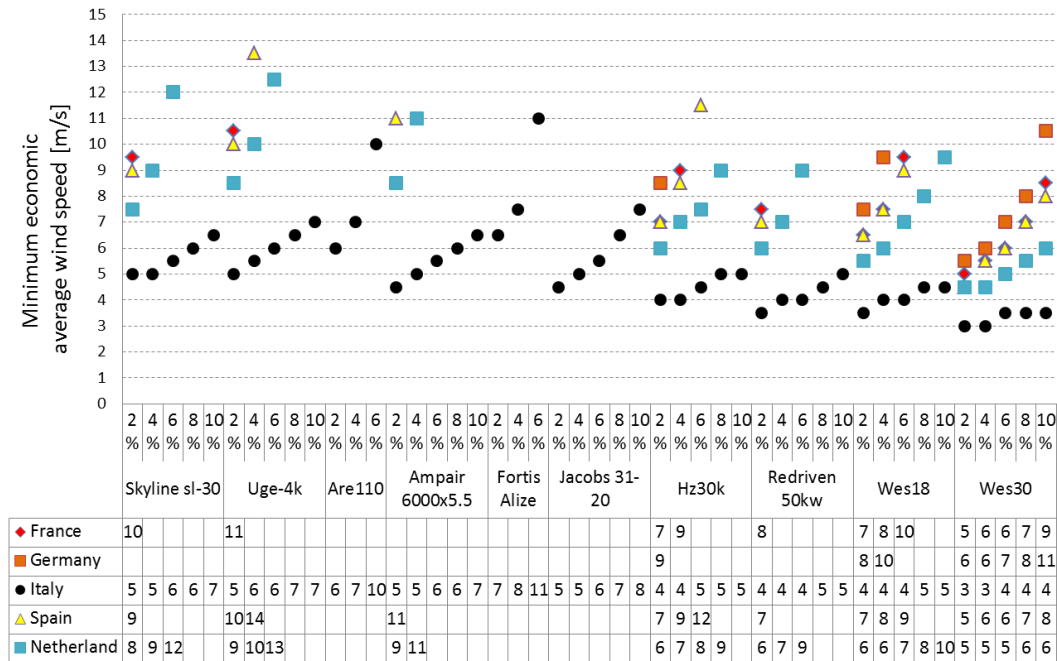


Figure 2.21 Economic wind speed thresholds for each country varying the OCC (from 2% to 10%). 100% financed scenario

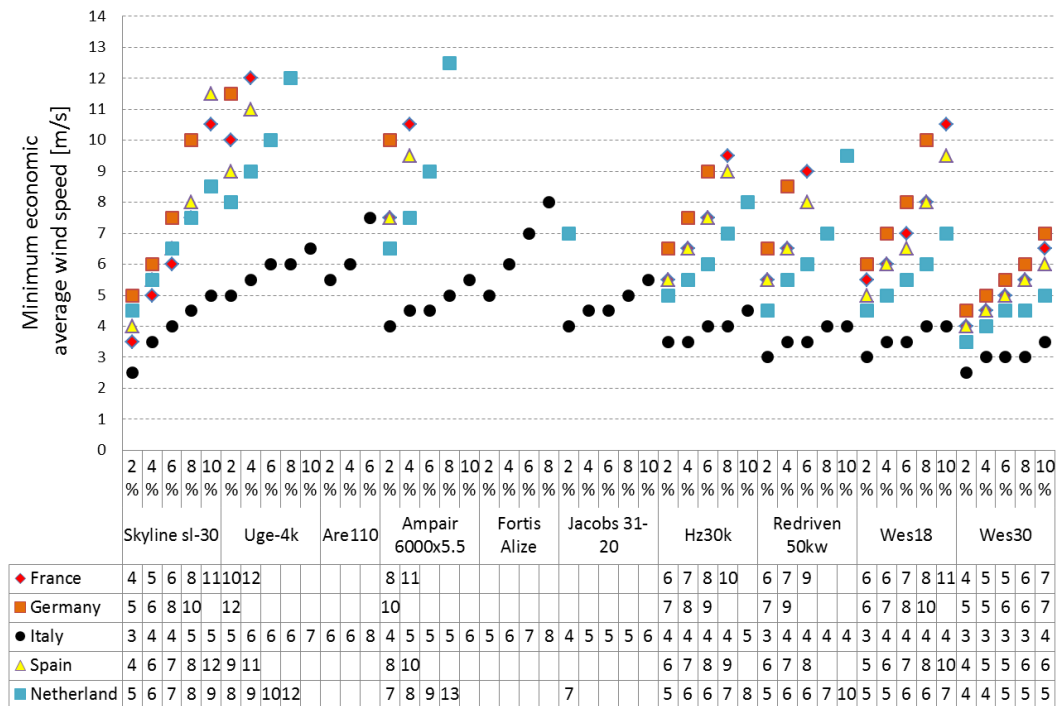


Figure 2.22 Economic wind speed thresholds for each country varying the OCC (from 2% to 10%). 0% financed scenario

### 2.2.7 Conclusions and further research

This *Paragraph* presents an economic analysis of the installation and use of SWTs for some of the main EU countries (France, Germany, Italy, Spain and The Netherlands) proposing an economic performance model that considers the most relevant technical and economic factors that influence the profitability of such systems. Ten SWTs are evaluated in this analysis, with rated power ranging from 2.5 to 200kWp, and their relevant technical features are collected. Moreover, SWTs purchase, transportation, installation and operative costs are determined and analyzed highlighting their components and trends. An economic model, applied to each considered country, allows studying the economic feasibility of wind turbines. The model includes SWT economic factors, e.g. purchasing, transportation and installation costs, the wind speed quality, the national the incentive legislation and other relevant economic and financial drivers, e.g. opportunity cost of capital, inflation rate, financing interest rate, tax level, etc.

Major outcomes deal with the *NPV* curves varying the SWT model, the site average wind speed and the financing plan. Moreover the wind threshold values making such systems economically feasible are determined and discussed for each country. Finally, the obtained results, referred to year 2012, have shown that in the considered countries a set of conditions affect SWT profitability. Among them, the national incentive schemes still played a crucial role in the reference year. Particularly, the results have demonstrated the economic profitability and competitiveness of the most cost-effective SWTs in the five considered EU countries in accordance with the respective anemological conditions.

Further research needs to extend and perform such feasibility analysis enlarging the geographical application of the economic model to the entire EU continent and to other extra-EU countries, e.g. the USA, Japan and the Middle/Far East, identifying similarities, differences and new opportunities to spread the diffusion of SWT renewable energy plants. In addition, the analysis of SWT economic profitability in absence of supporting policies and incentives and the study of SWT designed to meet the energy demand of a specific user is also of interest.

### 2.2.8 Final remarks

The results, shown in this *Paragraph*, highlight the convenience of the most cost-effective SWTs, and even more for WTs due to economy of scale reasons, with the incentive scheme proposed by each considered country in 2012 and their anemological conditions. Such aspect has led to a significant growth of the wind power sector in the EU area as demonstrated by the 2011 and 2012 installations reported in Table 2.15. Considering the Italian context, the distributed energy production from SWTs has rapidly grown, achieving 9MWp only in 2011, with an increase from 1.5MW in 2009 to 13.3MW at the end of 2011 (Fera *et al.*, 2014)

Table 2.15 2011 and 2012 wind power installations and total capacity in the five considered EU countries (EWEA, 2013; WWEA, 2014)

Country	Installed 2011 [MW]	Total capacity end 2011 [MW]	Installed 2012 [MW]	Total capacity end 2012 [MW]
France	979	6,607	892	7,499
Germany	1,860	29,075	2,240	31,315
Italy	940	6,737	1,407	8,144
Spain	997	21,673	1,123	22,796
The Netherlands	59	2,328	63	2,391

However, as for the PV sector, several European governments have amended the incentive schemes with cuts, even retroactive, making the investments in WTs and SWTs less profitable. Italy and Spain are the most evident cases. Such aspects are clarified in the wind power installations for 2013 and the first half-year of 2014 presented in Table 2.16.

Table 2.16 2013 and half-year 2014 wind power installations and total capacity in the five considered EU countries (EWEA, 2013; WWEA, 2014)

Country	Installed 2013 [MW]	Total capacity end 2013 [MW]	Installed Half-year 2014[MW]	Total capacity Half-year 2014[MW]
France	755	8,254	338	8,592
Germany	3,345	34,660	1,830	36,490
Italy	407	8,551	30	8,581
Spain	163	22,959	0.1	22,959
The Netherlands	302	2,693	-	-

Germany continued his growth confirming his leadership in the European area and its third positions worldwide. France experienced a constant decrease of wind power installations, while Italy and Spain had a dramatic reduction from 1,407MW and 1,123MW, respectively, of 2012 to almost no wind power installations in the first half of 2014. Thus, the wind power sector requires proper and clear supporting policies to continue its development. In the SWT context, Fera *et al.* (2014) demonstrates their potential and economic feasibility even in the Italian context concluding that specific program of incentives for development and research in the field of the energy generation and management are crucial to make SWTs contribute to the energy generation and distribution.



## References

- Ardente, F., Beccali, M., Cellura, M., & Lo Brano, V., 2008. Energy performances and life cycle assessment of an Italian wind farm. *Renewable and Sustainable Energy Reviews*, 12(1), 200–217.
- Bishop, J. D. K., & Amaratunga, G. a. J., 2008. Evaluation of small wind turbines in distributed arrangement as sustainable wind energy option for Barbados. *Energy Conversion and Management*, 49(6), 1652–1661.
- Bolinger, M., & Wiser, R., 2009. Wind power price trends in the United States: Struggling to remain competitive in the face of strong growth. *Energy Policy*, 37(3), 1061–1071.
- Bortolini, M., Gamberi, M., Graziani, A., Manzini, R., & Pilati, F., 2014. Performance and viability analysis of small wind turbines in the European Union. *Renewable Energy*, 62, 629–639.
- Bowen, A., Huskey, A., Link, H., Sinclair, K., Forsyth, T., Jager, D., ... Smith, J., 2009. Small Wind Turbine Testing Results from the National Renewable Energy Lab, (July).
- Carta, J. a., Ramírez, P., & Velázquez, S., 2009. A review of wind speed probability distributions used in wind energy analysis. *Renewable and Sustainable Energy Reviews*, 13(5), 933–955.
- Doddamani, S.S., Jangamshetti, S. H., 2008. Economic Index for Selection of Wind Turbine Generator at a Site. In 2008 IEEE international conference on sustainable energy technologies, 622–627.
- Dunlop, J., 2006. Wind Power Project Returns—What Should Equity Investors Expect? *The Journal of Structured Finance*, 12(1), 81–89.
- Elmore, A. C., & Gallagher, R., 2009. Using Regional Climate Center Data to Predict Small Wind Turbine Performance, (January), 14–19.
- Fera, M., Iannone, R., Macchiaroli, R., Miranda, S., Schiraldi, M.M., 2014. Project appraisal for small and medium size wind energy installation: The Italian wind energy policy effects. *Energy Policy* 74, 621–631.
- Kelleher, J., & Ringwood, J. V., 2009. A computational tool for evaluating the economics of solar and wind microgeneration of electricity. *Energy*, 34(4), 401–409.
- KPMG, 2011. KPMG's Corporate and Indirect Tax Survey 2011.

- Krohn, S., Morthorst, P.E., Awerbuch, S., 2009. The economics of wind energy. Belgium: European Wind Energy Association; 2009.
- Li, Z., Boyle, F., & Reynolds, A., 2012. Domestic application of micro wind turbines in Ireland: Investigation of their economic viability. *Renewable Energy*, 41, 64–74.
- Lu, X., McElroy, M. B., & Kiviluoma, J., 2009. Global potential for wind-generated electricity. *Proceedings of the National Academy of Sciences of the United States of America*, 106(27), 10933–8.
- Mithraratne, N., 2009. Roof-top wind turbines for microgeneration in urban houses in New Zealand. *Energy and Buildings*, 41(10), 1013–1018.
- Mostafaeipour, a., Sedaghat, A., Dehghan-Niri, A. a., & Kalantar, V. (2011). Wind energy feasibility study for city of Shahr Babak in Iran. *Renewable and Sustainable Energy Reviews*, 15(6), 2545–2556.
- Pantaleo, A., Pellerano, A., Ruggiero, F., & Trovato, M., 2005. Feasibility study of off-shore wind farms: an application to Puglia region. *Solar Energy*, 79(3), 321–331.
- Peacock, a. D., Jenkins, D., Ahadzi, M., Berry, A., & Turan, S., 2008. Micro wind turbines in the UK domestic sector. *Energy and Buildings*, 40(7), 1324–1333.
- Risø National Laboratory., 1989. *European Wind Atlas*.
- Šimi, Z., Boži, M., & Šljivac, D., 2009. Small Wind Turbine Power Curve Comparison. In *IEEE AFRICON conference 2009*, 1–6.
- Simic, Z., Havelka, J. G., & Bozicevic Vrhovcak, M., 2013. Small wind turbines – A unique segment of the wind power market. *Renewable Energy*, 50, 1027–1036.
- Sinisuka, N. I., & Nugraha, H., 2013. Life cycle cost analysis on the operation of power generation. *Journal of Quality in Maintenance Engineering*, 19(1), 5–24.
- Stockton, K. M., 2004. Utility-scale wind on islands: an economic feasibility study of Ilio Point, Hawai'i. *Renewable Energy*, 29(6), 949–960.
- The European Wind Energy Association, 2012. *Annual report 2012 - United in tough times*.
- Valentine, S. V., 2010. A STEP toward understanding wind power development policy barriers in advanced economies. *Renewable and Sustainable Energy Reviews*, 14(9), 2796–2807.

- Valentine, S. V., 2011. Understanding the variability of wind power costs. *Renewable and Sustainable Energy Reviews*, 15(8), 3632–3639.
- Villanueva, D., & Feijóo, A., 2010. Wind power distributions: A review of their applications. *Renewable and Sustainable Energy Reviews*, 14(5), 1490–1495. doi:.rser.2010.01.005
- Walters, R., & Walsh, P. R., 2011. Examining the financial performance of micro-generation wind projects and the subsidy effect of feed-in tariffs for urban locations in the United Kingdom. *Energy Policy*, 39(9), 5167–5181.
- Wizelius, T., 2007. *Developing wind power projects: theory and practice*. UK: Earthscan.
- World Wind Energy Association, 2009. *World Wind Energy Report 2009*.
- World Wind Energy Association, 2010. *World Wind Energy Report 2010*.
- World Wind Energy Association, 2014. *Half-year Report 2014*.
- Yue, C.-D., Liu, C.-M., & Liou, E. M. L., 2001. A transition toward a sustainable energy future: feasibility assessment and development strategies of wind power in Taiwan. *Energy Policy*, 29(12), 951–963.

## Legislations

- French Government. Arrêté du 17 novembre 2008 vent. Arrêté du 17 Novembre 2008 fixant les conditions d'achat de l'électricité produite par les installations utilisant l'énergie mécanique du vent; 2008.
- German Government. EEG, act on granting priority to renewable energy sources (Renewable energy sources Act) 01/01/2009. SDLWindV; 2009. Ordinance on System Services by Wind Energy Plants 03/07/2009.
- Italian government, L 244/07. Legge 24 Dicembre 2007, n. 244. Disposizioni per la formazione del bilancio annuale e pluriennale dello Stato. Legge finanziaria 2008; 2008.
- Spanish government, RD 661/2007. Real Decreto 661/2007, de 25 de mayo, por el que se regula la actividad de producción de energía eléctrica En régimen especial; 2007.
- Dutch government. SDE. Besluit stimulerend duurzame energieproductie; 2008.



## 3. Energy Storage Technology

### *Review of the energy storage technologies for the RES management*

Nowadays, the fossil fuels still have the main incidence on the energy sector even if their price volatility and their relevant environmental impact are encouraging and favoring the spread of the renewable energy sources (RESs). However, the intermittent and random nature of the RESs logically suggests the adoption of energy storage systems (ESSs) to meet the load request compensating the gap between the energy availability and the energy demand. In addition, the previous analysis in *Paragraph 2.1* shows the significant role of energy self-consumption, due to the gap between the energy purchased and sold to the grid, in the RES lifetime profitability and the adoption of ESSs increases the share of self-consumption.

Several energy storage technologies exist and several studies show their applicability and economic feasibility for the RES management. In the 90s, Spiers *et al.* (1995), Ro and Rahman (1998) and Sutanto and Lachs (1998) evaluate the integration of battery energy storage (BES) systems to the Photovoltaic (PV) systems, while, Chiang *et al.* (1998) investigate the effectiveness of the BES systems for a sustainable energy development. In the recent literature, Kousksou *et al.* (2014) present an updated review of the state of the art of different energy storage technologies and Mahlia *et al.* (2014) discuss the available methods and recent development on energy storage. Subero *et al.* (2014), Akinyele and Rayudu (2014) and Beaudin *et al.* (2014) review the state of the energy storage technologies suitable for the integration and management of intermittency in RES, while Castillo *et al.* (2014) investigate grid-scale energy storage applications for RES integration describing their essential characteristics and services.

According to the mentioned scientific contributions, the next *Paragraph 3.1* briefly reviews the main functions provided by ESSs, their applications and the available technologies with focus on RESs integration and management. Finally, *Paragraph 3.2* describes more in details the characteristics and operation of battery energy storage (BES) systems, particularly suitable for PV plant and small wind turbine (SWT) energy storage and subject to further analysis in the next *Chapter 4*.

### 3.1 Energy storage system overview

The adoption of ESSs is significantly increasing to ensure energy fruition in the remote areas, to balance the intermittent and random nature of the RESs and to overcome several grid lacks, e.g. blackouts, overloads, low grid quality, etc. In details, the main functions and applications, for on-grid and off-grid applications, of ESSs are in the following:

- *Renewable integration*: minimization of the intermittency effect of RESs and increase their penetration in power grids, thus, allowing renewable generation to be dispatched
- *Different power sources integration*: improvement of the management of different power sources, e.g. transient conditions and switches, in off-grid applications, including RESs and fossil fuel based generators
- *Energy arbitrage*: it involves storing electricity at off-peaks when the cost is low, and selling it at peak demands periods when the cost is high
- *Load levelling*: utilization of the stored energy at peak periods, reducing the requirements of peaking generators (*load shifting* and *peak shaving* operations)
- *Load balancing*: adjusting power output as demand fluctuates in order to maintain power balance in the system
- *Power quality optimization*: Improvement of the quality of the electrical power, i.e. voltage and frequency regulation and stability, transient voltages and currents management, harmonic content control, reactive power regulation etc.
- *Spinning reserve*: reduce the requirement for idling generators in power systems. Such generators are dedicated to compensate any sudden failure of major generators
- *Uninterruptible power supply (UPS)/Black start*: Emergency power sources to address short and long interruptions, voltage peaks and flickers
- *Congestion relief*: reduction of network flows in transmission constrained systems either by increasing the capacity of the lines or providing alternative pathways for the electricity
- *Investment deferral*: use of storage to avoid/defer transmission and distribution infrastructure investment

Several energy storage technologies, briefly described in Table 3.1, are currently adopted to satisfy the aforementioned operations.

Table 3.1 Summary of the main ESS technologies (Kouskou et al., 2014)  
Energy storage technology review

Thermal energy storage (TES)	Sensible heat storage	Energy is stored changing the temperature of the storage mean
	Latent heat storage	During the energy storage process the thermal medium changes phase (Phase change materials PCM), releasing or absorbing the latent heat.
	Thermo-chemical energy storage	Energy is absorbed or released through a reversible endothermic chemical reaction
Electrical energy storage (EES)	Pumped hydro storage (PHS)	Method to store and produce electricity to supply high peak demands by pumping water from a lower reservoir to an upper reservoir. When the power demand is high water flows from the upper to the lower reservoir activating the turbines to generate electricity
	Compressed air energy storage (CAES)	Energy is stored by compressing air within an air reservoir using a compressor powered by off-peak/low-cost electric energy
	Flywheel energy storage (FES)	Energy is stored in the rotational mass of a flywheel. The kinetic energy stored in a flywheel is proportional to the mass and the square of its rotating speed
	Battery energy storage (BES)	A battery is an electrochemical device able to deliver, in the form of electric energy, the chemical energy generated by electrochemical reactions
	Hydrogen based energy storage (HES)	The hydrogen offers the advantage of storage and transportation. After production, the hydrogen can be stored in compressed tanks and when needed, can power a fuel cell stack providing energy
	Flow battery energy storage (FBES)	A flow battery is charged and discharged by a reversible chemical reaction between two liquid electrolytes, contained in separate tanks
	Capacitor and super-capacitor energy storage (SC)	Capacitors store energy as electric charge between two plates metal or conductive separated by an insulating material known as a dielectric when a voltage differential is applied across the plates
	Superconducting magnetic energy storage (SMES)	The superconducting magnetic energy storage system is an energy storage device that stores electrical energy in magnet field without conversion to chemical or mechanical forms

The essential characteristics of ESSs can be summarized with the following parameters, which common values for different ESSs are in Table 3.2.

- *Energy storage capacity [kWh]:* the amount of energy that can be stored
- *Typical power output [kW]:* the amount of power that can be discharged within the typical discharge duration
- *Energy density [Wh/L- Wh/kg]:* the nominal storage per unit volume or mass
- *Power density [W/L – W/kg]:* The maximum available power per unit volume or mass
- *Charge/Discharge duration:* the time needed for the storage to fully charge or discharge
- *Response time [s]:* the time needed for the storage to start providing output
- *Lifetime [years or cycles]:* the number of cycles and/or years that a storage technology will continue to operate
- *Roundtrip efficiency [%]:* the ratio of energy discharge by the system to the energy required (including losses) to charge the system over each cycle

- *Capital cost [€/kW or €/kWh]:* the cost of the storage technology per unit of power discharge [\$/-€/kW] or energy storage capacity [\$/-€/kWh]

Table 3.2 ESSs characteristics (Kouskou et al., 2014; Castillo et al. 2014)

ESS	Roundtrip efficiency [%]	Capacity [MW]	Energy density [Wh/L]	Capital [\$/kW]	Capital [\$/kWh]	Response time	Lifetime [years]
TES	30-60	0-300	80-250	200-300	3-50	-	5-40
PHS	75-85	100-5,000	0.5-1.5	600-2,000	5-100	ms	40-60
CAES	50-89	3-400	30-60	400-2,000	2-100	ms	20-60
Flywheel	93-95	0.25	10-30	350	5,000	< ms	≈15
Pb-acid battery	70-90	0-40	30-50	300	400	ms	5-15
Ni-Cd battery	60-65	0-40	50-75	500-1,500	800-1,500	ms	10-20
Na-S battery	80-90	0.05-8	150-240	1,000-3,000	300-500	ms	10-15
Li-on battery	85-90	0.1	74-299	4,000	2,500	ms	5-15
Fuel cells	25-50	0-50	800-10,000	5,00-1500	10-20	< s	5-15
Flow battery	75-85	0.3-15	10-50	600-1,500	150-1,000	ms	5-15
Capacitors	60-65	0.05	0.05-5	400	1,000	ms	≈5
Supercapacitors	90-95	0.3	2.5-15	300	2,000	ms	>20
SMES	95-98	01-10	0.5-5	300	10,000	ms	>20

### 3.2 Battery energy storage (BES) system overview

The use of RESs as completely reliable primary sources makes the energy storage a crucial factor. BES systems are particularly suitable for conventional RESs, as PV and wind systems, to store the energy during the RES availability and releasing it during the user request periods. In such a way, the RES systems are designed to supply a greater percentage of the user energy demand.

BES systems are currently the most common, cost-effective and reliable ESS systems. The existing battery technologies differ for the materials used as electrodes, *i.e.* anode and cathode, and the electrolytes, which provide electron transfer between the electrodes. The most common technologies are lead-acid, lithium-based, nickel-based and sodium-sulphur batteries. Rydh and Sandèn (2005a, 2005b) and Battke *et al.* (2013) compare the performances and costs of different technologies for batteries concluding that a leading technology has yet to emerge even if the lead-acid batteries are the most commonly used for the stand-alone power systems (Wenham *et al.*, 2007).

Among them, the operative fundamentals about lead-acid and lithium-ion batteries are summarized in Figure 3.1, including the common cost ranges, roundtrip efficiency, *i.e.* the efficiency of a complete charge/discharge process, and life-time.



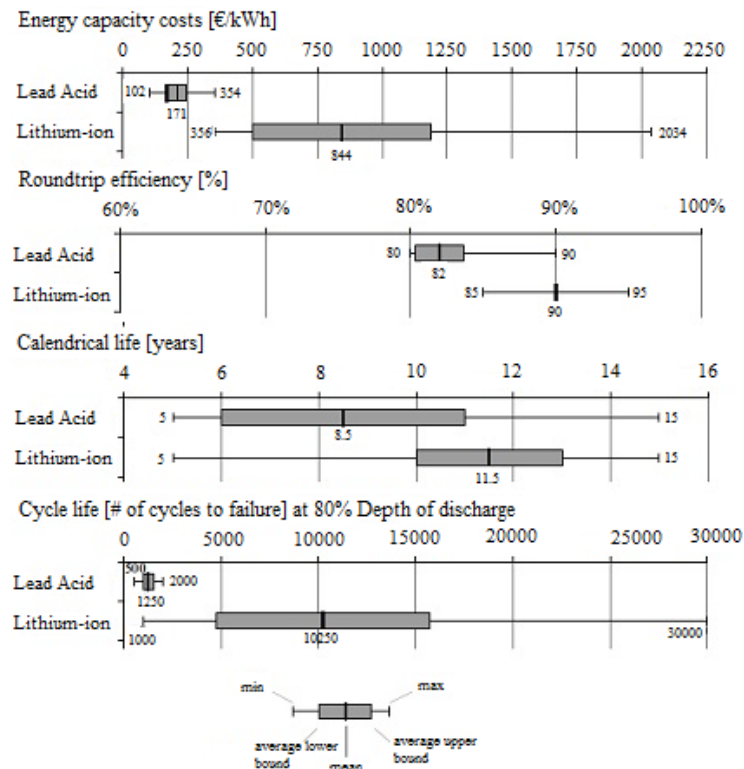


Figure 3.1 Lead-acid and lithium-ion batteries comparison (Battke et al., 2013)

**Lead-acid batteries.** They are the most mature and cheapest energy storage devices. Lead-acid batteries are based on chemical reactions involving lead dioxide (cathode electrode), lead (anode electrode) and sulphuric acid which act as the electrolyte. Lead-acid batteries have low costs, good reliability and efficiency, while their major disadvantages are the performance decrease with low and high ambient temperatures, the relatively short life-time, the required maintenance, the low specific energy and power. In addition, lead-acid batteries present difficulties to provide frequent power cycling, often in partial states of charge, which lead to premature failure due to sulphation.

**Lithium-based batteries.** Lithium battery technology consists of two main types, lithium-ion and lithium-polymer cells. Their high energy and power density make them attractive for wide ranges of application, from portable electronics to satellite applications. For lithium-ion batteries, the self-discharge rate is very low and battery lifetime reaches a relevant number of cycles with high efficiencies. However, the life-time is temperature dependent and the special packaging and internal overcharge protection circuits significantly increase their cost (Kousksou et al., 2014).

### 3.2.1 BES definitions and terms

Electrochemical battery operations and performances are mainly identified by the following parameters:

- Nominal voltage: reference battery voltage (V). It represents a suitable approximated value to identify the battery voltage, which continuously varies during the charging and discharging operations

- Open circuit voltage (OCV): the voltage (V) between battery terminals with no load applied
- Capacity: the total amount of the electrical charge  $Q$  that can be drawn from the battery before a specified cut-off voltage is reached. In the industrial contexts, charge capacity is measured in Ampere-hours (Ah). Practically, the capacity is determined as the integral of the discharge current over the discharge time, starting from the fully charged state and ending at the fully discharged state (Equation 3.1)

$$Q = \int_0^{t_D} I(t) dt = I \cdot t_D \text{ for constant current} \quad (3.1)$$

Where:

- $I$  is the discharge current (A)
- $t_D$  is the discharge time (h)

If the cutoff voltage is ignored the battery voltage continues to fall and damaging processes may result. Manufacturers frequently specify the rated capacity of their batteries, in Ah, given a fixed discharge rate. For example, a battery with a rated capacity of 100Ah for a 10 hours discharge period (C/10 discharge rate) is able to provide 10A for 10 hours. The rated capacity of the batteries is usually expressed for different discharge periods, e.g. C/20, C/10, C/5, C/3, C/1 discharge rates, since it varies with the discharge rate. The higher the discharge rate, the lower the cell capacity is (refer to *sub-Paragraph 3.2.2* for details);

- State of charge (SOC): the SOC measures the fraction of the original charge left at a given time:

$$SOC(t) = \left[ 1 - \frac{1}{Q_n} \int_0^t I(\tau) d\tau \right] \cdot 100\% \quad (3.2)$$

Where:

- $Q_n$  is the nominal charge capacity (Ah);
- Depth of discharge (DOD): DOD is the percentage of the battery capacity that has been discharged, expressed as a percentage of maximum capacity. Thus, DOD is the complement of SOC;
- Cycle life: The number of charge-discharge cycles the battery can perform before it fails to meet specific performance criteria. The battery capacity, and therefore the operating life, is affected by the rate and depth of cycles (DOD) and the environmental conditions such as the temperature and the humidity. The parameter state of health (SOH), which represents the ratio between the current available capacity and the nominal capacity, defines the battery current status.

Several contributions in the literature models degradations of the performances of batteries during the ageing process (Riffoneau *et al.*, 2011). As example, Table 3.3 shows the maximum number of cycles for a commercial lead-acid battery as a function of the *DOD* and the temperature.

*Table 3.3 Cycle life for a lead-acid battery as a function of DOD and temperature*

Temperature	20°C	25°C	30°C	35°C	40°C
<i>DOD (%)</i>	<i>Cycle life (Times)</i>				
10	9,400	6,640	4,700	3,320	2,350
20	7,700	5,450	3,850	2,725	1,925
30	6,240	4,400	3,120	2,200	1,560
40	4,960	3,500	2,480	1,750	1,240
50	3,820	2,700	1,910	1,350	955
60	2,840	2,000	1,420	1,000	710
70	2,120	1,500	1,060	750	530
80	1,700	1,200	850	600	425
90	1,360	950	680	475	340
100	1,060	750	530	375	265

A BES system consists of single or multiple cells, connected in series, parallel or even a mix of both depending on the desired output voltage and capacity. The connection in parallel of two identical batteries doubles the capacity at the same nominal voltage, while the connection in series doubles the nominal voltage at the same capacity. The cell connections are to be done with cells of the same type, manufacturer and state of charge, after the check of their correct efficiency (Wenzl, 2009).

### 3.2.2 Charge/Discharge process

The voltage of a battery is given by its OCV and over-voltages occurring due to diffusion processes, electrochemical reactions and ohmic resistances. The battery voltage is always above the OCV during charging and below OCV during discharging as in Figure 3.2. The battery voltage during the discharging process, which typical curve is in Figure 3.3, is expressed according to the following Equation 3.2.

$$U_{Battery} = U_{OpenCircuit} - IR - \eta_{reaction} - \eta_{diffusion} \quad (3.3)$$

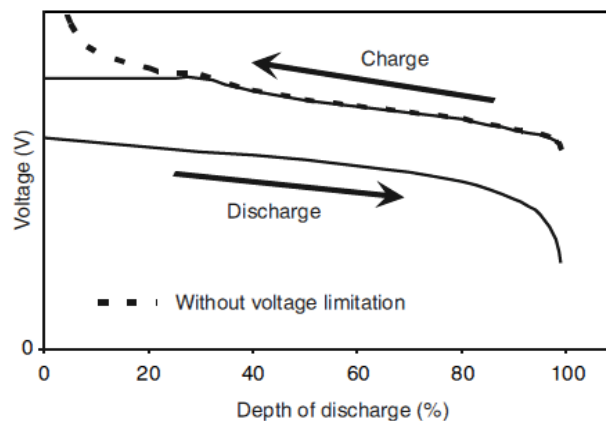


*Figure 3.2 Schematic of the voltage during a constant current discharge and charge*

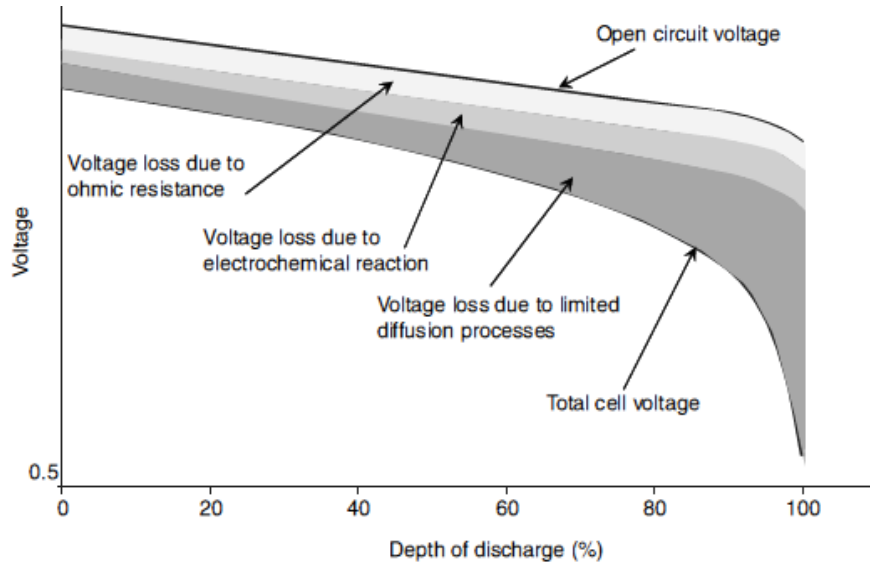


Figure 3.3 Schematic of the discharge curve of a battery with different voltage losses

The ohmic voltage drop,  $IR$ , is caused by the ohmic resistances of all the elements in the current path of the battery. The reaction over-voltage,  $\eta_{reaction}$ , is caused by the charge transfer resistance, positive during charging and negative during discharging, and, finally, diffusion over-voltage,  $\eta_{diffusion}$ , occurs if concentration gradients in the electrolyte are present. During the discharging process, the increase of the voltage losses significantly affects the battery capacity because the battery voltage quickly equals the cut-off voltage, interrupting the discharging process. From a physical point of view, the amount of charged molecules does not change due to the discharge conditions. Only self-discharge processes can reduce the available capacity. Thus, the limitation of the discharge capacity is not a coulombic limitation but, simply, a problem with the voltage level during discharging. This behaviour is described by the so-called Peukert law. The discharge current  $I$  of a battery decreases with the increase of the "constant current" discharge time,  $t$ , as in Equation 3.34.

$$I^n \cdot t = constant \quad (3.4)$$

Where:

- $n$  is the Peukert coefficient, function of the battery type and model

A Peukert coefficient equals to  $n = 1$  means that the available battery capacity does not depend on the discharge rate that is unrealistic in the practise where the Peukert coefficient is greater than 1. In particular, lead-acid batteries have strong dependencies on the discharge rate, while lithium-based technologies are less affected by the discharge rate. The Figure 3.4 highlights the discharge curves for batteries with different impact of the current rates on the available capacity.

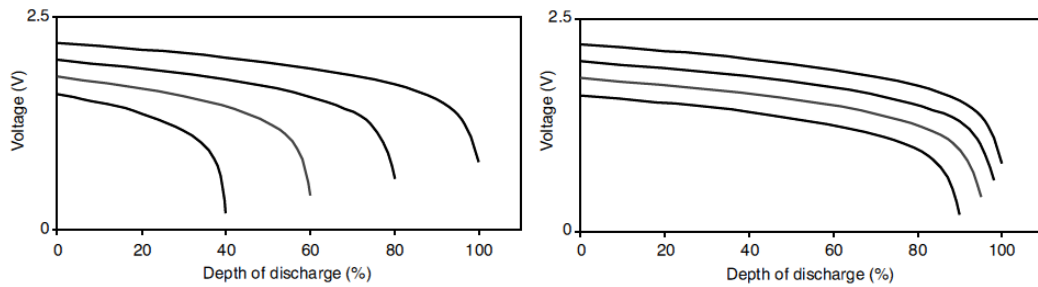


Figure 3.4 Schematic of discharge curves for a battery with a strong impact of current rate on the available capacity (e.g. lead-acid batteries) and a battery with lower impact of current rates (e.g. lithium-ion batteries)

High discharge currents decrease the capacity and high charge/discharge currents increase the energy dissipation and the temperature, due to ohmic resistances, influencing the battery health and efficiency. For this reason, it is appropriate to limit and properly control the charging and discharging processes to avoid inefficient battery utilization (Sauer, 2009).

### 3.2.3 Impact of the temperature on the performance of BES systems

The temperature has a significant impact on the electrical performance of BES systems. Generally, the performances increase with a temperature increase even if aging and self-discharge processes are accelerated by high temperatures. The BES system capacity is, also, affected by the external temperature. A capacity decrease of 1% per degree occurs below 20°C. For these reasons, BES systems are typically stored in a 20-25°C controlled rooms (Wenham *et al.*, 2007).

## References

- Akinyele, D. O., & Rayudu, R. K. (2014). Review of energy storage technologies for sustainable power networks. *Sustainable Energy Technologies and Assessments*, 8, 74–91.
- Batke, B., Schmidt, T. S., Grosspietsch, D., & Hoffmann, V. H. (2013). A review and probabilistic model of lifecycle costs of stationary batteries in multiple applications. *Renewable and Sustainable Energy Reviews*, 25, 240–250.
- Beaudin, M., Zareipour, H., Schellenberglabe, A., & Rosehart, W. (2010). Energy storage for mitigating the variability of renewable electricity sources: An updated review. *Energy for Sustainable Development*, 14(4), 302–314.
- Castillo, A., & Gayme, D. F. (2014). Grid-scale energy storage applications in renewable energy integration: A survey. *Energy Conversion and Management*, 87, 885–894.
- Chiang, S. J., Chang, K. T., & Yen, C. Y. (1998). Residential photovoltaic energy storage system. *IEEE Transactions on Industrial Electronics*, 45(3), 385–394.
- Kousksou, T., Bruel, P., Jamil, A., El Rhafiki, T., & Zeraoui, Y. (2014). Energy storage: Applications and challenges. *Solar Energy Materials and Solar Cells*, 120, 59–80.
- Mahlia, T. M. I., Saktisahdan, T. J., Jannifar, A., Hasan, M. H., & Matseelar, H. S. C. (2014). A review of available methods and development on energy storage; technology update. *Renewable and Sustainable Energy Reviews*, 33, 532–545.
- Riffonneau, Y., Bacha, S., Barruel, F., & Ploix, S. (2011). Optimal Power Flow Management for Grid Connected PV Systems With Batteries. *IEEE Transactions on Sustainable Energy*, 2(3), 309–320.
- Ro, K., & Rahman, S. (1998). Battery or fuel cell support for an autonomous photovoltaic power system. *Renewable Energy*, 13(2), 203–213.
- Rydh, C. J., & Sandén, B. a. (2005a). Energy analysis of batteries in photovoltaic systems. Part I: Performance and energy requirements. *Energy Conversion and Management*, 46(11-12), 1957–1979.
- Rydh, C. J., & Sandén, B. a. (2005b). Energy analysis of batteries in photovoltaic systems. Part II: Energy return factors and overall battery efficiencies. *Energy Conversion and Management*, 46(11-12), 1980–2000.

- Sauer, D. U. (2009). Batteries: Charge-Discharge Curves. Reference Module in Chemistry, Molecular Sciences and Chemical Engineering. Encyclopedia of Electrochemical Power Sources, 443–451.
- Spiers, D. J., & Rasinkoski, A. D. (1995). Predicting the service lifetime of lead/acid batteries in photovoltaic systems. *Journal of Power Sources*, 53(2), 245–253.
- Sutanto, D., & Lachs, W. . (1998). Battery energy storage systems for sustainable energy development in Asia. *Electric Power Systems Research*, 44(1), 61–67.
- Toledo, O. M., Oliveira Filho, D., & Diniz, A. S. A. C. (2010). Distributed photovoltaic generation and energy storage systems: A review. *Renewable and Sustainable Energy Reviews*, 14(1), 506–511.
- Wenham, S.R., Green, M.A., Watt, M.E., Corkish, R. (2007). *Applied photovoltaics*. (Earthscan, Ed.). United Kingdom.
- Wenzl, H. (2009). Batteries: Capacity. Reference Module in Chemistry, Molecular Sciences and Chemical Engineering. Encyclopedia of Electrochemical Power Sources, 395–400.
- Yekini Suberu, M., Wazir Mustafa, M., & Bashir, N. (2014). Energy storage systems for renewable energy power sector integration and mitigation of intermittency. *Renewable and Sustainable Energy Reviews*, 35, 499–514.





## 4. Hybrid Energy System Design

### *Design of grid connected and off-grid hybrid energy systems*

A hybrid energy system (HES) represents a system in which renewable energy sources (RESs), *e.g.* photovoltaic (PV) plant, small wind turbines (SWTs) *etc.*, fossil fuel based energy sources, *e.g.* diesel generators, and energy storage systems are integrated to meet a certain a certain load demand at any time.

The interest in HESs is increasing for both grid connected applications, in order to increase the energy self-consumption due to the increasing electricity prices and the intermittent and random nature of RESs, and off-grid applications, *e.g.* telecommunication system, remote village energy supply, *etc.* Indeed, in most rural areas of developing countries, grid connected electric power supply is economically not realistic due to high cost of paying for the energy amid constricted energy potential of the inhabitants. In addition, supply of electricity with diesel based fuel becomes very much expensive while HES becomes competitive with diesel only generation (Mohammed *et al.*, 2014).

A reference diagram for a generic grid connected and off-grid HES architecture is in Figure 4.1. The system integrates RESs, *i.e.* PV plants and SWTs, battery energy storage (BES) system, electric conversion devices, *i.e.* AC-DC, DC-AC, AC-AC, DC-DC conversion units and bidirectional inverters, the connections to the user AC and DC loads through AC and DC bus bars, and the secondary or backup power source, represented by a an electric generator for off-grid applications and by the national grid for grid connected systems. Energy sources and electric conversion devices are properly controlled and synchronized in order to guarantee their proper operations and switch between them, meet the energy demand and manage the BES system charging/discharging processes avoiding the risk of overcharging and overvoltage conditions.

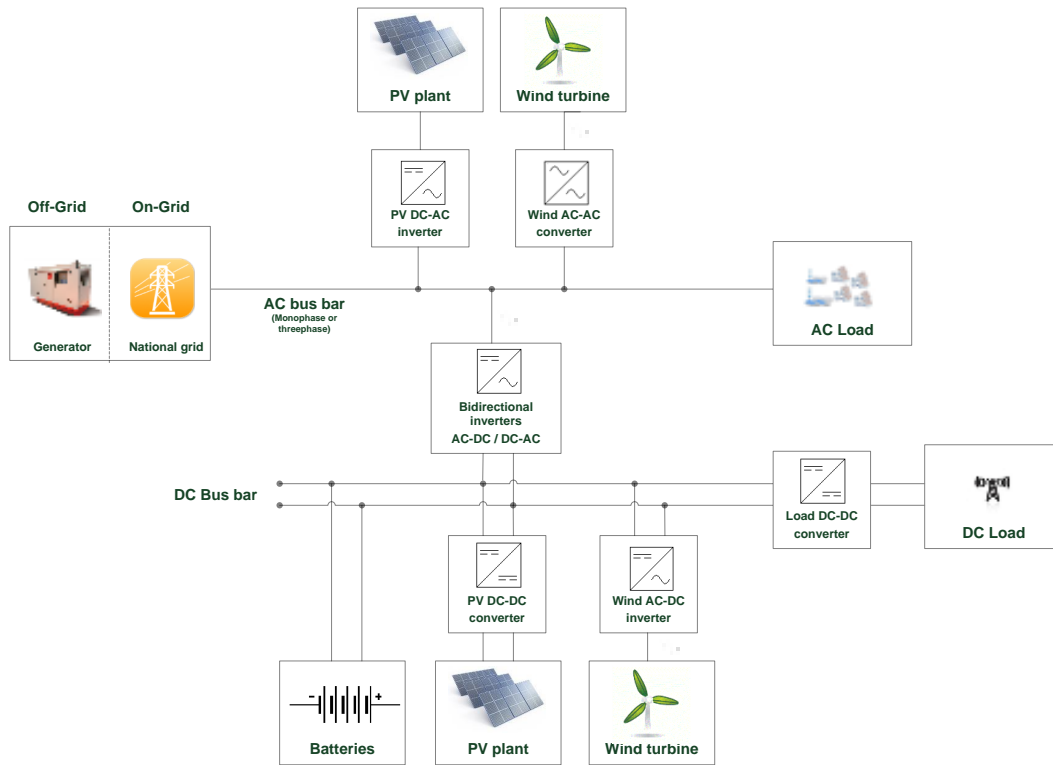


Figure 4.1 Reference diagram for a generic HES

All the introduced energy conversion processes are affected by their correspondent electric conversion efficiencies listed in Table 4.1 together with operative values, taken from the standard practice and literature (Wenham *et al.*, 2007).

Table 4.1 Standard electric conversion efficiencies for PV-BES systems

Electric conversion process	Converter	Efficiency range
DC/DC conversion (including MPPT)	PV DC-DC Converter	90-95%
DC/DC conversion	Load DC-DC Converter	92-95%
DC/AC conversion	Inverter/Bidirectional inverters	92-95%
AC/DC conversion	Bidirectional inverters	92-95%
AC/DC conversion	Wind AC-DC inverter	92-95%
AC/DC conversion	PV AC-DC inverter	92-95%
AC/AC conversion	Wind AC-AC Converter	92-95%
Battery roundtrip efficiency	Battery	80-95%

Both the energy production of each HES source and the load demand fluctuates and the HES has the purpose to meet the load generating energy at any time by optimally using each energy source, and storing excess energy for the later use in deficit generating conditions. The consequent optimization problems are to compute the optimal size and/or the operation control of the system with the aim of minimizing the total cost throughout the useful life of the installation, while responding to the load energy requirements, the unmet load, its environmental impact and other key objective functions (Kusakana & Vermaak, 2014). Khatib *et al.* (2013) present a review of HES integrating a PV plant, while Upadhyay & Sharma (2014) review the configurations, control and sizing

methodologies of HESs highlighting the technological, economic, socio-political and environmental factors involved in the HES evaluation criteria. The following *Paragraphs* present techno-economic models, and the related case studies, about the design and development of a grid-connected PV-BES HES and an off-grid PV-BES-Diesel generator HES preceded by a brief review of issues and scientific contributions on grid connected and off-grid HES.

#### 4.1 Grid-connected hybrid energy system (HES): overview

Grid connected HES generally refers to the integration of RESs, mostly PV plants and SWTs, and energy storage systems (ESSs), while the fossil fuel generators has, eventually, the function of emergency power source or back-up source in case of grid instability and unreliability. ESSs are generally considered an effective means for reducing the intermittency of electricity generated by RESs and to compensate/manage the negative impacts of grid connected distributed generation and its increasing levels of penetration on electricity grids (Eltawil & Zhao, 2010; Passey *et al.*, 2011). However, it currently remains unclear when and under which conditions ESSs, particularly BES systems, can be profitably operated in residential PV systems without supporting policy. In the following, some scientific contribution studying the feasibility and profitability of grid connected HES are presented and briefly described:

- Riffoneau *et al.* (2011) presents an optimal power flow management of a grid connected PV-BES system performing peak-shaving operation in order to decrease the cost for the owner of the system
- Colmenar-Santos *et al.* (2012) point out the profitability of a grid-connected PV facilities in Spain for household electricity self-sufficiency taking into account the technical and economic impact of storage systems
- Daud *et al.* (2013) presents an improved control strategy for a grid connected PV-BES systems for mitigating PV plant output power fluctuations
- Nottrott *et al.* (2013) develop a linear programming routine to optimize the energy storage dispatch schedule for a grid-connected PV-BES system
- Bayod-Rujula *et al.* (2013) propose sizing criteria of a HES, integrating PV plant and wind turbine, with battery storage focusing on self-consumption and considering interaction with the grid
- Hoppman *et al.* (2013) show the economic viability of storage solutions for small grid connected PV systems in Germany
- Murphy *et al.* (2014) consider the contribution of a grid connected PV-Diesel generator HES for energy supply in unreliable electric grid
- Finally, Scozzari *et al.* (2014) simulate and optimize an electricity storage system to be coupled to a small PV plant applied to an industry load, to calculate its profitability in the Italian regulatory context

In this context, the next *Paragraph 4.2* proposed a techno-economic analysis of a grid connected PV-BES HES. According to the results about PV plant profitability presented in the *Paragraph 2.1* and the decreasing contribution of national policies to support PV plants, PV plant find effective applications if the energy production is dedicated to local self-consumption, while the grid parity concept is extended to a comparison of PV energy generation costs toward the grid electricity tariff. The adoption of BES system and the study of the user energy demand to increase the self-consumption share of a specific energy user are investigated.

## 4.2 Grid-connected PV-BES HES design

This *Paragraph*, based on Bortolini *et al.* (2014), proposes a technical and economic model for the design of a PV-BES HES, in which the energy demand is mainly satisfied by the PV-BES HES purchasing the electricity from the grid if necessary, only. The model includes, as input, the irradiation level, the temperature and the energy demand profiles considering the whole system lifetime. Such data are hourly accounted within an entire reference year of analysis to evaluate a reliable PV system power size and BES system capacity able to minimize the levelized cost of the electricity (*LCOE*). The proposed model is applied to define the configuration of such a system for the new buildings of the Engineering and Architecture School at the Bologna University located in Bologna, Italy (latitude 44.49 North, longitude 11.34 East). A multi-scenario analysis is assessed varying the PV-BES system key parameters to define the best conditions minimizing *the LCOE* and making the proposed technical solution profitable.

According to the introduced purposes, the reminder of this paper is organized as follows: the next *sub-Paragraph 4.2.1* introduces the PV-BES system architecture defining the strategy and the logic of control adopted for energy dispatching and the load supply. The model to design the PV-BES system is analytically described in the *sub-Paragraph 4.2.2*, while the *sub-Paragraph 4.2.3* presents the introduced application including the definition of the model parameters and revising the input data. The obtained results are extensively discussed in the *sub-Paragraph 4.2.4* before drawing the paper conclusions in the last *sub-Paragraph 4.2.5* together with suggestions for further research.

### 4.2.1 PV-BES HES architecture

In a grid connected PV-BES HES, the grid plays a back-up function if the energy produced by the PV system and the energy available in the BES system are not able to satisfy the user load. Figure 4.2 shows a typical layout for a grid connected PV-BES system, including hourly power flow directions. The adoption of bidirectional inverters to charge the batteries through the grid is suggested in the case of grid instability to guarantee the energy supply during the grid lacks. Furthermore, the grid connection introduces the advantage of perfect power source availability and the possibility to sell the PV plant energy overproduction, if present.

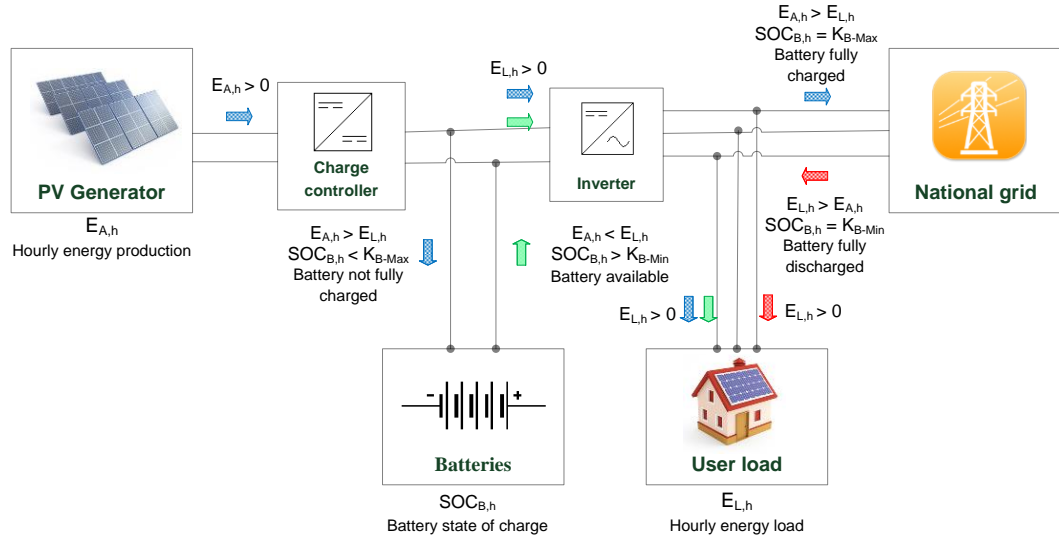


Figure 4.2 Reference diagram for the grid-connected PV-BES HES

At first, the battery physical constraints are in the following *Equation 4.1*, for each hour,  $h$ . The hourly state of charge,  $SOC_{B,h}$ , cannot exceed the maximum capacity,  $K_B^{max}$ , and it has to be higher than the minimum capacity,  $K_B^{min}$ , defined through the so-called maximum allowable depth of discharge,  $DOD$ , as in *Equation 4.2*.  $K_B^{min}$  and  $K_B^{max}$  are physically defined by specific voltage limits. When the battery voltage reaches such limits, the charge controller and the inverter interrupt the charging or the discharging process, respectively. The charging/discharging processes should be limited by a maximum charging/discharging current. Such a limit depends upon either the adopted battery charge controller/inverter or the physical battery limit to avoid significant capacity efficiency decreases or damages.

$$K_B^{min} \leq SOC_{B,h} \leq K_B^{max} \quad (4.1)$$

$$K_B^{min} = (1 - DOD) \cdot K_B^{max} \quad (4.2)$$

The HES aims to satisfy the hourly energy demand thanks to the energy produced by the PV modules or by the energy stored in the BES system. The grid works as a backup energy source if the PV-BES system is not able to fully satisfy the energy demand. Therefore, the hourly energy balance is defined in the following *Equation 4.3*.

$$E_{L,h} = E_{A,h} + E_{B,h} + E_{G,h} \quad (4.3)$$

The PV plant operates to meet the energy demand, while the energy surplus, if present, is firstly directed to the BES system, until the full charge, and, then, it is sold to the grid. On the contrary, in the case of low irradiance and during the night-time hours, the BES system supplies the energy deficit until  $SOC_{B,h}$  decreases to its minimum level. Then, the grid supplies the further lack of energy as a perfect power source. Figure 4.3

summarizes, through a flow-chart, the aforementioned management rules that univocally define, for each studied hour,  $h$ , the energy flows among the PV modules, the BES system, the load and the electric grid. Such logic of control and management is the basis for the proposed analytic model. It simulates the behaviour of the PV-BES HES. Such an approach, fully described in the next *sub-Paragraphs*, is able to predict the PV-BES energy performances and its costs.

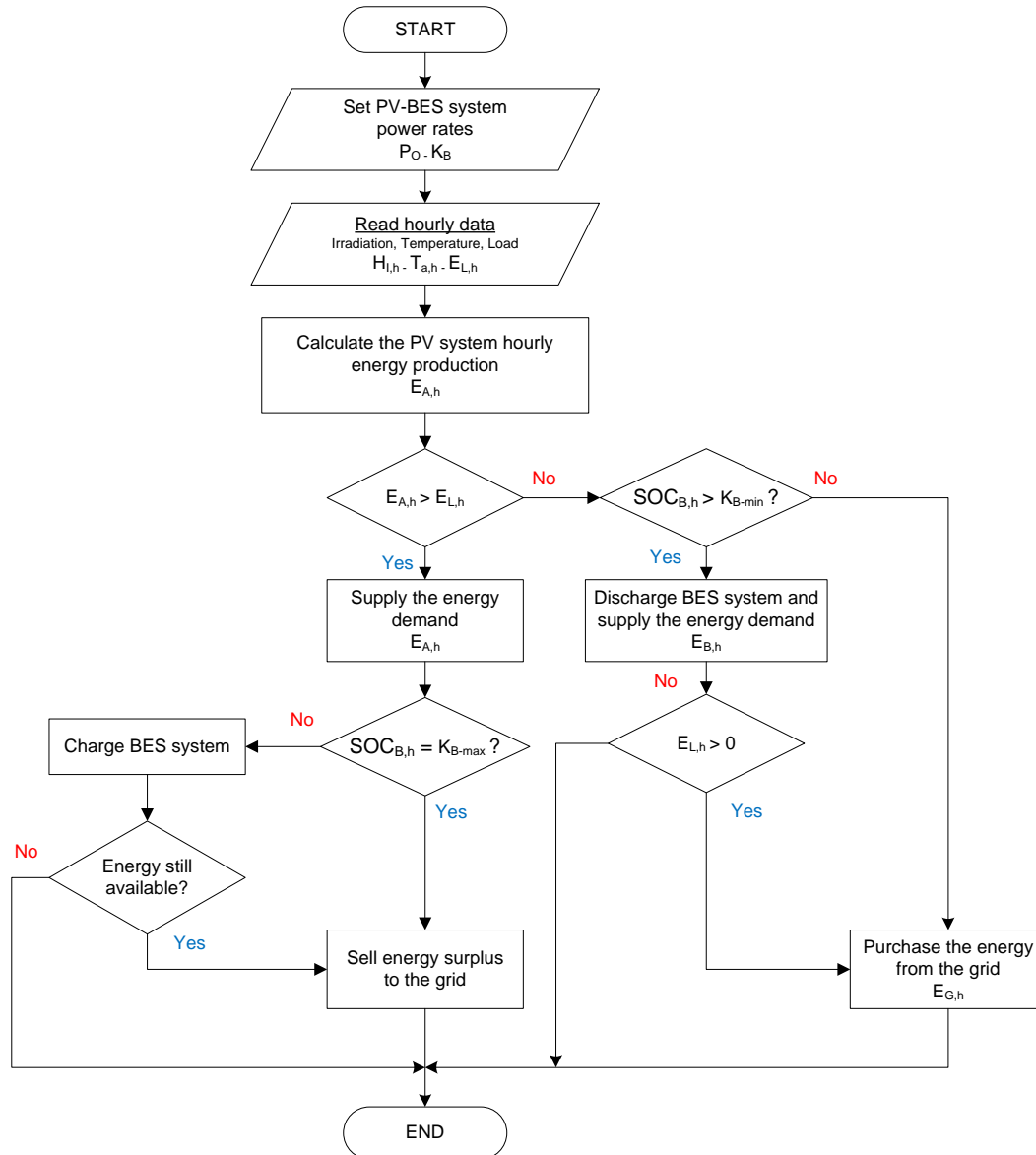


Figure 4.3 Energy flow control chart for each studied hour,  $h$

#### 4.2.2 PV-BES analytic model

This *sub-Paragraph* presents both the analytic model of the PV-BES HES and the economic model used to compute the *LCOE* assessing the system economic profitability. A parametric tool, implementing such models according to the previous energy flow control algorithm is developed in Microsoft Visual Basic for Applications™ environment and is used for the application and multi-scenario analysis in which the PV plant size and

the BES system capacity are varied into defined ranges to determine the best configuration of the whole system.

#### 4.2.2.1 PV plant analytic model

Focusing on the PV system, the model quantifies the hourly yield of the PV arrays,  $E_{A,h}$ , according to Equation 4.4 (Markvart, 2000).

$$E_{A,h} = H_{I,h} \cdot A_a \cdot \eta_{PV,h} \quad (4.4)$$

Where:

- $H_{I,h}$  is the total in-plane irradiation for the hour  $h$  [ $\text{kWh/m}^2$ ]
- $A_a = P_o / (\eta_{module} \cdot H_{I,r})$  is the effective PV module area, which depends on the PV plant nominal power  $P_o$  [ $\text{kWp}$ ] and the module efficiency  $\eta_{module}$  [%]. The lower the module efficiency, the higher the PV module area has to be.  $P_o$  refers to standard test conditions, *i.e.* solar spectrum of AM 1.5, module temperature of  $25^\circ\text{C}$  and reference in-plane irradiance,  $H_{I,r}$ , of  $1\text{kW/m}^2$  (IEC, 1998)
- $\eta_{PV,h}$  is the PV system overall efficiency for hour  $h$

As example, a  $1\text{kWp}$  PV plant produces  $1\text{kWh}$  if it operates in the standard test conditions for 1 hour. Irradiation levels lower than  $1\text{kW/m}^2$  and temperatures higher than  $25^\circ\text{C}$  reduce the PV plant yield. The model assumes a direct correlation between the energy production and the irradiation level. Such an assumption is acceptable because only significant low irradiation levels may further reduce the module performance due to the voltage drops. Figure 4.4 highlights the influence of the irradiance and the temperature on the electrical performances of a commercial mono-crystalline PV module showing a slight voltage drop if the irradiance decreases.

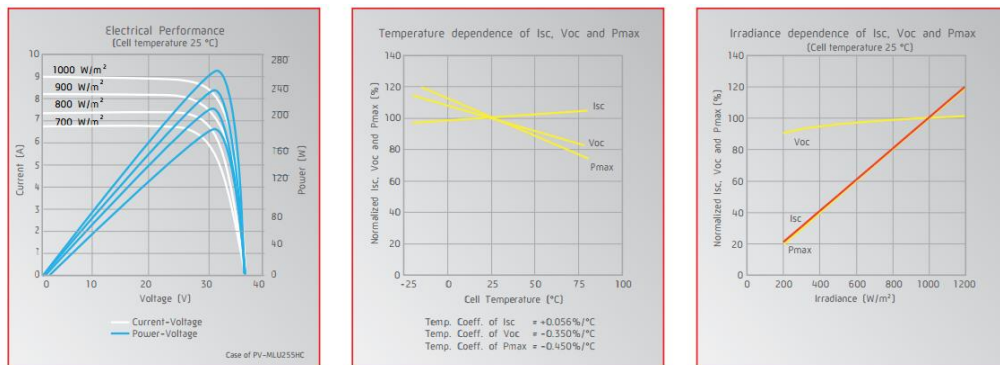


Figure 4.4 Irradiance and temperature influence on the PV module performance

The overall PV system efficiency,  $\eta_{PV,h}$ , depends on the reference module conversion efficiency, the power conditioning efficiency,  $\eta_{pc}$ , the efficiency decrease due to the cell temperature,  $\eta_{temp}$ , and the annual progressive PV module degradation,  $\eta_d$ , decreasing the PV plant performance in each year,  $j$ . Furthermore, the DC/AC electric conversion is affected by the inverter efficiency,  $\eta_{inv}$ . Wiring losses are assumed to be included in the

energy conversion device efficiency losses, while soiling and self-shading effects are neglected considering proper module maintenance and an adequate spacing between the PV arrays.

$$\eta_{PV,h} = \eta_{module} \cdot \eta_{pc} \cdot \eta_{temp,h} \cdot \eta_{inv} \cdot (1 - (j - 1) \cdot \eta_d) \quad (4.5)$$

Considering the temperature effect, the PV module efficiency decreases linearly as defined in *Equation 4.6* and *Equation 4.7* (Hernández-Moro & Martínez-Duart, 2013).

$$\eta_{temp,h} = [1 - \beta \cdot (T_{c,h} - T_{c,ref})] \quad (4.6)$$

$$T_{c,h} = T_{a,h} + [(NOCT - 20)/800] \cdot H_{I,h} \quad (4.7)$$

Where:

- $\beta$  is the temperature coefficient of solar cell efficiency [ $1/^\circ\text{C}$ ]
- $T_{c,h}$  is the PV cell temperature for hour  $h$  [ $^\circ\text{C}$ ]
- $T_{c,ref}$  is the PV cell reference temperature [ $^\circ\text{C}$ ]
- $T_{a,h}$  is the ambient temperature for hour  $h$  [ $^\circ\text{C}$ ]
- $NOCT$  is the normal operating cell temperature [ $^\circ\text{C}$ ]

In previous *Equations*,  $\beta$  and  $NOCT$  depends on the considered PV module technology and type. Such specifications are, generally, provided by the manufacturers. Considering silicon PV technology,  $\beta$  generally ranges from  $0.4\%/^\circ\text{C}$  to  $0.6\%/^\circ\text{C}$ , while  $NOCT$  ranges from  $45^\circ\text{C}$  to  $49^\circ\text{C}$ .

#### 4.2.2.2 BES system analytic model

The BES system capacity is expressed by both the nominal capacity,  $K_B$  and the number of autonomy hours,  $AH$ .  $AH$  represents the number of hours that a fully charged battery is able to supply the energy demand considering an average hourly load,  $E_{L,a}$  and the discharging process efficiency,  $\eta_{ach}$ .

$$AH = (K_B \cdot \eta_{inv} \cdot \eta_{ach} \cdot DOD) / E_{L,a} \quad (4.8)$$

The BES system capacity, efficiency and maximum number of cycles are heavily affected by the external temperature. A decrease of 1% per degree occurs below  $20^\circ\text{C}$ . On the contrary, high temperatures accelerate the aging and the battery self-discharge (Wenham *et al.*, 2007). For these reasons, BES system is assumed to be stored in a  $20^\circ\text{C}$  controlled room. During the charging process, *i.e.* when the PV production,  $E_{A,h}$ , exceeds the energy demand,  $E_{L,h}$ ,  $SOC_{B,h}$  is increased according to *Equation 4.9*.



$$SOC_{B,h} = \max\{SOC_{B,h-1} \cdot (1 - \sigma) + [(E_{A,h} - E_{L,h})/\eta_{inv}] \cdot \eta_{ch}, K_B^{max}\} \quad (4.9)$$

Where:

- $\sigma$  is the BES system hourly self-discharge rate [%]
- $\eta_{ch}$  is the BES system charging efficiency [%]

The charging process ends when either the BES system reaches the maximum capacity or the energy storage of the available energy is completed. On the contrary, if the PV production,  $E_{A,h}$ , cannot satisfy the energy demand,  $E_{L,h}$ , the battery starts the discharging process, in case of available energy stored, until the lower capacity limit is reached or the load demand is completely met (*Equation 4.10*).

$$SOC_{B,h} = \min\{SOC_{B,h-1} \cdot (1 - \sigma) - (E_{L,h} - E_{A,h})/(\eta_{inv} \cdot \eta_{dch}), K_B^{min}\} \quad (4.10)$$

In both *Equation 4.9* and *Equation 4.10* the initial BES system *SOC* is  $SOC_{B,0} = K_B^{min}$ .

#### 4.2.2.3 Economical model

The PV-BES system economic assessment includes the *LCOE* and the lifetime system study. In the following, details about such economic performance analysis are provided. The *LCOE* is a widely adopted index to assess the economic feasibility of power systems based on RESs or other sources (Branker *et al.*, 2011; Bazilian *et al.*, 2013; Hernández-Moro & Martínez-Duart, 2013). In the present context, the *LCOE* represents the equivalent grid electric tariff that makes the discounted value of the revenues,  $R_j$ , equals to the discounted value of the costs,  $C_j$ , during the economic lifetime of the PV-BES HES. The *LCOE* represents the unitary cost of the produced electricity and it allows the economic comparison of different power generation technologies. The following *Equation 4.11* introduces the *LCOE* expression as the balance between revenues and costs during the whole system lifetime.

$$\sum_{j=1}^n \frac{R_j}{(1+OCC)^j} = \sum_{j=1}^n \frac{LCOE \cdot (1+g)^{j-1} \cdot E_j}{(1+OCC)^j} = C_0 + \sum_{j=1}^n \frac{C_j \cdot (1+g)^{j-1}}{(1+OCC)^j} \quad (4.11)$$

Where:

- $OCC$  is the opportunity cost of capital [%]
- $g$  is the inflation rate [%]
- $C_0$  is the PV-BES system turnkey cost [€]

From *Equation 4.11*, *LCOE* is equal to the ratio between the sum of the system costs and the overall PV plant energy production, both discounted and affected by the inflation.

$$LCOE = \left( C_0 + \sum_{j=1}^n \frac{C_j \cdot (1+g)^{j-1}}{(1+OCC)^j} \right) / \sum_{j=1}^n \frac{E_j \cdot (1+g)^{j-1}}{(1+OCC)^j} \quad (4.12)$$

Particularly, the objective function of the proposed model deals with the cost minimisation to meet the energy demand so that, in *Equation 4.13*, the annual energy production,  $E_j$ , is replaced by the reference year energy demand,  $E_L$ .

$$LCOE = \left( C_0 + \sum_{j=1}^n \frac{C_j \cdot (1+g)^{j-1}}{(1+OCC)^j} \right) / \sum_{j=1}^n \frac{E_L \cdot (1+g)^{j-1}}{(1+OCC)^j} \quad (4.13)$$

#### 4.2.2.4 Lifetime PV-BES cost analysis

The PV-BES HES costs include several contributions due to the PV modules, the inverter, the battery banks and the battery charge controller. The PV module and installation costs,  $C_{PV}(P_o)$ , and the inverter costs,  $C_{inv}(P_o)$ , are expressed as a function the PV rated power  $P_o$ . In particular,  $C_{PV}(P_o)$  includes the purchasing and installations costs of multiple components, e.g. cells, mechanical and electrical connections, mountings and electrical output conversion devices, etc. Nowadays, silicon technologies, i.e. Amorphous (a-Si), Mono-crystalline (m-Si) and Poly-crystalline (p-Si) modules, are the dominant and widely adopted technologies for PV applications. The PV module and installation costs for different silicon technologies are obtained through a market research, including EU and extra EU manufacturers. Figure 4.5 summarizes the results presenting the trend of the turnkey costs (VAT excluded) as a function of the system plant size for both the EU and the extra EU manufacturers and considering a-Si and m-Si/p-Si technologies (Bortolini *et al.*, 2013).

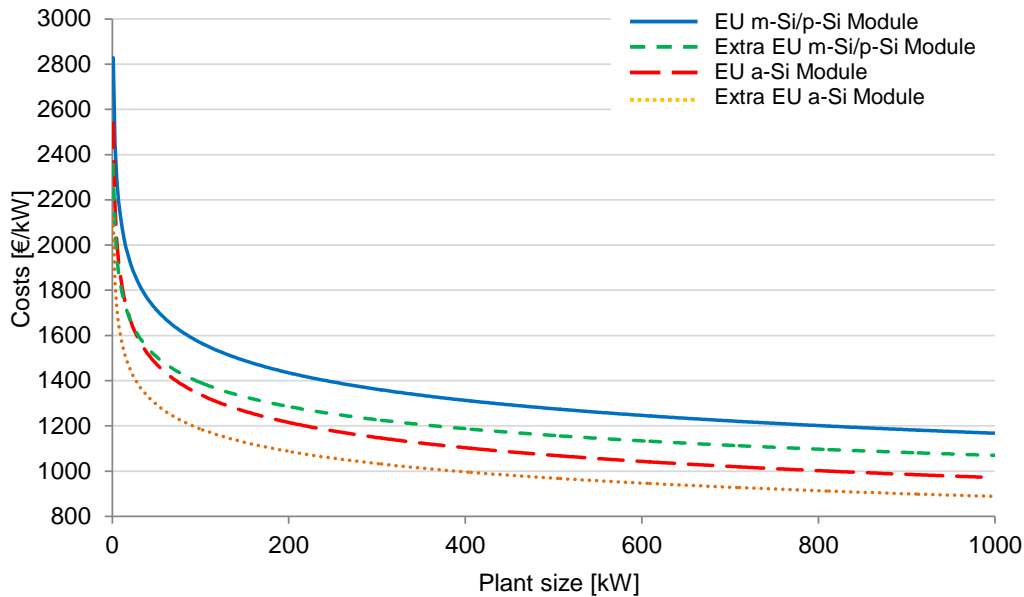


Figure 4.5 Trend for turnkey PV system costs (2012-2013)

The regression functions, to evaluate the PV system turnkey costs for a generic plant size are in the following *Equations 4.15-4.18*.

$$C_{PV}(P_o) = c_{module} \cdot P_o \quad (4.14)$$

$$c_{module}^{EU\ cSi} = 2828.7 \cdot P_o^{-0.128} \quad (4.15)$$

$$c_{module}^{Extra\ EU\ cSi} = 2539.9 \cdot P_o^{-0.139} \quad (4.16)$$

$$c_{module}^{EU\ aSI} = 2356.4 \cdot P_o^{-0.114} \quad (4.17)$$

$$c_{module}^{Extra\ EU\ aSI} = 2115.8 \cdot P_o^{-0.126} \quad (4.18)$$

Finally, the battery bank cost and the charge controller cost are proportional to the battery capacity and the input current, respectively. *Equation 4.19* presents the PV-BES system turnkey cost drivers, composing  $C_0$ .

$$C_0 = C_{PV}(P_o) + C_{inv}(P_o) + C_{cc} \cdot P_o / V_B + C_B \cdot K_B \quad (4.19)$$

Concerning the operating annual costs during the system lifetime, the maintenance activities,  $C_j^{OM\&I}$ , and the component replacement (inverter,  $C_j^I$ , batteries,  $C_j^B$ , charge controller,  $C_j^C$ ) are required to prevent failures and the performance decreases. Furthermore, the amount of energy purchased from the grid introduces an additional cost,  $C_j^E$ , proportional to the grid electricity tariff,  $e_c$ , while the energy sold to the grid, proportional to the electricity market price,  $e_p$ , is computed in the following *Equation 4.20* as an opportunity cost,  $C_j^S$ .

$$C_j = C_j^{OM\&I} + C_j^E + C_j^B + C_j^I + C_j^C - C_j^S \quad (4.20)$$

### 4.2.3 Case study

The proposed model is validated through a case study about the design of a grid connected PV-BES HES to meet the energy demand of the Engineering and Architecture School of the Bologna University, located in Bologna, Italy (latitude 44.49 North, longitude 11.34 East). All the input data are presented in this *Paragraph*, while the key outcomes are in the *sub-Paragraph 4.2.4*.

#### 4.2.3.1 Temperature and irradiation profiles

Figure 4.6 and Figure 4.7 show the hourly temperature and irradiation profiles for Bologna geographical site. Data are referred to the average monthly conditions and they come from the Photovoltaic Geographical Information System (PVGIS) of the Joint Research Center (JRC). Irradiation data are measured considering an optimal inclination angle of the solar collector equals to 36 degrees. The aggregate global annual irradiation level is of 1715 kWh/m<sup>2</sup>/year (PVGIS, 2013).

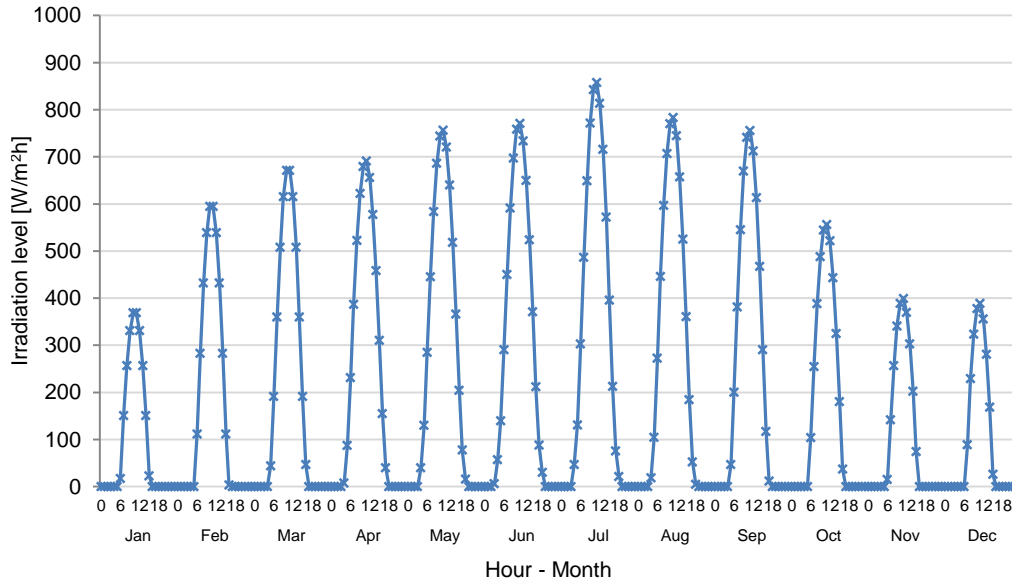


Figure 4.6 Monthly average irradiation profile for Bologna, Italy

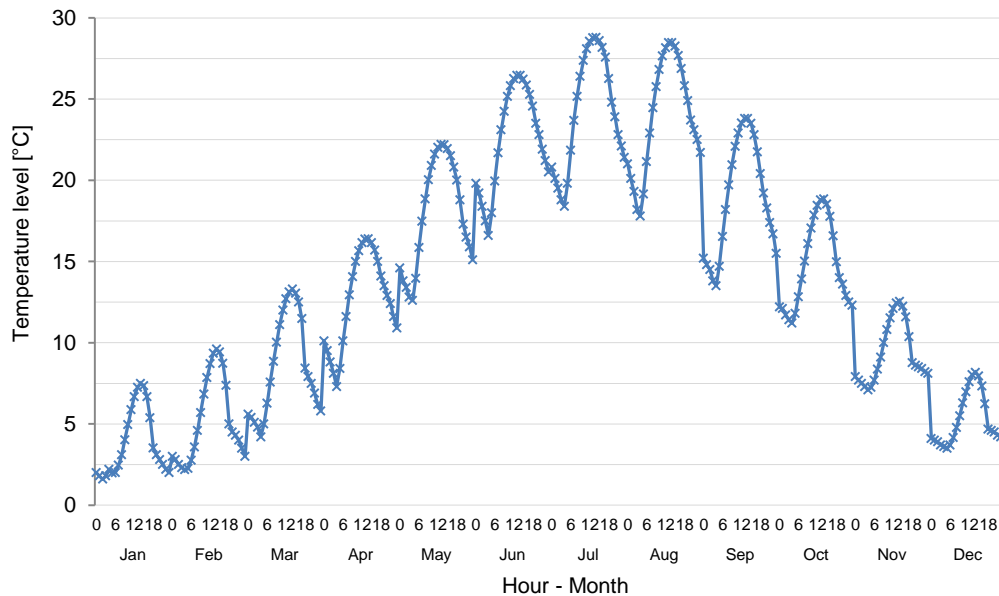


Figure 4.7 Monthly average temperature profile for Bologna, Italy

#### 4.2.3.2 Load profile

The hourly load profile for the university complex is depicted in Figure 4.8 and Figure 4.9. It highlights an average load of 55kW (the red dashed line) and a base-load demand ranging from 30kW to 50kW during the night-time and the weekends, representing the 30-50% of the daily peak. This means that it is potentially profitable to store energy to meet the night-hour energy demand. Furthermore, June and July show the highest demand of electric energy due to the significant load from air conditioning, while August is marked by the lowest energy consumption due to the activity summer break.

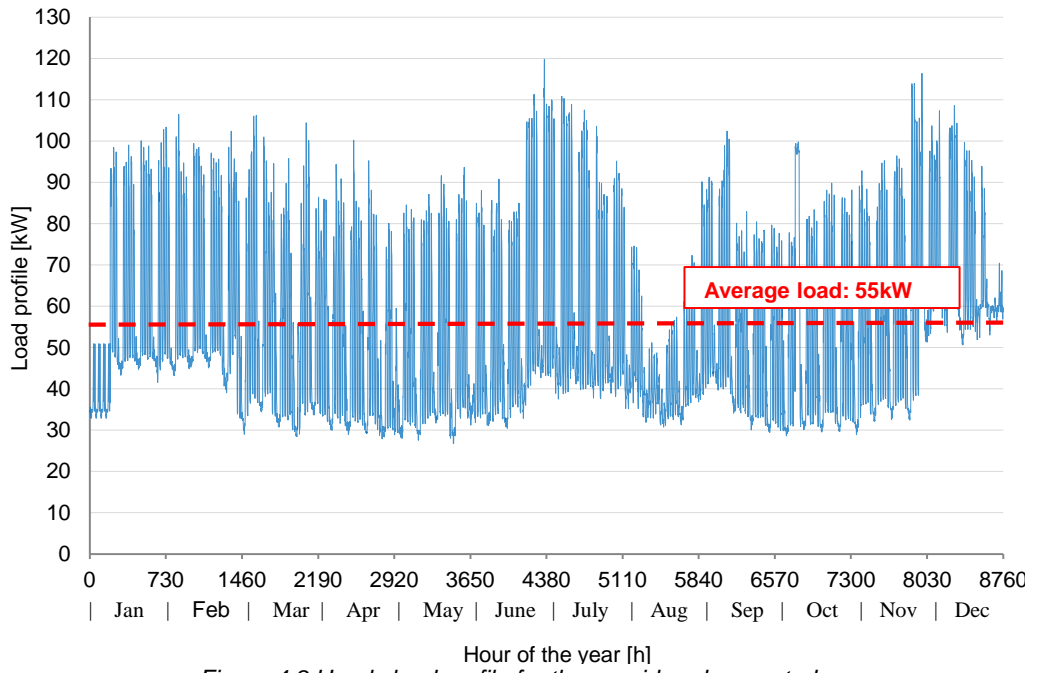


Figure 4.8 Hourly load profile for the considered case study

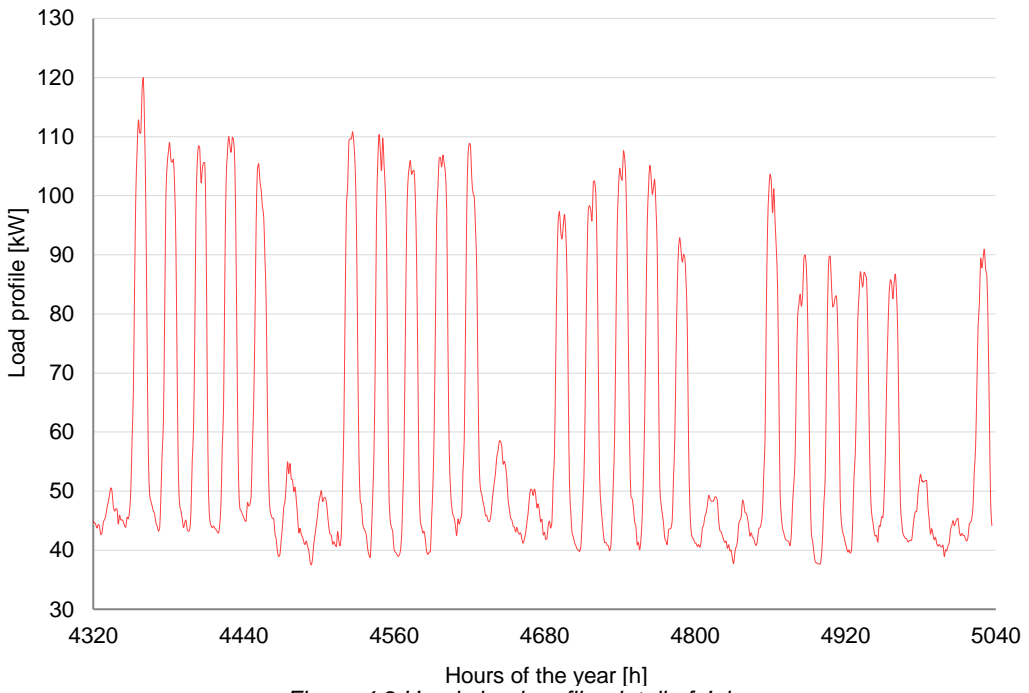


Figure 4.9 Hourly load profile, detail of July

## 4.2.3.3 Input Data

In the next Tables 4.2-4.4, the boundary conditions for the previously introduced parameters and the other input data included in the analytic model are reported adopting fix values or ranges of variation according to the standard practice and the available data from industrial component datasheets.

Table 4.2 Case study adopted values and ranges: PV plant

PV plant		
Parameter	Adopted value/range	References
$P_o$	50-600kWp, step 25kWp	
$H_{I,r}$	1kW/m <sup>2</sup>	(IEC, 1998)
$n$	25 years	(Diaf <i>et al.</i> , 2008; Shaahid <i>et al.</i> , 2009; Ismail <i>et al.</i> , 2013)
$\eta_d$	0.005	(Banker, 2011; Thevenard & Pelland, 2013)
$\eta_{module}$	0.14	
$\eta_{pc}$	0.95	(Rydh & Sandén, 2005a; Rydh & Sandén, 2005b; Eitawil & Zhao, 2013)
$\eta_{inv}$	0.92	(Rydh & Sandén, 2005a; Rydh & Sandén, 2005b; Wenham <i>et al.</i> , 2007)
$\beta$	0.005/°C	(Kaabeche <i>et al.</i> , 2011; Tina & Scandura, 2012)
$NOCT$	47°C	(Riffonneau <i>et al.</i> , 2011; Tina & Scandura, 2012)
$T_{c,ref}$	25°C	(IEC, 1998)
$C_{PV}(P_o)$	$2539.9 \cdot P_o^{-0.139}$	(Bortolini <i>et al.</i> , 2013)
$C_{inv}(P_o)$	$0.0325 \cdot P_o^2 + 196,25 \cdot P_o + 350.95$	(Bortolini <i>et al.</i> , 2013)
$C_j^{OM\&I}$	$0.01 \cdot P_o$ for $j = 1, \dots, n$	(Diaf <i>et al.</i> , 2008; Bortolini <i>et al.</i> , 2013)
$C_j^I$	$0.0325 \cdot P_o^2 + 196,25 \cdot P_o + 350.95$ for $j = 10, 20$ only	(Rydh & Sandén, 2005a; Rydh & Sandén, 2005b; Diaf <i>et al.</i> , 2008; Bortolini <i>et al.</i> , 2013)

Table 4.3 Case study adopted values and ranges: BES system

BES system		
Parameter	Adopted value/range	References
$K_B$	0-850kWh, 0-10h, step 0.5h	Equation 4.8
$\sigma$	0.00583% (0.14% per day)	(Markvart & Castaner, 2003)
$\eta_{ach}$	0.895	(Rydh & Sandén, 2005a; Rydh & Sandén, 2005b; Battke <i>et al.</i> , 2013)
$\eta_{ch}$	0.895	(Rydh & Sandén, 2005a; Rydh & Sandén, 2005b; Battke <i>et al.</i> , 2013)
$DOD$	0.80	(Rydh & Sandén, 2005a; Rydh & Sandén, 2005b; Wenham <i>et al.</i> , 2007; Battke <i>et al.</i> , 2013)
$C_B$	150€/kWh	(Solarbuzz, 2013)
$V_B$	96V	
$C_{cc}$	4.38€/A	(Solarbuzz, 2013)
$C_j^B$	equal to the installation cost for $j = 6, 12, 18$ only	(Thevenard & Pelland, 2013; Battke <i>et al.</i> , 2013)
$C_j^C$	equal to the installation cost for $j = 10, 20$ only	(Muselli <i>et al.</i> , 2000)

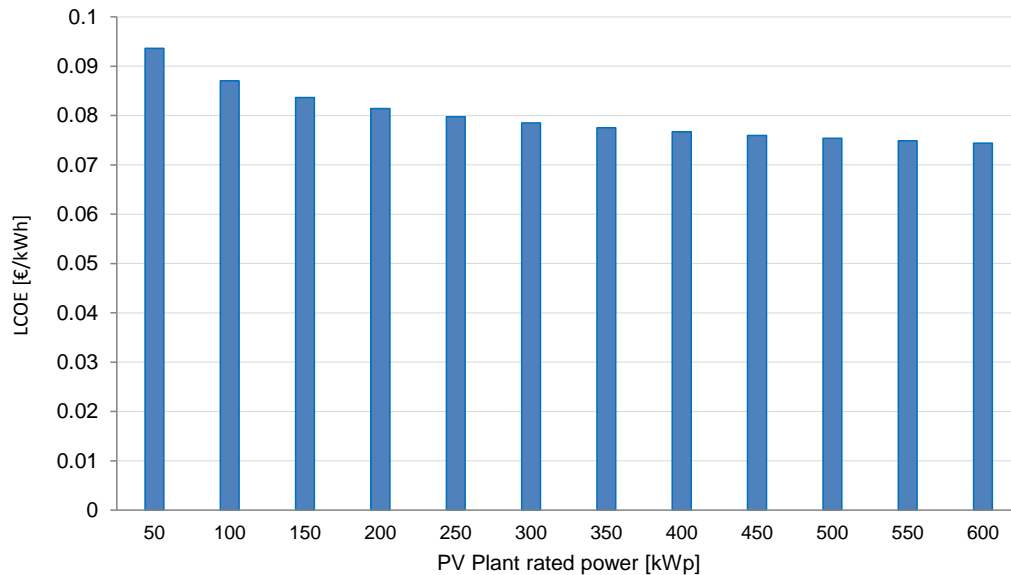
Table 4.4 Case study adopted values and ranges: financial and environmental param.

Financial and environmental parameters		
Parameter	Adopted value/range	References
$H_{I,h}$	See Figure 4.6	(PVGIS, 2013)
$T_{a,h}$	See Figure 4.7	(PVGIS, 2013)
$E_{L,h}$	See Figure 4.8-4.9	
$e_c$	0.20€/kWh	(EC, Eurostat, 2013)
$e_p$	0.04€/kWh	(Bortolini <i>et al.</i> , 2013)
$g$	0.03	(EC, Eurostat, 2013)
$OCC$	0.05	

A wide range of system configurations occur and they are examined and compared to determine the best plant configuration. For each scenario the  $LCOE$  is calculated together with the hourly energy yield, the energy request from the grid, the energy surplus and the battery state of charge. The key results and outcomes are compared and discussed in the following *sub-Paragraph 4.2.4*.

#### 4.2.4 Results and discussions

First of all, the  $LCOE$  values of different PV plant rated powers are calculated according to *Equation 4.12* (referred to the annual PV plant energy production) and the results are presented in Figure 4.10. Suh result represents the cost of the PV plant for each kWh produced.

Figure 4.10  $LCOE$  values for different PV rated powers (2013 extra EU c-Si technology)

The impact of PV-BES HES on the user energy demand costs is evaluated as follows. According to *Equation 4.8* and the parameter values defined in previous Table 4.3, each hour of storage autonomy, *i.e.*  $AH = 1$ , corresponds to, approximately, 85kWh of the BES system capacity (see *Equation 4.21*).

$$K_B^{AH=1} = (55kWh \cdot 1AH) / (0.92 \cdot 0.895 \cdot 0.80) \cong 85kWh \quad (4.21)$$

Figure 4.11 shows the *LCOE* values (according to Equation 4.13 and referred to the annual energy demand) for the main configurations of PV plant rated power and BES capacity. As previously explained, the results are comparable to the electricity grid tariff, assumed equal to 0.20€/kWh, represented with the red dashed line.

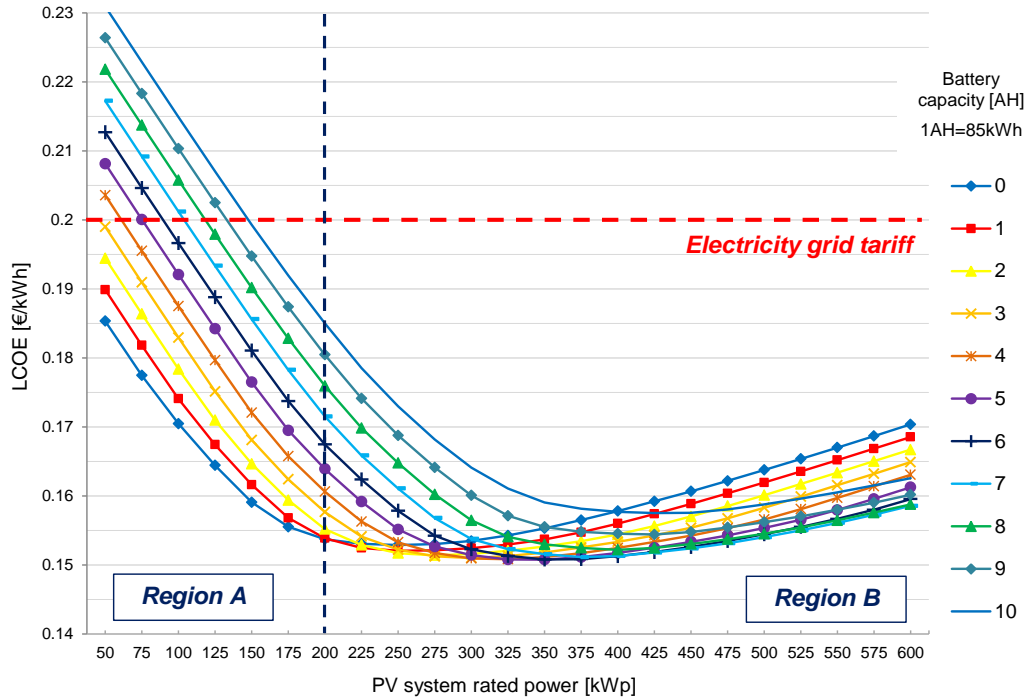


Figure 4.11 *LCOE* values for different PV rated powers and BES system capacities

PV plants without BES system ( $AH = 0$ ) lead to *LCOE* values lower than 0.20€/kWh for all the tested scenarios. Furthermore, the graph defines two distinct regions depending on the PV system rated power. From 0 to 200kWp, *i.e.* the Region A, BES system is not convenient, while its adoption becomes profitable with PV rated powers higher than 200kWp, *i.e.* the Region B. Furthermore, the higher the PV rated power, the higher the required BES system capacity is. The best scenario, presenting a *LCOE* value of 0.151€/kWp, is for 350kWp and 5.5 autonomy hours of the BES system. Details of such a scenario are summarized in Table 4.5 together with the correspondent data for the grid only and PV only benchmarks.

Table 4.5 PV-BES HES and traditional system best scenarios

Parameter	PV-BES HES	Grid only	PV only
PV rated power	350kWp	0kWp	250kWp
BES system capacity	5.5h (467.5kWh)	0h	0h (0kWh)
<i>LCOE</i>	0.151€/kWh	0.200€/kWh	0.153€/kWh
Yearly energy production	463'413kWh	0 kWh	331'010kWh
Yearly energy demand	480'214kWh	480'214kWh	480'214kWh
Yearly energy purchase	142'385kWh	480'214kWh	248'871kWh
Yearly energy surplus	101'860kWh	0 kWh	97'750kWh
Energy self-consumed	70.3%	0.0%	48.2%



Furthermore, in the following Figure 4.12 to Figure 4.15, the hourly trends of the parameters included in Table 4.5 are presented for the PV-BES HES *LCOE* best scenario. Figure 4.12 shows the average monthly energy production before power conditioning and the DC/AC conversion. The effect of the ambient temperature on the module efficiency generates an energy production peak of about 210-220kWh from March to September, except for July with 240kWh.

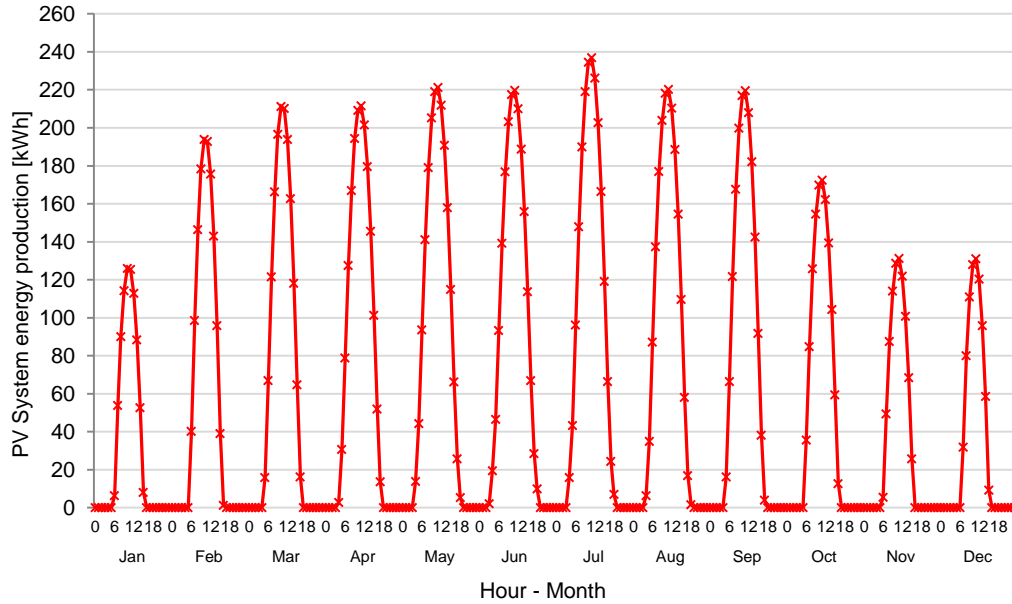


Figure 4.12 Monthly average energy produced by PV system

The hourly state of charge of the BES system, relating the amount of the stored energy to both the electric load and the irradiation level for each hour of the day, according to the energy flow control algorithm of Figure 4.3, is exemplified in Figure 4.13 detailing the trend for the month of April.

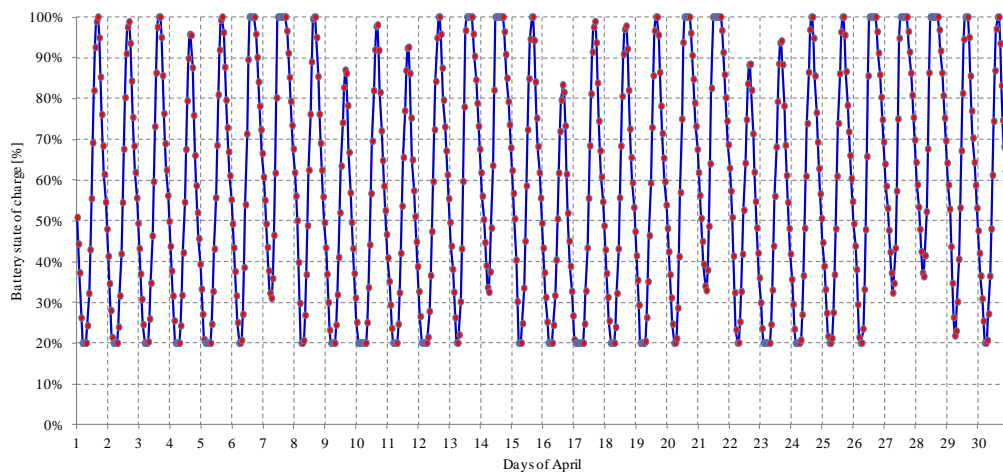


Figure 4.13 Hourly detail of the battery state of charge for the month of April

Aggregately, the monthly average trend of  $SOC_{B,h}$  is presented in the following Figure 4.14. The BES system is not exploited during the low irradiation periods, while the maximum capacity is frequently reached from March to September. The average  $SOC_{B,h}$  is of about 225kWh with 39% of fully discharged condition, i.e.  $SOC_{B,h} = K_B^{min}$ , and 16%

of fully charged condition, i.e.  $SOC_{B,h} = K_B^{max}$ , occurrences. The  $SOC_{B,h}$  trend reflects the amount of energy surplus and the energy purchased from the grid shown in Figure 4.15. Energy purchase is equal to the 30% of the whole energy demand and is required, especially, in the winter period and during the July peak, while the energy surplus corresponds to the 22% of the global energy production and it is concentrated during the high irradiation periods.

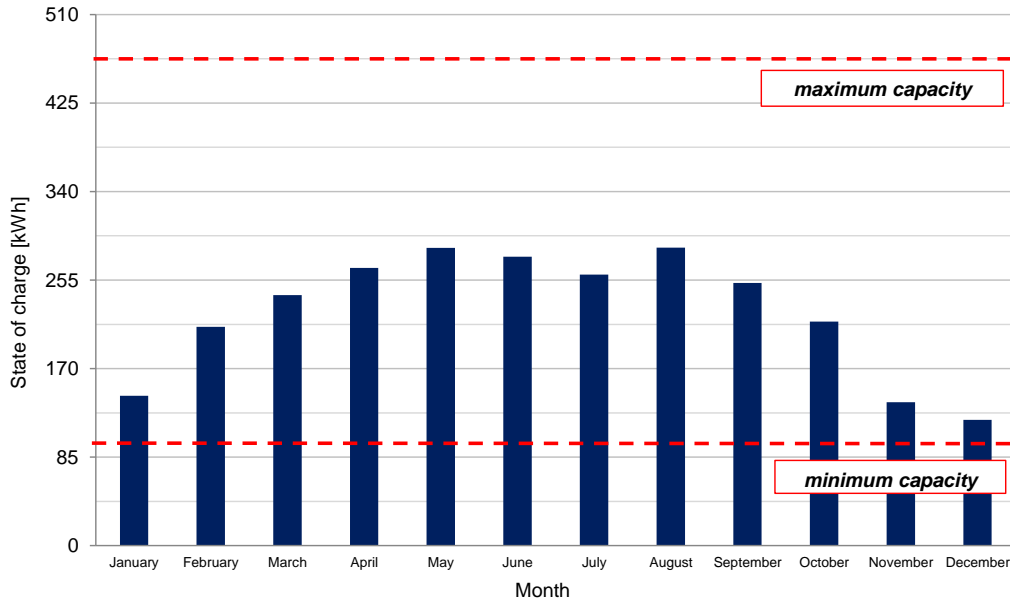


Figure 4.14 Average monthly BES system state of charge,  $SOC_{B,h}$

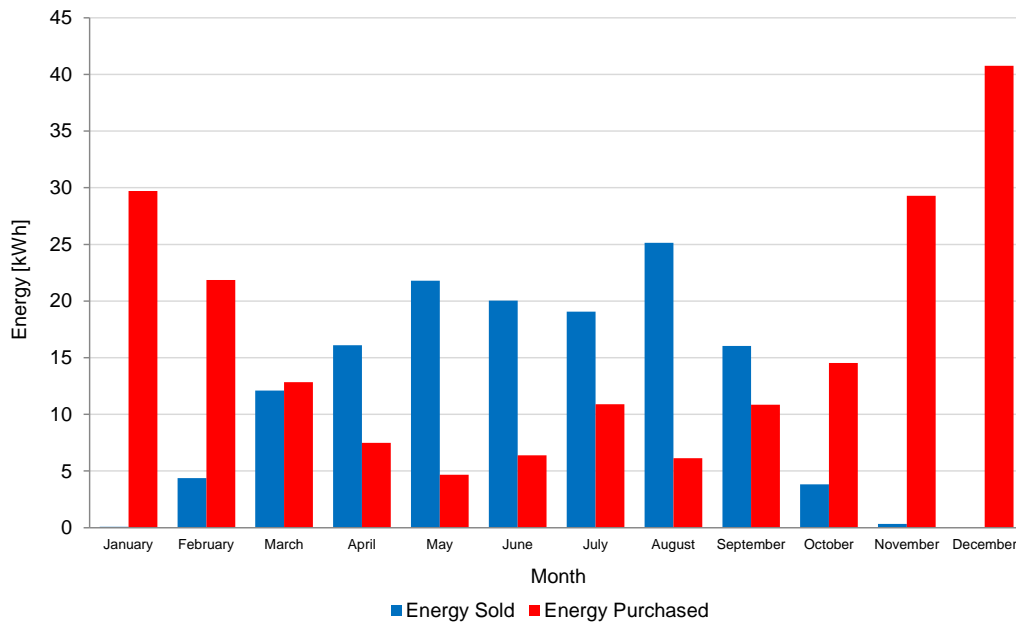


Figure 4.15 Average monthly energy surplus and energy purchased from the grid

Finally, the charge/discharge processes are of interest. The trend of charge/discharge current is represented in Figure 4.16. The maximum charge and discharge currents are respectively 1300A and 1000A.

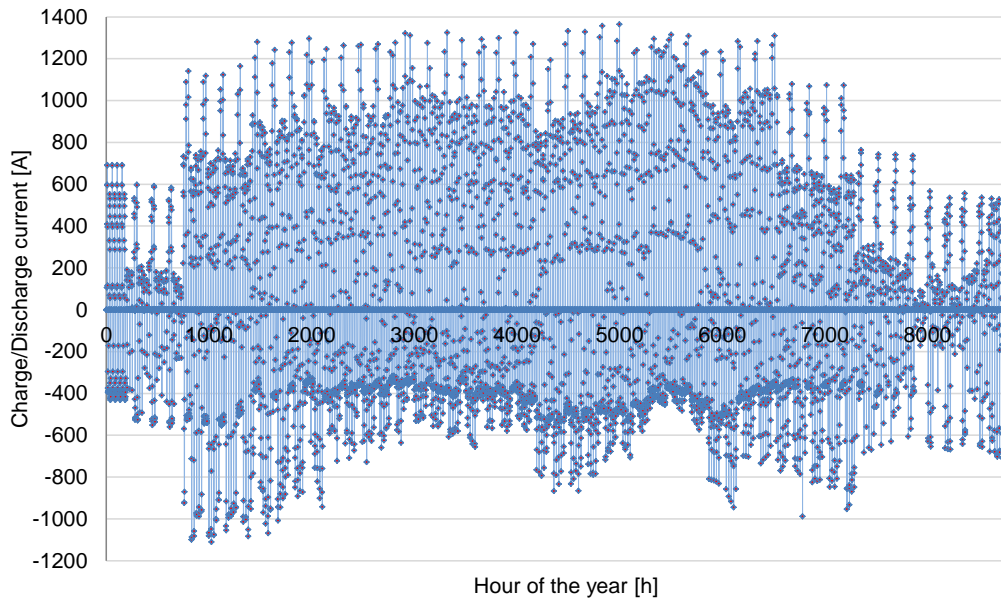


Figure 4.16 Battery Charge/Discharge currents

A 467.5kWh BES system with a nominal voltage of 96V means a nominal capacity of about 5000Ah. The maximum discharge current corresponds to a C/5 discharge rate which represents an acceptable critical value to guarantee the reliable battery operations, while the charge currents overcome the typical suggested value for standard load and batteries (1/10 of the nominal capacity equals to 500A) the 50% of charging hours. The introduction of current limitations for charge and discharge processes or the battery capacity increase depends on the properties of the adopted battery. As example, VRLA batteries allows higher charge current.

Concerning costs, Figure 4.17 shows the PV-BES HES cost distribution for the best scenario. The energy purchase and the system turnkey costs cover 75% of the total costs, while the maintenance activities, including component replacements, cause the remaining 25% of the total costs. Among them, the incidence of the BES system purchase and replace represents the 27% of the total costs.

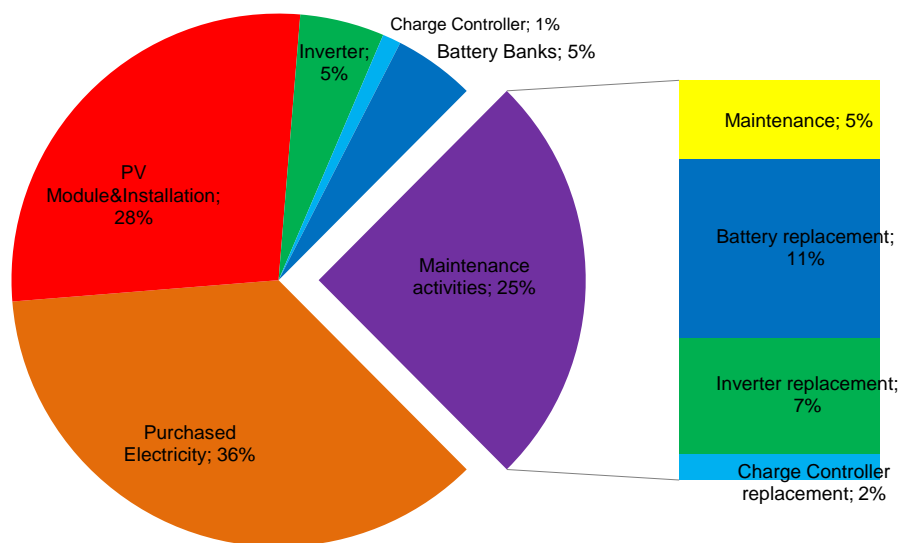


Figure 4.17 PV-BES system cost distribution for the best economic scenario

Finally, the technical feasibility of the PV–BES HES, defining the PV array specifications (See Table 4.6), is addressed verifying whether the considered university complex offers the necessary rooftop area to install the PV modules with a global rated power of 350kWp. Fig. 4.18 shows the university complex layout highlighting the available solar collector rooftop area,  $A_a^{max}$ , equal to 8000m<sup>2</sup>. Considering a standard ratio between the PV module area and the required surface, the so-called packing factor, of 3, the upper limit to the PV power capacity possible to install is of about 400kWp. In the selected configuration, the required rooftop area to install the 350kWp PV power modules is close to 7000m<sup>2</sup>, confirming the feasibility of the chosen PV–BES HES.

Finally, concerning the required space for the BES system installation, the common volume requirement is of about 0.0134m<sup>3</sup>/kWh so that a volume of 6.27m<sup>3</sup> is necessary in the chosen configuration. Such a value, properly increased due to the space for utilities, connections and further devices, fits with the available space in the engine room of the university complex.

Table 4.6 Design parameters for the PV-BES system

PV module		Inverter		PV array	
MPPT voltage	35.1V	AC Voltage	480V	Nameplate capacity	349kWp
MPPT current	8.13A	AC Power	50kW	Number of modules	1222
Open circuit voltage	44.3V	Efficiency	92%	Number of inverters	7
Short circuit current	8.65A	Max DC Voltage	600V	Module per string	13
Number of cells in series	72	Max AC Current	170A	String in parallel	94
Cells area	1.75m <sup>2</sup>			Total module area	2358 m <sup>2</sup>
Module area	1.93m <sup>2</sup>			String open circuit voltage	575.9V
Efficiency	14.8%			String MPPT voltage	456.3V
				Packing factor	3
				Required area	7074m <sup>2</sup>

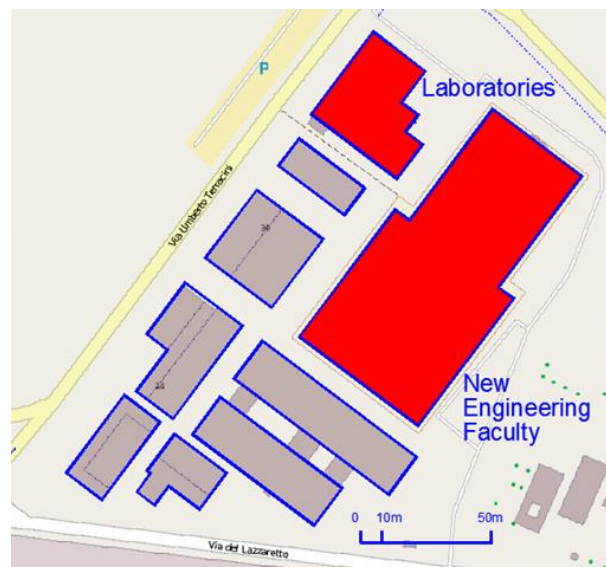


Figure 4.18 University complex layout and available rooftop area

#### 4.2.5 Conclusions

This *Paragraph* presents a technical and economic model to support the design of a grid-connected PV plant with BES system. The energy demand is supplied by both the PV-BES system and the grid, used as a back-up source. The proposed model is based on an energy flow control algorithm oriented to meet the energy load profile with PV-BES HES firstly. The model is useful to design such a system determining the PV rated power and the battery capacity that minimize the *LCOE* of the PV-BES HES. The amount of energy purchased from the grid introduces an additional cost proportional to the grid electricity tariff, while the energy sold to the grid, proportional to the electricity market price, is computed as an opportunity cost. As a consequence, the obtained *LCOE* values can be directly compared with the grid electricity tariff, showing immediately the competitiveness and profitability of the PV-BES HES configuration.

The main input refer to the hourly energy demand profile, the hourly available irradiation and the temperature levels measured at the installation location.

The model is applied to design the PV-BES HES for the new buildings of the Engineering and Architecture School at the Bologna University, Italy. Several scenarios are tested varying the system rated power and capacity. Considering 0.20€/kWh as energy purchase cost and 0.04€/kWh as energy selling price, the best PV-BES HES configuration leads to a *LCOE* equal to 0.151€/kWh with an energy cost reduction of 24.5% compared to the grid electricity price and an energy self-consumption rate around 70%. This result is comparable with the PV only solution (No BES system) which leads to a *LCOE* equal to 0.153€/kWh with an energy cost reduction of 23.5% and an energy self-consumption rate up to 48%. The technical feasibility of the proposed plant is, finally, checked matching the required PV surface to the available rooftop area.

Concluding, the results, referred to the year 2013, show the economic profitability of a PV plant designed to meet the energy demand of the user in a location with medium-high irradiation level ( $\approx 1,700 \text{ kWh/m}^2 \text{ year}$ ), and therefore oriented to self-consumption, while the competitiveness of storage systems is connected to the gap between the purchase cost and selling price of electricity from the grid. However, the high BES system costs due to the initial investment and the maintenance activities and the eventual presence of incentives and benefits on the energy sold to the grid can make the investment not particularly attractive.

Further activities focus on the application of the proposed model to other scenarios, e.g. off-grid solutions, to compare its performances under several constraints and different location features. The multi-objective system design is another interesting research path to develop considering both the economic and the environmental performances with the final aim to define the system configuration that contemporary minimizes the *LCOE* and the most widely adopted environmental impact indicators, like the carbon footprint.

### 4.3 Off-grid HES design: overview

The adoption of off-grid HES introduces benefits and risks. Hazelton *et al.* (2014) reviews the existing literature to identify claimed and demonstrated benefits and risks for HES. The most commonly identified benefits are those that are easy to measure: reduced cost and improved electrical services. Other benefits such as the social or environmental benefits are less commonly demonstrated, but are frequently claimed. The major risks identified included incorrect system sizing due to load uncertainty, challenges related to community integration, equipment compatibility issues, inappropriate business models and risks associated with geographical isolation. Akikur *et al.* (2013) review studies of HES suitable for electrification in rural area and Table 4.7 present some of these contribution considering HESs with the integration of PV plants, BES units and other RES or traditional energy sources with particular attention to the PV-BES-Diesel generator HES configuration, on which it is developed a techno-economic model in the next Paragraph 4.4.

Table 4.7 Multisource energy production system review.

Energy production and storage devices							References
PV	SWT	Fuel cell	Diesel engine	Micro turbine	Micro-hydro	Battery	
							Tan <i>et al.</i> (2010) Wisseem <i>et al.</i> (2012) Glavin <i>et al.</i> (2012)
✓						✓	Kazem <i>et al.</i> (2013) Rezk & El-Sayed, (2013) Mulder <i>et al.</i> (2013) Semaoui <i>et al.</i> (2013)
✓	✓					✓	Protogeropoulos <i>et al.</i> (1997) Celik (2002) Yang <i>et al.</i> (2008) Diaf <i>et al.</i> (2008) Kaabechee <i>et al.</i> (2011)
✓		✓				✓	Li <i>et al.</i> (2009) Avril <i>et al.</i> (2010) Jallouli <i>et al.</i> (2012) Silva <i>et al.</i> (2013)
✓			✓			✓	Muselli <i>et al.</i> (1999) Muselli <i>et al.</i> (2000) Shaahid & Elhadidy (2007) Shaahid & Elhadidy (2008) Shaahid & El-Amin (2009) Hrayshat (2009) Saheb-Koussa <i>et al.</i> (2009) Rehman & Al-Hadhrami (2010) Khatib <i>et al.</i> (2011) Kaldellis <i>et al.</i> (2012) Khelif <i>et al.</i> (2012) Ismael <i>et al.</i> (2013a) Suresh Kumar & Manoharan (2014)
✓				✓		✓	Ismael <i>et al.</i> (2013b)
✓	✓		✓			✓	Elhadidy and Shaahid (2004)
✓	✓	✓	✓			✓	Dufo-López & Bernal-Agustin (2008)
✓	✓		✓		✓	✓	Kusakana & Vermaak (2014)

#### 4.4 Off-grid PV-BES-Diesel generator HES design

Energy in remote regions is generally supplied by off-grid fossil fuel based generators. The integration of PV plant and a BES system is an effective solution to increase the energy supply reliability, the system autonomy and lifetime, to reduce generator working hours, to decrease the fuel consumption and the maintenance operations and to improve the generator management, *i.e.* preheating, cooling and transient conditions. In this context, BES systems have a crucial role in the operation and management of the HES, in addition to the storage of exceeding energy produced by the RESs. Furthermore, the decrease of PV plant component prices, the technology consolidation and innovation of BES systems and energy conversion devices create favorable economic and technical conditions for their exploitation.

In the recent literature, several contributions propose analysis to evaluate the technical and economic feasibility of off-grid energy production systems integrating diesel generators, PV plants and energy storage solutions (See Table 1.7).

Muselli *et al.* (2009), Muselli *et al.* (2000) and Kaldellis *et al.* (2012) study sizing methodologies for a HES, integrating PV plant, and their approaches are applied to evaluate the installation in European remote areas. Rehman and Al-Hadhrami (2010), Shaahid and Elhadidy (2007), Shaahid and Elhadidy (2008) and Shaahid and El-Amin (2009) offer several contributions to the technical and economic assessment of PV-BES-Diesel generator HES in Saudi Arabia, while Khatib *et al.* (2011), Ismail *et al.* (2013) and Suresh Kumar and Manoharan (2014) evaluate such systems in the South Far East region. Finally Khelif *et al.* (2012) analyze the feasibility of a PV-Diesel generator HES in the North Africa region.

This *Paragraph* presents a technical and economic model for the design of an off-grid PV-BES-Diesel HES for any installation site. The previously mentioned contributions evaluate the effectiveness and the optimum component sizes of such systems in high irradiation regions, while the proposed model is applied to study the best technical solution for a HES to be installed in a remote village in Yakutsk (Russia), a location marked by a medium irradiation level, *i.e.*  $\sim 1400\text{kWh/m}^2\text{year}$ , in collaboration with the company Margen S.p.A. The aim is to determine the PV plant rated power and the BES system capacity able to minimize the *LCOE*. The costs due to the generator operation, *i.e.* fuel consumption and maintenance activities, are accounted as additional costs. As a consequence, the obtained *LCOE* values can be directly compared with the only generator scenario, showing immediately the competitiveness and profitability of the PV-BES system integration.

The model takes into account the hourly energy demand, the irradiation and the temperature profiles for the installation site calculating the hourly PV plant yield, the battery charge-discharge processes and the generator energy request. A multi-scenario analysis is carried out varying the PV plant and BES system capacity.

According to the introduced purposes, the reminder of this *Paragraph* is organized as follows: the next *sub-Paragraph 4.4.1* introduces the HES architecture, defining the strategy and the logic of control adopted for energy dispatching and the load supply. The *sub-Paragraph 4.4.2* analytically describes the model to design the HES, while *sub-Paragraph 4.4.3* presents the introduced case study including the definition of the model parameters and revising the input data. The obtained results are extensively discussed in *sub-Paragraph 4.4.4* before drawing the conclusions together with suggestions for further research in the *sub-Paragraph 4.2.5*. Finally, the *sub-Paragraph 4.2.6* includes technical details of the developed HES in collaboration with the company Margen S.p.A. and currently installed in Yakutsk (Russia).

#### 4.4.1 PV-BES-Diesel generator HES architecture

A reference diagram for the off-grid HES, including the energy flow directions, is in Figure 4.19. The HES integrates the diesel generator, the PV plant, the battery banks, the AC main distribution unit, which is connected to the load, the electric conversion and control devices. The PV plant can directly supply the AC load through a PV inverter, which includes a maximum power point tracking device, electric protections, reactive and exceeding power management.

The battery charge/discharge processes, the generator start/stop signals and the modulation of the power coming from the PV inverter are controlled through the bidirectional inverter, which also protects the batteries avoiding both the risk of overcharge and excessive discharge.

The BES system stores the exceeding energy produced by the PV plant optimizes the diesel generator management, e.g. management of pre-heating, cooling times and transient conditions, and guarantees the energy supply during generator failure or low irradiation periods. The diesel generator charges the BES only in case of extended low charge conditions to prevent the battery degradation.

The BES system physical constraints are defined in the following *Equation 4.22*, for each working hour,  $h$ . The hourly state of charge,  $SOC_{B,h}$ , cannot exceed the maximum capacity,  $K_B^{max}$ , and it has to be higher than the minimum capacity,  $K_B^{min}$ , defined through the so-called maximum allowable depth of discharge,  $DOD$ , as in *Equation 4.23*.

$$K_B^{min} \leq SOC_{B,h} \leq K_B^{max} \quad (4.22)$$

$$K_B^{min} = (1 - DOD) \cdot K_B^{max} \quad (4.23)$$

The system aims to satisfy the user load thanks to the PV plant production, the energy stored in the BES system and the diesel generator in case of the PV-BES system is not able to fully supply the required hourly energy demand.



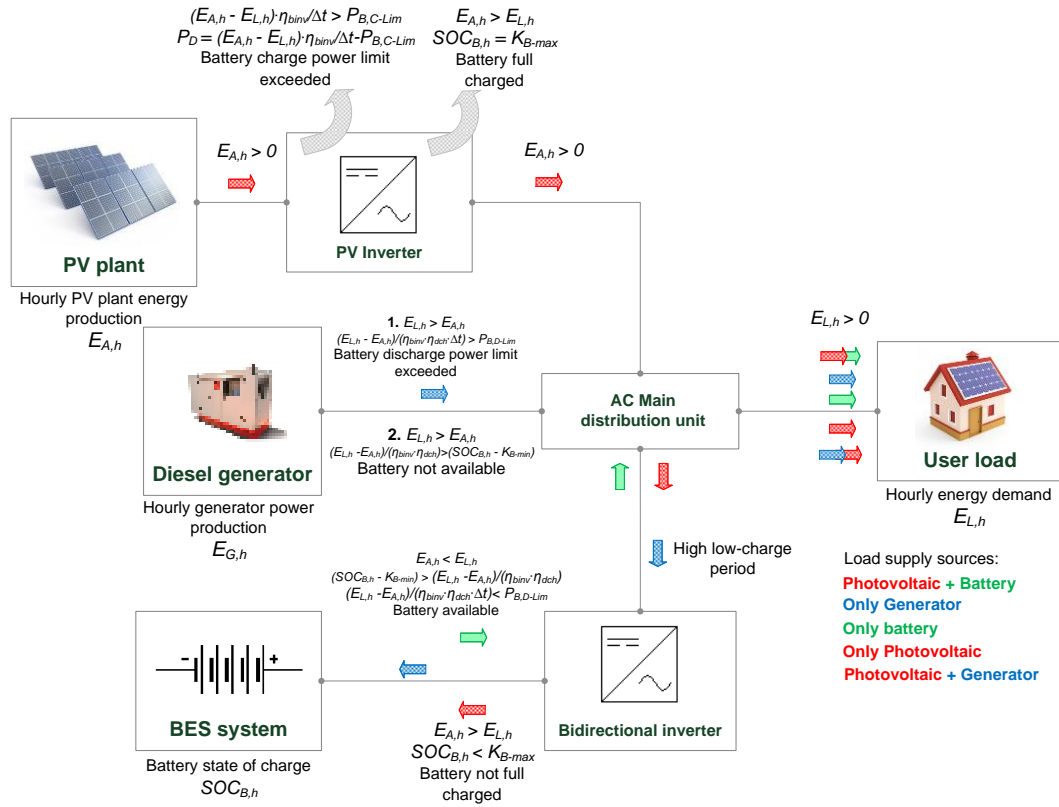


Figure 4.19 Reference diagram for the off grid HES

The hourly energy balance is in the following Equation 4.24.

$$E_{L,h} = E_{A,h} + E_{B,h} + E_{G,h} \quad (4.24)$$

The PV plant operates to meet the energy demand, while the energy surplus, if present, flows to the BES system, until it is fully charged. The exceeding energy is dissipated through the PV inverter. The battery charging process is limited by the technical battery limits in the charging power,  $P_{B,C}^{Lim}$ . The charging power is controlled by the bidirectional inverter and eventual exceeding energy is directly dissipated by the PV inverter. On the contrary, in the case of low irradiance and during the night-time hours, BES system supplies the energy deficit until the  $SOC_{B,h}$  decreases to its minimum level or the required power overcomes the battery discharging power limit,  $P_{B,D}^{Lim}$ . In such two cases, the bidirectional inverter requests the diesel generator to supply the load. The PV plant works in parallel to the diesel generator and the BES system, while the battery charge/discharge processes are stopped when the diesel generator supplies the load.

The flowchart in Figure 4.20 summarizes the management rules to define, for each studied hour,  $h$ , the electric energy flows through the system. Such logic of control and management is the basis for the developed analytic model simulating the behavior of the HES. Such approach leads to assess the system performances and costs.

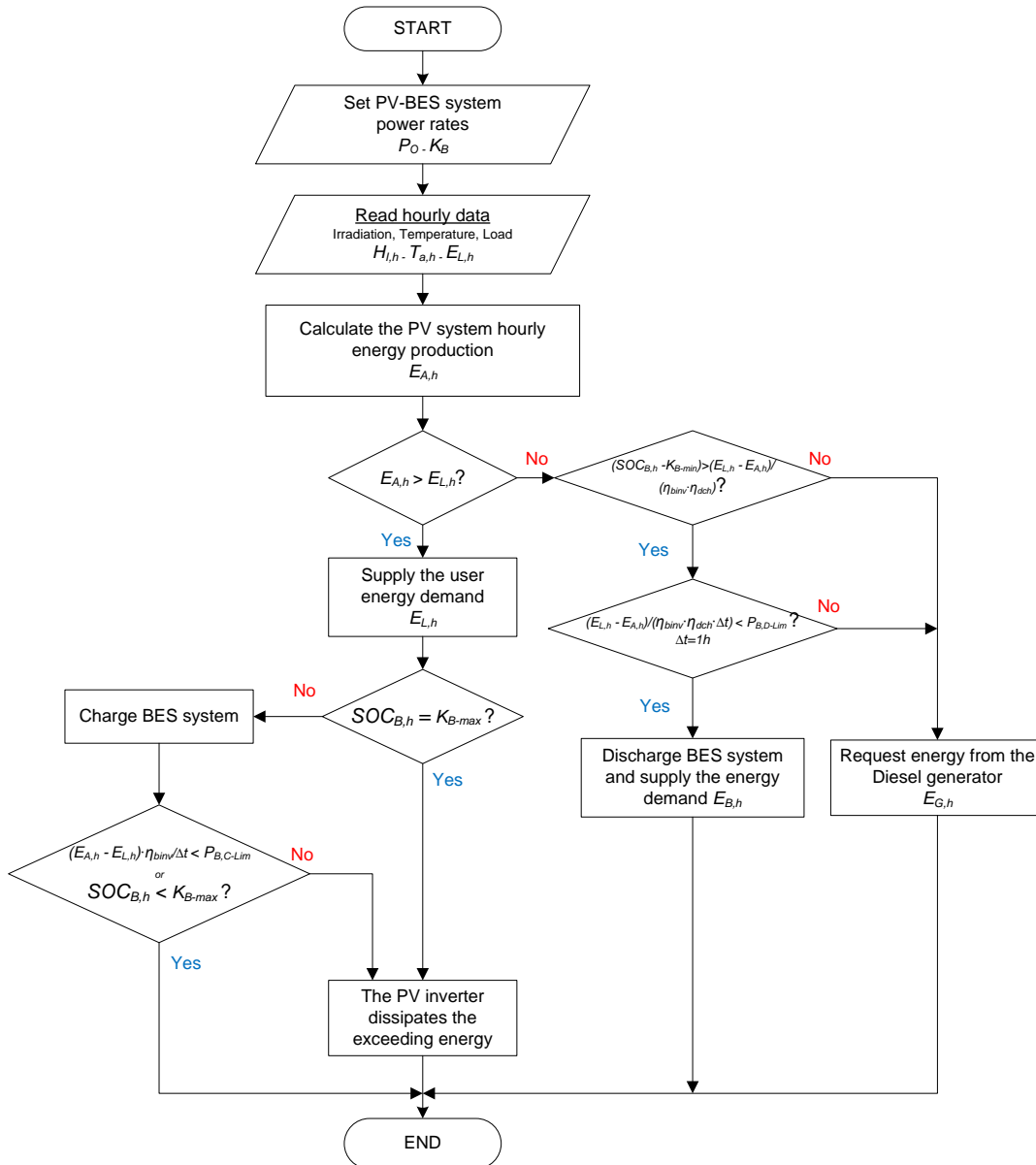


Figure 4.20 Electric energy flow control chart for each studied hour,  $h$

#### 4.4.2 Analytic model

This *sub-Paragraph* presents both the analytic model of the HES and the economic model to compute the *LCOE*. A parametric tool, implementing such models according to the introduced energy flow control algorithm, is developed in Microsoft Visual Basic for Applications™ environment. A multi-scenario analysis, in which the PV system size and the BES system capacity are varied into defined ranges, allows identifying the best technical configuration.

##### 4.4.2.1 PV plant analytic model

Focusing on the PV plant, the model quantifies the hourly yield of the PV arrays,  $E_{A,h}$ , according to *Equation 4.25* and considering the effect of the efficiency decrease due to the PV module degradation (Markvart, 2000).

$$E_{A,h} = H_{I,h} \cdot A_a \cdot \eta_{PV,h} \quad (4.25)$$

Where:

- $H_{I,h}$  is the total in-plane irradiation for the hour  $h$  [kWh/m<sup>2</sup>]
- $A_a = P_o / (\eta_{module} \cdot H_{I,r})$  is the effective PV module area, which depends on the PV plant nominal power  $P_o$  [kWp] and the module efficiency  $\eta_{module}$  [%]. The lower the module efficiency, the higher the PV module area has to be.  $P_o$  refers to standard test conditions, i.e. solar spectrum of AM 1.5, module temperature of 25°C and reference in-plane irradiance,  $H_{I,r}$ , of 1kW/m<sup>2</sup> (IEC, 1998)
- $\eta_{PV,h}$  is the PV system overall efficiency for hour  $h$

The overall PV system efficiency depends on the reference module conversion efficiency,  $\eta_{module}$ , the electrical energy efficiency,  $\eta_e$ , the efficiency decrease due to the cell temperature,  $\eta_{temp,h}$ , and the progressive PV module degradation,  $\eta_d$ . Furthermore, the DC/AC electric conversion is affected by the bidirectional inverter efficiency,  $\eta_{binv}$  (see Equation 4.26).

$$\eta_{PV,h} = \eta_{module} \cdot \eta_e \cdot \eta_{temp,h} \cdot \eta_{binv} \cdot (1 - (j - 1) \cdot \eta_d) \quad (4.26)$$

The PV module efficiency decreases linearly with the temperature respect to the reference condition of 25°C as defined in Equation 4.27 (Hernández-Moro & Martínez-Duart, 2013).

$$\eta_{temp,h} = 1 - \beta \cdot (T_{c,h} - T_{c,ref}) \quad (4.27)$$

$$T_{c,h} = T_{a,h} + [(NOCT - 20)/800] \cdot H_{I,h} \quad (4.28)$$

Where:

- $\beta$  is the temperature coefficient of solar cell efficiency [1/°C]
- $T_{c,h}$  is the PV cell temperature for hour  $h$  [°C]
- $T_{c,ref}$  is the PV cell reference temperature [°C]
- $T_{a,h}$  is the ambient temperature for hour  $h$  [°C]
- $NOCT$  is the normal operating cell temperature [°C]

In Equations 4.27-4.28,  $\beta$  and  $NOCT$  depends on the considered PV module type. Such specifications are from the manufacturer datasheet.

#### 4.4.2.2 BES system analytic model

The BES system capacity is expressed by both the nominal capacity,  $K_B$ , and the number of autonomy hours,  $AH$ .  $AH$  is the number of hours that a fully charged battery is able to

supply the energy demand considering the average hourly user load,  $E_{L,a}$ , and the discharging process efficiency,  $\eta_{dch}$ . (see Equation 4.29).

$$AH = (K_B \cdot \eta_{binv} \cdot \eta_{dch} \cdot DOD) / E_{L,a} \quad (4.29)$$

The temperature has a significant impact on the electrical performance of BES systems. Generally, the performances increase with a temperature increase but aging and the self-discharge processes are accelerated. The BES system available capacity is also affected by the external temperature. A capacity decrease of 1% per Celsius degree occurs below 20°C. For these reasons, BES systems are typically stored in 20-25°C controlled rooms (Wenham et al., 2007).

During the charging process,  $SOC_{B,h}$  is increased according to Equation 4.30.

$$SOC_{B,h} = \max \{SOC_{B,h-1} \cdot (1 - \sigma) + (E_{A,h} - E_{L,h}) \cdot \eta_{binv} \cdot \eta_{ch}, K_B^{max}\} \quad (4.30)$$

Where:

- $\sigma$  is the BES system hourly self-discharge rate [%]
- $\eta_{ch}$  is the BES system charging efficiency [%]

The battery charging process is restricted by the maximum battery power charge limit,  $P_{B,C}^{Lim}$ , defined by the battery technical limitations in the charging current,  $I_{B,C}^{Lim}$ , in order to avoid improper charging process, battery degradation and efficiency decrease.  $I_{B,C}^{Lim}$  is defined through the BES system maximum charge rate,  $C_n^C$ , and the nominal capacity  $I_B$  expressed in Ah.

$$(E_{A,h} - E_{L,h}) \cdot \eta_{binv} / \Delta t < P_{B,C}^{Lim} = I_{B,C}^{Lim} \cdot V_B \quad \Delta t = 1hour \quad (4.31)$$

$$I_{B,C}^{Lim} = I_B / C_n^C \quad (4.32)$$

$$I_B = K_B \cdot 1000 / V_B \quad (4.33)$$

The charging process ends if the BES system reaches the maximum capacity or the process to store the available energy is completed. On the contrary, if the PV production,  $E_{A,h}$ , cannot satisfy the energy demand,  $E_{L,h}$ , the battery starts its discharging process in the cases of available energy and a power request lower than the power discharge limit,  $P_{B,D}^{Lim}$ . If the requested power exceeds the power discharge limit or the hourly energy demand exceeds the remaining battery capacity, the demand is satisfied through the generator (see Equation 4.34), otherwise the discharging process continues until the load demand is completely met (see Equation 4.37).

$$SOC_{B,h} = SOC_{B,h-1} \cdot (1 - \sigma) \quad \text{If} \begin{cases} (E_{L,h} - E_{A,h})/\eta_{binv} \cdot \eta_{dch} > (SOC_{B,h} - K_B^{min}) \\ (E_{L,h} - E_{A,h})/(\eta_{binv} \cdot \eta_{dch} \cdot \Delta t) > P_{B,D}^{Lim} \end{cases} \quad (4.34)$$

$$P_{B,D}^{Lim} = I_{B,D}^{Lim} \cdot V_B \quad \Delta t = 1 \text{ hour} \quad (4.35)$$

$$I_{B,D}^{Lim} = I_B / C_n^D \quad (4.36)$$

$$SOC_{B,h} = SOC_{B,h-1} \cdot (1 - \sigma) - (E_{L,h} - E_{A,h})/\eta_{binv} \cdot \eta_{dch} \quad \text{Otherwise} \quad (4.37)$$

In *Equations 4.30-4.34-4.37* the initial BES system state of charge is supposed to be  $SOC_{B,h} = K_B^{max}$ . It is also possible to set a discharge power limit higher than  $P_{B,D}^{Lim}$  for a limited period to handle generator transient conditions, e.g. pre-heating and cooling time, power source switches, etc., to guarantee the proper system operation.

#### 4.4.2.3 Economical model

The HES system economic assessment includes the *LCOE* and the lifetime system study. The aim is to determine the impact of the PV plant and BES system integration in a traditional diesel generator system evaluating their economic profitability. The *LCOE* is a widely adopted index to assess the economic feasibility of systems based on RESs (Hernández-Moro & Martínez-Duart, 2013). In the present context, the *LCOE* represents the equivalent energy cost that makes the discounted value of the revenues,  $R_j$ , equals to the discounted value of the costs,  $C_j$ , during the economic lifetime of the HES. Therefore, the *LCOE* represents the unitary cost of the produced electricity and it allows the economic comparison of different power generation technologies. The following *Equation 4.38* introduces the *LCOE* expression, as the balance between revenues and costs during the whole system lifetime.

$$\sum_{j=1}^n \frac{R_j}{(1+OCC)^j} = \sum_{j=1}^n \frac{LCOE \cdot (1+g)^{j-1} \cdot E_j}{(1+OCC)^j} = C_0 + \sum_{j=1}^n \frac{C_j \cdot (1+g)^{j-1}}{(1+OCC)^j} \quad (4.38)$$

Where:

- $OCC$  is the opportunity cost of capital [%]
- $g$  is the inflation rate [%]
- $C_0$  is the PV-BES system turnkey cost [€]

From *Equation 4.38*, *LCOE* is the ratio between the sum of the system costs and the overall energy production, both discounted and affected by the inflation rate.

$$LCOE = \left( C_0 + \sum_{j=1}^n \frac{C_j \cdot (1+g)^{j-1}}{(1+OCC)^j} \right) / \sum_{j=1}^n \frac{E_j \cdot (1+g)^{j-1}}{(1+OCC)^j} \quad (4.39)$$

The goal of the proposed model is the cost minimization to meet the energy demand so that, in *Equation 4.40*, the annual energy production,  $E_j$ , is replaced by the reference year global energy demand,  $E_L$  (Bortolini *et al.*, 2014).

$$LCOE = \left( C_0 + \sum_{j=1}^n \frac{C_j \cdot (1+g)^{j-1}}{(1+OCC)^j} \right) / \sum_{j=1}^n \frac{E_L \cdot (1+g)^{j-1}}{(1+OCC)^j} \quad (4.40)$$

#### 4.4.2.4 Lifetime hybrid energy system cost analysis

The impact of the integration of the PV plant and the BES system to a traditional system is evaluated through a lifetime cost analysis. The initial investment due to the diesel generator is not accounted because of the purpose is to compare the HES with a traditional diesel generator, which is necessary for an off-grid independently by the adoption of additional energy sources and storage solutions. The diesel generator rated power should be sized on the maximum user load to ensure the energy supply in the case of solar absence and battery completely discharged.

The PV-BES HES costs include several contributions due to the PV plant installation, the inverter, the battery banks, the bidirectional inverter, the AC main distribution unit, the communication and the remote control devices. The former two costs,  $C_{PV}(P_o)$  and  $C_{inv}(P_o)$ , are functions of the PV rated power,  $P_o$ . The AC main distribution unit cost,  $C_{AC}(P_{max})$  is function of the maximum user load, the battery bank costs is proportional to the battery capacity,  $K_B$ , and, finally, the bidirectional inverter,  $C_{binv}$ , and control device costs,  $C_{cd}$ , are assumed to be constant according the user load profile level. The PV-BES HES turnkey cost expression is presented in *Equation 4.41*.

$$C_0 = C_{PV}(P_o) + C_{inv}(P_o) + C_{AC}(P_{max}) + c_B \cdot K_B + C_{binv} + C_{cd} \quad (4.41)$$

Concerning the operating annual costs, the maintenance activities,  $C_j^{OM\&I}$ , and the component replacement, *i.e.* inverter,  $C_j^I$ , batteries,  $C_j^B$ , and bidirectional inverter,  $C_j^{binv}$ , prevent failures and the performance decrease. Furthermore, the diesel generator introduces additional costs due to fuel consumption,  $C_j^{Gf}$ , proportional to the energy supplied, the fuel cost,  $c_f$ , and the generator specific consumption, function of the generator working power with respect to its maximum power,  $f_{G,h}(P_{G,h}/P_G^{max})$ , and the maintenance operations,  $C_j^{Gm}$ , proportional to the number of working hours and the maintenance hourly cost,  $c_m$ .

$$C_j = C_j^{OM\&I} + C_j^B + C_j^I + C_j^{binv} + C_j^{Gf} + C_j^{Gm} \quad (4.42)$$

The HES *LCOE* value is compared with that referred to a traditional diesel generator ( $P_o = 0$ ,  $K_B = 0$ ), which works 8760 hours per year directly supplying the load. The *LCOE* of a traditional diesel generator can be evaluated, according to *Equation 4.43*, calculating the

unit energy cost,  $e_G$ , for the reference year  $j = 1$  considering maintenance operation for 8760 hours and the average specific fuel consumption per produced kWh,  $f_G$ .

$$e_G = c_f \cdot f_G / \rho_f + (c_m \cdot 8760) / E_L \quad (4.43)$$

The described model is able to carry out the technical and economic design of HESs for any installation site and specific system configuration. In the next *sub-Paragraph*, the model is applied to determine the optimal configuration of a PV-BES-Diesel generator HES to be installed in a remote village in Yakutsk (Russia), developed in collaboration with the company Margen S.p.A.

#### 4.4.3 Case study

The proposed model is implemented to design a PV-BES-Diesel generator HES to meet the energy demand of a remote village located in Yakutsk, Russia (Latitude 62.02° North, Longitude 129.44° East).

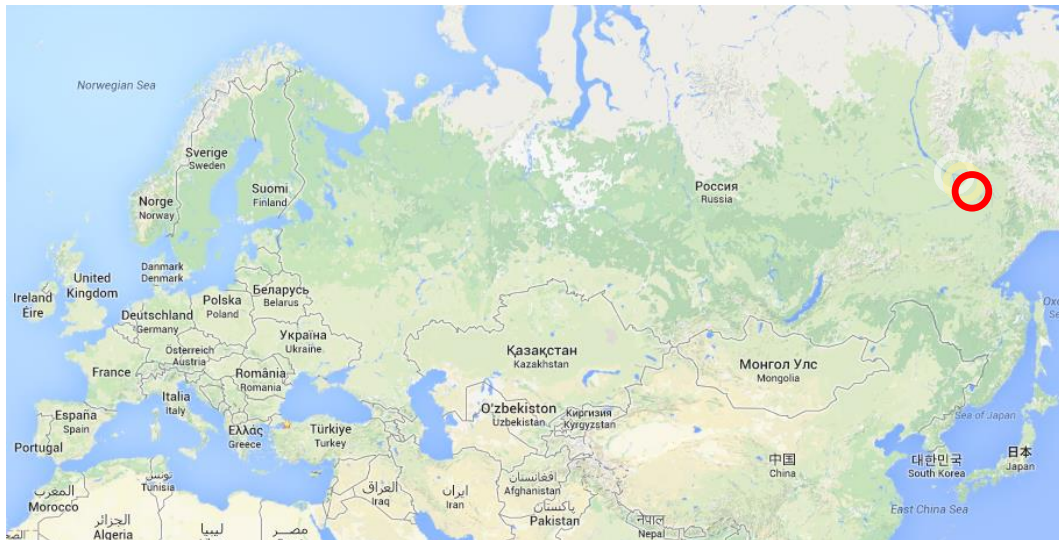


Figure 4.21 Yakutsk - Remote village location

The main purpose is to identify the optimal PV-BES HES configuration, to be integrated with traditional diesel generators, in order to minimize the *LCOE* of the whole HES.

All the input data are presented in these *sub-Paragraphs* with deep attention to the hourly temperature, the irradiation and load profiles for the considered reference year and the main technical aspects.

##### 4.4.3.1 Temperature and irradiation profiles

Figures 4.22-4.24 show the irradiation and the temperature profiles for Yakutsk. The temperature profile is referred to the monthly average high temperature condition, which corresponds to the daylight time. The presence of snow and ice on PV modules during the dramatic low temperature period from November to February may lead to PV plant performance reductions. The irradiation levels on November, December, January and

February cover respectively the 2.9%, 0.7%, 1.4%, 7.0% of the yearly irradiation and the PV modules cleaning should be concentrated in February. Anyway, the monthly precipitation during the winter period is limited (average 0.42mm/month) with an average number of precipitation days per month equal to 3.5 (2.0 in February) (Pogodaiklimat, 2014). The irradiation profile is referred to the hourly conditions estimated with the help of the PV-Watts calculator of the National Renewable Energy Laboratory (NREL, 2014). The graph refers to an optimal inclination angle of the solar collector equal to 44°. The aggregate global annual irradiation level is of 1,437 kWh/m<sup>2</sup> year and the average daily irradiation level is of 3.94 kWh/m<sup>2</sup> day (See Figure 4.23).

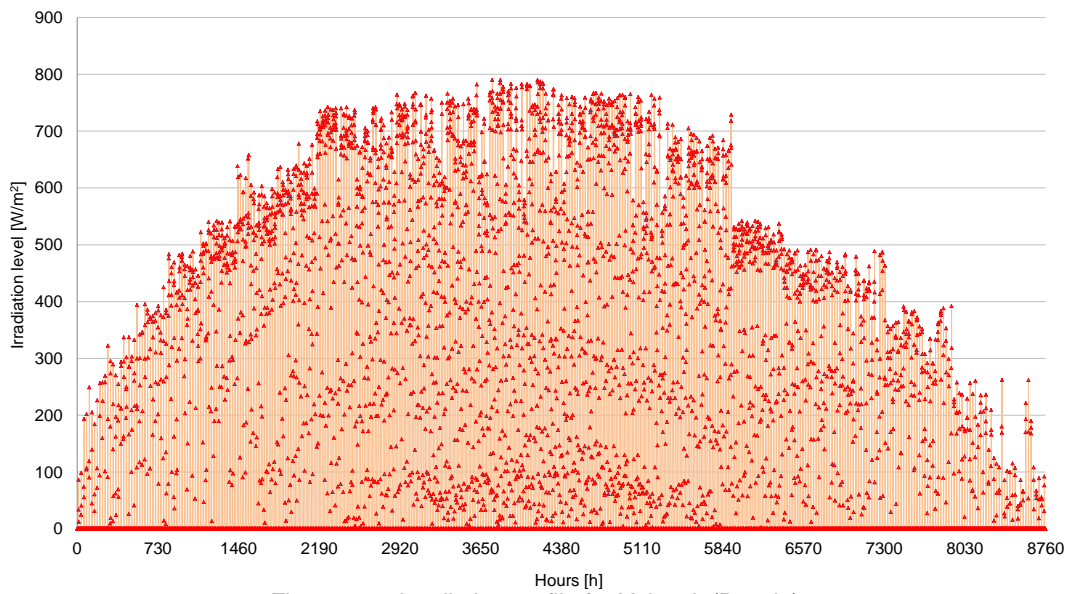


Figure 4.22 Irradiation profile for Yakutsk (Russia)



Figure 4.23 Russian irradiation map



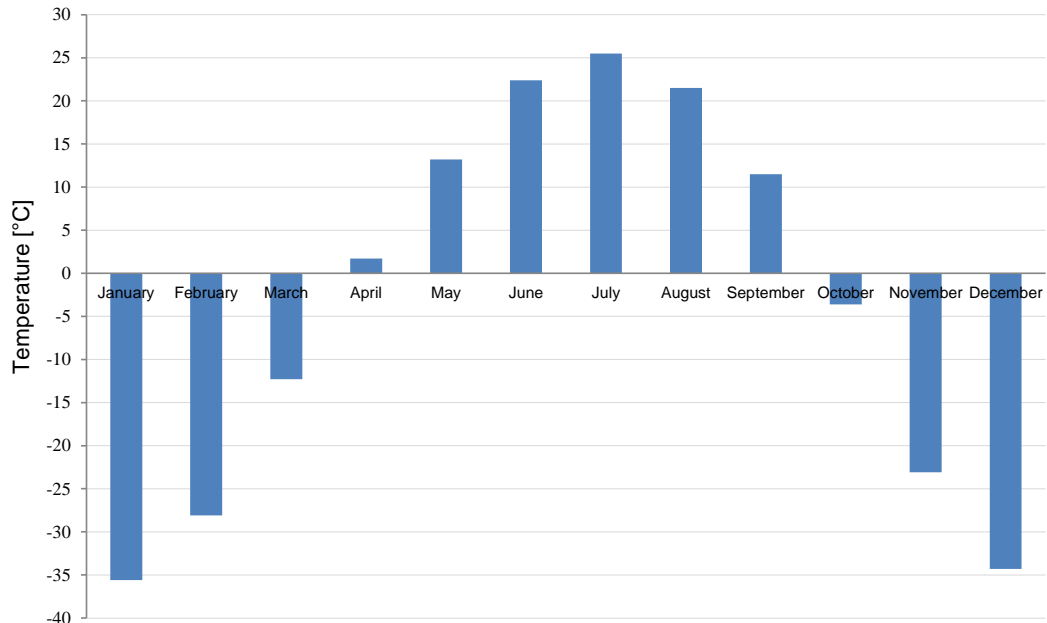


Figure 4.24 Temperature profile for Yakutsk (Pogodaiklimat, 2014)

#### 4.4.3.2 Load profile

The hourly load profile of the remote village is presented in Figure 4.25. It shows an average load of about 16kW (the red dashed line), a base load of 8-10kW, a maximum load,  $P_{max}$ , of 30kW and a yearly energy request of about 138MWh.

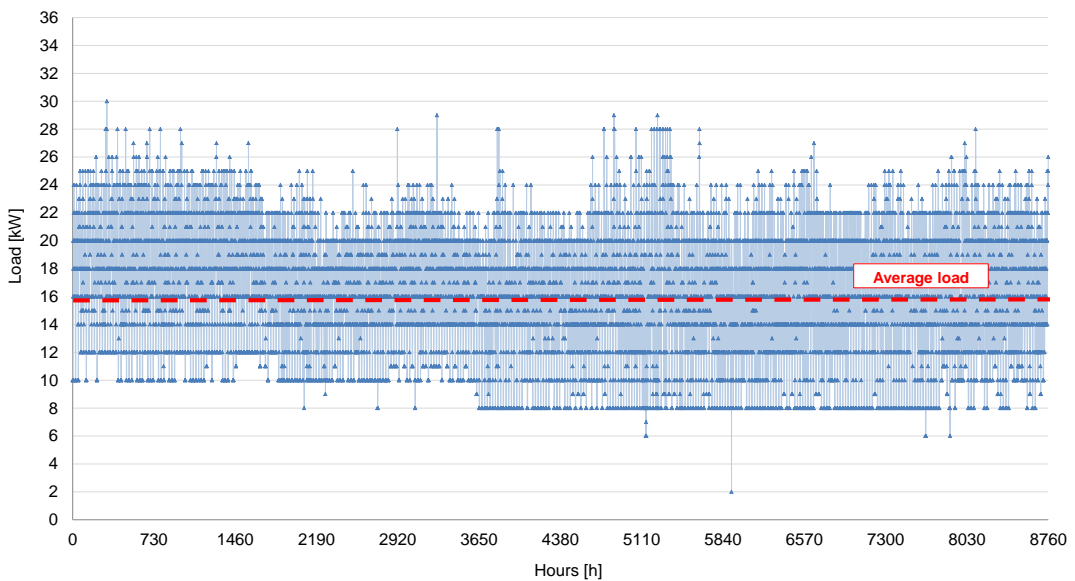


Figure 4.25 Hourly load profile for the remote village in Yakutsk (Russia)

#### 4.4.3.3 Off-grid HES detailed architecture

The HES architecture to supply the remote village in Yakutsk is in Figure 4.26. It is a three phase PV-BES-Diesel generator HES including the following functional units:

- 2 x 33.3 Maximum power - 31.3kW Continuous power (COP) diesel generators. The adoption of two generators guarantees the energy supply during the maintenance operations or failures to any of the two

generators. The generators work alternatively to equally distribute the working hours and, therefore, the maintenance activities

- PV plant based on multi-crystalline PV module technology
- BES system based on valve-regulated lead acid (VRLA) batteries
- One or more three phase PV inverters according to the identified PV plant rated power
- 3 x 6kW COP bidirectional inverters, one for each phase. The master bidirectional inverter is the HES control unit. It is synchronized with the other two slave bidirectional inverters, the AC main distribution unit and the three phase inverters. In addition, it controls the BES system charging/discharging operations and the generator power requests. The size of bidirectional inverters is in accordance to the user load profile. Particularly, they are able to continuously supply 18kW, close to the average user load demand, 24kW for 30 minutes, 27kW for 5 minutes and 33kW for few seconds
- Control and monitoring devices

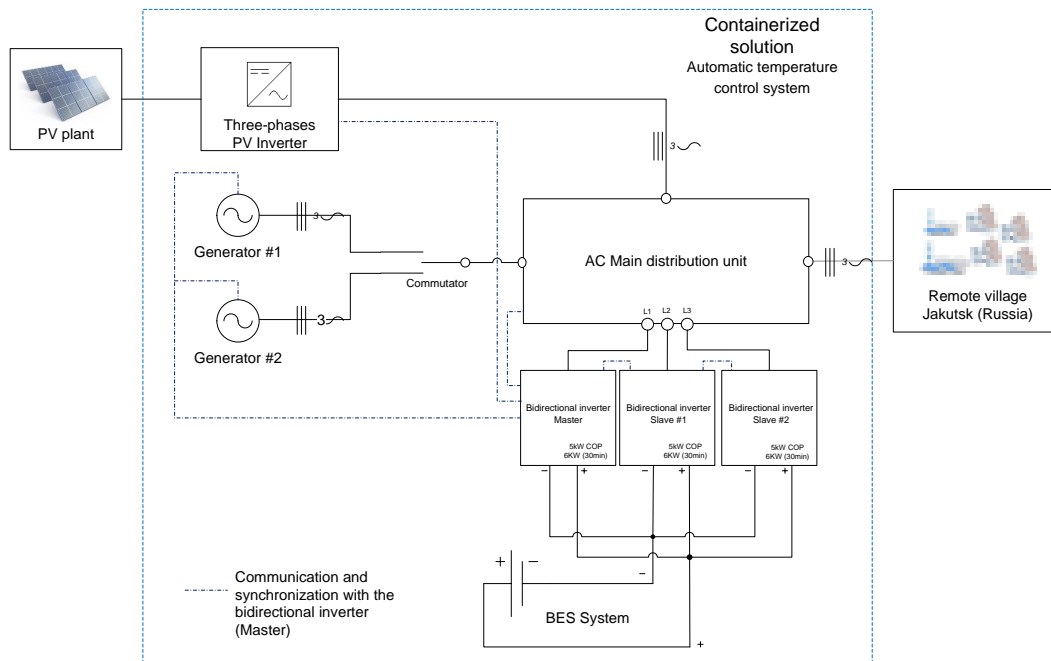


Figure 4.26 Case study - HES architecture

The system is provided in containers equipped with a proper temperature control systems to avoid component performance decrease and damages. The temperature control system is specifically required for the Yakutsk extreme climate. In the following, the boundary conditions for the previously mentioned parameters and the input data included in the analytic model of such functional units are fully reported adopting fix values or ranges according to the real industrial component datasheets and referring to the standard literature.

#### 4.4.3.4 PV-BES system parameters

The PV-BES integrated system includes the PV plant, the BES system and the electric conversion devices.

The PV plant input data, presented in Table 4.8, refers to high quality multi-crystalline modules manufactured in the European area.

Table 4.8 PV plant main parameters

Parameter	Description	Value - Range	Reference
$C_j^{OM\&I}$	PV-BES operation and maintenance cost for year $j$	$0.01 \cdot P_o$ for $j = 1, \dots, n$	Bortolini <i>et al.</i> , 2013
$C_{PV}(P_o)$	PV plant installation cost	See Table 4.9 & Equation 4.44	Real market data
$P_o$	PV plant rated power	10-120kWp, step 5	Multi-scenario analysis
$H_{I,r}$	Yearly module reference in-plane irradiance	1kW/m <sup>2</sup>	IEC, 1998
$n$	PV plant lifetime	25 years	Ismail <i>et al.</i> , 2013b
$NOCT$	Normal operating cell temperature	47°C	Tina & Scandura, 2012
$T_{c,ref}$	PV cell reference temperature	25°C	IEC, 1998
$\eta_d$	PV module annual degradation ratio	0.5%/year	Thevenard & Pelland, 2013
$\eta_{module}$	PV module efficiency	15%	Technical datasheet
$\beta$	Temperature coefficient of solar cell efficiency	0.005/°C	Tina & Scandura, 2012

The PV plant installation cost includes the PV module cost, the installation and labor costs, the supporting structure costs and the engineering cost. Table 4.9 shows such costs for the five considered PV plant rated powers, from 3kWp to 150kWp obtained through a market survey (year of reference 2014).

Table 4.9 PV Plant Installation Costs (2014)

PV plant rated power [kWp]	Module costs [€/kWp]	Labor and installation costs [€/kWp]	Supporting structure costs [€/kWp]	Engineering costs [€/kWp]	PV plant total costs [€/kWp]
3	690	400	300	250	1,640
10	690	400	300	115	1,505
35	670	400	300	85	1,455
75	640	400	300	85	1,425
150	620	400	300	60	1,380

The impact of the modules in the total cost is 45%, while the remaining percentage is covered by the installation and labor costs (27%), the supporting structure costs (20%) and the engineering costs (8%). The following correlation function between PV installation cost and its rated power allows calculating  $C_{PV}(P_o)$ .

$$C_{PV}(P_o) = (1,690.3 \cdot P_o^{-0.041}) \cdot P_o \quad (4.44)$$

The BES system adopts batteries based on the valve regulated lead acid (VRLA) technology, which is a mature and cheap technology and suitable for this kind of applications. The input data of BES system are presented in Table 4.10, while Table 4.11

presents the input data of the electric conversion devices, both in accordance with the standard literature and the technical datasheets of commercial units.

Table 4.10 BES system parameters

Parameter	Description	Value - Range	Reference
$C_B$	BES system unitary cost	150€/kWh	Real market data
$C_j^B$	PV-BES system battery replacement cost for year $j$	150€/kWh for $j=7,13,19$ only	(Battke <i>et al.</i> , 2013) Technical data sheet
$C_n^C$	BES system charge rate	6	Technical data sheet
$C_n^D$	BES system discharge rate	4	Technical data sheet
$DOD$	Depth of discharge	70%	(Battke <i>et al.</i> , 2013) Technical data sheet
$K_B$	BES system nominal capacity	1-5AH, step 0.5AH	Multi-scenario analysis
$V_B$	BES system voltage	48V	
$\sigma$	BES system hourly self-discharge rate	0.067%/day	Technical data sheet
$\eta_{ch}$	BES system charging efficiency	90%	(Battke <i>et al.</i> , 2013)
$\eta_{dch}$	BES system discharging efficiency	90%	(Battke <i>et al.</i> , 2013)

Table 4.11 PV-BES system electric conversion device parameters

Parameter	Description	Value - Range
$C_{AC}(P_{max})$	AC distribution unit cost (function of $P_{max}$ )	100€/kW
$C_{binv}$	Bidirectional inverters cost	7,500€
$C_{cd}$	Control devices cost	1,250€
$C_{inv}(P_o)$	PV inverter cost (function of $P_o$ )	225€/kW
$C_j^{binv}$	PV-BES system bidirectional inverter cost for year $j$	7,500€ for $j=9,17$ only
$C_j^I$	PV-BES system inverter cost for year $j$	225/kWp for $j=9,17$ only
$P_{max}$	User peak demand	35kW
$\eta_e$	PV electrical efficiency	95%
$\eta_{binv}$	Bidirectional inverter efficiency	94%
$\eta_{inv}$	PV inverter efficiency	96%

#### 4.4.3.5 Diesel generator and other parameters

The identified diesel generators are able to provide a maximum power of 39.2kW, for a limited period, and a continuous power of 37.2kW. The alternator efficiency is of 85% leading to a maximum net power of 33.3kW and a continuous net power of 31.3kW making the generators able to satisfy the remote village demand peaks (see Figure 4.23), even in the case of solar absence and full-discharged battery.

The accounted costs due to the generator operations are a function of the maintenance activities and the fuel consumption. The required maintenance activity data are in Table 4.12 and the overall costs is expressed as a function of each operating hour. The generator specific fuel consumption, expressed in kg/kWh, is a function of the supplied power. Figure 4.27 shows its trend, while the estimation of the specific fuel consumption for each supplied power level is obtained through the correlation functions in *Equations 4.45-4.46*. The transport costs of fuel and spare parts are not accounted in the analysis

but the remote positions of the village may lead to significant logistic costs, increasing the convenience and profitability of the PV-BES system integration. Finally, Table 4.13 summarizes all the parameters and input data related to the diesel generators and to the environmental and economic issues.

Table 4.12 Diesel generator maintenance program

Maintenance activity	Maintenance frequency [h]	Cost [€]	Cost [€/h]
Oil, air and fuel filter replacement	1,000	95	0.095
Blower belt, distribution kit and valve cover gasket replacement	2,500	295	0.118
Complete generator revision	12,000	4,150	0.346
Total costs [€/h]		0.559 €/h	
Total costs [€/h], including ≈ 10% of labor cost		0.6 €/h	

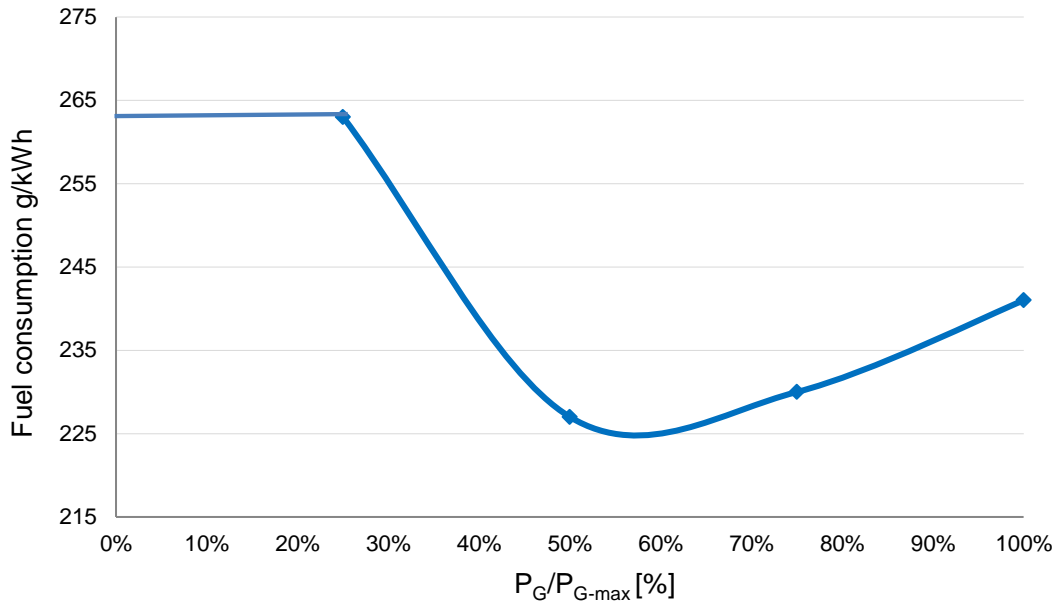


Figure 4.27 Generator fuel consumption as a function of power supplied

$$f_{G,h} \left( \frac{P_{G,h}}{P_G^{max}} \right) = \left[ -0.330 \cdot \left( \frac{P_{G,h}}{P_G^{max}} \right) + 0.808 \cdot \left( \frac{P_{G,h}}{P_G^{max}} \right)^2 - 0.605 \cdot \left( \frac{P_{G,h}}{P_G^{max}} \right) + 0.369 \right]$$

$$\text{if } 0.25 < \frac{P_{G,h}}{P_G^{max}} < 1 \quad (4.45)$$

$$f_{G,h} \left( \frac{P_{G,h}}{P_G^{max}} \right) = 0.263 \quad \text{if } 0 < \frac{P_{G,h}}{P_G^{max}} < 0.25 \quad (4.46)$$

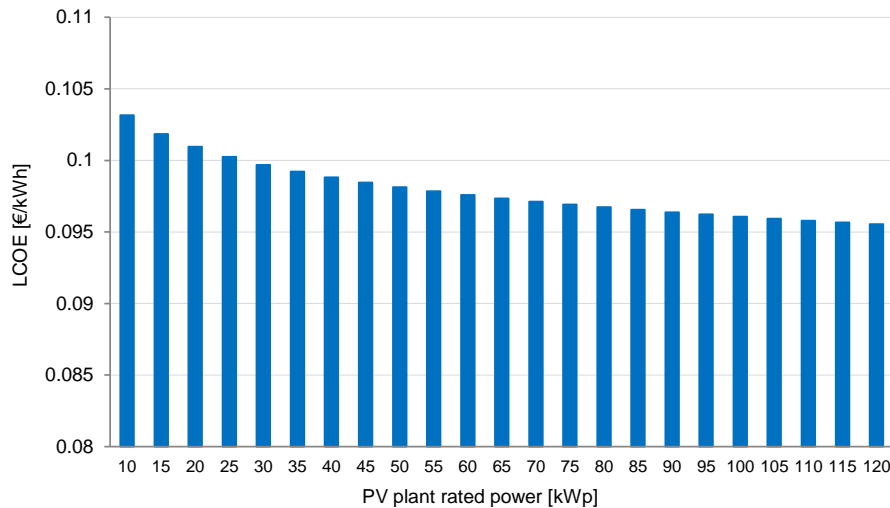
Table 4.13 Diesel generator and environmental/economic parameters

Parameter	Description	Value - Range
<i>Diesel generator parameters</i>		
$c_f$	Generator fuel cost	0.7€/l
$c_m$	Generator maintenance cost	0.6€/h (See Table 4.12)
$f_{G,h} \left( \frac{P_{G,h}}{P_G^{max}} \right)$	Generator specific fuel consumption for hour $h$	See Fig. 4.27 and Equations 4.45-4.46
$P_G^{max}$	Generator maximum net power	33.3kW
$\rho_f$	Fuel density	0.835kg/l
<i>Environmental and economic parameters</i>		
$E_{L,h}$	Energy load for hour $h$	See Figure 4.25
$H_{I,h}$	Total in-plane irradiation for hour $h$	See Figure 4.22
$g$	Inflation	3%
$OCC$	Opportunity cost of capital	5%
$T_{a,h}$	Ambient temperature for hour $h$	See Figure 4.24

A wide range of system configurations, *i.e.* 207, occur and they are examined and compared to determine the best plant configuration. For each scenario the *LCOE* is evaluated together with the hourly energy yield, the energy request from the generator, the fuel consumption, the generator working hours, the energy surplus, the battery state of charge and cycles. The key results and outcomes are compared and discussed in the following *sub-Paragraph 4.4.4*.

#### 4.4.4 Results and discussions

First of all, the *LCOE* values of different PV plant rated powers are calculated according to Equation 4.39 (referred to the PV plant energy production) and the results are presented in Figure 4.28. The values are comparable with the results of the previous analysis (See Figure 4.10). The slight *LCOE* increase is due to the adoption of high quality EU manufactured PV modules instead of extra EU PV modules and the presence of a lower irradiation level.

Figure 4.28 *LCOE* values for different PV rated powers (2014 EU c-Si technology)

According to Equation 4.29 and the parameter values defined in previous Table 4.10, each hour of storage autonomy, *i.e.*  $AH = 1$ , corresponds to, approximately, 25kWh of the BES system capacity (see Equation 4.47).

$$K_B^{AH=1} = (16 \cdot 1AH) / (0.7 \cdot 0.9 \cdot 0.94) \cong 25kWh \quad (4.47)$$

The minimum BES capacity is assumed to be equal to 25kWh (1 AH) to guarantee the proper HES operation. Figure 4.29 shows the *LCOE* values for the main configurations of PV rated power and BES capacity. The results are compared with the *LCOE* of a traditional diesel generator system with the hypothesis of adoption of the same generator type, represented through the red line. Such unitary energy cost, corresponding to the *LCOE* with no PV plant and BES system integrated, is calculated according to Equation 4.43 and presented in Equation 4.48.

$$e_G = 0.7 \cdot 0.232 / 0.835 + (0.6 \cdot 8760) / 138,129 = 0.232\text{€}/kWh \quad (4.48)$$

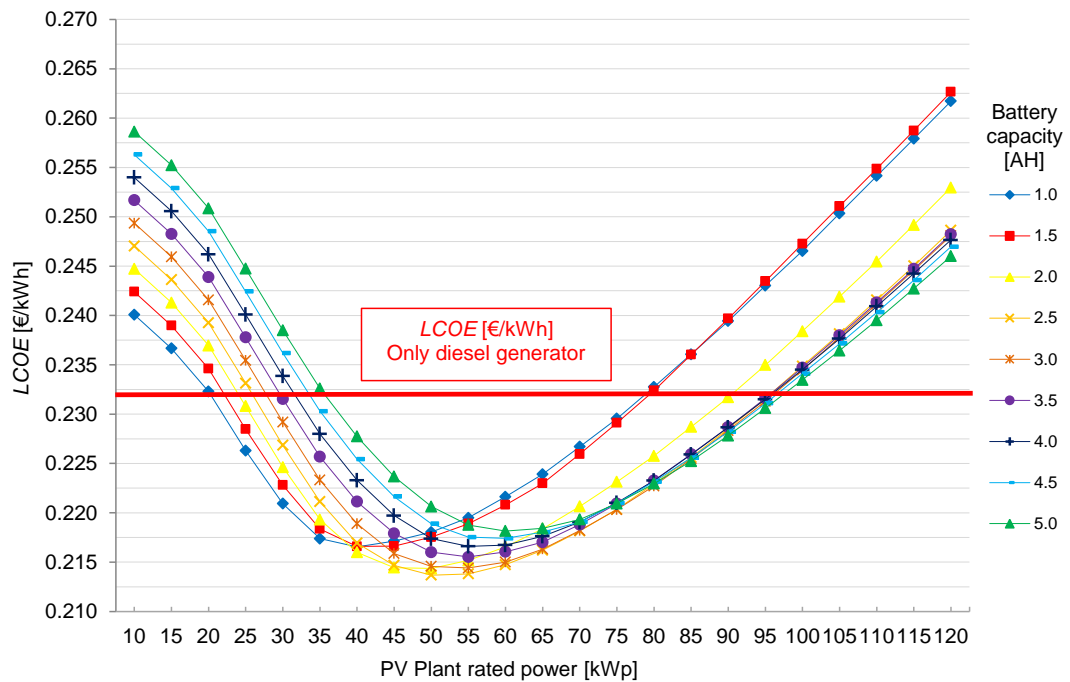


Figure 4.29 *LCOE* values for different PV rated power and BES system capacity

Table 4.14 summarizes the results and *LCOE* for the optimum scenarios for the different battery capacities.

Table 4.14 LCOE results for different HES scenarios

PV plant rated power [kWp]	Battery capacity [AH]	Yearly energy demand [kWh]	Yearly PV energy production [kWh]	Yearly PV energy stored [kWh]	Yearly PV energy dissipated [kWh]	Yearly Gen energy production [kWh]	Yearly Gen working hours [h]	Yearly Gen starts [n°]	Yearly fuel consumption [kg]	Yearly battery cycles [n°]	LCOE [€/kWh]
0	0	138,129	0	0	0	138,129	8,760	1	32,023	0	0.2324
40	1	138,129	48,854	1,533	6,572	96,353	6,923	308	22,707	236	0.2165
40	1.5	138,129	48,854	2,813	5,059	95,265	6,796	326	22,421	255	0.2166
50	2	138,129	61,068	6,346	9,292	88,462	6,165	519	20,730	296	0.2144
50	2.5	138,129	61,068	8,444	6,812	86,681	6,052	552	20,317	299	0.2137
55	3	138,129	67,175	10,796	8,780	83,326	5,850	579	19,538	310	0.2144
55	4	138,129	67,175	13,520	5,559	81,007	5,861	582	19,091	310	0.2166
60	5	138,129	73,281	17,391	5,948	76,578	5,608	467	18,068	318	0.2182

The optimum PV plant rated power ranges from 40 to 60kWp. The choice of the BES capacity depends upon the installer priorities, e.g. fuel consumption, maintenance operations, low initial investment and payback time, emergency BES autonomy hours, etc. The battery banks can be also extended or reduced during the three programmed replacements according to the HES behavior experienced in the previous years and the bidirectional inverter power limit. In addition, Table 4.15 highlights the initial investment and yearly savings due to the integration of PV-BES system and an estimate of the investment payback time.

Table 4.15 Economic profitability of the different HES scenarios

PV plant rated power [kWp]	Battery capacity [AH]	Initial investment [€]	Yearly fuel savings [€]	Yearly maintenance savings [€]	Payback time estimation [years]
40	1	83,122	6,521	1,102	10.9
40	1.5	84,997	6,721	1,178	10.8
50	2	102,991	7,905	1,557	10.9
50	2.5	104,866	8,194	1,625	10.7
55	3	114,756	8,740	1,773	10.9
55	4	118,506	9,053	1,739	11.0
60	5	130,245	9,768	1,891	11.2

The relatively high payback time results are due to the assumed low fuel cost, i.e. 0.7€/l, and the irradiation level of the Yakutsk region, i.e. about 1,400 kWh/m<sup>2</sup>year. However, further considerations about the significant costs and technical issues concerning the transportation of fuel and spare parts to such a remote area, not accounted in this analysis, are required to better estimate the savings due to the fuel consumption and the maintenance operation reductions.

Concerning the best scenario, i.e. 50kWp-2.5AH, the LCOE reduction is of about 8% compared to a traditional diesel generator. The HES installation is also economically sustainable excluding the PV energy production during the winter period, when the snow and ice may cover the PV modules. Particularly the LCOE reductions is of about 7%, 6.5%, 4.5%, 3% excluding the PV energy production respectively for December-January, November-December, from December to February and from November to February.



Finally, Figure 4.30 shows the lifetime HES cost distribution, discounted to the year 0, in order to satisfy the remote village overall energy demand.

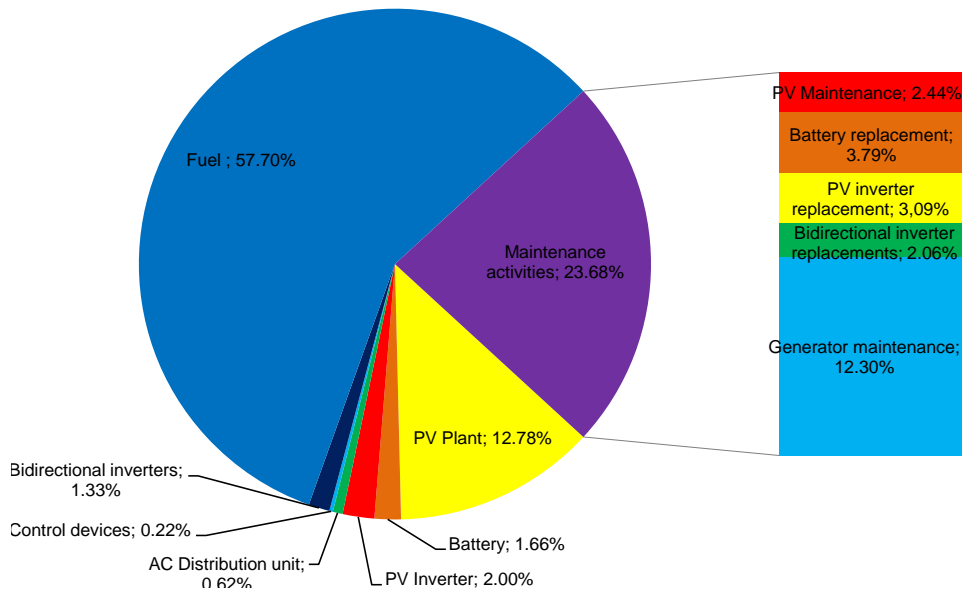


Figure 4.30 HES cost distribution for the best scenario

The PV-BES turnkey costs cover about the 19% of the total costs, while the cost due to the fuel consumption has the main incidence, *i.e.* about the 58%. As a consequence, better conditions for the PV-BES, *e.g.* fuel cost and irradiation level, creates favorable conditions to increase the PV plant rated power and BES system capacity. The maintenance activities cause the remaining 24% of the total costs. Among them, the cost due to the generator operation has the larger incidence, *i.e.* about the 50% of maintenance activity costs, confirming the great opportunity of the PV-BES integration.

#### 4.4.5 Conclusions and further research

This *sub-Paragraph* presents the study of a PV plant and a BES system integrated in a traditional off-grid diesel generator. The development of a technical and economic model for the design of an off-grid PV-BES-Diesel generator HES system allows determining the PV system rated power and the BES system capacity able to minimize the *LCOE*. The model is able to design HESs for any installation site and in this *sub-Paragraph* it is applied to evaluate the optimum configuration of a PV-BES-Diesel generator HES, developed in collaboration with the company Margen S.p.A., to be installed in Yakutsk (Russia) to supply the energy demand of a remote village. The results highlight the technical feasibility and the moderate economic profitability of such a system for a context with a medium irradiation level, *i.e.*  $\sim 1,400 \text{ kWh/m}^2 \text{ year}$ , and a relatively low fuel cost, *i.e.*  $0.7 \text{ €/l}$ . Considering the best PV rated power and BES capacity configuration, a *LCOE* reduction of about 8% occurs, compared to a traditional diesel generator.

Further research mainly deals with the accounting of fuel and spare part transport costs to the remote village and the application of the technical and economic model to different locations, *i.e.* different environmental and economic conditions and load profiles. In

addition, the economic analysis may be integrated with the assessment of the environmental impact of the system, considering manufacturing, transportation, utilization and maintenance processes.

#### 4.4.6 Final remarks

The PV-BES-Diesel generator HES system has been developed and installed in Yakutsk (Russia) to meet the energy demand of a remote village. A representation of the system is in the Figures 4.32 and 4.33, while a technical single-line diagram is in Figure 4.34 in the appendix A-4.4. The innovative part of the research project is the integration of energy conversion devices, *i.e.* bidirectional inverters, PV inverter and AC distribution unit, to the diesel generator control board and PLC. The energy conversion devices are supplied by SMA company, leader in the solar inverter sector. The following components are integrated in the system:

- PV plant (20kWp)
- BES system (100kWh - 48V, 2000Ah)
- 2 x Diesel Generators (39.2kW Prime Power)
- Diesel generators control board
- Programmable logic control (PLC) for management of diesel generators
- 3 x Bidirectional inverters Sunny Island 8.0H, 1 x Master and 2 x Slaves. The Sunny Island master controls the HES, the battery charge/discharge processes, the generator start/stop signals and the modulation of the power coming from the PV inverter. The Sunny Islands are in communication and the master is connected to monitoring and control devices systems through RS485 protocol (Sunny Remote control and Sunny Webbox)
- Three-phase multicluster box: It is the AC distribution unit that can include 2 x clusters composed by 3x Bidirectional inverters and three-phases PV inverter. The current solution has only 1 cluster and the choice of multicluster box derives from the customer request to extend the system in the future increasing PV plant rated power and battery capacity. The multicluster box communicates with bidirectional inverters and synchronizes power sources.
- Batfuse box: Fuses to protect Sunny Islands from overcurrents.
- Sunny tripower 17000L (17KW): Three-phases inverter with reactive power supply, transformerless. The Sunny tripowers communicates with the Sunny Islands through RS485 protocol.
- Sunny webbox: Central measurement data acquisition and diagnostic unit for the monitoring of the HES.
- Sunny sensors: Measuring system for environmental data, including an integrated irradiation and external module temperature sensors.
- Sunny remote control: Control and visualization unit.

The system also includes energy supply for auxiliaries and a manual bypass line in order to directly connect the diesel generator to the load in case of energy conversion device failures.

In addition the following features are provided:

- 30 Feet artic container with high insulation level
- Temperature control system (Automatic recirculation gate for radiator air, ventilation system, electric heater)
- Fuel tank 300l with automatic fuel transfer system, fuel counter and fuel prefilter
- Fuel heater
- Oil tank with manual refill 30l
- Anti-intrusion security system
- Energy meter
- Smoke and fire-detection

The configuration, originally 20kWp PV plant and 100kWh BES system capacity, is going to be updated increasing the PV plant power up to 40kWp according to the model results. Particularly, the Figure 4.31 show the *LCOE* values for the current (0.251€/kWh) and future (0.228€/kWh). The economic profitability, considering 100kWh as BES system capacity, can be further improved increasing the PV plant rated power up to 60kWp (0.218€/kWh).

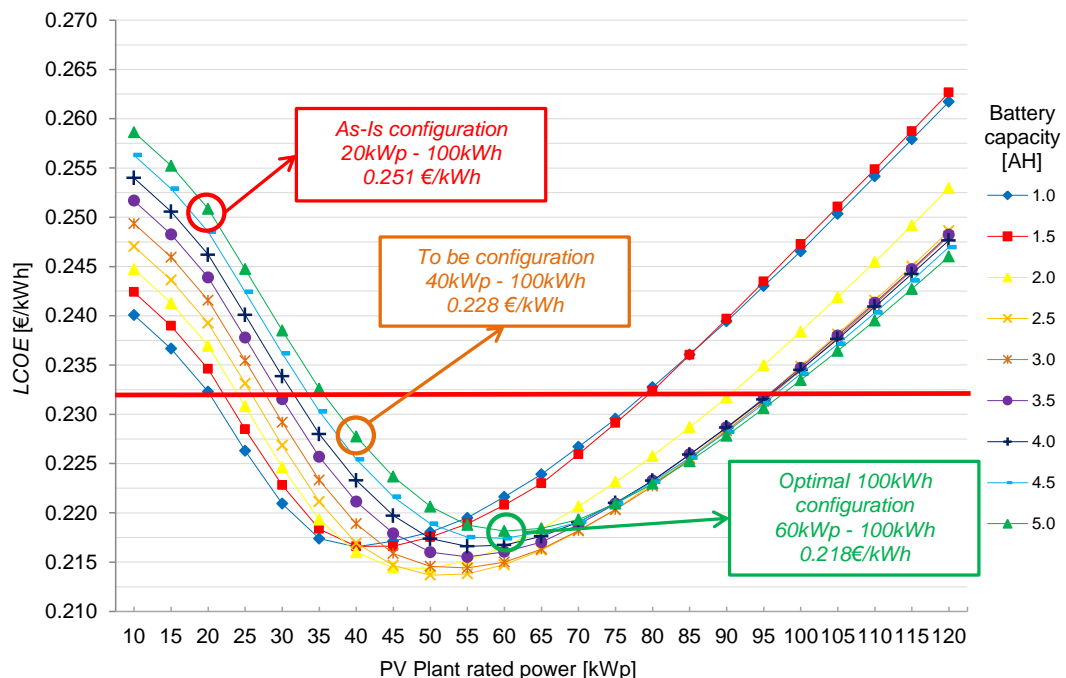




Figure 4.32 Installed 20kWp PV Plant – Yakutsk



2xGensets 35kW

Control board - Gensets



Bidirectional inverters (three-phases system)

VRLA batteries - 100kWh



PV inverter (three-phases)

Figure 4.33 HES: 2 x Diesel generators, 20kWp PV plant, 100kWh BES system

#### 4.4.7 Acknowledgements

The authors would like to acknowledge the company Margen S.p.A. (Italy) for the financial and technical support to the project.

# Appendix A-4.4

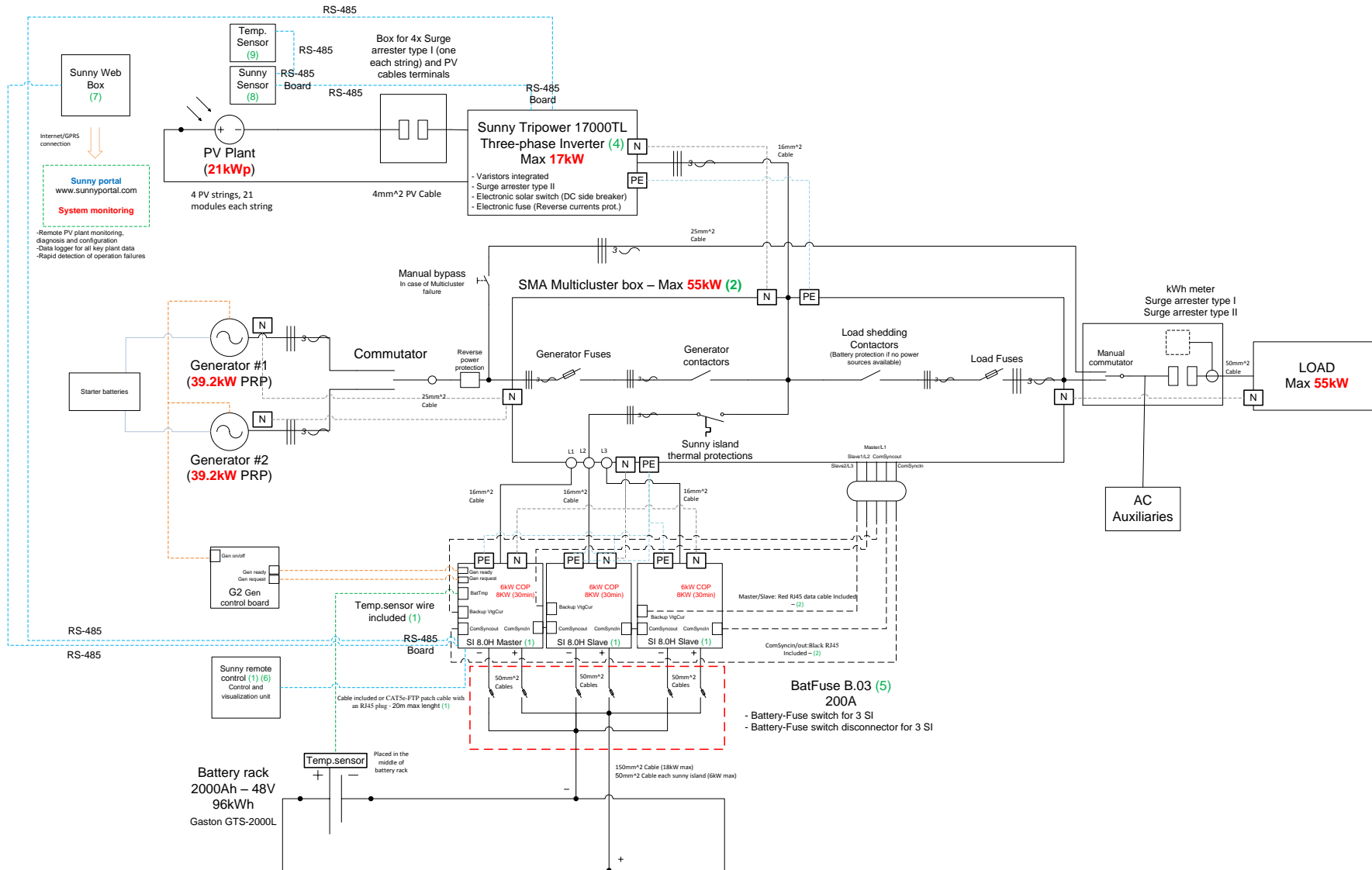


Figure 4.34 PV-BES-Diesel generator HES single-line diagram

## 4.5 Off-grid PV-BES-SWT-Diesel generator HES design

This *Paragraph* presents the configuration and technical details of a PV-BES-SWT-Diesel generator HES to be installed in a remote location in Russia to supply a telecommunication station in Russia. The HES system has been developed in collaboration with the company Margen S.p.A.

### 4.5.1 PV-BES-SWT-Diesel generator HES architecture

The PV-BES-SWT-Diesel generator HES architecture is in Figure 4.35, while the more detailed single-line diagram is in Figure 4.36 (Appendix A-4.5.)

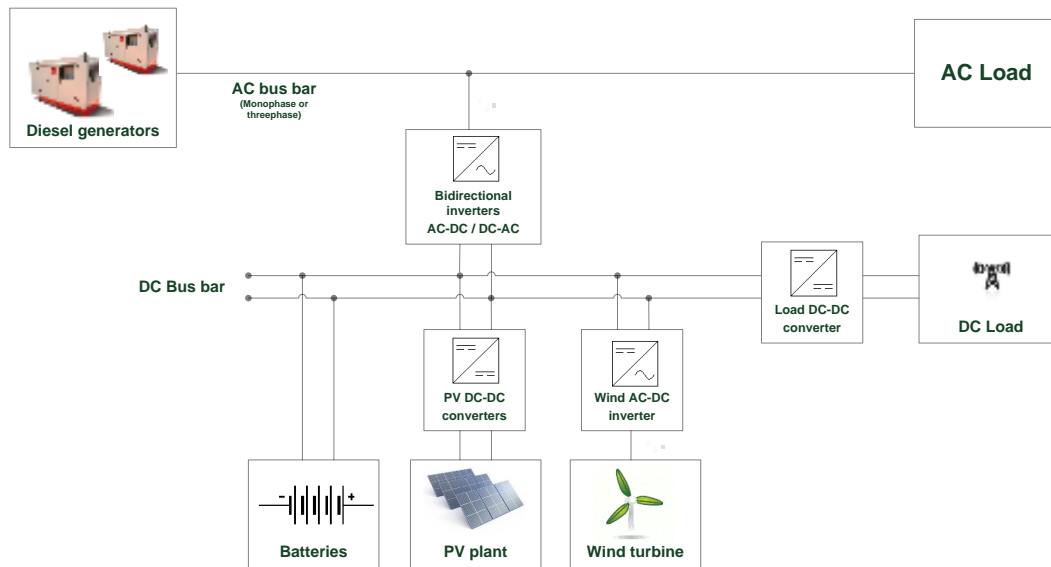


Figure 4.35 PV-BES-WT-Diesel generator HES architecture

The system integrates two diesel Generators, the PV plant, the SWT, the battery banks, the electric conversion and control devices and the DC bus bar, which is connected to the telecommunication system. The system also includes AC supply for the auxiliaries of the telecommunication system. The PV plant and SWT are connected to the DC bus bar through a solar charge controller and a wind AC/DC converter, respectively, and they can supply directly the DC load or charge the battery.

The battery charge/discharge processes, the generator start/stop signals and the modulation of the power coming from the PV inverter and SWT are controlled through the bidirectional inverter, which also protects the batteries avoiding both the risk of overcharge and excessive discharge. In details, the system is composed by the following functional modules:

- PV plant (10kWp, 2.5kWp each string)
- Wind turbine (10kWp)
- Battery BES system (196kWh, 2 racks of 48V and 2000Ah)
- 2 x Diesel Generators (24kWe)

- Diesel generators control board
- PLC for management of diesel generators
- 4 x 2.5kW Solar charge controller (one each string)
- 10kW Wind power controller (AC/DC conversion)
- 3 x Bidirectional inverters, 1 each phase
- DC bus bar and 48V/24V converter for auxiliaries
- Monitoring and control system devices

In addition the following features are provided:

- 30 Feet artc container with high insulation level
- Temperature control system (Automatic recirculation gate for radiator air, ventilation system, electric heater)
- 15000-litre double-walled storage tank to be buried, with flow control valve, pit and coating made of plastic reinforced by fibre glass, gap filling and leak sensor
- Fuel heater
- Oil tank with manual refill 30l
- Anti-intrusion security system
- Energy meter
- Smoke and fire-detection

#### *4.5.2 Further developments*

Further research deals with the development of an analytic model for the techno-economic assessment of the PV-BES-SWT-Diesel generator HES, similarly to the analysis referred to the PV-BES-Diesel generator HES. In addition, a multi-objective design, evaluating both tech-economic and environmental aspects, is of interest for future research activities.

#### *4.5.3 Acknowledgements*

The authors would like to acknowledge the company Margen S.p.A. (Italy) for the financial and technical support to the project.

Appendix A-4.5

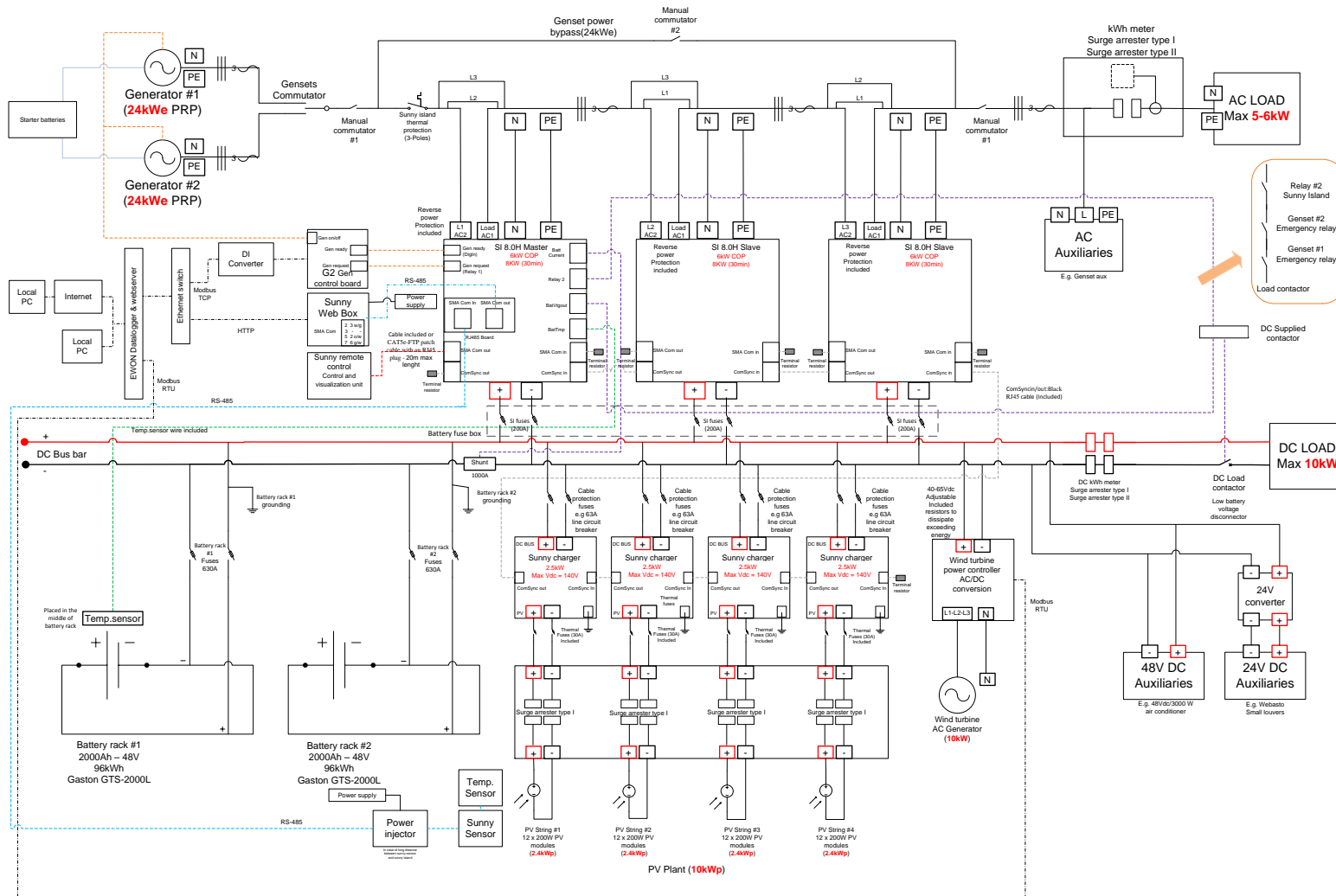


Figure 4.36 PV-BES-WT-Diesel generator HES single-line diagram



## References

- Akikur, R. K., Saidur, R., Ping, H. W., & Ullah, K. R. (2013). Comparative study of stand-alone and hybrid solar energy systems suitable for off-grid rural electrification: A review. *Renewable and Sustainable Energy Reviews*, 27, 738–752.
- Avril, S., Arnaud, G., Florentin, A., & Vinard, M. (2010). Multi-objective optimization of batteries and hydrogen storage technologies for remote photovoltaic systems. *Energy*, 35(12), 5300–5308.
- Battke, B., Schmidt, T. S., Grosspietsch, D., & Hoffmann, V. H. (2013). A review and probabilistic model of lifecycle costs of stationary batteries in multiple applications. *Renewable and Sustainable Energy Reviews*, 25, 240–250.
- Bayod-Rújula, Á. a., Haro-Larrodé, M. E., & Martínez-Gracia, A. (2013). Sizing criteria of hybrid photovoltaic–wind systems with battery storage and self-consumption considering interaction with the grid. *Solar Energy*, 98, 582–591.
- Bazilian, M., Onyeji, I., Liebreich, M., MacGill, I., Chase, J., Shah, J., ... Zhengrong, S. (2013). Re-considering the economics of photovoltaic power. *Renewable Energy*, 53, 329–338.
- Bortolini, M., Gamberi, M., & Graziani, A. (2014). Technical and economic design of photovoltaic and battery energy storage system. *Energy Conversion and Management*, 86, 81–92.
- Bortolini, M., Gamberi, M., Graziani, A., Mora, C., & Regattieri, A. (2013). Multi-parameter analysis for the technical and economic assessment of photovoltaic systems in the main European Union countries. *Energy Conversion and Management*, 74, 117–128.
- Branker, K., Pathak, M. J. M., & Pearce, J. M. (2011). A review of solar photovoltaic levelized cost of electricity. *Renewable and Sustainable Energy Reviews*, 15(9), 4470–4482.
- Celik, a. . (2002). Optimisation and techno-economic analysis of autonomous photovoltaic–wind hybrid energy systems in comparison to single photovoltaic and wind systems. *Energy Conversion and Management*, 43(18), 2453–2468.
- Colmenar-Santos, A., Campiñez-Romero, S., Pérez-Molina, C., & Castro-Gil, M. (2012). Profitability analysis of grid-connected photovoltaic facilities for household electricity self-sufficiency. *Energy Policy*, 51, 749–764.

- Diaf, S., Belhamel, M., Haddadi, M., & Louche, A. (2008). Technical and economic assessment of hybrid photovoltaic/wind system with battery storage in Corsica island. *Energy Policy*, 36(2), 743–754.
- Elhadidy, M. a., & Shaahid, S. M. (2004). Promoting applications of hybrid (wind+photovoltaic+diesel+battery) power systems in hot regions. *Renewable Energy*, 29(4), 517–528.
- Eltawil, M. a., & Zhao, Z. (2010). Grid-connected photovoltaic power systems: Technical and potential problems—A review. *Renewable and Sustainable Energy Reviews*, 14(1), 112–129.
- Eltawil, M. a., & Zhao, Z. (2013). MPPT techniques for photovoltaic applications. *Renewable and Sustainable Energy Reviews*, 25, 793–813.
- Glavin, M. E., & Hurley, W. G. (2012). Optimisation of a photovoltaic battery ultracapacitor hybrid energy storage system. *Solar Energy*, 86(10), 3009–3020.
- Hernández-Moro, J., & Martínez-Duart, J. M. (2013). Analytical model for solar PV and CSP electricity costs: Present LCOE values and their future evolution. *Renewable and Sustainable Energy Reviews*, 20, 119–132.
- Hoppmann, J., Volland, J., Schmidt, T. S., & Hoffmann, V. H. (2014). The economic viability of battery storage for residential solar photovoltaic systems – A review and a simulation model. *Renewable and Sustainable Energy Reviews*, 39, 1101–1118.
- Hrayshat, E. S. (2009). Techno-economic analysis of autonomous hybrid photovoltaic-diesel-battery system. *Energy for Sustainable Development*, 13(3), 143–150.
- Ismail, M. S., Moghavvemi, M., & Mahlia, T. M. I. (2013a). Design of an optimized photovoltaic and microturbine hybrid power system for a remote small community: Case study of Palestine. *Energy Conversion and Management*, 75, 271–281.
- Ismail, M. S., Moghavvemi, M., & Mahlia, T. M. I. (2013b). Techno-economic analysis of an optimized photovoltaic and diesel generator hybrid power system for remote houses in a tropical climate. *Energy Conversion and Management*, 69, 163–173.
- Jallouli, R., & Krichen, L. (2012). Sizing, techno-economic and generation management analysis of a stand alone photovoltaic power unit including storage devices. *Energy*, 40(1), 196–209.

- Kaabeche, A., Belhamel, M., & Ibtouen, R. (2011). Techno-economic valuation and optimization of integrated photovoltaic/wind energy conversion system. *Solar Energy*, 85(10), 2407–2420.
- Kazem, H. a., Khatib, T., & Sopian, K. (2013). Sizing of a standalone photovoltaic/battery system at minimum cost for remote housing electrification in Sohar, Oman. *Energy and Buildings*, 61, 108–115.
- Khatib, T., Mohamed, A., & Sopian, K. (2013). A review of photovoltaic systems size optimization techniques. *Renewable and Sustainable Energy Reviews*, 22, 454–465.
- Khatib, T., Mohamed, A., Sopian, K., & Mahmoud, M. (2011). Optimal sizing of building integrated hybrid PV/diesel generator system for zero load rejection for Malaysia. *Energy and Buildings*, 43(12), 3430–3435.
- Khelif, A., Talha, A., Belhamel, M., & Hadj Arab, A. (2012). Feasibility study of hybrid Diesel–PV power plants in the southern of Algeria: Case study on AFRA power plant. *International Journal of Electrical Power & Energy Systems*, 43(1), 546–553.
- Kusakana, K., & Vermaak, H. J. (2014). Hybrid diesel generator/renewable energy system performance modeling. *Renewable Energy*, 67, 97–102.
- Li, C.-H., Zhu, X.-J., Cao, G.-Y., Sui, S., & Hu, M.-R. (2009). Dynamic modeling and sizing optimization of stand-alone photovoltaic power systems using hybrid energy storage technology. *Renewable Energy*, 34(3), 815–826.
- Markvart, T. (2000). *Solar Electricity*, 2nd Edition. Wiley, USA.
- Markvart, T., Castaner, L. (2003). *Practical Handbook of Photovoltaic Fundamentals Applications*. (Elsevier UK, Ed.).
- Mohammed, Y. S., Mustafa, M. W., & Bashir, N. (2014). Hybrid renewable energy systems for off-grid electric power: Review of substantial issues. *Renewable and Sustainable Energy Reviews*, 35, 527–539.
- Murphy, P. M., Twaha, S., & Murphy, I. S. (2014). Analysis of the cost of reliable electricity: A new method for analyzing grid connected solar, diesel and hybrid distributed electricity systems considering an unreliable electric grid, with examples in Uganda. *Energy*, 66, 523–534.

- Muselli, M., Notton, G., & Louche, A. (1999). Design of Hybrid-Photovoltaic Power Generator, With Optimization of Energy Management. *Solar Energy*, 65(3), 143–157.
- Muselli, M., Notton, G., Poggi, P., & Louche, A. (2000). PV-hybrid power systems sizing incorporating battery storage: an analysis via simulation calculations. *Renewable Energy*, 20(1), 1–7.
- Nottrott, a., Kleissl, J., & Washom, B. (2013). Energy dispatch schedule optimization and cost benefit analysis for grid-connected, photovoltaic-battery storage systems. *Renewable Energy*, 55, 230–240.
- Passey, R., Spooner, T., MacGill, I., Watt, M., & Syngellakis, K. (2011). The potential impacts of grid-connected distributed generation and how to address them: A review of technical and non-technical factors. *Energy Policy*, 39(10), 6280–6290.
- Protopoulos, C., Brinkworth, B. J., & Marshall, R. H. (1997). Sizing and techno-economical optimization for hybrid solar photovoltaic/wind power systems with battery storage. *International Journal of Energy Research*, 21 (6), 465–479.
- Rehman, S., & Al-Hadhrani, L. M. (2010). Study of a solar PV–diesel–battery hybrid power system for a remotely located population near Rafha, Saudi Arabia. *Energy*, 35(12), 4986–4995.
- Rezk, H., & El-Sayed, A. H. M. (2013). Sizing of a stand alone concentrated photovoltaic system in Egyptian site. *International Journal of Electrical Power & Energy Systems*, 45(1), 325–330.
- Riffonneau, Y., Bacha, S., Barruel, F., & Ploix, S. (2011). Optimal Power Flow Management for Grid Connected PV Systems With Batteries. *IEEE Transactions on Sustainable Energy*, 2(3), 309–320.
- Rydh, C. J., & Sandén, B. a. (2005a). Energy analysis of batteries in photovoltaic systems. Part I: Performance and energy requirements. *Energy Conversion and Management*, 46(11-12), 1957–1979.
- Rydh, C. J., & Sandén, B. a. (2005b). Energy analysis of batteries in photovoltaic systems. Part II: Energy return factors and overall battery efficiencies. *Energy Conversion and Management*, 46(11-12), 1980–2000.
- Saheb-Koussa, D., Haddadi, M., & Belhamel, M. (2009). Economic and technical study of a hybrid system (wind–photovoltaic–diesel) for rural electrification in Algeria. *Applied Energy*, 86(7-8), 1024–1030.

- Scozzari, R., & Santarelli, M. (2014). Techno-economic analysis of a small size short range EES (electric energy storage) system for a PV (photovoltaic) plant serving a SME (small and medium enterprise) in a given regulatory context. *Energy*, 71, 180–193.
- Semaoui, S., Arab, A. H., Bacha, S., & Azoui, B. (2013). Optimal Sizing of a Stand-alone Photovoltaic System with Energy Management in Isolated Areas. *Energy Procedia*, 36, 358–368.
- Shaahid, S. M., & El-Amin, I. (2009). Techno-economic evaluation of off-grid hybrid photovoltaic–diesel–battery power systems for rural electrification in Saudi Arabia—A way forward for sustainable development. *Renewable and Sustainable Energy Reviews*, 13(3), 625–633.
- Shaahid, S. M., & Elhadidy, M. A. (2007). Technical and economic assessment of grid-independent hybrid photovoltaic–diesel–battery power systems for commercial loads in desert environments. *Renewable and Sustainable Energy Reviews*, 11(8), 1794–1810.
- Shaahid, S. M., & Elhadidy, M. A. (2008). Economic analysis of hybrid photovoltaic–diesel–battery power systems for residential loads in hot regions—A step to clean future. *Renewable and Sustainable Energy Reviews*, 12(2), 488–503.
- Silva, S. B., Severino, M. M., & de Oliveira, M. a. G. (2013). A stand-alone hybrid photovoltaic, fuel cell and battery system: A case study of Tocantins, Brazil. *Renewable Energy*, 57, 384–389.
- Suresh Kumar, U., & Manoharan, P. S. (2014). Economic analysis of hybrid power systems (PV/diesel) in different climatic zones of Tamil Nadu. *Energy Conversion and Management*, 80, 469–476.
- Tan, C. W., Green, T. C., & Hernandez-Aramburo, C. a. (2010). A stochastic method for battery sizing with uninterruptible-power and demand shift capabilities in PV (photovoltaic) systems. *Energy*, 35(12), 5082–5092.
- Thevenard, D., & Pelland, S. (2013). Estimating the uncertainty in long-term photovoltaic yield predictions. *Solar Energy*, 91, 432–445.
- Tina, G. M., & Scandura, P. F. (2012). Case study of a grid connected with a battery photovoltaic system: V-trough concentration vs. single-axis tracking. *Energy Conversion and Management*, 64, 569–578.

- Upadhyay, S., & Sharma, M. P. (2014). A review on configurations, control and sizing methodologies of hybrid energy systems. *Renewable and Sustainable Energy Reviews*, 38, 47–63.
- Wenham, S.R., Green, M.A., Watt, M.E., Corkish, R. (2007). *Applied photovoltaics*. (Earthscan, Ed.). United Kingdom.
- Wissem, Z., Gueorgui, K., & Hédi, K. (2012). Modeling and technical–economic optimization of an autonomous photovoltaic system. *Energy*, 37(1), 263–272.
- Yang, H., Zhou, W., Lu, L., & Fang, Z. (2008). Optimal sizing method for stand-alone hybrid solar–wind system with LPSP technology by using genetic algorithm. *Solar Energy*, 82(4), 354–367.

### *Legislations*

- International Standard IEC 61724:1998, Photovoltaic system performance monitoring - Guidelines for measurement, data exchange and analysis.

### *Web references*

- European Commission, Eurostat, <http://epp.eurostat.ec.europa.eu/>. Last access: August, 2013.
- Joint Research Center (JRC) – Institute for Energy and Transport (IET). Photovoltaic Geographical Information System (PVGIS), <http://re.jrc.ec.europa.eu/pvgis/index.htm>, Last access: September, 2013.
- National Renewable Energy Laboratory (NREL). (2014). PV Watts tool. <http://rredc.nrel.gov/solar/calculators/pvwatts>. Last access: July, 2014.
- Pogodaiklimat. (2014). <http://www.pogodaiklimat.ru/>. Last access: July, 2014.
- Solarbuzz - Solar market research and analysis, <http://www.solarbuzz.com>, Last access: August, 2013.

# 5. Solar Concentrating Technology

## *Review of solar concentrating principles and technologies*

The purpose of this *Chapter* is to provide a conceptual background of solar concentration principles and a review of the available technical plant engineering solutions. The topics discussed are the basis and provide the right framework for the two experimental activities conducted to develop a concentrating photovoltaic (CPV) prototype and the thermal energy storage (TES) system described, respectively, in the following *Chapter 6* and *Chapter 7*.

### *5.1 Solar concentration background*

The physical principle at the base the solar concentration is elementary: the incident solar rays are either reflected by a surface, or their trajectory is partially deflected by the crossing of appropriate transparent surfaces in order to focus the incident solar rays on a smaller area than the source. The rays collecting surface is called *solar collector*, while the surface to which the rays are focused is called *solar receiver*.

Inside the atmosphere, solar radiation is the sum of three components:

- *Diffuse component*: the fraction of solar radiation scattered from the sky and from the surroundings and not directly incident on the target surface
- *Beam component* (Direct radiation): the fraction of solar radiation coming straight from the Sun and not subjected to any deviation or distortion phenomena
- *Reflected component*: The solar radiation fraction incident on the target surface after the reflection from Earth ground, sea and/or other artificial surfaces. It depends on the so-called local *Albedo* and needs to be considered in presence of tilted target surfaces

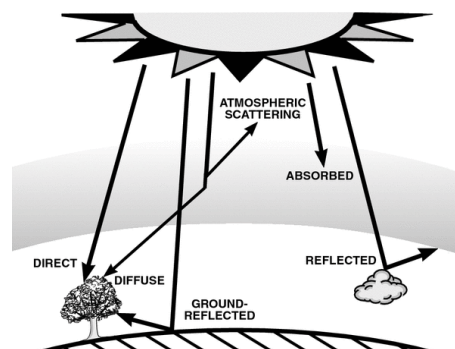


Figure 5.1 Different components of solar radiation

Solar concentrators are generally able to capture only the beam component of the solar radiation since diffuse or scattered and reflected radiations are not associated with a specific direction as for the beam fraction, as show in Figure 5.1. However, a portion a diffuse radiation can be collected but it is difficult to be estimated, especially during cloudy days, and it is usually neglected.

The optical concentration ratio,  $CR_O$ , is defined as the ratio of the solar flux,  $I_r$ , on the solar receiver to the flux,  $I_a$ , on the solar collector, while the geometric concentration ratio  $CR$ , measured in suns, is based on the solar receiver area,  $A_r$ , and solar collector aperture area,  $A_a$ , *i.e.* the area in which the solar radiation enters the collector.

$$CR_O = \frac{I_r}{I_a} \quad (5.1)$$

$$CR = \frac{A_r}{A_a} \quad (5.2)$$

$CR_O$  takes into account the optical losses and represents the true concentration ratio. However, it has no relationship with the receiver area and, therefore, with thermal losses which are proportional to such an area.  $CR$  is associated with the specific solar concentrator with another important parameter, *i.e.* the *acceptance angle*  $2\theta_{max}$ . The acceptance angle is the maximum angle within which light can be collected. The concentrator is then said to have an *half acceptance angle*  $\theta_{max}$ , or a total acceptance angle  $2\theta_{max}$  since it accepts light within an angle  $\theta_{max}$  to the optical axis. Its value depends on the concentration of the optic and the refractive index in which the receiver is immersed. The acceptance angle is linked to precision of the solar concentrator tracking and optical systems and its tolerance errors. The smaller the acceptance angle is, the more precision is required. Figure 5.2 explains the concept for an ideal concentrator: when the radiation angle of incidence  $\alpha$  is lower or equal than  $\theta_{max}$  all the rays collected by the solar collector are captured by the solar receiver, while when  $\alpha$  overcomes  $\theta_{max}$  all the rays are not captured by the solar receiver. Imperfections in the tracking and optical systems also contribute to decrease the acceptance angle.

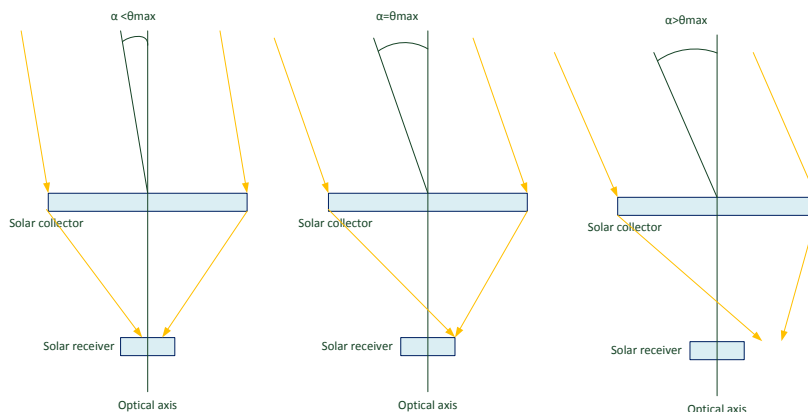


Figure 5.2 Acceptance angle examples in an ideal concentrator



The concentration of the solar radiation is achievable with two different strategies:

- Reflection through *solar mirrors*, which reflect the incident radiation and concentrate it to a focus area, *i.e.* the *solar receiver*, located over the mirror. According to the major literature, four main solar mirror configurations are currently available and installed in solar concentrating systems.
  1. *Parabolic troughs*: Parabolic troughs are line-focus systems. Their collectors are the mirrored surfaces of a linear parabolic concentrator focusing the direct solar radiation to the receiver located along the focal line of the parabola
  2. *Parabolic dishes*: Parabolic dish reflectors are point-focus collectors that track the sun in two axes, concentrating the solar radiation to a receiver located on the dish focal point
  3. *Heliostats*: Heliostats are usually a plane mirror, which turns so as to keep reflecting sunlight toward a predetermined target. The target may be a physical object, distant from the heliostat, or a direction in space. The reflective surface of the mirror is kept perpendicular to the bisector of the angle between the directions of the sun and the target as seen from the mirror.
  4. *Linear Fresnel reflectors*: A linear Fresnel reflector consists of an array of linear mirror strips, behaving as Fresnel lenses, which concentrates light to a fixed receiver mounted on a linear tower support
  
- Refraction through *solar lenses*, which refract the incident radiation and concentrating it to a focus area, *i.e.* the receiver, generally located under the lens plane. In this configuration a relevant parameter is the so-called focal length expressing the distance over which initially collimated rays are brought to the focus. This length is, consequently, the distance between the collector and the receiver. For concentrating purposes, converging lenses are required.

Details about reflection and refraction solar concentration strategies and their integration in existing CSP and CPV plants are in the following *Paragraph 5.2* and *Paragraph 5.3* (Goswami *et al.*, 2008; Pavlović *et al.*, 2012; Baharoon *et al.*, 2015).

## 5.2 Concentrating solar power (CSP) technology

In CSP plants, the solar radiation is concentrated through a solar collector into a solar receiver, where a heat transfer fluid (HTF) is heated up to several hundred Celsius degrees. The HTF is used to either directly or indirectly, *i.e.* heating up a second HTF in a proper heat exchanger, supply common thermodynamic cycles, *i.e.* Rankine, Brayton and Stirling cycles, for electricity generation (*power block*). Figure 5.3 represents a schematic representation of a CSP plant. In order to compensate the intermittent and random nature of solar radiation and increase the power block working hours, the CSP plant can integrate a fossil fuel based back-up power systems, *e.g.* a traditional boiler, and a thermal energy storage (TES) system.

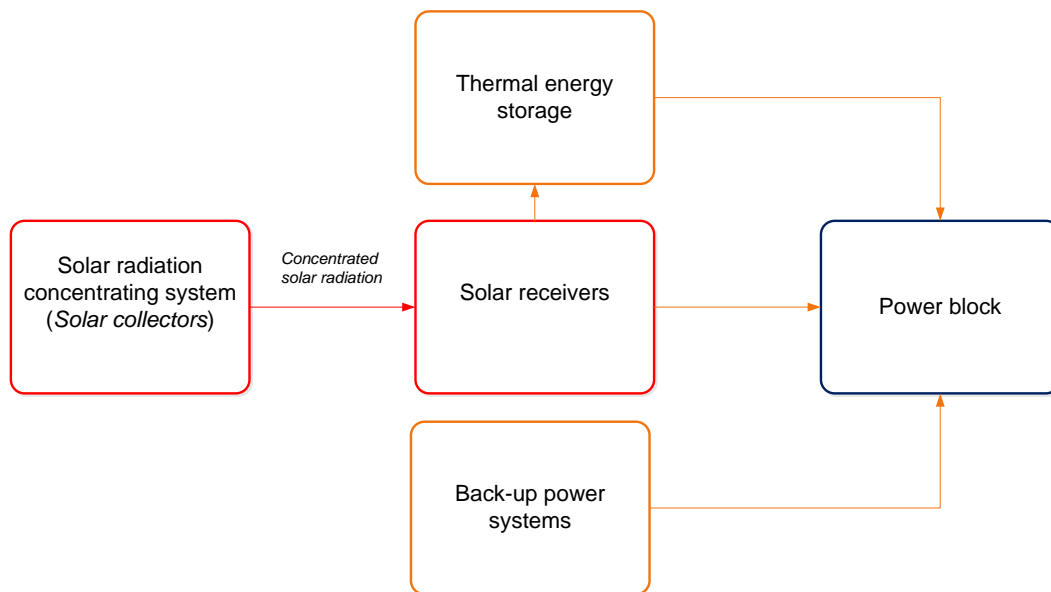


Figure 5.3 CSP plant schematic

Table 5.1 gives an overview of the CSP plants installed worldwide and the ongoing projects and the respective adopted technology. The four adopted technologies, *i.e.* parabolic trough collectors (PTC), tower solar power (TSP), Stirling dish collector (SDC) and linear Fresnel collector (LFC), are based on reflection strategy using solar mirrors to reflect and concentrate the solar radiation. More details are explained in more details in the following *Paragraphs*.

Table 5.1 CSP plants installed worldwide and ongoing projects (Baharoon et al., 2015)

CSP Plant technology	Active	Power [MW]	Under-construction	Power [MW]	Under-development	Power [MW]
Parabolic trough collector (PTC)	62	2,751.41	20	2,122	4	400
Tower solar power (TSP)	8	602	4	602	5	1,000
Stirling dish collector (SDC)	-	-	1	1.5	-	-
Linear Fresnel collector (LFC)	6	59.65	5	166	-	-
Total	76	3,413.06	30	2,891.5	9	1,400

PTCs are the most common commercially available solar concentrator with the first commercial plant built in the 1984. PTC is a mature technology, proven technically and

economically and able to guarantee an effective integration with conventional plants and with energy storage solutions. PTC-based active CSP plants represent the 95.7% of the total generating capacity of CSP plants. Considering under-construction projects, the percentage is 73.40% and decrease to 28.57% for under-development projects, reflecting the increasing importance of the other available technologies.

TSP technology is a recent technology, well established since the success of first commercial plant installed in 2007. The adoption of TSP technology is suitable for large scale CSP plants due to the system complexity and economy of scale reasons. Eight active projects are currently working (64.42MW installed, 2.24%), four are under-construction (602MW, 20.8%) and five under-development (1000MW, 71.43%) showing the increasing competitiveness of such a technology.

Concerning, SDC technology, its special design allows the use for remote and small-grid applications and the installation in sloped surface. Among all the CSP technologies it has the highest overall efficiency, *i.e.* peak solar to electricity conversion efficiency ranges from 29.4% to 31.25%, and zero water consumption for the wet/dry cooling system.

Although, the technology has currently only one under-construction commercial project due to the prohibitive cost and the difficult integration with storage solutions and traditional power plant. The generating capacity of this project is 1.5 MW (0.052% of the total generating capacity of under-construction CSP projects).

Finally, LFC technology has the lowest efficiencies among all the CSP technologies and the improvement in its optimal efficiency can make LFC a direct competitor for PTC technology. The lowest land use is a significant advantage is urban area or in case of integration with conventional plant with low land availability. Only six LFC projects with a total capacity of 59.65MW are active (2.07% of total CSP plant capacity) and 5 plants under-construction with a total generating capacity of 166MW (5.74%) (Pavlović *et al.*, 2012; Baharoon *et al.*, 2015).

### 5.2.1 Parabolic trough collector (PTC) technology

PTC technology adopts parabolic-shaped solar mirrors with a focusing system running along their focal line. Geometrically, the parabolic shape has the property that, for any line parallel to its axis, the angle between it and the normal surface is equal to the angle between the normal and a line to the focal point. Because of the solar radiation arrives to the Earth through parallel rays and by the Snell law the angle of reflection is equal to the angle of incidence, all the rays parallel to the axis of the parabola are reflected to the focus. Figure 5.4 shows such property,  $F$  is the focus.

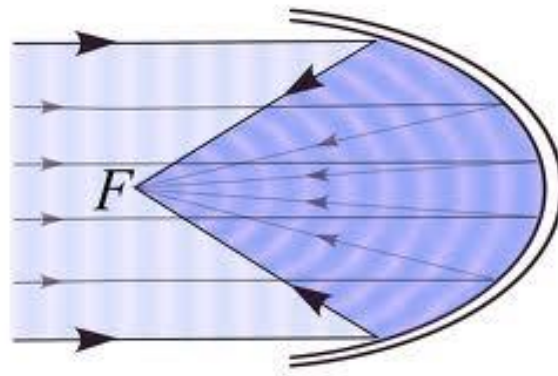


Figure 5.4 Reflection of solar radiation through parabolic mirror

One axis tracking technology is required with north-south axis direction providing more energy in summer, while east-west axis direction with better performance in winter. The tracking system rotates the collector in its single axis reflecting the direct component of solar radiation onto the receiver tube, located in the focal line, which contains the HTF, generally synthetic oil, molten salts or pressurized water.

The HTF reaches temperatures between 400°C to 500°C either generating steam to supply a conventional Rankine thermodynamic cycle in case of synthetic oil and molten salts or directly supplying the Rankine cycle in case of pressurized water. Figure 5.5 shows a picture of a series PTCs and a power plant using pressurized water as HTF and integrating a TES system.

The peak solar to electricity conversion efficiency is 23-27%, while the annual solar to electricity conversion efficiency is 15-16% (Baharoon *et al.*, 2015).

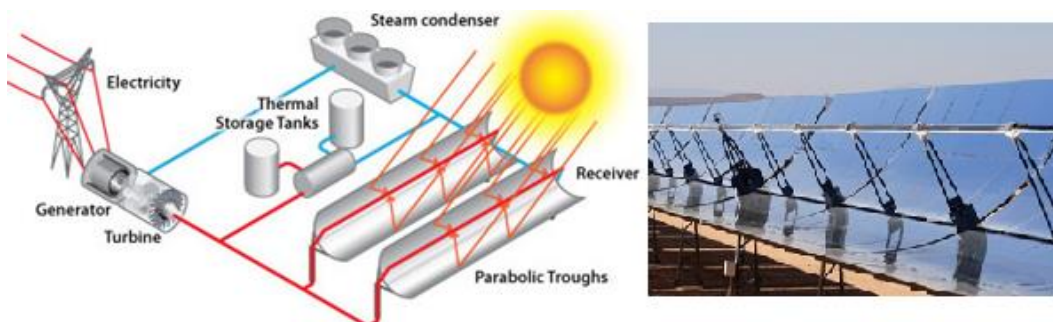


Figure 5.5 PTC-based CSP plant

### 5.2.2 Tower solar power (TSP) technology

TSP technology, also known as central receiver technology, adopts a number of two-axis controlled flat solar mirrors, *i.e.* heliostats, which reflects the direct component of solar radiation onto a central receiver located at the top of a power tower heating up a proper HTF.

The TSP plant can be designed in three different configurations with the aim to reduce the blocking and shading effects and to improve the solar field optical efficiency

- Vertical plane receiver with a north-facing heat transfer surface and the solar field located in the northern hemisphere of the tower
- Cylindrical receiver with an exterior heat transfer surface and the solar field located around the tower (circle configuration)
- Receiver with an enclosed heat transfer surface and the solar fields located north of the receiver

The available HTFs are several including molten salts, open air, pressurized water, superheated steam, pressurized air, *etc.* able to supply Rankine and Brayton thermodynamic cycles with temperature ranging between 200°C (Pressurized water) to about 700°C (air). The adoption of molten salts allows using the salts as HTF and energy storage medium at temperature up to 565°C, increasing significantly the energy storage capacity. The main disadvantage is that the water consumption for cleaning the heliostats and for cooling the exhaust wet steam from turbine is higher than the other solar technologies.

Figure 5.6 present a picture of TSP plant and a scheme of such technology using pressurized water as HTF to supply a Rankine thermodynamic cycle, while Figure 5.7 show a 30MW TSP CSP plant, designed with the software IPSE Pro, adopting molten salts as HTF and superheated steam to supply a Rankine thermodynamic cycle.

Central receiver technology is generally preferred for large scale utility power plants, *i.e.* rated power greater than 100MW, due to the technology complexity and economy of scale reasons. The peak solar to electricity conversion efficiency is 20-27%, while the annual solar to electricity conversion efficiency is 15-17% (Baharoon *et al.*, 2015).

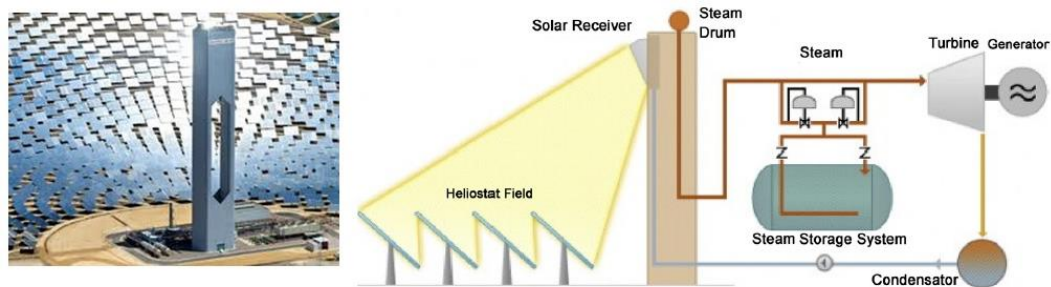


Figure 5.6 TSP-based CSP plant (Pavlović, 2012)

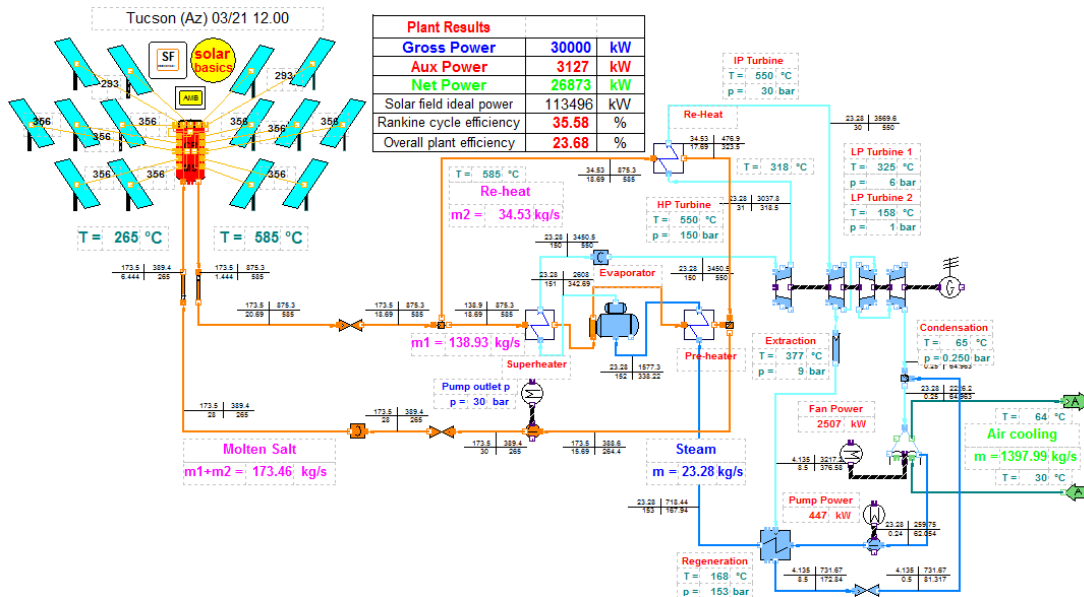


Figure 5.7 TSP-based CSP plant adopting molten salts as HTF and superheated steam as working fluid designed with IPSE Pro Software

### 5.2.3 Stirling dish collector (SDC) technology

SDC technology uses a two-axis controlled parabolic dish-shaped mirror, which reflects the direct component of solar radiation to a central receiver located at the focal point of the parabolic dish. The generated high temperature, up to 1000°C, is converted into electricity through a micro-turbine or Stirling engine. The available working fluids for the Stirling engine are either helium or Hydrogen. Concerning, SDC technology, its special design allows the use for remote and small-grid applications and the installation in sloped surface. Among all the CSP technologies it has the highest overall efficiency, *i.e.* peak solar to electricity conversion efficiency ranges from 29.4% to 31.25%, and zero water consumption for the wet/dry cooling system.



Figure 5.8 SDC-based CSP plant (Pavlović, 2012)

### 5.2.4 Linear Fresnel collector (LFC) technology

SDC is one tracking technology using a fixed collector and an elevated inverted linear fixed receiver. The collector has a parabola shape and it is composed by a number of flat ground mounter mirrors, which each rotates to reflect the direct component of solar radiation onto a linear receiver, *i.e.* a long, selectively coated absorber tube. The main advantages of such technology are the fixed receiver, the flexibility on the choice of the HTF (thermal oil, water, molten salts *etc.*) and the low capital costs due to the light structural support, flat reflectors and fixed receiver without moving joints. However, blocking and shading effects of adjacent mirrors, shading of the fixed receiver and impossibility to reach an ideal parabola reduce the optical efficiency. The design and development of compact linear Fresnel collector (CLFC) can further reduce the cost and land use making the technology competitive with PTC-based plant. The peak solar to electricity conversion efficiency is 18-22%, while the annual solar to electricity conversion efficiency is 8-10% (Baharoon *et al.*, 2015). Figure 5.9 shows a picture of a series LFCs and a power plant using pressurized water as HTF.

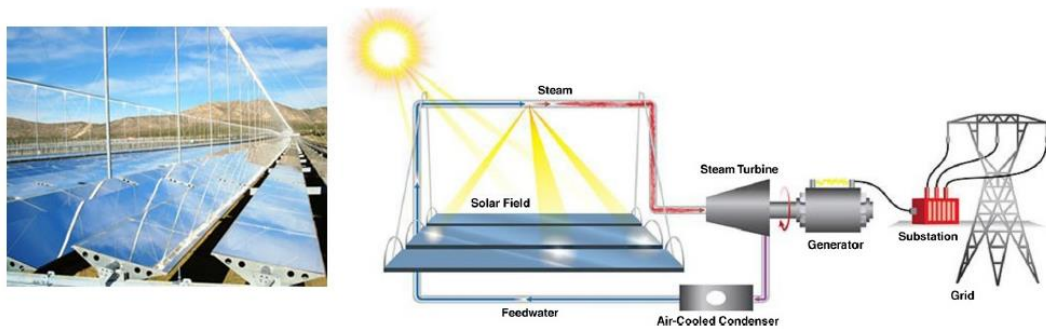


Figure 5.9 LFC-based CSP plant (Pavlović, 2012)

Concluding the overview on CSP plants, Table 5.2 compares the main features of the described technologies.

Table 5.2 Main features of the described CSP plant technologies (Baharoon *et al.*, 2015)

Parameter	PTC	TSP	SDC	LFC
Focus technique	Line focus	Point focus	Point focus	Line focus
Tracking system	1-Axis	2-Axis	2-Axis	1-Axis
Peak solar to electricity conversion efficiency	23-27%	20-27%	29.4-31.3%	18-22%
Annual solar to electricity conversion	15-16%	15-17%	26%	8-10%
Water consumption for wet/dry cooling [m <sup>3</sup> /MWh]	3-4/0.2	3-4/0.2	0	3-4/0.2
Land use [m <sup>2</sup> /MWh/year]	6-8	8-12	8-12	4-6
Cost (100MWe at 2000kWh/m <sup>2</sup> year) [€/kWh]	0.265	0.230 Storage	-	0.230 Buffer
Cost (100MWe at 2500kWh/m <sup>2</sup> year) [€/kWh]	0.187 Storage	0.210	-	0.200 Buffer
Storage type	Direct-indirect (Molten salts)	Direct (Molten salts) Buffer (Water)	No	Buffer (Water)
Storage hours (h)	0.5-12	1-15	0	0.5-1
Operating temperature [°C]	310-393 (Oil) 340 (Water) 550 (Molten salts)	250-500 (Water) 565 (Molten salts) 680 (Air)	250-700 (Hydrogen or Helium)	250-300 (Water-HTF)

The cost per unit of energy produced decrease in case of storage integration emphasizing the significant importance of TES solutions. In this context, in the next *Chapter 7*, an experimental activity for the development and experimental tests of a TES prototype for a central receiver CSP plant is presented. Such prototype refers to a central receiver CSP plant working with air as HTF and working fluid in a Brayton cycle.

### 5.3 Concentrating photovoltaics (CPV) technology

CPV systems adopt PV solar cells to directly convert solar radiation to electrical power energy, without the interaction to any thermal vector, *e.g.* steam, heat fluids, *etc.*, as in CSP plants. In such systems, adopting line-focus or point-focus geometries, an array of PV cells is located on the solar receiver and it is lighted by the concentrated solar radiation. The main purpose of CPV system is to reduce the cost of electricity produced replacing the PV cell surface, *i.e.* an expensive material, with cheaper optical devices, *i.e.* mirrors and lenses, able to concentrate the solar radiation on a small and high efficient PV cells. The opportunities offered by CPV toward flat-plane systems are the following:

- Superior conversion efficiency, *i.e.* over 20%
- Higher annual capacity factor, especially, toward fix plane plants
- Low material availability requirements
- Less toxic material usage
- Ease of recycling
- Ease of rapid manufacturing scale-up
- High local manufacturing content
- Possibility to compete on costs

However, the requirement of a solar tracking system, in order to capture the direct component of solar radiation, and a cooling system, in order to avoid electric conversion efficiency decrease and solar cell damages, increases the complexity and costs of such a technology. CPV systems have been developed together with development of PV technology but such complexity and the size of the CPV industry have delayed the large-scale diffusion of these systems.

CPV systems are classified according to the concentration ratio of the solar radiation incident onto the cell: low concentration (LCPV) with a concentration ratio ranging between 1 and 40 suns, medium concentration (MCPV) with a concentration ratio ranging between 40 and 300 suns and high concentration (HCPV) with a concentration ratio ranging between 300 and 2000 suns. Among them, HCPV systems have a major interest in the industrial and scientific contexts and they offer best perspectives in terms of efficiency and costs reduction (Muñoz *et al.*, 2010; Pérez-Higueras *et al.*, 2011).

In the following *sub-Paragraphs*, a brief description of the current available technologies is presented with particular attention to point-focus Fresnel lens-based HCPV plant. Such technology is used in the prototype described in the following *Chapter 6*.



### 5.3.1 CPV solar cells

Solar cells are a key component for all PV systems. Great progresses in materials and cell layout, *i.e.* the position of the photosensitive surface, bonding and wires, by-pass diode, *etc.*, are done together with an increasing miniaturization of cell size. A detailed classification of PV solar cells is in Miles *et al.* (2005). Figure 5.10 summarizes the major cell typologies and promising frontiers.

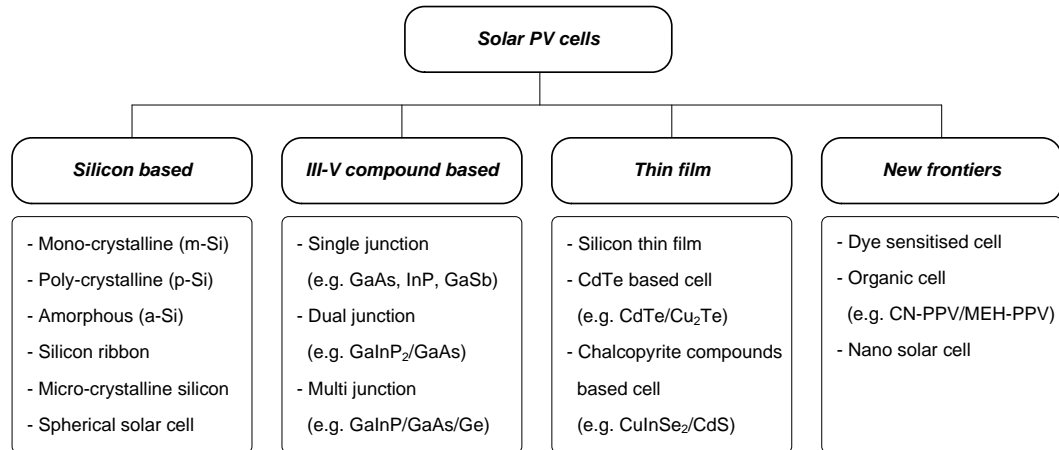


Figure 5.10 Solar PV cell classification

In CPV systems great attention is paid to guarantee high cell conversion efficiency levels, even tolerating a cost increase for the higher quality of the adopted cells. This is due to the compensation introduced by the low requested receiver surface replaced by the optic collector concentrating the solar radiation. Such reasons explain the great interest in multi-junction PV (MJPV) solar cells for CPV systems. To understand the operating principle and the potential strength of MJPV cells the concept of optical band gap needs to be introduced. In PV applications, the optical band gap is an energy range, proper of each material, and it determines the portion of the solar spectrum that the material can absorb. Table 5.3 lists the band gap of some of the most common semi-conductors adopted in the PV sector.

Table 5.3 Energy band gap of the most commonly adopted semi-conductors

Semi-conductor	Energy Band Gap (eV) at 302K
Silicon (Si)	1.12
Indium Selenide (InSe)	1.3
Gallium Arsenide (GaAs)	1.4
Cadmium Telluride (CdTe)	1.47
Cadmium Selenide (CdSe)	1.7
Gallium Phosphide (GaP)	2.25
Copper Sulfide (CuS)	1.2
Cadmium Sulfide (CdS)	2.25
Germanium (Ge)	0.8
Indium Nitride (InN)	0.9
Gallium Nitride (GaN)	3.4

Considering an ideal single-junction PV cell with a proper band gap  $E_g$  and a photon incident on the cell with an energy  $E_\lambda$  equal to:

$$E_\lambda = h \cdot \frac{c}{\lambda} \quad (5.3)$$

Where:

- $h$  is the Planck constant [ $\text{m}^2\text{kg/s}$ ]
- $c$  is the speed of light [ $\text{m/s}$ ]
- $\lambda$  is the photon wavelength [ $\text{m}$ ]

Two possibilities occur. If  $E_\lambda < E_g$  the photon is not absorbed and it does not contribute to the PV phenomena. Otherwise, if  $E_\lambda \geq E_g$  the photon is absorbed. In such latter case, a portion of energy, equal to  $E_g$ , can be converted to electrical power, while the excess is dissipated through heat. As a consequence, a single-junction PV cell is sensible to a specific range of the solar spectrum correspondent to its energy band gap. Because of the energy band gap depends on the PV cell semi-conductor, to enlarge the sensible range several materials are adopted. MJPV cells follow such a principle and they integrate several layers of different semi-conductors. The upper layer has the highest band gap, while the lowers are stacked in descending order of their band gaps. From such a perspective, the ideal solar cell should include hundreds of different layers, each one tuned to a small range of light wavelengths, from ultraviolet to infrared. Difficulties in manufacturing limit the number of layers to few units. Nowadays, triple junction PV (TJPV) cells represent a standard for MJPV cells. Figure 5.11 shows a 3D scheme of a TJPV cell. As explained, the top, middle and bottom sub-cells are in descending order of their energy band gap. The tunnel junctions are added to provide a low electrical resistance and optically low-loss connection between each couple of adjacent sub-cells.

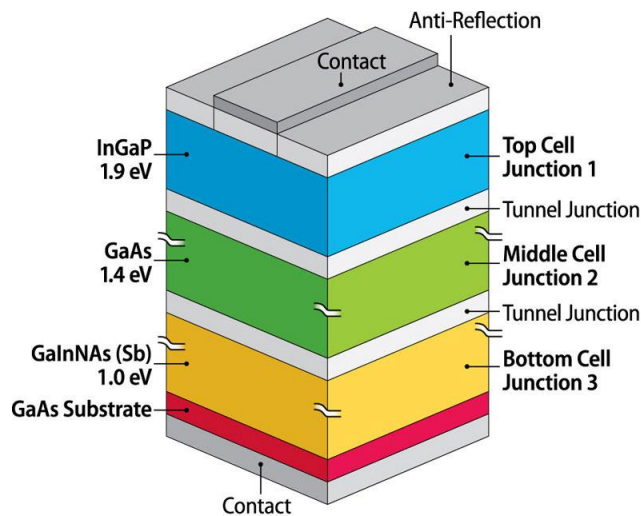


Figure 5.11 TJPV solar cell layout, example

Despite the higher costs, CPV modules using MJPV cells can achieve electric conversion efficiencies up to 39%, while CPV modules integrating silicon PV cells convert solar radiation into electricity with efficiency around 27%. In addition, the efficiency evolution, from 1986 to 2010, shows an exponential growth for MJPV cells, while for silicon cells a slight variation occurred (Pérez-Higueras *et al.*, 2011).

### 5.3.2 Cell cooling and heat recovery

In PV systems, only a fraction of the incoming sunlight striking the cell is converted to electrical energy. The remainder of the absorbed energy is converted to thermal energy, *i.e.* heat, and it causes the temperature to rise unless the heat is efficiently dissipated to the environment. Considering CPV, this phenomenon is critical due to the high light flux concentrated to the small receiver area. Temperatures on the receiver surface can reach hundreds of Celsius degrees, especially in presence of high concentration ratios. As a consequence, unforced heat dissipation, by natural air recirculation, is not sufficient to maintain reasonable cell temperatures. A receiver cooler is, generally, required. This is also to avoid the cell efficiency degradation due to its high working temperature.

Royne *et al.* (2005) investigate the cooling of PV cells under concentrated illumination. Their review of such issue points out two strategies, *i.e.* passive and active cooling, for cell cooling:

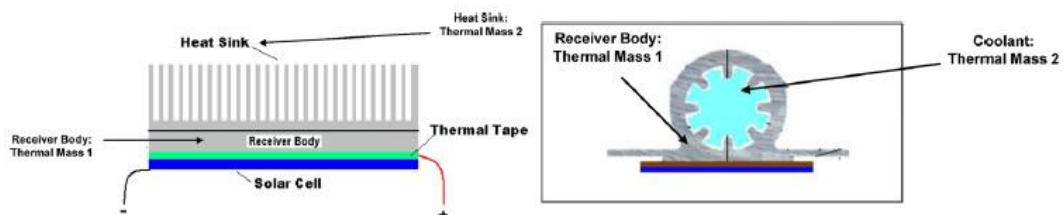


Figure 5.12 Active and passive cooling (Vivar *et al.*, 2012)

Passive cooling transfers heat without using any additional HTF. Typical passive coolers are made up of linear fins located on all the available heat sink surfaces to increase the heat exchange area. Such solutions work well at low and medium concentration ratios, *i.e.* up to 300x, they do not require pipes and other additional circuits and they are cost effective especially for point-focus geometry concentrators.

On the contrary, active cooling is a type of heat transfer that uses powered devices, such as fans or pumps, to cool a surface, *i.e.* the cells. It generally requires installing and controlling a circuit for cooling fluid circulation. Its cost is higher than for passive coolers, the simplicity lower but the performances are, frequently, higher (see Royne *et al.* (2005) for a comparison between passive and active coolers). Such a cooling strategy fits well with high concentration solar plants, *i.e.* up to 2000x, linear-focus geometries and it allows to easily collect and to recover heat thanks to the presence of the cooling fluid. The prototype described in the next *Chapter* includes an active cooling circuit and heat recovery system using purified water as cooling fluid.

### 5.3.3 CPV plant technologies

The IEC 62108 norm, the first standard developed exclusively for CPV technology, covers five different technologies, shown in Figures 5.13-15.

- Point-focus dish CPV technology
- Linear-focus trough CPV technology
- Point-focus Fresnel lens CPV technology
- Linear-focus Fresnel lens CPV technology
- Heliostat CPV technology

The solar collector, integrating the optical devices, used to concentrate the solar radiation onto the solar receiver, integrating the PV cells, are based on the same principles of solar collectors of CSP plants described in the previous *sub-Paragraphs*. CPV systems can also integrate point-focus Fresnel lenses, which behavior and principles are explained in the following *Paragraph 5.3.4*.

In addition, CPV plants usually integrate a secondary optics element (SOE). SOE are used to increase the optical system efficiency by catching refracted light that otherwise would miss the receiver, compensating assembly and tracking errors, better the tracking tolerance, increasing the angle of acceptance, and enhance the flux uniformity on the cell, avoiding the decrease of electric conversion efficiency.

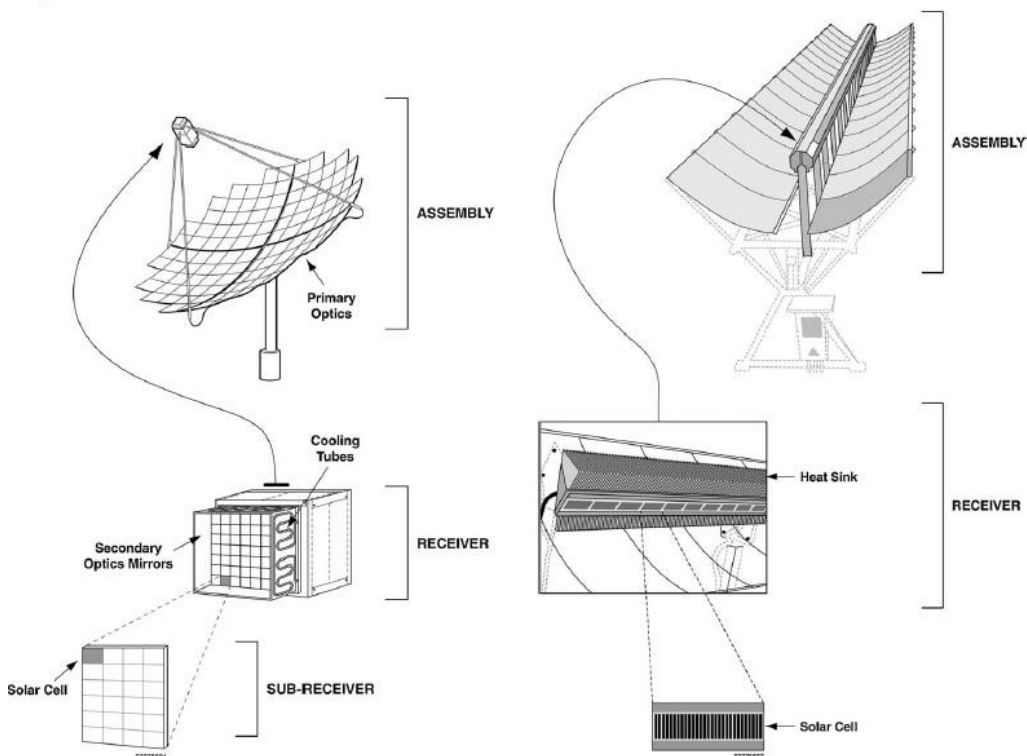


Figure 5.13 Point-Focus Dish and Linear-Focus Trough (Muñoz et al., 2010)

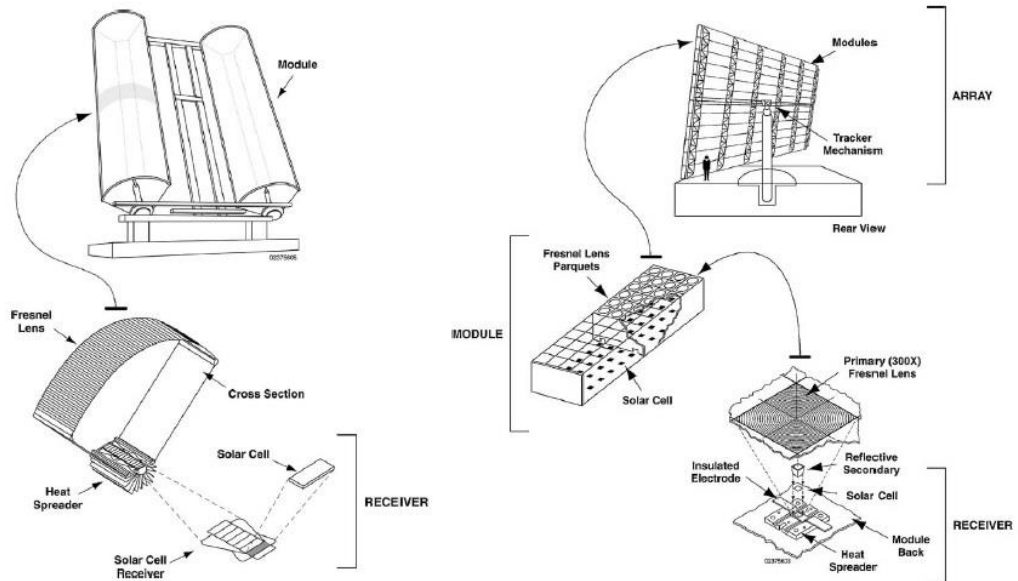


Figure 5.14 Point-Focus and Linear-Focus Fresnel Lenses (Muñoz et al., 2010)

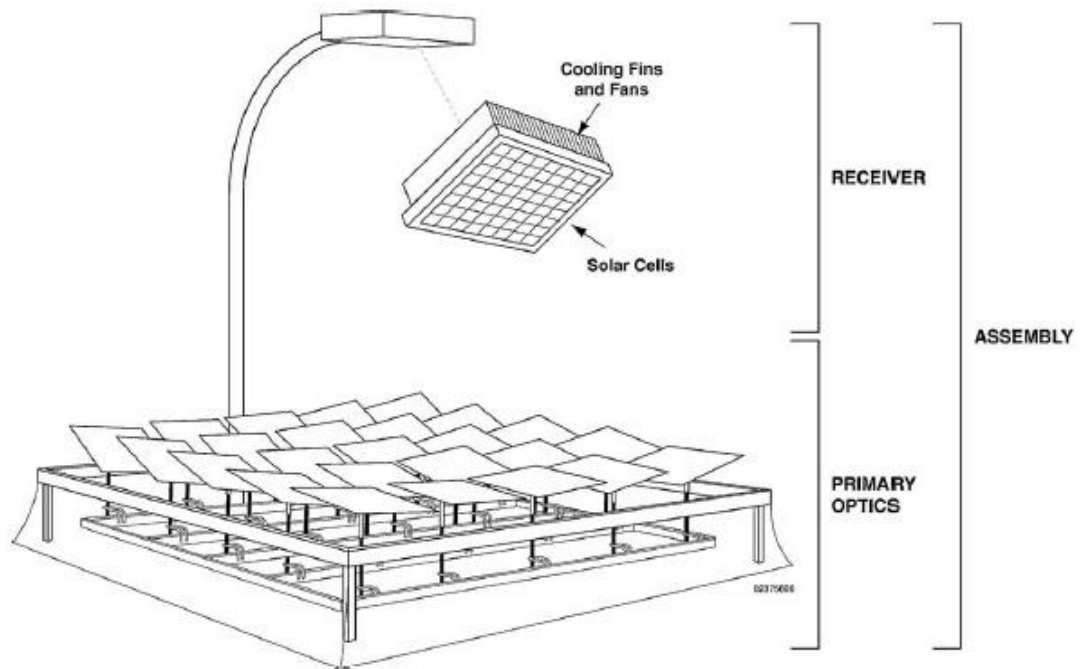


Figure 5.15 Heliostat CPV (Muñoz et al., 2010)

The CPV market is still small compared to traditional PV and CSP plants but interest is increasing due greatly to higher efficiency levels in locations with high insolation and low moisture. The first large-scale project started its operation 2011, and, by mid-2012, more than 100 plants totaling as much as 100 MW were operating in at least 20 countries worldwide (REN21, 2013).

### 5.3.4 Fresnel lens refraction optic

This *Paragraph* focuses on the properties and principles of Fresnel lenses, adopted in the developed CPV prototype. The concentration of light to a point focus was originally made

with biconvex or plano-convex converging lenses. In such lenses, a collimated beam of light travelling parallel to the lens axis is focused to a spot on the axis (Figure 5.16).

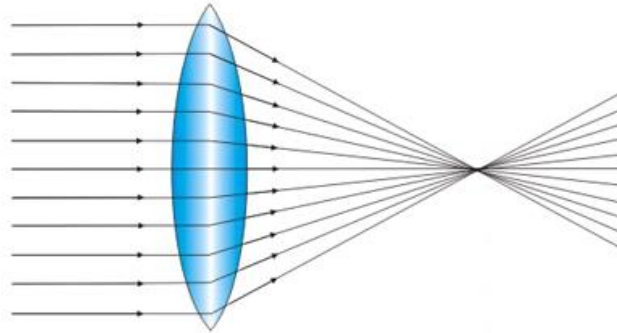


Figure 5.16 Biconvex converging lens

Strong weaknesses of such lenses are their weight, dimensions and the high focal length. In 1748, G.L. Leclerc starts to investigate how to overcome such troubles and, in 1820, A.J. Fresnel builds the first prototype of a new lens, taking its name, for a lighthouse application. Fresnel lens is a flat optical component with the surface made of several small concentric grooves, approximating by a flat surface the curvature at that position of conventional convex lenses (Sierra & Vázquez, 2005), so that the excess non-refractive portions of conventional lenses are removed preserving the focusing profile (Lo & Arenberg, 2006). Figure 5.17 proposes the equivalent Fresnel of a plano-convex lens. The thickness and the material reductions are evident.

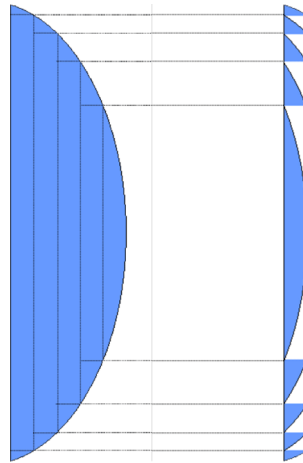


Figure 5.17 Equivalent Fresnel of a plano-convex lens

Nowadays, Fresnel lenses represent the standard optics for collectors in all solar refraction plants. Two basic configurations of the Fresnel lenses are feasible and they define a same number of refraction plant design typologies: linear and point-focus Fresnel lenses. The former has linear parallel grooves and it focuses the solar radiation on a line, *i.e.* the receiver should be linear, while the latter presents spotted circular focuses and it is used for point-focus geometry receivers. Developments in concentrating solar energy applications integrating Fresnel lenses are still in progress. The adoption of such a technology to concentrate the solar radiation is more recent than for reflection

through mirrors. Xie *et al.* (2011) fully review this sector presenting an useful classification of the major improvements in concentrating solar energy Fresnel lens systems. The large amount of contributions, both theoretical and experimental, are proposed after the '80s and they consider the so-called non imaging Fresnel lenses, *i.e.* lenses designed with the specific purpose of concentrating light rather than forming an image. Such a technology is recognized to be very competitive for solar collectors due to the possibility of having high concentration ratios, *e.g.* higher than 1000x, optical efficiencies, together with light-weight and cost effectiveness due to the adoption of low cost materials, like poly-methyl-methacrylate (PMMA), for lens manufacturing. Such strengths justify the adoption of this concentrating technology for the proposed CPV prototype described in the next *Chapter 6*.

## References

- Baharoon, D. A., Rahman, H. A., Omar, W. Z. W., & Fadhl, S. O. (2015). Historical development of concentrating solar power technologies to generate clean electricity efficiently – A review. *Renewable and Sustainable Energy Reviews*, 41, 996–1027.
- Goswami, D.Y., Kreith, F., Kreider, J. F. (2008). *Principles of Solar Engineering*, Second Edition. (CRC Press, Ed.).
- Lo, A., Arenberg, J., (2006). New architecture for space telescopes uses Fresnel lenses. SPIE newsroom – The international Society for Optical Engineering.
- Miles, R.W., Hynes, K.M., Forbes, I., (2005). Photovoltaic solar cells: an overview of state-of-the-art cell development and environmental issues. *Progress in Crystal Growth and Characterization of Materials* 51:1-42.
- Muñoz, E., Vidal, P. G., Nofuentes, G., Hontoria, L., Pérez-Higueras, P., Terrados, J., ... Aguilera, J. (2010). CPV standardization: An overview. *Renewable and Sustainable Energy Reviews*, 14(1), 518–523.
- Pavlović, T. M., Radonjić, I. S., Milosavljević, D. D., & Pantić, L. S. (2012). A review of concentrating solar power plants in the world and their potential use in Serbia. *Renewable and Sustainable Energy Reviews*, 16(6), 3891–3902.
- Pérez-Higueras, P., Muñoz, E., Almonacid, G., & Vidal, P. G. (2011). High Concentrator PhotoVoltaics efficiencies: Present status and forecast. *Renewable and Sustainable Energy Reviews*, 15(4), 1810–1815.
- REN21 Renewable energy policy network for the 21st century. (2013). *RenewableS 2013 GLOBAL STATUS REPORT*.

- Royne, A., Dey, C.J., Mills, D.R., (2005). Cooling of photovoltaic cells under concentrated illumination: a critical review. *Solar Energy Materials and Solar Cells* 86:451-483.
- Sierra, C., Vázquez A.J., (2005). High solar Energy concentration with a Fresnel lens. *Journal of Materials Science* 40:1339-1343.
- Vivar, M., Clarke, M., Pye, J., & Everett, V. (2012). A review of standards for hybrid CPV-thermal systems. *Renewable and Sustainable Energy Reviews*, 16(1), 443–448.
- Xie, W. T., Dai, Y. J., Wang, R. Z., & Sumathy, K. (2011). Concentrated solar energy applications using Fresnel lenses: A review. *Renewable and Sustainable Energy Reviews*, 15(6), 2588–2606.



## 6. Concentrating PV/T Prototype

### *Design, development and performance tests of a small-scale concentrating photovoltaics prototype with thermal recovery (CPV/T)*

The technical and economic sustainability of Photovoltaic (PV) systems is heavily affected by the cost and performances of the adopted PV cells. Concentrating Photovoltaic (CPV) technology represents an effective alternative to reduce the PV cell surface and, at the same time, to increase the global conversion efficiency. Such systems include optic elements to concentrate the solar radiation to a small area where high-efficiency PV cells are located. Particularly, the adoption of multi-Junction photovoltaic (MJPV) solar cells, is encouraged to increase the power conversion performance. This *Chapter* presents full details about the design, development and experimental tests, carried out in the 2011-2012 period, of a Fresnel lens Concentrating Photovoltaic Thermal (CPV/T) prototype for the micro-cogeneration of electrical power and thermal energy. The two axis controlled prototype integrates five different functional modules to guarantee the required features. Basically, the MJPV cells allow power production, while Water Heat Exchangers (WHEs) are installed for both the cell cooling and the recovery of thermal energy. The operative concentration factor is up to 800x through eight non-imaging Fresnel lenses integrated to the solar collector. Furthermore, a two axes solar tracker assures sun collimation during day-time. The prototype control, together with the monitoring of the environmental conditions and the energy conversion performances, is provided thanks to a semi-automatic real-time interface developed adopting LabView® Integrated Development Environment (IDE).

This *Chapter* focuses on the description of the hardware components, *i.e.* the mechanical, hydraulic and electrical devices, their integration to the plant and the experimental analysis assessed to study both the solar collimation accuracy and the prototype overall energy performances. The two axis tracking system control strategy, briefly described in this *Chapter*, is provided and fully discussed in Bortolini *et al.* (2012).

### *6.1 CPV technology overview and prototype objectives*

With reference to the 2010-2011 period, PV silicon solar cells was generally able to produce electricity with a conversion efficiency lower than 26% (Green *et al.*, 2010), while MJPV cells, III–V components based, reached values close to 42% (Guter *et al.*, 2009 & Pan *et al.*, 2011) representing an efficient solution to convert the sun rays to power

energy. Unfortunately, due to their high cost, these cells are not convenient for standard flat-plane modules. Crystalline silicon represents, actually, the most adopted material to produce PV modules. The CPV technology allows reducing the receiver surface due to the concentration of the sun rays to a small area, *i.e.* focus point. Consequently, in such energy plants, the adoption of MJPV cells becomes feasible and potentially profitable (Wenham *et al.*, 2007). However, its complexity and the size of the CPV industry have delayed the evolution and high-scale establishment of these systems. The pioneer multi-megawatt project came on line in 2011, and, by mid-2012, only 100 plants for a total power of about 100 MW were operating in at least 20 countries worldwide, compared to the 100GW traditional PV global capacity installed at the end of 2012 (Muñoz *et al.*, 2010; REN21, 2013).

Considering CPV applications, the literature proposes several contributions. Zubi *et al.* (2009) present the state of the art of high concentration photovoltaics. These energy conversion systems adopt parabolic mirrors or lenses to convey the sun rays to the solar receiver with a concentration factor usually above 400 *suns*. El Gharbi *et al.* (2011) analyze and compare such optic technologies, while Xie *et al.* (2011) and Chemisana *et al.* (2009) focus and review the applications integrating Fresnel lenses. Sonneveld *et al.* (2011) and Chemisana (2011) review and describe building integrated concentrating PV systems highlighting the current state of the art and the possible future scenarios.

Solar concentration systems generally require a cooling circuit to control the receiver temperature preventing damages to the cells and the decrease of their conversion efficiency level. Chemisana *et al.* (2011) estimate an average decrease of the cell electrical performances equal to 0.14% per Celsius degree. Even if a cooling hydraulic circuit is often necessary, nowadays, few applications integrate a thermal recovery unit to solar concentrators. Combined Heat and Power (CHP) systems are not often developed, especially for small size solar energy systems, *i.e.* micro-cogeneration, while a large number of contributions consider CHP plants integrated to plane modules. Immovilli *et al.* (2008) focus this aspect in deep. Finally, solar concentrators are able to capture only the beam fraction of the solar radiation. A sun tracking system represents a crucial device to increase the solar conversion efficiency. Aim of this device is to guarantee the best collimation between the solar collector and the sun, from sunrise to sunset, so that the former is always orthogonal to the direction of the sun rays (Rumyantsev *et al.*, 2004). Bortolini *et al.* (2012) describe the design and test of a sun tracking system based on a feedback control algorithm applied to a Fresnel lens small scale module.

This *Chapter* present a research activity concerning about the design, development and field-test of a CPV/T prototype for the distributed micro-cogeneration of heat and power. The purpose is to investigate CPV/T technology in a small scale plant solution highlighting the potential and critical issues of such technology for distributed generation of energy. The developed energy system allows studying the electric and thermal conversion efficiencies together with an assessment of the solar collimation accuracy.

Furthermore, an analysis of the expected manufacturing costs highlights the crucial drivers affecting an investment in such solar energy plants.

The experimental relevance of such a research activity is confirmed by the support of the Fondazione Cassa di Risparmio di Trento e Rovereto, Italy, through a sponsorship to the MiSTICo Project (Micro-Sistemi e Tecnologie Innovative per la COgenerazione da energia solare) focusing on CPV technology and involving the Universities of Padova, Bologna and Trento and the Bruno Kessler Foundation - Trento, Italy. The research project includes prototypal and experimental connotation. Improvements, changes and further tests are still required even if a final plant layout solution is already obtained and assembled.

The reminder of this *Chapter* is organized as follows: the next *Paragraph 6.2* describes the developed prototype, giving full details about its functional modules. *Paragraph 6.3* introduces the aforementioned economic analysis of the system manufacturing costs, while, in *Paragraph 6.4*, the outcomes of a set of field-tests are discussed highlighting the perspectives for such an energy system. Conclusions are in *Paragraph 6.5* together with suggestions for further research and the prototype improvement.

## 6.2 CPV/T Prototype description

The description of the prototype follows a “general to detail” approach and a functional perspective. At first, the plant is presented as a whole proposing its general features and the global structure. The five functional modules are, then, investigated highlighting their role to make the plant working effectively and the choices made for their design and development.

The CPV/T prototype is a stand-alone plant, designed to be installed at the ground level or on a plane roof facing the sun during the whole day, e.g. south-oriented location. Actually, such a system is on the south-east oriented plane roof at the University of Bologna - Department of Industrial Engineering laboratories. The installing location geographical coordinates are: latitude  $\phi$  44.5136° North, longitude  $L$  11.3184° East

The following five functional modules are integrated to the CPV/T prototype:

- support steel structure
- solar collectors and receivers
- solar biaxial tracking system
- real-time motion control and monitoring system
- hydraulic circuit for cell cooling and thermal recovery

In addition, an auxiliary weather station monitors the profiles of the global and beam radiation, the air temperature, the wind speed and direction in order to estimate the plant performances and to measure the weather conditions with the support of the semi-automatic real-time interface developed adopting LabView© Integrated Development Environment (IDE).

The following Figure 6.1 shows, respectively, a frontal and back view of the developed prototype, including the main components/functional modules and their reciprocal positions. The grey flat surface is the plane roof where the plant is located.

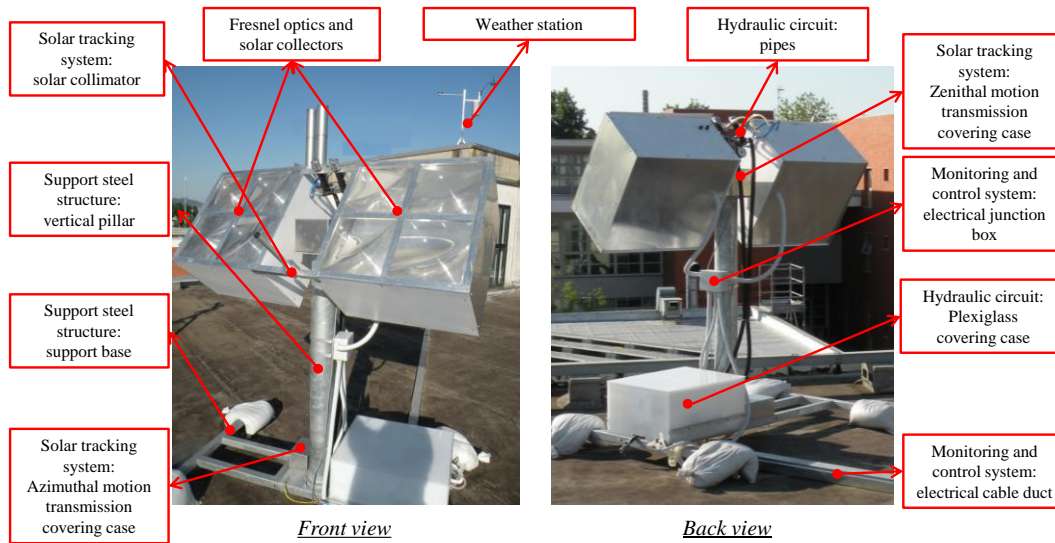


Figure 6.1 CPV/T prototype, front and back views

The overall dimensions are, approximately, of 1.6x1.7x2m height and the weight is of 120kg. A set of eight squared 330x330mm Fresnel lenses, fixed on a reticular frame, made of several welded aluminum squared profiles, *i.e.* the solar collector, concentrates the incident radiation on an equivalent number of solar receivers located in correspondence of the lens foci. Each of them includes a high efficiency triple-junction photovoltaic (TJPV) solar cell installed on a WHE with the purpose of both cell cooling and thermal recovery. Furthermore, the biaxial solar tracker guarantees the highest captation of solar radiation during the day by aligning the system position to the direction of the incident sun rays. The solar tracker consists of two mechanical actuators able to rotate both the collector and the receiver along two solar coordinates, *i.e.* the azimuthal and zenithal axes of motion, so that the surface of the Fresnel lenses is always orthogonal to the direction of the incident radiation. An electronic remote controller implements a closed loop algorithm for solar tracking. At last, the hydraulic circuit integrated to the prototype allows the cooling of the cells and the heat recovery supplying the cooling fluid, *i.e.* purified water, to the WHEs.

Further details about each of them are provided in the next *Paragraphs* of this *Chapter* together with a quantitative description of the design choices.

### 6.2.1 Support steel structure

The support structure of the developed prototype is made of two elements, both realized with galvanized steel, *i.e.* the support base and the vertical pillar (see Figure 6.2). The former, whose dimensions are 1.6x1.0m, prevents the tip over of the whole plant and it is made of four squared 50x50mm welded tubular profiles. A 320x320mm galvanized steel plate is screwed in the center of the base and supports the latter structural element, *i.e.*

the vertical pillar, and the azimuthal tracking system. Its height is of 1.4m and the diameter of 140mm. On top of the pillar, it is located a 1.6m horizontal shaft supported by a 300x200mm galvanized steel plate. The horizontal shaft supports an aluminum reticular frame which integrates solar collectors and solar receivers.

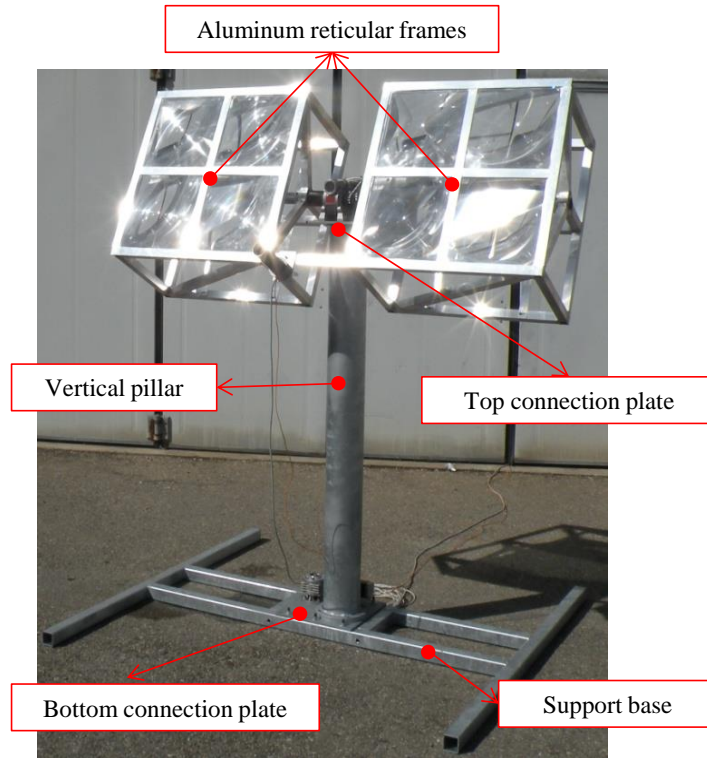


Figure 6.2 CPVT prototype, support steel structure

Figure 6.2 clearly shows the pillar while the shaft is not immediately visible because it is located inside the solar collection modules. Figure 6.3, taken during the prototype assembly, depicts the horizontal shaft on top of the vertical pillar, together with the zenithal tracking system described in the following.

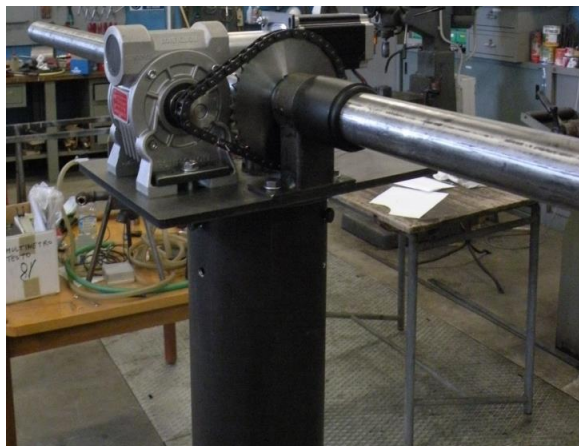


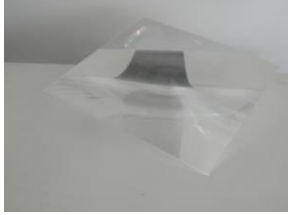
Figure 6.3 Support steel structure: the vertical pillar and the horizontal shaft

### 6.2.2 Solar collectors

The designed solar collector detects the incident radiation on a wide surface and concentrates it to a smaller area where the receivers, including the TJPV cells, are

located. As introduced, eight non-imaging point-focus PMMA Fresnel lenses are used and they represent the key elements of the collector. Their geometric and optic features are summarized in Table 6.1.

*Table 6.1 Features of the adopted Fresnel lenses*

Dimensions	330x330mm	
Thickness	3mm	
Focal length	350mm	
Refractive index	1.491	
Groove	1mm	
Abbe number	58	

To properly support and refer the lenses two identical frames are designed, for four lenses each. Such frames are located at the two sides of the pillar and they are in-built with the horizontal shaft. The geometric constraints that need to be considered for the frames design are the lens dimensions and shape, their focal length and the shaft diameter. A picture of the developed frame, together with the integration in the prototype, is in Figure 6.4.

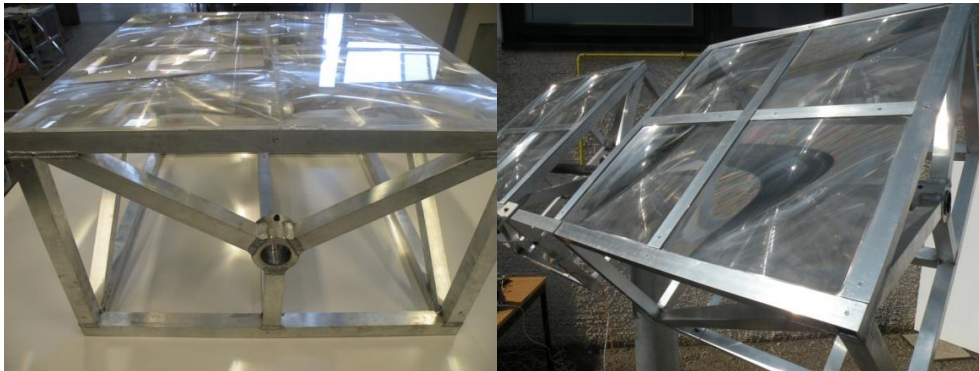


*Figure 6.4 Solar collector aluminum frame and integration in the prototype*

The reticular frames are built with welded aluminum tubular profiles to join low weight to an acceptable stiffness. Their dimensions are of 666x666mm and the height is of 400mm. Such dimensions fit with a set of 2x2 lenses to be installed on top of each frame thanks to several screwed aluminum sheets and further fixed with silicone to prevent rain seepage. The lateral surface of each frame includes three profiles welded to create a “Y” configuration around a central ring. The hole diameter is of 42mm and it fits with the previously introduced horizontal shaft for the collector support and the motion transmission. The shaft and the modules are screwed up so that they are in-built and their movement is coordinated.

Finally, to prevent the rain and the humidity to seep inside the collector from the four lateral surfaces and the bottom of each module, ten metal protection plates are screwed to the tubular profiles. Each of them fits with the lateral/bottom dimensions of the reticular frame. For such protection plates, the adoption of aluminum instead of cheaper plastic materials is required to prevent combustion phenomena in case of the concentrated sun

rays fall out of the receivers in the event of an accident. At last, the adoption of the screws to tighten up the plates to the frames allows to easily removing them if adjustments to the receivers are necessary and/or other devices located inside the collector and under the lens plane need to be manipulated.

### 6.2.3 Solar receivers

The solar receiver is the plant functional module, hit by the concentrated radiation, whose purpose is the energy conversion and heat recovery thanks to the solar cells and the cooling fluid. For such reasons the solar receivers represent the key elements of the whole prototype, *i.e.* the other modules are designed to maximize the solar receiver performances. The description of such a module is split into two *sub-Paragraphs*. The former provide the features of the TJPV cells integrated to the plant receivers, while the latter *sub-Paragraph* describes the layout and the working principle of the heat exchangers, supporting and cooling the cells.

#### 6.2.3.1 Triple-junction photovoltaic (TJPV) Cells

The solar receivers integrated to the prototype include a set of commercial high efficiency TJPV cells, specifically designed for concentration plants.

The three junctions are made of Indium-Gallium-Phosphide (InGaP), Indium-Gallium-Arsenide (InGaAs) and Germanium (Ge), while the cell layout and electrical features, together with the spectral response, highlighting the sensible wavelengths for each junction, are in the following figures and table.

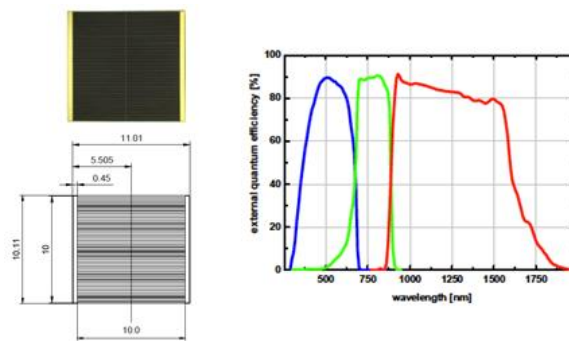


Figure 6.5 TJPV cell layout and spectral response

Table 6.2 TJPV cell electrical features

Sun concentration [Suns]	$I_{SC}$ [A]	$V_{OC}$ [V]	$I_{MP}$ [A]	$V_{MP}$ [V]	FF [%]	$\eta$ [%]
200x	2.740	3.054	2.674	2.687	85.9	35.9
300x	4.114	3.089	4.010	2.702	85.3	36.1
500x	6.838	3.120	6.610	2.710	84.0	35.8
700x	9.533	3.151	9.236	2.681	82.4	35.4
1000x	13.693	3.185	13.301	2.601	79.3	34.6

\* measurement conditions: 1.5AM, 1000W/m<sup>2</sup>, 25°C.

(Legend:  $I_{SC}$  = short circuit current,  $V_{OC}$  = open circuit voltage,  $I_{MP}$  &  $V_{MP}$  = maximum power point current and voltage, FF = fill factor,  $\eta$  = efficiency)

The TJPV cells are located, as shown in Figure 6.6, in a ceramic, *i.e.* aluminum oxide, 80x80mm squared plate able to guarantee the proper electric connection and cell cooling. The ceramic plate presents four holes for the integration and installation in the WHE.

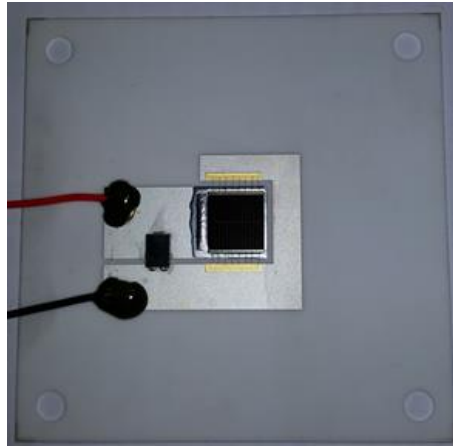


Figure 6.6 TJPV cell connected in a ceramic 80x80mm squared plate

### 6.2.3.2 Water heat exchangers (WHEs)

As introduced, the solar receivers are located under the solar collector plane, close to the lens focus points. Each of them integrates a TJPV cell fixed on a heat exchanger for cooling and heat recovery. Figures 6.7 and 6.8 show a 3D render and a picture of the described receiver and the integration with the ceramic plate. Overall dimensions of such a units are of 80x80x20(height)mm and they are made of polyvinylchloride. The electric and hydraulic connections of both the cells and the WHEs are in series, while the maximum lens concentration factor is of 800x.

Particularly, the cold fluid enters the exchangers from a single inlet and flows directly under the TJPV cell area filling an empty zone milled between the exchanger base and the ceramic plate on which the cells are located. Four lateral outlets allow the hot fluid to exit and convey it to the one lateral outlet hole. Finally, to ease the positioning of the receivers in correspondence of the lens focus points a set of two screws are used and a same number of holes are milled on the bar fixed on the bottom of the reticular frames. The effective positioning of the receivers on the lens focus points can be done manually.

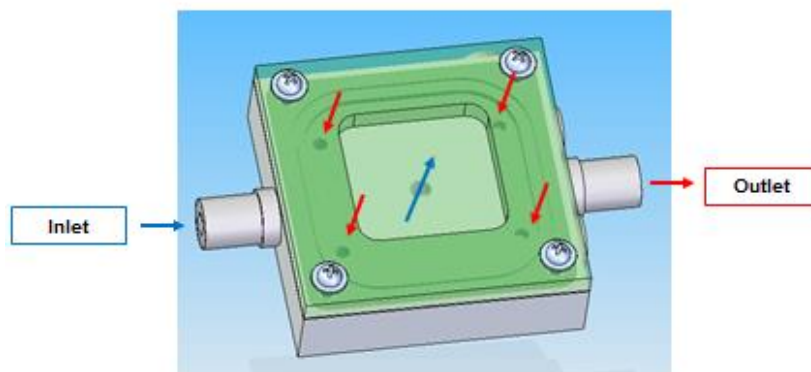


Figure 6.7 Polyvinylchloride WHE 3D render



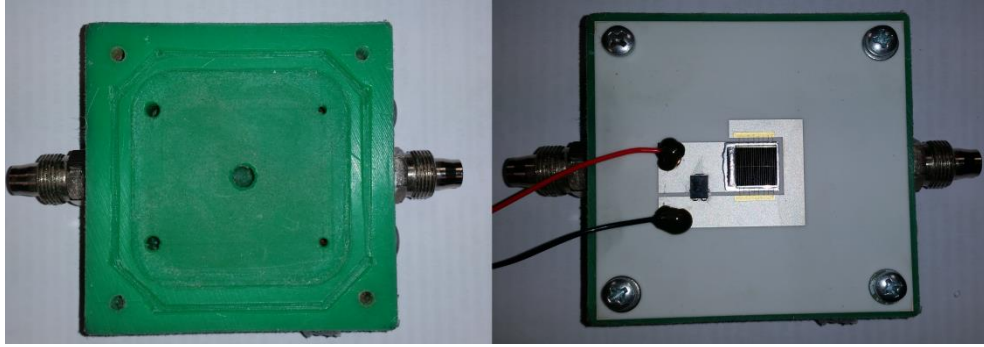


Figure 6.8 WHE integrating TJPV cell

#### 6.2.4 Solar biaxial tracking system

In concentrating solar plants the direct radiation is the only available for the PV conversion process. Consequently, to maximize the solar radiation captation, the accurate collimation between the prototype orientation and the sun ray direction is required. Due to the apparent motion of the sun toward the Earth, the solar collector position needs to be continuously checked and changed so that the lens plane is always, approximately, orthogonal to the ray direction.

Single and dual axes tracking systems are, commonly, feasible depending on the number of the controlled axes of motion. Particularly, single axis trackers generally follow the daily East-West Sun trajectory and neglect the sun rise above the horizon. Dual axes trackers provide a bi-axial motion control along both the two sun trajectories. In concentrating solar plants, due to the aforementioned possibility to convert the sole direct component of the solar radiation, a bi-axial motion control is generally strongly required. The developed prototype follows such a guide-line.

From the hardware perspective, two independent kinematic mechanisms are developed for the two selected motion axes:

- Zenithal kinematic mechanism to align the prototype along the solar altitude angle, which represents the angle between the observer horizon and the line to the sun. The solar altitude complementary angle is the Zenith angle
- Azimuthal kinematic mechanisms to follow the daily motion of the Sun from east to west, according to the solar azimuth angle

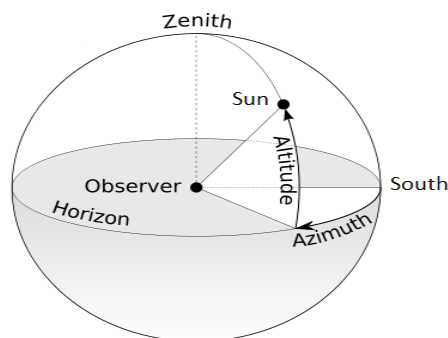


Figure 6.9 Solar azimuth and solar altitude angles

Both mechanisms adopt a stepper motor as their actuator. The motors are identical for the two motion axes and they present a holding torque of 3Nm, a phase current of 4.2A DC and an angular step resolution of 1.8 degrees. The last parameter is crucial to guarantee a high accuracy in sun collimation.

For both motion axes, the actuators are coupled with a gear reducer (gear ratio equal to 100) and, then, with a chain drive motion transmission system (gear ratio equal to 4). As a consequence, the global angular resolution is, theoretically,  $4.5 \times 10^{-4}$  degrees per step.

The tracking mechanisms are installed in two different positions of the prototype. For the zenithal axis of motion the tracker is on a plate on top of the pillar and it is directly coupled with the horizontal shaft that supports the reticular frames containing the lenses and the receivers (See Figure 6.10)



Figure 6.10 Zenithal tracking mechanism

On the contrary, the Azimuthal tracker (See Figure 6.11) is connected to the bottom plate and the transmission of motion is made thanks to a vertical shaft coaxial to the pillar which rotates the top plate. The friction generated by the contact between the rotating plate and the steel bush is reduced by using steel spheres, while two ball bearings supports the vertical shaft. Two limit switches prevents the system to assume wrong and dangerous positions.

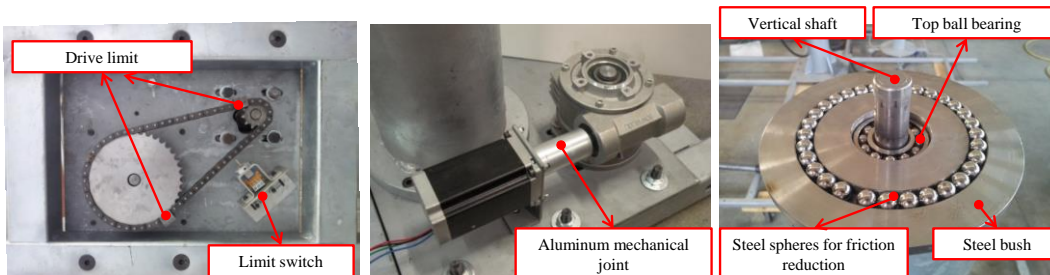


Figure 6.11 Azimuthal tracking mechanism

Finally, two aluminum capsules are integrated to protect each tracking mechanism from the rain and other atmospheric agents (see Figure 6.1).

The developed solar tracking system integrates not only the described actuators for motion transmission but, also, a further device, called solar collimator in the following, to directly sense the solar irradiation level and drive the algorithms for solar tracking. Figure 6.12 shows a picture of the solar collimator after its integration to the solar collector.

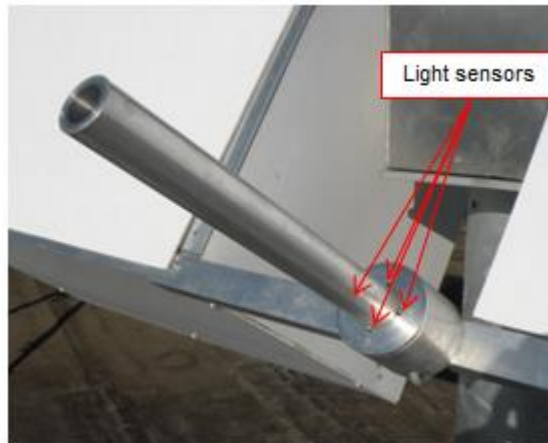


Figure 6.12 Solar collimator integrated to the solar collector

Such a device is made of two elements: the circular base, integrating four light sensors, and a central 250mm long stem. The collimator is installed so that the base lies on a plane parallel to the solar collector. The operating principle is based on the shadow generated by the central stem. Particularly, if the sun rays are orthogonal to the base no shadow is generated and the system is correctly oriented. On the contrary, if the sun rays hit the collimator obliquely a shadow is generated and a misalignment occurs. The four sensors, installed at the corners of two orthogonal diameters of the stem, detect the presence of a shadow decreasing the transduced electrical signal, driving the prototype realignment. A picture of the adopted sensors and of the polar characteristic working curve is in Figure 6.13.

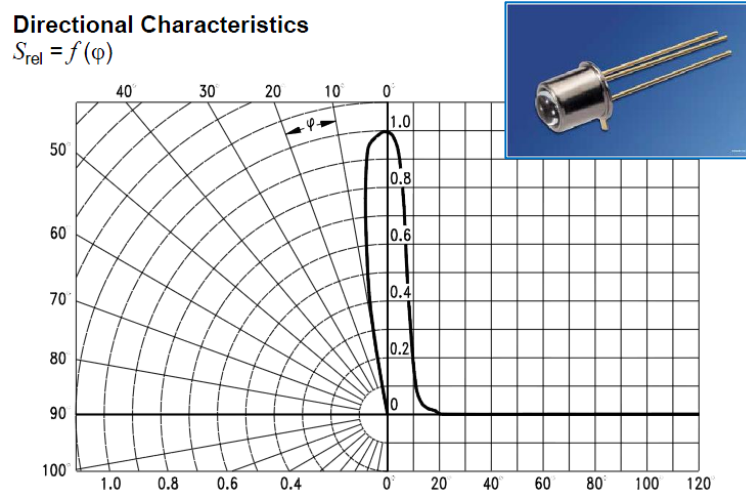


Figure 6.13 Light sensors, picture and polar characteristic curve

The narrow polar curve generates a relevant decrease of the transduced current signal for low values of the angular gap between the sun ray direction and the collimator position. If such a gap, called  $\varphi$  in Figure 6.13, is approximately equal to  $10^\circ$  the transduced error decreases of about the 80% of the nominal value. A gap of  $20^\circ$  transduces a null signal. The choice of such sensors allows increasing the accuracy in sun collimation: low angular misalignments are clearly detected by the control system.

Finally, from an electrical point of view the light sensors work as variable resistors. Given a constant feeding voltage, they reduce or increase the current intensity in function of the illuminance they are exposed to. The electric measurement system is represented in Figure 6.14. The voltage is of 24V and four auxiliary resistors of  $1200\Omega$  each are added in series to further reduce the current intensity so that it fits with the  $\pm 20\text{mA}$  range of the analog input slot for current data acquisition.

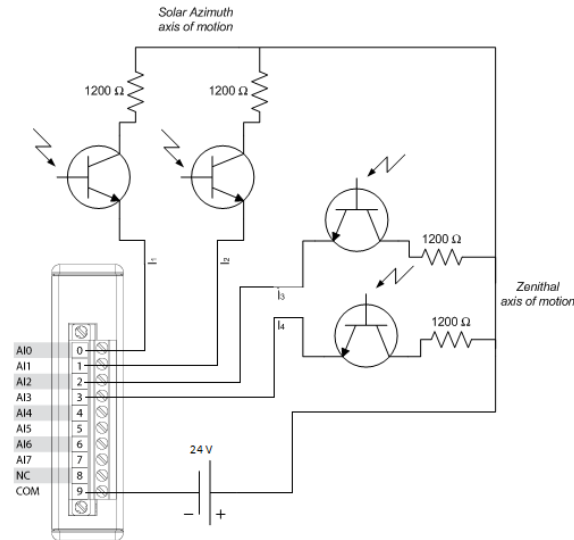


Figure 6.14 Light sensor electrical acquisition circuit

#### 6.2.4.1 Motion control strategy

As previously mentioned, the motion control strategy is fully discussed in Bortolini *et al.* (2012). In this *Paragraph*, a brief description of the motion control strategy implemented in the solar biaxial tracking system is provided. The purpose is to ensure the accurate collimation between the sun and the prototype during day-time preventing the occurrence of danger states through the monitoring and early detection of environmental criticalities (e.g. strong wind, pouring rain, *etc.*). Such control strategy is performed through a real-time LabView™ platform.

Basically, the implemented solar tracking system operates as an on-off controller along the two controlled motion axes, *i.e.* solar altitude and solar azimuth. For each motion axis the actuators are enabled if the angular alignment displacement between the prototype and the sun current positions is higher than a defined limit. Actuators are switched-off when such gap becomes lower than a different (coherent) value. The alignment gap sign defines the rotation direction (See Figure 6.15).

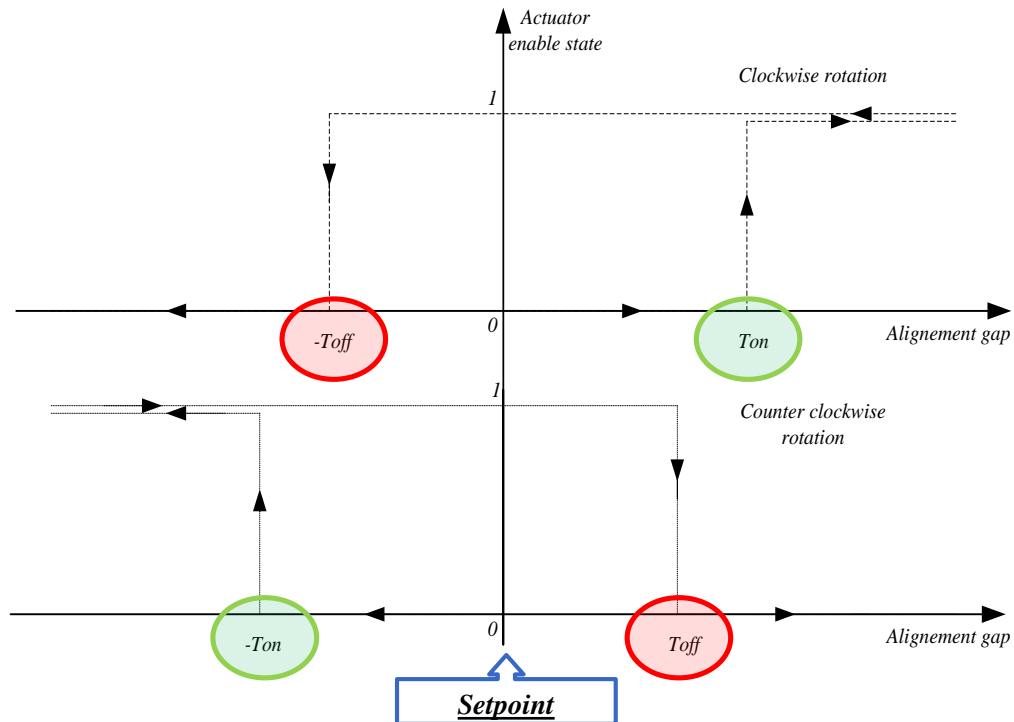


Figure 6.15 On-off control of the implemented solar tracking system

Both kinematic mechanisms are driven by two different control loops working separately or coordinately.

- a Forward loop control based on the well-known astronomic solar equations (See Figure 6.16). The alignment gap is the difference between the current solar Alt/Azimuth angles and the prototype position computed counting the step number since a defined reference position, *i.e.* zero. Such strategy has a great steadiness but low accuracy (mechanical and prototype positioning errors are not compensated).

*Solar Altitude -  $\theta$*

$$\sin(\theta) = \cos(\delta) \cos(\omega) \cos(\phi) + \sin(\delta) \sin(\phi)$$

*Solar Azimuth -  $\gamma$*

$$\cos(\gamma) = \frac{\sin(\theta) \sin(\phi) - \sin(\delta)}{\cos(\theta) \cos(\phi)}$$

where:

$\phi$  : location latitude

$\omega$  : hour angle

$\delta$  : solar declination

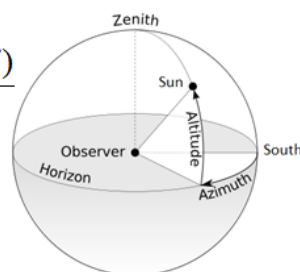


Figure 6.16 Astronomic solar equations

- a Feedback loop control based on the difference between two retroactive signals transduced by a set of phototransistors, used as light sensors, and integrated into a sun collimator. In presence of a misalignment the stem shades some sensors.

The alignment gap is the difference between the two transduced signals of the motion axis. Such strategy has a great accuracy but low steadiness, especially during partially cloudy days.

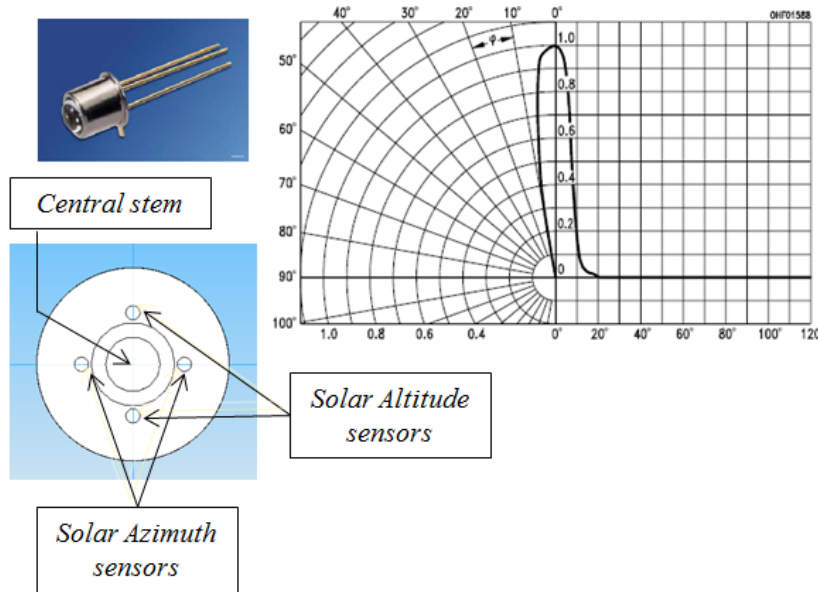


Figure 6.17 Light sensors feedback loop control strategy

Forward and feedback control strategies present complementary strengths and weaknesses. As a consequence, their effective integration, *i.e.* hybrid control strategy, allows increasing the tracking accuracy and the energy conversion performances of solar modules and plants.

Generally, a hybrid strategy for solar tracking implements a switching procedure between forward and feedback control algorithms as a function of the environmental conditions and the current system position. Depending on these factors, the opportunity to switch from forward loop to feedback control or *vice-versa* is considered. The next Figure 6.18 proposes the flow-chart diagram of the proposed switching procedure. The algorithm is based on the four signals transduced by the same sensors adopted for the feedback control strategy and described in the previous paragraphs. Basically, if at least one of the four devices is directly illuminated, *i.e.* the correspondent transduced electrical signal is higher than a defined setpoint, the feedback control module is activated and the associate algorithm is executed. Otherwise, the forward loop module is used to track the sun. The decisional parameter adopted to evaluate the opportunity to switch between the two control modules is defined as follows:

$$M_s = \max\{Az_1 + Az_2, Alt_1 + Alt_2\} \quad (6.1)$$

Where  $Az_1, Az_2, Alt_1, Alt_2$  indicate the transduced signals for both azimuthal and zenithal axes of motion. The feedback control module is run to align the system to the current sun position if  $M_s$  is higher than a defined setpoint, called  $T_{fd}$ . Otherwise, if  $M_s$  is lower than the setpoint  $T_{fo}$  and the feedback control module is running, the switch to the forward

loop module occurs. The values of the setpoint  $T_{fd}$  and  $T_{fo}$  need to be defined according to the output signal range of the adopted light sensors and must prevent an oscillatory behaviour of the system, *i.e.* the cyclical switch between the two control modules. Finally, when the control strategy is selected the correspondent algorithm runs in accordance with the procedures described in the previous paragraphs.

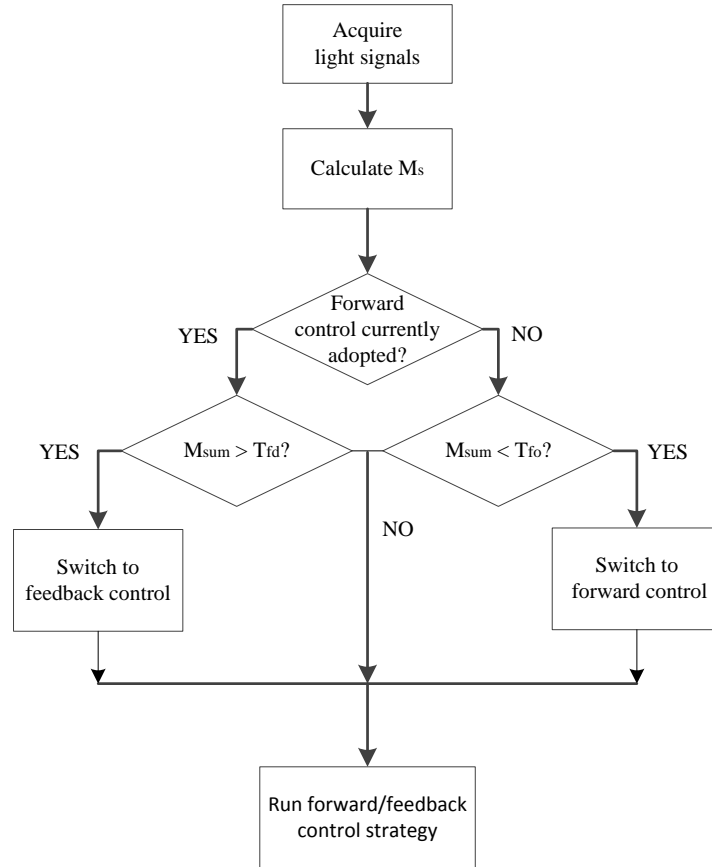


Figure 6.18 Hybrid control strategy, flow-chart of the switching procedure

The introduced strategy defines three regions on the  $(t, M_s)$  plane according to the next Figure 6.19.

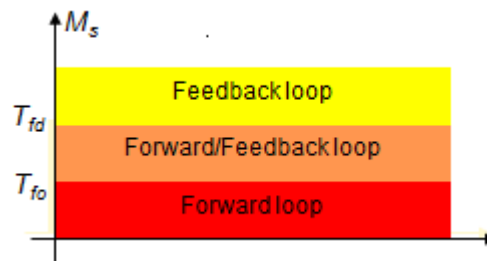


Figure 6.19 Best tracking strategy as a function of  $M_s$

In the intermediate region, *i.e.*  $T_{fo} < M_s < T_{fd}$ , the current tracking strategy still runs until the lower or upper limit is reached. Such a region avoids the continuous switch between the forward loop and feedback strategies.

Finally, the time dependent main loop of control manages the transient states, *i.e.* startup and switch-off, and the danger condition detection.

Three day-periods are distinguished:

- *Day-time*: the prototype tracks the sun according to the best tracking strategy
- *Early-morning*: the prototype moves to sunrise position
- *Night-time*: the prototype moves to safety rest position

In case of danger condition detection all processes are stopped, the prototype moves to safety rest position and external input is waited, *i.e.* manual reboot.

### 6.2.5 Electronic variable load

Table 6.3 highlights that the TJPV cell working conditions, *i.e.* the voltage, current, solar irradiation level, cell surface temperature, affect its performances. Among those parameters, some of them are not directly controllable, *e.g.* the solar irradiation level, while others are, only, partially controllable, *e.g.* the cell temperature. On the contrary, the electrical parameters can be actively controlled to make the cell working at the maximum power point (MPP), *i.e.* the couple of values of the current and the voltage maximizing the extracted electrical power. The so called I-V, *i.e.* current-voltage, and P-V, *i.e.* power-voltage, curves, typical of each solar cell, clarify such a concept. An illustrative example, not directly referred to the described prototype, is in Figure 6.20. The MPP is the maximum of the P-V curve, while the couple of values  $(V_{MP}, I_{MP})$  represents the correspondent point on the I-V curve and it identifies the best working conditions maximizing the extracted electrical power. As expected, the MPP varies continuously during day-time due to the fluctuations of the aforementioned non totally controllable parameters. The goal of the electronic variable load module is to control the current and the voltage so that the operative working conditions are always close to the MPP. Such a module is composed by a variable load device, manually and/or electronically controllable, and a MPP tracking strategy, *i.e.* an algorithm to measure and control the current and the voltage variables to maximize the extracted power.

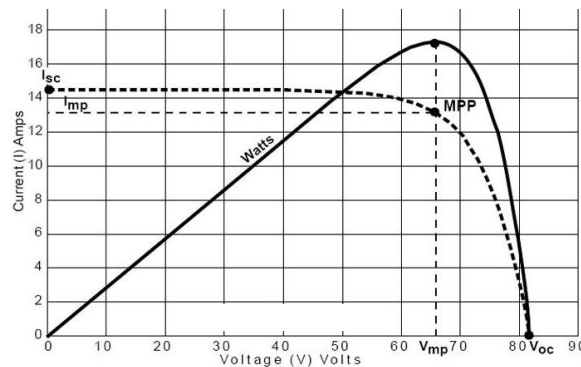


Figure 6.20 I-V and P-V curves, example

The tests to study the cell performances, when they are integrated to the plant, are executed adopting the commercial device represented in Figure 6.21 together with its admissible ranges of control and tolerances.





	Range	Tolerance
Voltage	0..160V	0.1%
Current	0..60A	0.2%
Power	0..400W	0.2%

Figure 6.21 Electronic variable load for MPP tracking

The adopted device allows a manual control of the electric parameters, through the visible knobs and screen, or can be connected to a remote controller, through the serial unit, for the automatic acquisition and control of the electric variables running a MPP tracking algorithm. Details about the adopted MPP strategy are not the purpose of this dissertation.

### 6.2.6 Real-time motion control and monitoring system

The developed prototype integrates a real-time remote control and monitoring system for the bi-axial solar tracking and the cyclic measure of both the environmental conditions and the operating parameters. The control and monitoring platform is developed with LabView™ Integrated Development Environment (IDE) and it runs on a NI C-RIO real-time industrial module. The next Figure 6.22 shows a commented picture of the hardware control board for input and output signal manipulation. In the following, a systematic description is provided.

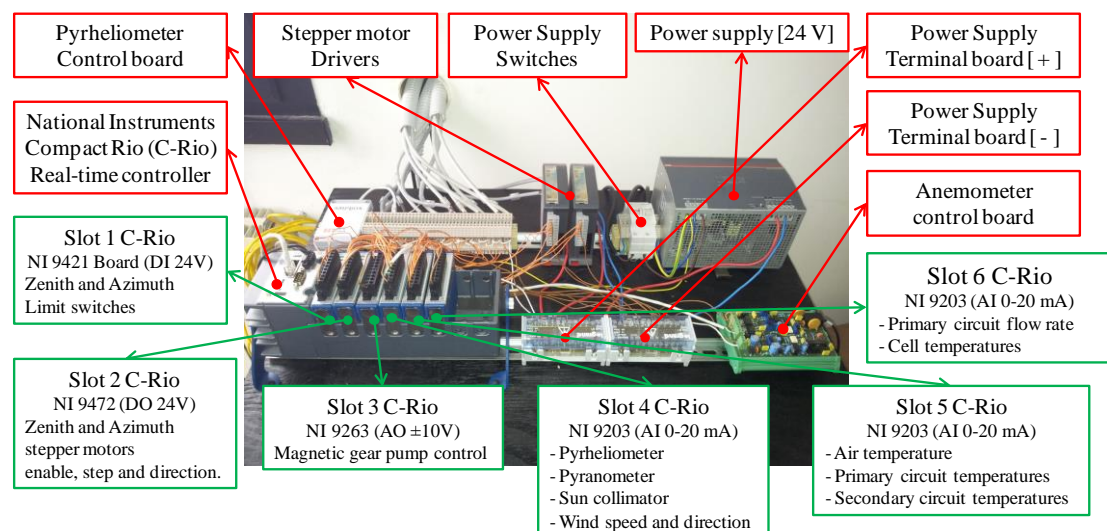


Figure 6.22 Hardware control board

The electrical power conversion efficiency strongly depends on the MPP tracking algorithm implemented through the electronic variable load. The voltage and the current levels of the electrical circuit, integrating the TJPV cells, are the key parameters affecting the extracted power, given the solar irradiance level and the concentration factor.

Because of the adoption of the commercial electronic load represented in Figure 6.21, the correspondent electrical data are immediately available on its screen and, currently, they do not need further sensors and devices for the acquisition.

Considering the thermal parameters, the description of the hydraulic cooling circuit in *Paragraph 6.2.7* and the plant scheme in Figure 6.24 point out the required sensors for the temperature, pressure and flow rate measurement. Despite the pressure manometers are traditional manual sensors, the other devices are connected to the NI C-RIO and the control board. Particularly, ten PT100 temperature sensors are installed. Their 4..20mA output signals are acquired through the ten channels of the current analog input Slot 5 and Slot 6. The cooling circuit flow rate is measured through a low volume rotating vane flow meter with an operative range of 0.015..0.7litres/min and a current output signal in the range 4..20mA. The aforementioned Slot 6 manages the load of such a data.

Finally, the  $\pm 10V$  analog output Slot 3 is used to control the magnetic gear pump installed in the primary loop of the hydraulic circuit. The speed range is 500..5000rpm. The pump installed in the secondary loop is controllable manually.

#### *6.2.6.1 Power supply unit*

Two levels of voltage are required for the complete system control. The grid tension of 220V AC supplies the power devices, *i.e.* the stepper motors, the gear pumps, the NI C-RIO real-time controller, while a 24V DC voltage supplies the control circuits to acquire and set the control signals. Despite the first voltage level is immediately available from the national grid, to obtain the low voltage level the 24V AC/DC transformer called “Power supply” in Figure 6.22 is required. The switches, installed next to the transformer, control the power supply of the whole board.

#### *6.2.6.2 Motion control unit*

The motion control unit feeds the stepper motors and it manages the light sensor signals for the bi-axial solar tracking. The low voltage electrical connections for the signal manipulations are in Figure 6.23.

Each motor is controlled by a step driver that modulates the feeding power through three low voltage digital signals set thanks to the digital output slot connected to the NI C-RIO controller, *i.e.* the Slot 2 of Figure 6.22. Such signals refer to:

- enable command: 1 if the motor is enabled, 0 otherwise
- direction command: 1 for clockwise driveshaft rotation direction, 0 for counter-clockwise rotation
- step command: 1 for single step command, 0 for no step command

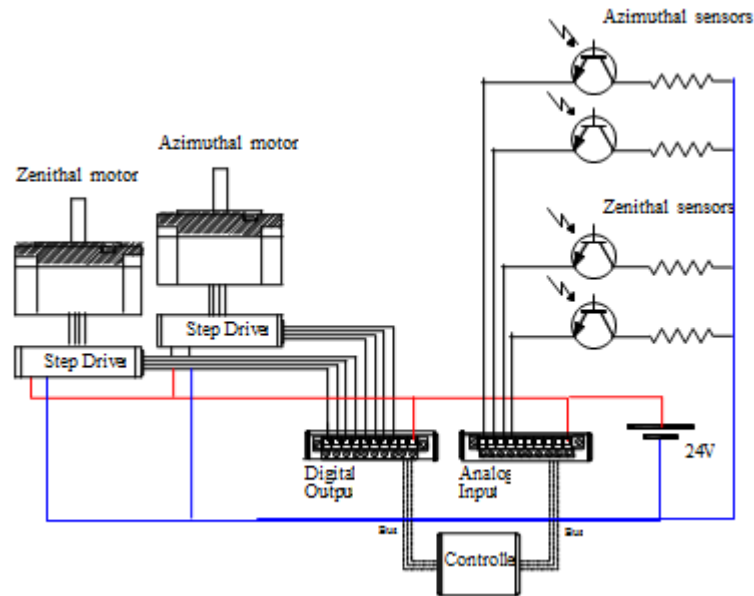


Figure 6.23 Motion control unit circuit

Particularly, to generate a sequence of motor steps, the enable command should be set to 1 and the step signal has to be sequentially switched from 0 to 1. Each switch generates the rotation of the motor shaft of a single step angle. Consequently, for each motion axis, the total number of generated steps is directly correlated to the angular rotation of the solar collector given a zero reference position. The right side of Figure 6.23 shows the connections to manage the four signals from the light sensors integrated to the solar collimator and previously described. Such connections are already introduced in Figure 6.14 together with the required analog input slot, *i.e.* the Slot 4 of Figure 6.22.

Finally, to prevent the solar collector to reach danger positions, generating its tip over or the damage of the electric and hydraulic circuits, two (M)ON-OFF-(M)ON limit switches are provided and their digital signal is acquired by the digital input slot connected to the NI C-RIO and named Slot 1 in Figure 6.22. Normally, the OFF signal is transduced indicating the system is in an admissible position. If the azimuthal and/or zenithal current position reaches a wrong value, *e.g.* the zenithal angle becomes lower than 0 or higher than 90 degrees, a short shaft hits the limit switch moving it to the momentary ON, *i.e.* (M)ON, position. The control system detects such a danger condition and it generates the immediate stop of the regular system motion.

### 6.2.7 Hydraulic circuit for cell cooling and thermal recovery

The hydraulic circuit, represented in the next Figure 6.24, both cools the TJPV cells and it recovers the thermal energy. The circuit deals with two closed loops integrating four heat exchangers each. The cold fluid, thanks to a magnetic driver gear pump, flows through the exchangers, cooling the cells. The flow rate is remotely controlled in the range 500..5000rpm of the gear pump. The hot fluid reaches a brazed fourteen plates heat exchanger for surface heat exchange with the purified water flowing in the second loop and directly feeding the users thanks to a circulation gear pump. In Figure 6.24, for the

sake of simplicity, the users are exemplified through a tank. Inlet and outlet temperatures for each exchanger are measured through a set of PT100 temperature sensors, while the flow rate is measured through a low volume rotating vane flow meter. Finally, the hydraulic circuit integrates a two liters expansion vessel, two deaerators and a safety valve calibrated to prevent the pressure to grow above 1.5bar.

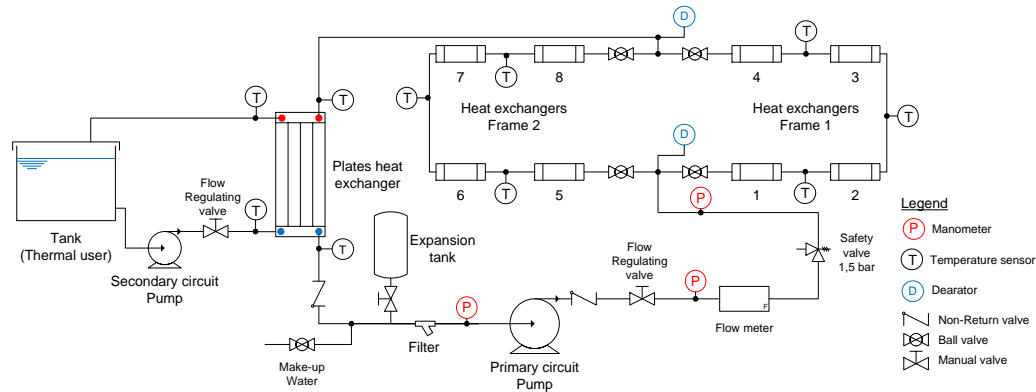


Figure 6.24 Hydraulic cooling circuit scheme

In the prototype final layout, except for the heat exchangers located in correspondence of the cell focus points, all the hydraulic devices are placed close to the base of the pillar inside a protection box, as shown in Figure 6.1. The next Figure 6.25 represents a detail of the several components included inside the aforementioned protection box. In addition to the hydraulic devices, the temperature and pressure sensors and the electrical box for signal acquirement and command setting are shown. The overall dimensions of the protection box, including all the major hydraulic circuit components, is of 600x500x300(height)mm and it fits with the width of the support base

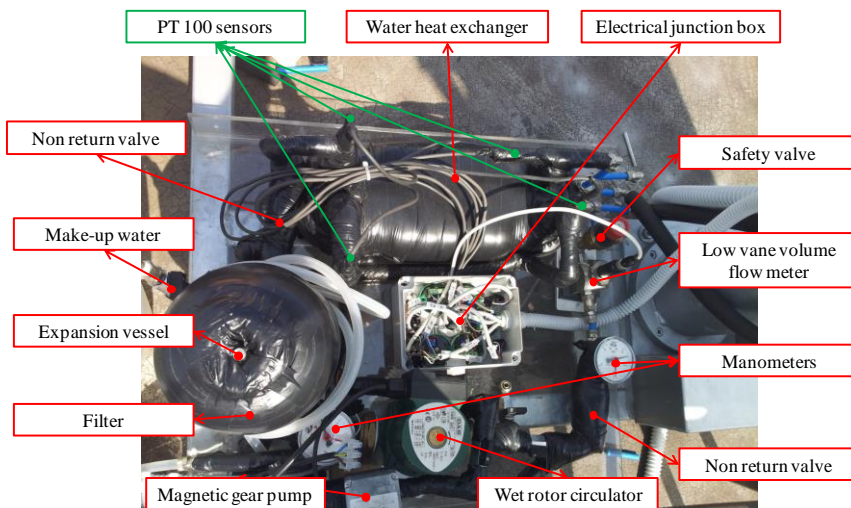


Figure 6.25 Hydraulic cooling circuit, key elements inside the protection box

### 6.2.8 Auxiliary weather station

The knowledge of the profiles of the most important environmental and weather parameters is a crucial data for the performance assessment. In the context of the developed prototype, the following parameters are monitored:

- the global irradiation on the horizontal surface (in  $W/m^2$ )
- the direct irradiation on a two axis tracked plane (in  $W/m^2$ )
- the air temperature (in Celsius degrees)
- the wind speed (in km/h) and direction (in degrees from the North)

The solar data are crucial for the prototype performance assessment, the air temperature is relevant for heat recovery and heat dispersion analysis and, finally, the wind speed needs to be controlled to stop the system and move it to a safety position in case of the tip over risk.

Except for the second parameter, requiring a specific device to track the sun, the other data are measured through three commercial sensors, *i.e.* a pyranometer, an air temperature thermometer and an anemometer, installed on a separate weather station placed close to the prototype but far from any disturb element, such as heat sources, shadows, *etc.*, and from the ground that, especially during the summer months, irradiates the reflected heat and light. The weather station is visible on top right of Figure 6.1, while a detail is in the next Figure 6.26.



Figure 6.26 Weather station integrating the pyranometer, the air temperature thermometer and the anemometer

Furthermore, the pyrhelimeter to measure the direct irradiation is installed on a separate commercial tracker and located next to the prototype. A picture of both the measurement device and the tracker is in Figure 6.27.



Figure 6.27 Pyrhelioscope for direct solar irradiation measurement

The pyrhelioscope is not directly integrated to the solar collector to prevent the measured data to be affected by the prototype solar collimation accuracy level.

The operative ranges of the four environmental condition sensors, together with their output signals sent to the control platform, are in the following Table 6.4.

Table 6.3 Features of the four adopted environmental condition sensors

Sensor	Details	Adopted operative range	Output signal range
Pyranometer	Delta Ohm - LP Pyra 03AC Sensitivity: 17.09mV/(kW/m <sup>2</sup> ) Impedance: 37.6Ω	0..2000W/m <sup>2</sup>	4..20mA
Pyrhelioscope	Kipp & Zonen - CHP1, AMPBOX Sensitivity: 8.03μV/(kW/m <sup>2</sup> ) Impedance: 30.3Ω	0..1600W/m <sup>2</sup>	4..20mA
Air thermometer	Italcoppie Pt-100, Transmitter Accuracy: ±0.12Ω at 0°C	-12..47°C	4..20mA
Anemometer	BitLine - Anemometer, Transmitter Speed sensitivity: 1km/h Direction sensitivity: 10 degrees	Speed: 0..150km/h Direction: 0..360degrees	Speed: 4..20mA Direction: 4..20mA

The output signals are the same for all the four devices to ease the integration of such sensors to the control platform. The identical ±20mA analog input Slot 4 and Slot 5 are used to acquire them.

### 6.3 Manufacturing cost analysis

Despite the proposed prototype is at a research stage of its life cycle and, consequently, it is far from an optimized large scale production, a realistic analysis of the rising manufacturing costs is, already, feasible. In addition, the support structure, tracking system and hydraulic circuit are oversized and they are suitable for the solar collectors integrating more than 8 solar receivers, *i.e.* TJPVs+WHEs. Such costs represent the initial investment in a solar energy system like the described prototype. A functional perspective drives the analysis of the rising costs. Direct materials and labour costs are computed separately. Table 6.5 and Figure 6.28 summarize the key data.

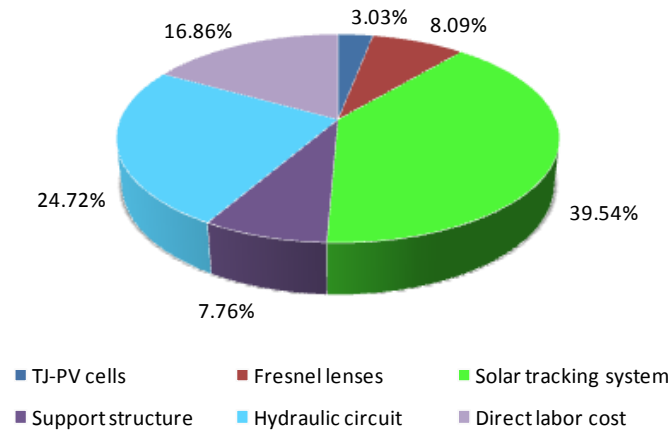


Figure 6.28 Functional cost analysis, percentages refer to the full manufacturing cost

Table 6.4 Prototype manufacturing costs

Description	# units/kg	Total cost [€]
TJPV cells	8 units	36.00
Fresnel lenses	8 units	96.00
Sun tracking system		469.00
<i>Gear reducer</i>	2 units	
<i>Chain drive system</i>	2 units	
<i>Stepper motor</i>	2 units	
<i>Microstepping driver</i>	2 units	
Support structure		92.00
<i>Galvanized steel structure (base, pillar and shaft)</i>	40kg	
<i>Aluminum frames (collector)</i>	8kg	
Hydraulic circuit		293.20
<i>Circulation pump</i>	1 unit	
<i>Heat exchangers</i>	8 units	
<i>Plate heat exchanger</i>	1 unit	
<i>Deareator</i>	1 unit	
<i>Expansion vassel</i>	1 unit	
<i>Filter</i>	1 unit	
<i>Piping</i>	1 unit	
Direct labor cost		200.00
Full production cost		1186.20

The solar tracking system and the hydraulic circuit are the two functional modules with the highest impact on the system global cost. However, as previously mentioned, they are oversized and they can be used for more than 8 solar receivers.

Such modules allow to track the sun and to recover thermal energy and they represent the main difference non-concentrating and concentrating PV plants. A trade-off analysis between the performances of flat plane PV systems and CPV/T plant is necessary to study if the increase of the conversion efficiency and energy production justify the CPV/T plant higher cost. Such an analysis represents a possible future development.

#### 6.4 Field-tests and experimental campaign

An experimental campaign to field-study the proposed prototype is assessed during the 2012 summer months in Bologna, Italy (latitude 44.51° North, longitude 11.32° East).

Three different tests are carried out. At first, the accuracy in sun collimation is analyzed as a key condition not to decrease the amount of the collected solar radiation. The second test focuses on a preliminary analysis of a single TJPV cell studying its electric features and curves when integrated to the proposed prototype. Finally, the system global conversion efficiency is investigated. The key outcomes for each experimental campaign are discussed in the next *sub-Paragraphs*.

#### 6.4.1 Accuracy in solar tracking

The accuracy of the adopted solar tracking system heavily affects the energy conversion efficiency. In particular, the electric performance of the TJPV cells strongly depends on the uniformity of the concentrated radiation on the cell surface and a significant performance decrease happens in case of a non-homogenous distribution of the solar irradiance flux. Therefore, the feedback loop tracking strategy proposed in the previous *Paragraph 6.2.4* is field-tested to experimentally investigate its performances in solar collimation. The measure of the shadow length generated by the collimator stem allows calculating the angular alignment gap between the sun and the prototype. Figure 6.29 clarifies such a concept.

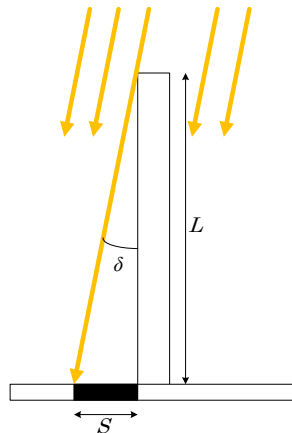


Figure 6.29 Accuracy in solar collimation, shadow related to the angular misalignment

Equation 6.2 correlates the angular misalignment between the sun rays and the solar collector,  $\delta$ , to the shadow and the stem length.

$$\delta = \tan^{-1} \left( \frac{S}{L} \right) \quad (6.2)$$

Furthermore, Figure 6.30 shows two pictures of the solar collimator taken immediately before and after the actuator switch on, *i.e.* when the gap is maximum and minimum.



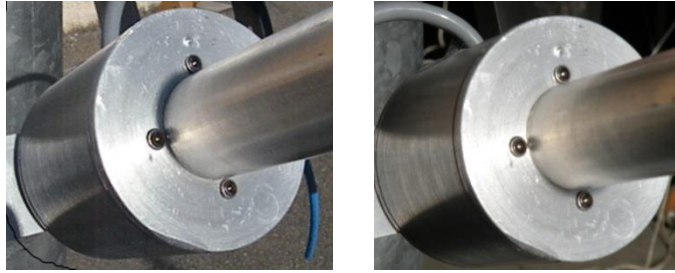


Figure 6.30 Shadow before and after the system realignment

The average experimental alignment gap is lower than  $0.8^\circ$  representing a limit value according to the optical properties of the adopted Fresnel lenses.

#### 6.4.2 Single TJPV cell electric conversion efficiency analysis

The present second field-test focuses on the analysis of the energy conversion performances of a single TJPV cell when integrated to the proposed prototype. A set of runs to calculate the experimental I-V, *i.e.* current-voltage, and P-V, *i.e.* power-voltage, curves are assessed under the environmental irradiance conditions represented in the graph of Figure 6.31. Particularly, the red curve refers to the global radiation on the horizontal plane, while the blue one shows the beam fraction on an optimally oriented surface. The monitored parameters also include the air temperature and the wind speed and direction. During the test,  $31.5^\circ\text{C}$  and light wind are measured.

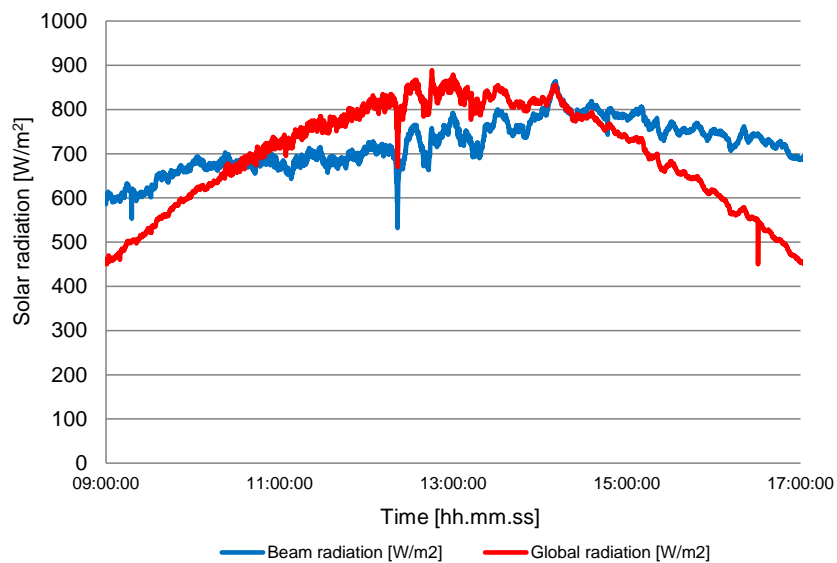


Figure 6.31 Global radiation and direct fraction profiles on July 23, 2012

The graph in Figure 6.32 shows a significant example of the experimental I-V and P-V curves for a single TJPV solar cell integrated to the Fresnel lens prototype. Particularly, the adopted cell extracts a maximum power of 8.7W when irradiated with a  $800\times$  concentrated solar radiation, while the cell conversion efficiency is equal to 15.8%.

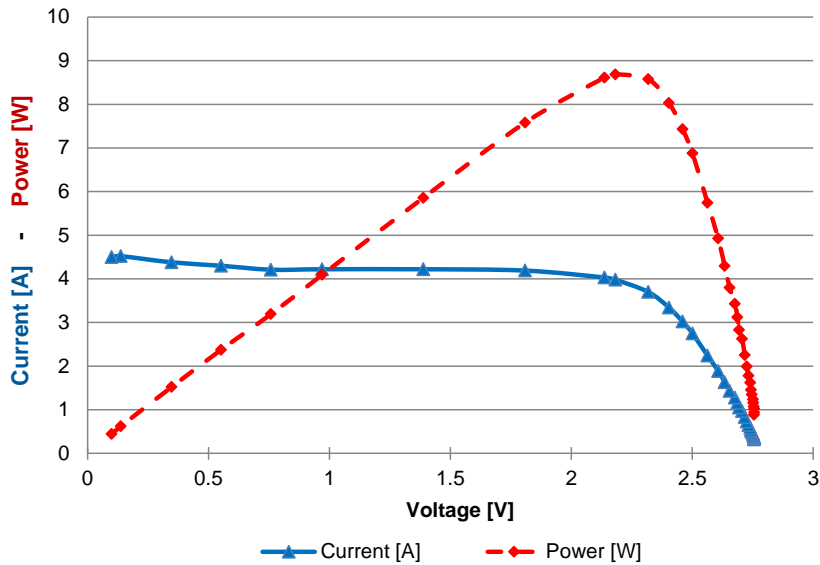


Figure 6.32 Experimental I-V and P-V curves for a single TJPV cell

The experienced electrical conversion efficiency is clearly lower than the rated power of the adopted TJPV cell (See Table 6.3). The identified causes and the adopted solutions to increase prototype performances are discussed in the next *sub-Paragraph* 6.4.3.

#### 6.4.3 Prototype electric and thermal conversion efficiency analysis

During the third field-test the study of both the prototype power and thermal recovery performances are assessed. In such test, for the sake of simplicity, only one of the two frames used as solar collectors is considered. Consequently, a series of four TJPV cells, fixed on a same number of heat exchangers, is adopted. The following Table 6.6 summarizes the key results of two of the most relevant runs.

Table 6.5 Prototype power and thermal performances

<b>Test #1</b>					
<b>Power generation</b>			<b>Thermal recovery</b>		
Direct radiation	779	W/m <sup>2</sup>	Flow rate	0.252	l/min
Collector area	0.3249	m <sup>2</sup>	Inlet temperature	28.2	°C
Incident direct radiation	253.10	W	Outlet temperature	38.3	°C
Produced electrical power	30.70	W	Recovered thermal power	177.57	W
<i>Power conversion efficiency</i>	12.13%		<i>Thermal conversion efficiency</i>	70.16%	
<b>Test #2</b>					
<b>Power generation</b>			<b>Thermal recovery</b>		
Direct radiation	769	W/m <sup>2</sup>	Flow rate	0.430	l/min
Collector area	0.3249	m <sup>2</sup>	Inlet temperature	29.0	°C
Incident direct radiation	249.85	W	Outlet temperature	34.6	°C
Produced electrical power	30.70	W	Recovered thermal power	167.99	W
<i>Power conversion efficiency</i>	12.41%		<i>Thermal conversion efficiency</i>	67.24%	

The experienced electrical conversion efficiency is of about 13%, while the thermal conversion efficiency is around 70%. The low value for the power efficiency is due to several causes. Among them the most relevant is the high dispersion of the concentrated

radiation around the focus points, as shown in Figure 6.33, due to the mechanical inaccuracies, sun tracking misalignments and chromatic aberrations of Fresnel lens, *i.e.* different focus point for different radiation wavelengths.



Figure 6.33 High dispersion of concentrated solar radiation around the focus point

Therefore, the adoption of single concentration optics, *i.e.* the aforementioned Fresnel lenses, is not adequate, by itself, to reduce the width of the concentrated light spot that, generally, is higher than the cell surface and non-homogenous. Consequently, a fraction of the concentrated solar radiation does not hit the cell surface, reducing the electrical conversion efficiency and increasing the thermal energy collected by the receivers.

To overcome such a weakness a secondary optic element (SOE) could be of help to increase the concentrated radiation acceptance angle with a foreseeable raise of the light flux hitting the cell and to increase, at the same time, the light flux homogenization on the cell area. Such a concept is shown in Figure 6.34.

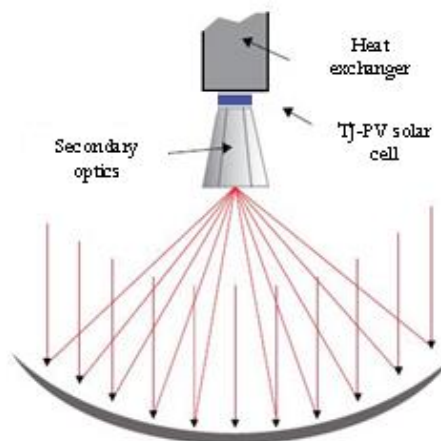


Figure 6.34 Secondary optic element concept

Considering the thermal recovery performances, the field-tests highlight acceptable values for such a parameter. From a realistic point of view, such performances are affected by two major phenomena. The former is the high air temperature experienced during the tests and the low temperature difference between the cooling water and the external temperature, preventing the cooling fluid heat dispersion through the pipelines. The latter is related to the aforementioned distribution of the concentrated radiation around the focus point and, particularly, to the rays falling out of the cell surface. Such a fraction of the concentrated radiation is totally available for heat recovery because it directly hits the heat exchanger surface without the cell intermediate surface. The

introduction of the SOE and other devices/strategies to increase the power conversion efficiency, probably, generates a parallel decrease of the thermal performances.

#### 6.4.3.1 Secondary optics development and field tests

The main purposes of a SOE are:

- compensate the chromatic aberration introduced by Fresnel lenses
- compensate the mechanical inaccuracies and misalignments
- homogenize the solar radiation incident on the TJPV cell

A truncated pyramid optic prism represents a typical effective but expensive solution to compensate the chromatic aberrations, mechanical inaccuracies and misalignments and homogenize the solar radiation incident on the TJPV cell. The cost of such SOE is significant for the developed small scale prototype with a limited number of TJPV cells. As a consequence, a cheap secondary optic has been developed to make a greater portion of the sun rays collected by the solar collector, hitting the TJPV cell. The SOE, shown in Figure 6.35, is an aluminum truncated pyramid able to increase the solar rays hitting the TJPV cell. However, it is not able to homogenize the solar radiation and a percentage of sun rays is reflected due to the presence of irregularities and impurities on the aluminum surface. The different solar rays distribution with the adoption of the secondary optic is depicted in Figure 6.36.

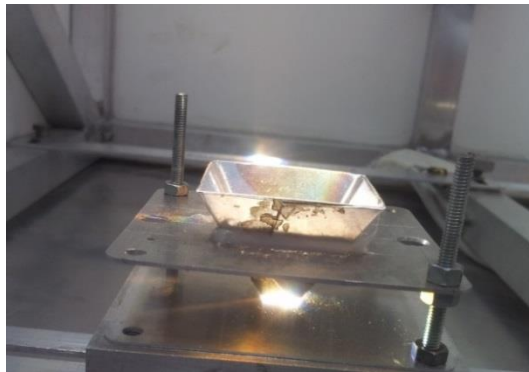


Figure 6.35 Developed aluminum truncated pyramid SOE



Figure 6.36 Different sun rays distribution with the adoption of the developed SOE

One single TJPV cells and four TJPV cells, integrated in their WHEs, are tested to evaluate the electric and thermal conversion efficiency on the prototype considering the

SOE benefits. Figure 6.37 present the prototype configuration during the tests of four TJPV cells.

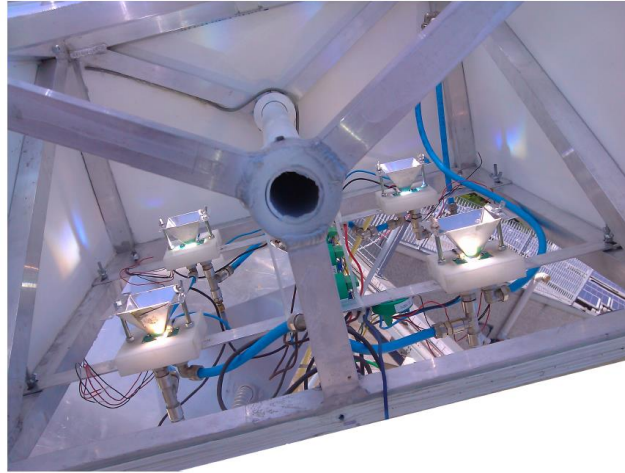


Figure 6.37 Test of 4 TJPV cells with SOE

The results, expressed in Table 6.7, show an increase of about 1% for one TJPV cell and 4% for four TJPV cells in the electrical efficiency but still too far from the TJPV cell nominal power (See Table 6.3). The reduction of the thermal conversion efficiency is due to the increase of electric efficiency and the heat dispersion through the aluminum SOE.

Table 6.6 Prototype power and thermal performances with SOE integration

<b>Test #3 - Single TJPV cell</b>				
<b>Power generation</b>			<b>Thermal recovery</b>	
Direct radiation	915	W/m <sup>2</sup>	Flow rate	0.454 l/min
Collector area	0.0812	m <sup>2</sup>	Inlet temperature	33.4 °C
Incident direct radiation	74.30	W	Outlet temperature	34.9 °C
Produced electrical power	12.50	W	Recovered thermal power	47.51 W
<i>Power conversion efficiency</i>	<i>16.82%</i>		<i>Thermal conversion efficiency</i>	<i>63.93%</i>
<b>Test #4 Four TJPV cells</b>				
<b>Power generation</b>			<b>Thermal recovery</b>	
Direct radiation	908	W/m <sup>2</sup>	Flow rate	0.431 l/min
Collector area	0.3249	m <sup>2</sup>	Inlet temperature	33.2 °C
Incident direct radiation	295.01	W	Outlet temperature	38.9 °C
Produced electrical power	46.75	W	Recovered thermal power	171.40 W
<i>Power conversion efficiency</i>	<i>15.85%</i>		<i>Thermal conversion efficiency</i>	<i>58.10%</i>

## 6.5 Conclusions and final remarks

A biaxial Fresnel CPV/T prototype for the distributed micro-cogeneration of heat and power has been designed, developed and field-tested. The system allows the production of electrical and thermal energy from the solar RES through the innovative concentrating technology. Details about the design choices of the five functional modules composing to the prototype are provided to study their technical features and their economic impact on the total manufacturing cost. Furthermore, a set of field-tests has been conducted during the 2012 summer months in Bologna, Italy. The main purposes of such an experimental campaign have been to verify the accuracy in sun collimation and to evaluate the

electrical and thermal conversion efficiency of both a single InGa/GaAs/Ge TJPV cell and of the whole prototype.

Experimental outcomes highlight an average alignment gap between the sun and the prototype solar collector lower than  $0.8^\circ$ , representing an limit value according to the optical properties of the adopted Fresnel lenses. Focusing on the conversion performances, both the electric efficiency of a single TJPV cell and of a series of four TJPV cells, connected in series, are investigated. In the former test, developed to characterize a single TJPV cell, the produced power is of 8.7W, while the electrical conversion efficiency is equal to 15.8%. In the latter test, results highlight an electrical conversion efficiency of about 13%, while the thermal conversion efficiency depends on the cooling fluid flow rate and outlet fluid temperature. The thermal conversion performance is around 70%. The development of a cheap SOE to compensate mechanical inaccuracies and sun tracking misalignments has slightly increased the electric conversion efficiency. For the single TJPV cell and four TJPV cells, the electric conversion efficiency has reached almost 17% and 16%, respectively, values still far from the TJPV cell nominal power. Such experimental results point out the complexity of CPV/T technology, which efficiency depends upon the integration of different components, *i.e.* solar collectors and receivers, tracking system, *etc.* The main reasons are the imperfection of concentrator geometry structure, the optical loss of the reflective mirrors, non-uniform illumination levels on the solar cell and the efficiency drop due to the temperature rise of the TJPV cell. Same critical issues are detected in some CPV and CPV/T prototypes presented in the major literature (Du *et al.*, 2012; Kandilli, 2013)

Concluding, CPV technology is an alternative to the more traditional photovoltaic (PV) technology based on flat-plate modules. From 2008 to 2013, the price of conventional crystalline silicon PV modules has decreased sharply from €3.5/W to €0.5/W. The challenge for CPV being to compete mainly with PV has therefore grown in similar proportions. Economies of scale represent the key factor that has been chiefly responsible for driving down the prices of PV modules (Leloux *et al.*, 2014). The additional costs due to the tracking system, cooling system, SOE and maintenance activities must be compensated by the increase in the energy conversion efficiency. The critical issues and challenges deal with a complex and expensive technology that still require research activities and industrial development to increase the efficiency and to reduce the costs. These evidences are also confirmed by the installation trend and the market of CPV plants worldwide, still significantly smaller than traditional PV market. However, the interest is increasing due to higher efficiency levels in locations with high direct normal insolation and low moisture level and it is expected that PV pricing will more or less plateau short- to mid-term, which may give CPV plants the unique opportunity to gain market share. Particularly, CPV continued its spread to new markets in 2013, with sizable projects completed in Australia, Italy, and the United States, and small pilots under way in Chile, Namibia, Portugal, Saudi Arabia, and elsewhere. China commissioned the world largest plant (50 MW) during 2013 and more than 165 MW was

operating in more than 20 countries, led by China and the United States. (REN 21, 2013; Gupta, 2013).

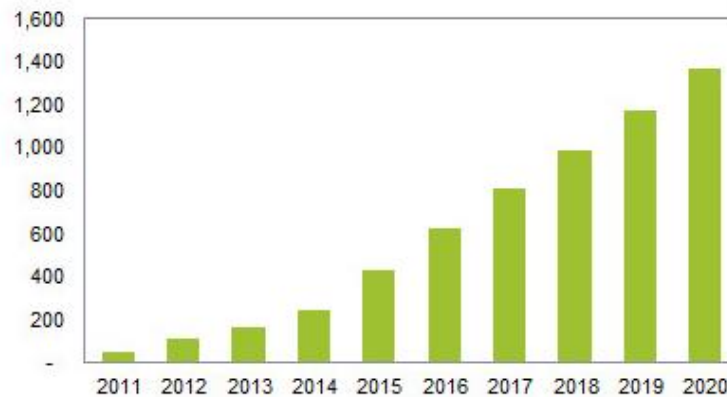


Figure 6.38 Global CV system installations and forecast (IHS, 2013)

Despite the still small installed capacity, various consultancy companies predict that the CPV market will grow to 500 MW by 2015 and 1 GW by 2010. As example, Figure 6.38 shows the CPV installations in the 2013 and a forecast of annual installed capacity until 2020 (PV Status report, 2013; IHS, 2013).

## Acknowledgements

The authors would like to thank the *Fondazione Cassa di Risparmio di Trento e Rovereto* for its significant support to the project.

## References

- Bortolini, M., Gamberi, M., Graziani, A., Manfroni, M., & Manzini, R. (2012). Hybrid Strategy for Bi-Axial Solar Tracking System. *Journal of Control Engineering and Technology*, 2(October), 130–142.
- Chemisana, D. (2011). Building Integrated Concentrating Photovoltaics: A review. *Renewable and Sustainable Energy Reviews*, 15(1), 603–611.
- Chemisana, D., Ibáñez, M., & Barrau, J. (2009). Comparison of Fresnel concentrators for building integrated photovoltaics. *Energy Conversion and Management*, 50(4), 1079–1084.
- Chemisana, D., Ibáñez, M., & Rosell, J. I. (2011). Characterization of a photovoltaic-thermal module for Fresnel linear concentrator. *Energy Conversion and Management*, 52(10), 3234–3240.

- Du, B., Hu, E., & Kolhe, M. (2012). Performance analysis of water cooled concentrated photovoltaic (CPV) system. *Renewable and Sustainable Energy Reviews*, 16(9), 6732–6736.
- European Commission. (2013). JRC SCIENTIFIC AND POLICY REPORT PV Status Report 2013.
- Gharbi, N. El, Derbal, H., Bouaichaoui, S., & Said, N. (2011). A comparative study between parabolic trough collector and linear Fresnel reflector technologies. *Energy Procedia*, 6, 565–572.
- Green, M. a., Emery, K., Hishikawa, Y., & Warta, W. (2010). Solar cell efficiency tables (version 36). *Progress in Photovoltaics: Research and Applications*, 18(5), 346–352.
- Gupta, R. (2013). CPV: Expansion and bankability required. *Renewable Energy Focus*, 14(4), 12–13.
- Guter, W., Schöne, J., Philipps, S. P., Steiner, M., Siefer, G., Wekkeli, A., ... Dimroth, F. (2009). Current-matched triple-junction solar cell reaching 41.1% conversion efficiency under concentrated sunlight. *Applied Physics Letters*, 94(22), 223504.
- Immovilli, F., Bellini, A., Bianchini, C., & Franceschini, G. (2008). Solar Trigeneration for Residential Applications, a Feasible Alternative to Traditional Micro-Cogeneration and Trigeneration Plants. 2008 IEEE Industry Applications Society Annual Meeting, 1–8.
- Kandilli, C. (2013). Performance analysis of a novel concentrating photovoltaic combined system. *Energy Conversion and Management*, 67, 186–196.
- Leloux, J., Lorenzo, E., García-Domingo, B., Aguilera, J., & Gueymard, C. a. (2014). A bankable method of assessing the performance of a CPV plant. *Applied Energy*, 118, 1–11.
- Muñoz, E., Vidal, P. G., Nofuentes, G., Hontoria, L., Pérez-Higueras, P., Terrados, J., ... Aguilera, J. (2010). CPV standardization: An overview. *Renewable and Sustainable Energy Reviews*, 14(1), 518–523.
- Pan, J.-W., Huang, J.-Y., Wang, C.-M., Hong, H.-F., & Liang, Y.-P. (2011). High concentration and homogenized Fresnel lens without secondary optics element. *Optics Communications*, 284(19), 4283–4288.
- REN21 Renewable energy policy network for the 21st century. (2013). *RenewableS 2013 GLOBAL STATUS REPORT*.



- Rumyantsev, V. D., Khvostikov, V. P., Khvostikova, O. A., Gazaryan, P. Y., Sadchikov, N. A., Vlasov, A. S., ... Andreev, V. M. (2004). Structural Features of a Solar TPV Systems, (June).
- Sonneveld, P. J., Swinkels, G. L. a. M., Tuijl, B. a. J. Van, Janssen, H. J. J., Campen, J., & Bot, G. P. a. (2011). Performance of a concentrated photovoltaic energy system with static linear Fresnel lenses. *Solar Energy*, 85(3), 432–442.
- Wenham, S.R., Green, M.A., Watt, M.E., Corkish, R. (2007). *Applied photovoltaics*. (Earthscan, Ed.). United Kingdom.
- Xie, W. T., Dai, Y. J., Wang, R. Z., & Sumathy, K. (2011). Concentrated solar energy applications using Fresnel lenses: A review. *Renewable and Sustainable Energy Reviews*, 15(6), 2588–2606.
- Zubi, G., Bernal-Agustín, J. L., & Fracastoro, G. V. (2009). High concentration photovoltaic systems applying III–V cells. *Renewable and Sustainable Energy Reviews*, 13(9), 2645–2652.



# 7. TES Prototype for CSP plants

## *Development and performance tests of a thermal energy storage prototype for CSP plants*

The second experimental activity deals with concentrating solar power (CSP) plants, a more developed and diffused technology than concentrated photovoltaics (CPV). CSP technology is unique among renewable energy sources (RESs) since it can easily be coupled with both thermal energy storage (TES) solutions and conventional fossil-fuel based power plant. Ongoing research efforts are in the areas of reflector and collector design and materials, heat absorption and transport, power production and thermal storage to make CSP more cost effective and, therefore, economically sustainable.

During the permanence at the Clean Energy Research Center (CERC) - University of South Florida (Tampa (FL) - United States) in the 2013, a research activity focused on the development and tests of a low cost storage solution for tower solar power (TSP) technology has been carried out. The aim was to develop a pilot scale TES prototype to investigate the effectiveness of the system for its future installation in a TSP plant installed by the company Sunborne in India. The system consists of a packed bed of pellets as the storage media and uses air as the heat transfer fluid (HTF). Such TES system may overcome the intermittent nature of sunlight and increase the capacity factor of the TSP plant and it is promising storage concept due to its single tank design and employment of cheap and abundant storage media such as sand and rock. This *Chapter*, after a brief introduction of TES solutions for CSP plants in *Paragraph 7.1*, describes the development and the performance tests of the prototype.

### *7.1 Thermal energy storage (TES) solutions for CSP Plants*

As previously discussed in *Paragraph 3.1*, energy storage systems (ESSs) are able to increase energy fruition in the remote areas, to balance the intermittent and random nature of the RESs and to overcome several grid lacks, e.g. blackouts, overloads, low grid quality, etc. ESSs coupled to CSP plant has the main purpose to increase the capacity factor of solar thermal power plant, i.e. the ratio of its actual output over a period of time, to its potential output if it were possible for it to operate at the nominal capacity continuously over the same period of time. The increase of capacity factor significantly affects the economic profitability of the plant since the power block unit is able to operate for a larger number of hours (See *Paragraph 5.2*)

In this context, TES system presents lower capital costs and very high operating efficiencies, up to 97%, when compared to mechanical and chemical storage technologies. Nowadays, 16 CSP plants, with rated power from 500kWe to 64MWe, worldwide take advantages of TES solution.

A TES system mainly consists of three functional modules:

- the storage medium: it stores the thermal energy either in form of sensible heat, fusion or vaporization latent heat or reversible chemical reactions. Synthetic oils and molten salts, used as sensible heat storage solutions, are currently the most widely storage mediums adopted in large scale CSP plant, while other storage materials are still investigated and under development
- the heat transfer mechanism: such mechanism has the purpose to supply or extract heat from the storage medium
- the containment system: it contains the storage medium, heat transfer mechanism and insulates the system from the external ambient in order to avoid heat dispersion and, therefore, the reduction of the TES roundtrip efficiency

The choice and combination of the mentioned functional modules aims to satisfy the following requirements to guarantee optimal performances, longevity and environmental/economic sustainability:

- High energy density
- Efficient heat transfer between the HTF and the storage medium
- Mechanical and chemical stability of the storage medium
- Chemical compatibility between the HTF, heat transfer equipment and the storage medium
- Full reversibility for a significant number of charging/discharging cycles
- Low thermal losses through the containment system
- Low capital and maintenance costs
- Low environmental impact

Three selection criteria are identified:

- Cost criteria for the selection of TES system functional modules, e.g. storage material, heat exchanger and TES enclosure
- Design criteria to determine the TES system operating conditions, e.g. maximum load, nominal temperature, operation strategy, and the integration into the power plant to meet the plant requirements (long-term vs short term storage, number of hours of storage etc.)
- Technical criteria to determine and evaluate the TES system technical properties/issues, e.g. the storage capacity, the charge/discharge rates efficiency, stability, lifetime, compatibility and safety

Figure 7.1 shows the main parts of a CSP plant and TES system, according to the scheme presented in the Figure 5.3 and discussed in *Paragraph 5.2*, while Figure 7.2 summarizes the main features of the three TES system selection criteria.

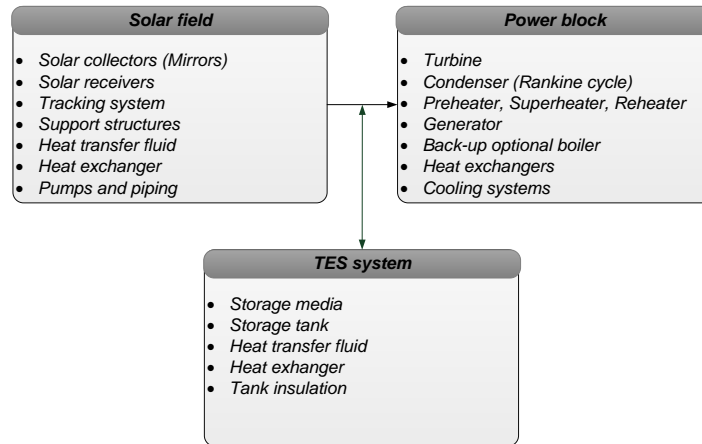


Figure 7.1 CSP plant and TES system main components

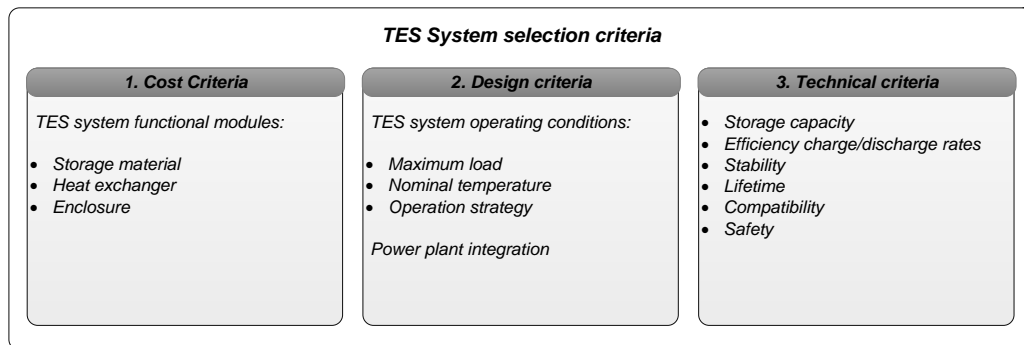


Figure 7.2 TES system selection criteria

This brief introduction on TES systems is concluded with a description of different technology currently available, shown in Figure 7.3. TES systems can be classified in either passive or active types. In active storage systems, the storage medium, in liquid or gas phases, circulates in the heat exchanger for energy transfer. Among them, three TES technologies are identified:

- Two-tank direct and indirect systems: In direct system, the fluid is stored in two tanks, containing the storage media at high temperature level and low temperature level. Fluid from the low-temperature tank flows through the solar receiver, increasing its temperature to the high temperature level, and it then flows to the high-temperature tank for storage. When required, fluid from the high-temperature tank flows through a heat exchanger, where it generates steam or heats up the power block working fluid for electricity production. The fluid exits the heat exchanger at a low temperature and returns to the low-temperature tank. Two-tank indirect systems work in the same way as two-tank direct systems, except different fluids are used as the heat-transfer and storage fluids. This system is used in plants in which the heat-transfer fluid is too expensive or not

suited for use as the storage fluid. The indirect system requires an extra heat exchanger, which adds cost to the system

- Single-tank thermocline systems: Fluids can also be used in a single tank system where a hot fluid such as synthetic oil is pumped into the top of a tank during the charging mode, gradually displacing a colder fluid. A thermal gradient is created within the system and is ideally stabilized and preserved by buoyancy effects. Such a system is called “thermocline storage” due to the thermal gradient that develops within the system. The hot fluid remains at the top and the cold fluid remains at the bottom, however, in these systems, it is difficult to separate the hot fluid from the cold fluid. A thermocline storage system has an additional advantage that the most of the storage fluid can be replaced with a low-cost filler material
- Steam accumulators: In addition to the use of synthetic oils and molten salts in active type storage, water can be used as the storage medium in systems called steam accumulators

Considering passive storage systems, a storage medium is charged and discharged transferring energy to a HTF flowing through it at different temperatures. Passive storage systems may utilize inexpensive solids such as rocks, sand or concrete for sensible heat storage materials, or phase change materials for storing thermal energy. Heat transfer can be more difficult because the storage medium is usually in solid phase rather than liquid phase. Two different types of passive storage systems are currently adopted:

- Systems with embedded or enhanced heat transfer structures, e.g. pipes embedded in a concrete storage module, integration of high conductivity heat exchanging mechanism, use phase change materials *etc.*
- Packed bed systems: Packed bed systems use sensible and latent heat storage material elements in different shapes and sizes and a HTF that flows between these elements for transferring heat to the storage material. Most of packed bed systems adopt a single-tank design to reduce the costs. These systems can maintain the thermal gradient when very low conductive materials such as rocks are used. Thermoclines with filler materials can be also defined as packed bed systems (Goswami et al., 2008; Kuravi et al., 2013).

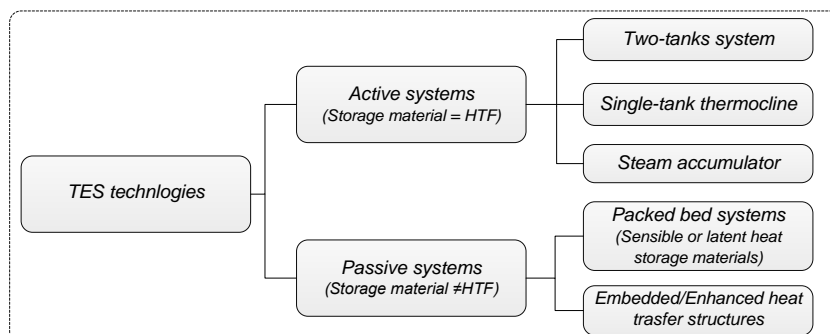


Figure 7.3 TES system available technologies

## 7.2 TES prototype

The developed TES system represents a low cost energy storage solution for a CSP plant based on TSP technology, which is described in the previous *Paragraph 5.2.2* and outlined in Figure 5.6. The single-tank design, the adoption of a packed bed of rock pellets as the storage media and air as HTF make the technology promising and economically sustainable. Figure 7.4 presents the architecture of the packed bed system. The solar radiation, reflected by the heliostats of the solar field, heats up the air flowing through the solar receiver. The high temperature air flow can both directly supply the power block thermal load and start the TES charging process. The solar field is generally designed, through the number and dimensions of the heliostats, to guarantee a specific number of energy storage hours. When the solar radiation is not available or not able to proper supply the power block thermal load, the TES system is discharged with a lower temperature air flow coming from the turbine outlet or the external ambient.

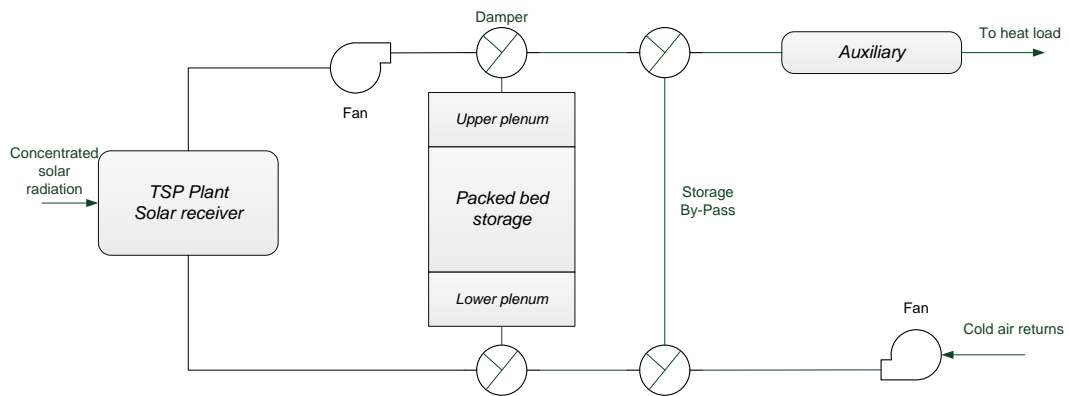


Figure 7.4 TES system architecture

The next *sub-Paragraphs* provide a description of prototype and the experimental test setup together with the results of the experimental analysis carried out to determine a pressure drop correlation that can reasonably predict pressure losses in a bed of highly irregular shaped solid pellets. Preliminary test results of charging/discharging processes are also presented.

### 7.2.1 TES prototype overview and experimental test set-up

A representation of the developed prototype is in Figure 7.5. The prototype allows simulating both charging and discharging cycles through two electric heaters (b-c), located at the inlet and outlet ducts of the insulated tank (a). The “charging” electric heater simulates the hot temperature air flow coming from the solar field, while the “discharging” electric heater simulates the lower temperature air flow coming from either the turbine outlet or external ambient. Discharging and charging processes are properly controlled through a control panel (d) able to regulate the switching on and the supplied power of both the electric heaters.

The temperature distribution in the packed bed of rocks is monitored thanks to a series of thermocouples placed in six layers along the bed height (6 thermocouples each layer). The thermocouples output signals are acquired through a National Instruments Platform (e) and the data-logging software NI Signal Express.

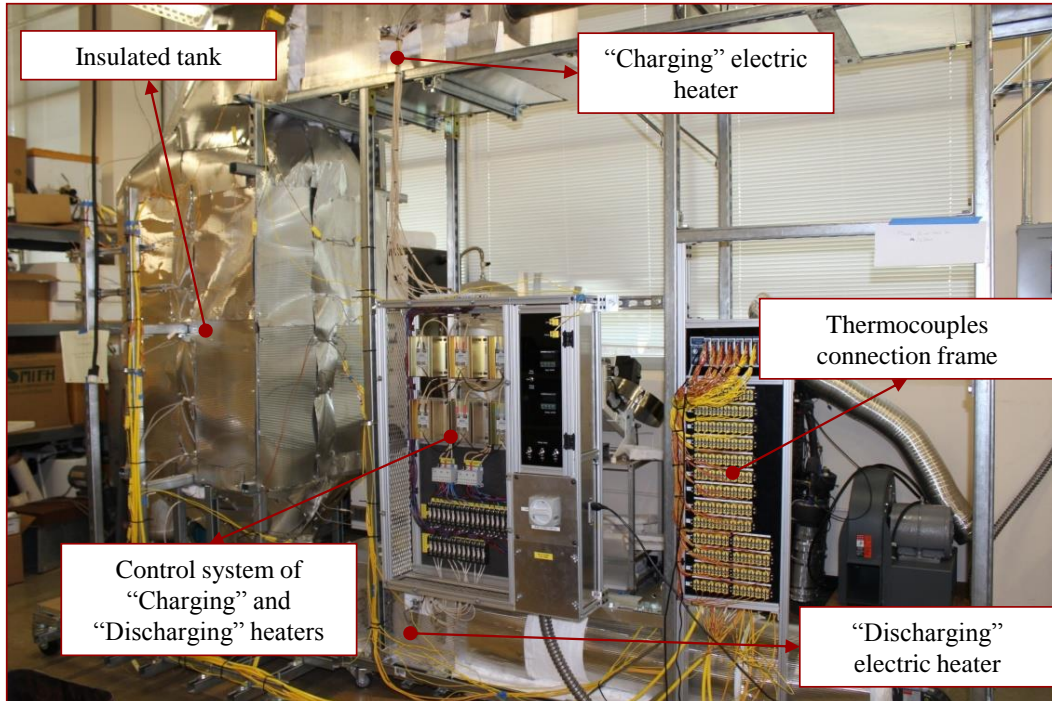


Figure 7.5 Architecture of the developed packed bed TES system

A schematic of the packed bed system is provided in Figure 7.6.

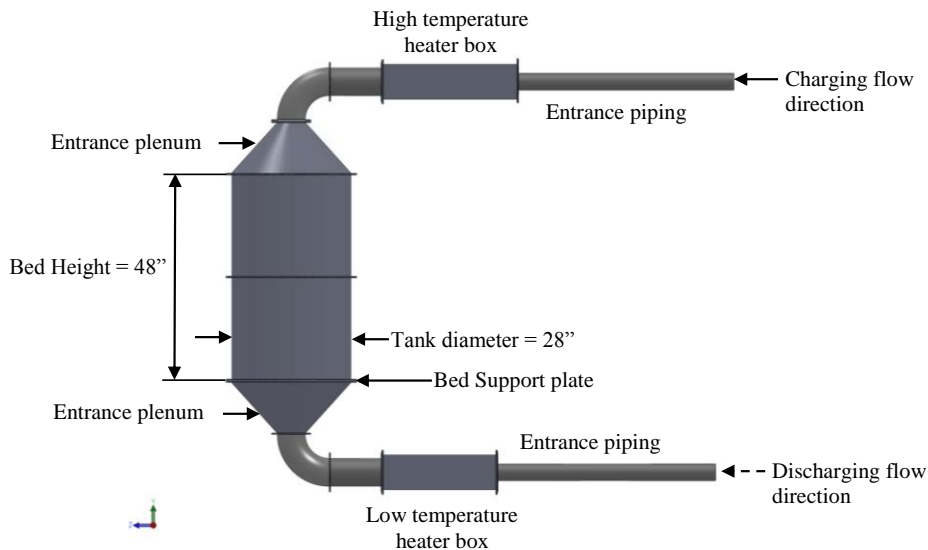


Figure 7.6 Schematic of the packed bed system

The final bed height is 0.889m and the bed diameter is 0.445m. The total tank height including the upper and lower plenums is 1.83m and the tank diameter is 0.711m. The difference between the tank diameter and the bed diameter is due to a 0.152m thick flexible ceramic wool insulation that lines the tank. A 9.53mm thick perforated carbon steel plate with 12.7mm holes and 48% open area is used to support the pellets. The



upper and lower elbows are 0.161m in diameter. A diffuser plate is installed at the exit of the lower elbow to reduce the effects of flow separation in the elbow, which creates non-uniform flow conditions.

The outside of the tank is insulated by 8 inches of ceramic fiber insulation and the inside of the tank is insulated by 2 inches of insulation, therefore the tank diameter is 4" greater than the packed bed diameter. The tank is made of carbon steel coated with a high temperature paint to minimize corrosion and is divided into two 24 inch flanged sections in order to facilitate ore placement and removal (Figure 7.7). Two 12 inch tall conical entrance plenums are placed above and below the bed. Flow conditioners, made of 304 stainless steel, are placed at each 90 degree elbow to ensure uniform flow into the bed. The total system height is approximately 103 inches, excluding the support structure. Two electric heaters are used for both charging and discharging modes in order to simulate real system conditions wherein the bed experiences a 300°C temperature differential. The packed bed support plate is designed by first assuming a 60 degree staggered pattern which is one of the strongest configurations for perforated plates. The maximum allowable bending stress of carbon steel at 400°C has been multiplied by a perforated plate modified strength coefficient in order to calculate the plate thickness. The strength coefficient is based on a ½ inch hole diameter and 11/16th inch pitch, which results in an open area of 48%. Stainless steel wire mesh is located on top of the plate to minimize the amount of small particles that may flow through the plate.

Volumetric flow rate is measured by an averaging pitot tube placed in the entrance piping. The pipe length is sized so that it meets upstream and downstream length requirements of the pitot tube. In order to size the Pitot tube and differential manometer, the system static pressure is estimated by calculating the pressure drop across all system components.



Figure 7.7 Flanged steel storage tank components

Temperature measurements within the ore and in the voids of the bed are measured by Omega instruments Inconel overbraided ceramic fiber insulated thermocouples. Figure 7.8a shows the thermocouples used for air temperature measurements. These are flexible, equipped with a shield to reduce radiative effects, and have bolt holes that can be used to align the thermocouples in the radial direction. Figure 7.8b shows the same thermocouples without the shield. These are inserted in the ore to measure their temperature.

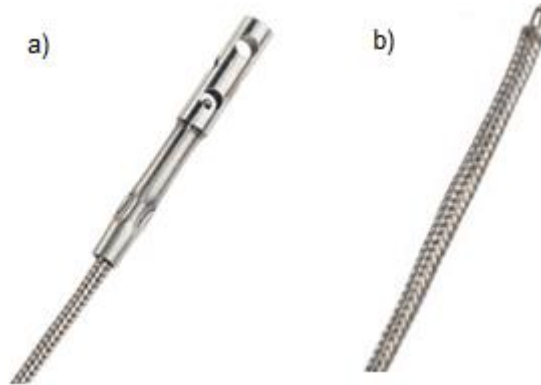


Figure 7.8 a) Shielded thermocouple for air measurements. b) Exposed tip thermocouple for iron ore temperature measurements

Six rows of thermocouples span the height of the packed bed to measure air temperature. The locations of the thermocouples are provided in Figure 7.9, while Figure 7.10 shows the one of the thermocouple row installed in the packed bed.

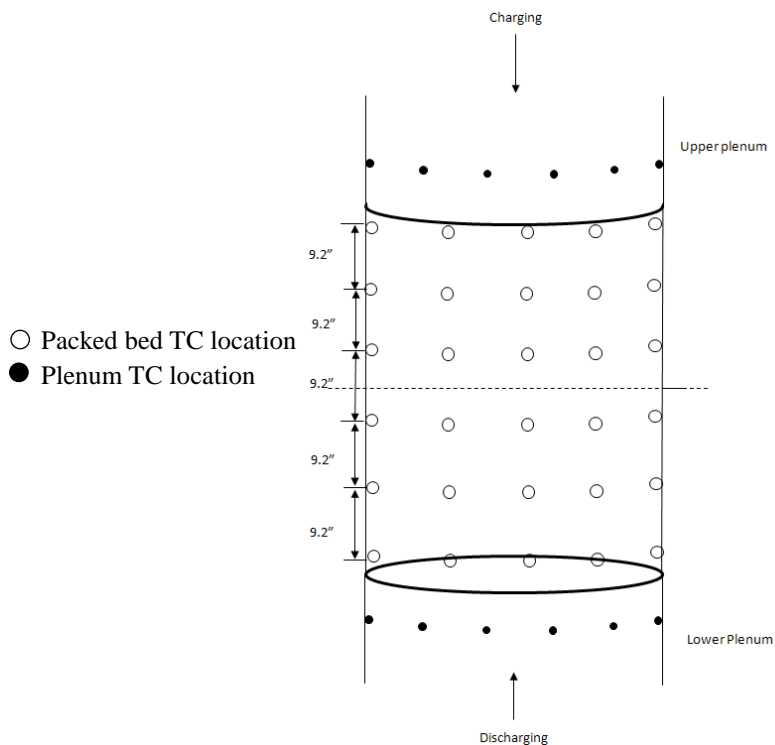


Figure 7.9 Thermocouple locations



Figure 7.10 Thermocouple row in the packed bed

The rows are spaced approximately 9.2 inches vertically apart and two rows in the upper and lower plenum are provided to measure the air entrance and exit temperature. The temperature of one ore is monitored by a thermocouple in the center of each row and there are 5 thermocouples measuring air in each row.

Finally, Table 7.1 summarizes the prototype system components and instruments.

Table 7.1 Iron ore prototype system components

<i>Component</i>	<i>Description</i>
Entrance piping	4" diameter, 60" length, 10 gauge, carbon steel
Heater box	304 Stainless steel
Elbow/Bed piping	304 Stainless steel, 6" diameter
Flow conditioner	304 Stainless steel, 6" diameter, 3/8" thickness
Packed bed plate	3/8" thick carbon steel, 1/2" diameter holes, 11/16" pitch
Tank	1/8" thick carbon steel, 48" height
Entrance plenum	1/8" thick carbon steel, 6"x28" diameter
Averaging pitot tube	Omega Instruments FPT-6100 High accuracy pitot tube; accuracy = $\pm 2\%$ of rate, repeatability = $\pm 0.1\%$ .
Digital manometer	Dwyer Mark III, 0-0.2491 kPa range; accuracy = $\pm 0.5\%$ of F.S. (1.245 Pa)
Thermocouples	Omega Instruments- XCIB, High temperature Inconel overbraided ceramic fiber insulated; accuracy is greater of 2.2°C or $\pm 0.75\%$ of reading.

### 7.2.2 Pressure drop model and experimental validation

The experimental analysis to measure the pressure drop along the packed bed and to validate a pressure drop correlation that can reasonably predict pressure losses in a bed of highly irregular shaped solid pellets is described and presented in Trahan *et al.* (2014). This *sub-Paragraph* introduces the experimental analysis procedure and discusses the main results, together with preliminary experimental tests to simulate charging and discharging cycles.

#### 7.2.2.1 Introduction

Laboratory-scale and pilot-scale packed bed systems have been tested and used to develop empirical correlations and validate numerical models that describe fluid flow and heat transfer in packed bed TES system. The models provide an avenue by which the parameters of a packed bed and their influence on performance and thermal behavior can be investigated. Within packed bed systems, pressure drop pumping losses can be significant. Thus, many studies focus on developing pressure drop correlations which are based on key parameters that affect the transport properties of a system. These parameters must be optimally chosen such that they minimize pressure losses without compromising heat transfer and efficiency.

Ergun *Equation* is one of the most widely adopted pressure drop correlation (Ergun, 1952).

$$\frac{\Delta P}{L} = A \cdot \frac{(1-\varepsilon)^2}{\varepsilon^3} \cdot \frac{\mu U}{D_p^2} + B \cdot \frac{(1-\varepsilon)}{\varepsilon^3} \frac{\rho U^2}{D_p} \quad (7.1)$$

Where

- the coefficient  $A$  is 150 and  $B$  is 1.75
- $\Delta P$  is the pressure drop of packed bed [Pa]
- $L$  is the height of packed bed [m]
- $\varepsilon$  is the void fraction
- $\mu$  is the dynamic viscosity of the fluid [kg/ms]
- $U$  is the superficial bed velocity, *i.e.* average velocity in a empty tank [m/s]
- $D_p$  is the particle diameter [m]
- $\rho$  is the density of the fluid [kg/m<sup>3</sup>]

Previous theories and equations on pressure loss through a bed have been utilized in conjunction with experimental data to establish the above relationship. The first term on the right-hand side represents viscous energy losses that dominate during laminar flow and the second term accounts for kinetic losses that govern in the turbulent regime. Experiments used in the development of the correlation included particles of various shapes such as spheres, cylinders, tablets, and crushed solids. The only factors considered in the analysis are fluid flow rate, particle diameter, fluid viscosity and density,

and fractional void volume. The correlation should be valid for hydraulic particle Reynolds numbers between 1 and 3000. The hydraulic particle Reynolds number differs from the particle Reynolds number that is typically used, in that it has a dependence on the void fraction. The hydraulic particle Reynolds number,  $Re_h$ , and particle Reynolds number,  $Re_p$ , are defined respectively as (Achenback, 1995).

$$Re_h = \frac{\rho U D_p}{\mu(1-\varepsilon)} \quad (7.2)$$

$$Re_p = \frac{\rho U D_p}{\mu} \quad (7.3)$$

Equation 7.1 has been successfully employed to predict the pressure drop of packed beds filled with regular-shaped spherical particles (Choi *et al.*, 2008, Li & Ma, 2011, Singh *et al.*, 2006). Numerous correlations have also been proposed, some of which simply alter the constants  $A$  and  $B$ , or modify the other bed parameters in order to develop a more accurate prediction of pressure drop for particle shapes that deviate from spherical. Modification has also been made by incorporating the shape factor, or particle sphericity, which is a measure of the degree to which the shape of the particle approaches the shape of a sphere. The sphericity,  $\psi$ , is defined in the following Equation 7.4 (Geldart, 1990).

$$\psi = \frac{\text{Surface of sphere of equal volume to the particle}}{\text{Surface area of the particle}} = \frac{\pi^{1/3}(6V_p)^{2/3}}{A_p} \quad (7.4)$$

In Ergun *et al.* (1952) there is little mention of the tank-to-particle diameter ratio,  $d/D_p$ , except that scatter in some of the data was likely due to a  $d/D_p$  ratio less than 10. It is speculated that packed beds with low tank-to-particle ratios are strongly influenced by the “wall-effect”, which is caused by increased void fraction and viscous friction at a rigid tank wall (Nemec & Levec, 2005). The ratio at which the wall effect is negligible has been inconsistently defined and there are opposing views on its exact effect on pressure drop (Eisfeld & Schnitzlein, 2001). For example, Meier *et al.* (1991) claim that the wall-effect can be neglected when  $d/D_p$  is greater than 40, whereas Torab & Beasley (1987) as well as Cohen & Metzner (1981) indicate a value of  $d/D_p > 30$ . Eisfeld and Schnitzlein (2001) have conducted an extensive analysis of more than 2300 data points from pressure drop experiments, mostly found in the literature, in order to investigate the wall-effect on pressure losses. They have concluded that the influence of the wall-effect is dependent on the Reynolds number, *i.e.* an increasing pressure drop due to the wall-effect appears in streamline or transitional flow and a decreasing or lack of pressure drop due to the wall emerges during turbulent flow. Moreover, Eisfeld and Schnitzlein (2001) have determined that for streamline flow, the wall-effect is significant when the  $d/D_p$  ratio is less than 10. They present a pressure drop correlation that has been developed in a study by Reichelt

(1972) in the form of the dimensionless friction factor and found that it is valid for particle Reynolds numbers of  $0.01 \leq Re_p \leq 17635$ , and tank-to particle diameter ratios of  $1.624 \leq d/D_p \leq 250$ :

$$f = \frac{K_1 A_w^2 (1-\varepsilon)^2}{Re_p \varepsilon^3} + \frac{A_w (1-\varepsilon)}{B_w \varepsilon^3} = \frac{\Delta P D_p}{\rho_f L U^2} \quad (7.5)$$

With the wall correction terms defined as:

$$A_w = 1 + \frac{2}{3 \left(\frac{d}{D_p}\right)^{(1-\varepsilon)}} \quad (7.6)$$

$$B_w = \left[ k_1 \left(\frac{D_p}{d}\right)^2 + k_2 \right]^2 \quad (7.7)$$

And  $k$  coefficients defined in Table 7.2 for different particle shapes.

**Table 7.2 Coefficient for Reichlet's Equation, Equation 7.2 (Eisfeld and Schnitzlein, 2001)**

Particle shape	Coefficients		
	$K_1$	$k_1$	$k_2$
Spheres	154	1.15	0.87
Cylinders	190	2.00	0.77
All particles	155	1.42	0.83

In *Equations 7.1 and 7.5*, the only packing parameters that are considered in the correlation are the particle diameter and the void fraction of the bed. Since the equivalent particle diameter,  $D_p$ , may be the same for different shape particles that exhibit dissimilar flow characteristics, Singh *et al.* (2006) have developed a new friction factor correlation that incorporates particle sphericity. Experiments have been conducted at particle Reynolds number ranging between  $1047 \leq Re_p \leq 2674$ , and on particles of different diameters, void fraction and sphericity in order to develop the following correlation:

$$f = 4.466 (Re_p)^{-0.2} \varepsilon^{-2.945} \{ \exp[11.85 (\log \psi)^2] \} = \frac{\Delta P \rho_f D_p}{L G^2} \quad (7.8)$$

Where  $G$  is the mass velocity of air or mass flow rate of air per unit bed cross-sectional area,  $[\text{kg/s m}^2]$ . The above pressure drop correlations based on Ergun, Singh *et al.*, and Eisfeld and Schnitzlein, are dependent on the particle diameter,  $D_p$ , which is equal to the diameter of the particle if it is a sphere. If the particle is non-spherical, an equivalent particle diameter must be used. In Ergun's correlation and Eisfeld and Schnitzlein's correlation this is defined as the Sauter-diameter, which is the diameter of a sphere with the same volume to surface area ratio as a non-spherical particle:

$$D_{sd} = \frac{6V_p}{A_p} \quad (7.9)$$

Ergun (1952) states that use of volume-to-specific surface of solid ratio was tested and is valid for many shapes including spheres, cylinders, and crushed materials such as coke and coal but does not extend to solids with holes or other special shapes. Singh *et al's* Equation incorporates an equivalent particle diameter by volume,  $D_v$ , defined as the diameter of a sphere having the same volume as the given particle:

$$D_v = \left(\frac{6}{\pi} V_p\right)^{1/3} = \frac{6V_p}{A_{sp}} = \frac{6V_p}{\psi A_p} = \frac{D_{sd}}{\psi} \quad (7.10)$$

Thus, the Equation 7.1 can be written as:

$$\frac{\Delta P}{L} = 150 \cdot \frac{(1-\varepsilon)^2}{\varepsilon^3} \cdot \frac{\mu U}{(\psi D_v)^2} + 1.75 \cdot \frac{(1-\varepsilon) \rho U^2}{\varepsilon^3 \psi D_v} \quad (7.11)$$

Li and Ma (2011) however, have conducted experiments and found that use of the Sauter diameter under-predicts the pressure drop when Ergun's *Equation* is used for non-spherical particles. This is due to the fact that the Sauter diameter only considers the specific surface area and does not explicitly account for the sphericity, or shape of the particle. Li and Ma (2011) have replaced the Sauter diameter with one that considers the sphericity and found that the flow resistance could be predicted with Ergun's *Equation*. The defined this particle diameter,  $D_{eq}$ , as:

$$D_{eq} = \psi D_{sd} = \psi^2 D_v = \frac{\psi^2 6V_p}{A_{sp}} = \frac{\psi 6V_p}{A_p} \quad (7.12)$$

From the above discussion, it is apparent that there are numerous ways to calculate pressure losses in a packed bed. In the present study, an attempt is made to find a correlation that is best suited for a packed bed of highly irregular shaped solid pellets with moderately low tank-to-particle diameter ratio. The pellets can be considered as crushed rock having flat, jagged surfaces.

### 7.2.2.2 Experimental test set-up

A schematic of the packed bed system is provided in Figure 7.11. The final bed height is 0.889m and the bed diameter is 0.445m. The total tank height including the upper and lower plenums is 1.83m and the tank diameter is 0.711m. The difference between the tank diameter and the bed diameter is due to a 0.152m thick flexible ceramic wool insulation that lines the tank and which will be used for future heat transfer experiments. A 9.53mm thick perforated carbon steel plate with 12.7mm holes and 48% open area is used to support the pellets. The upper and lower elbows are 0.161m in diameter. A diffuser plate is installed at the exit of the lower elbow to reduce the effects of flow separation in the elbow, which creates non-uniform flow conditions. Room temperature (23°C) air enters the bottom of the system through one of 3 blowers that are used to

achieve the desired flow rates. Velocity is measured with a hot wire anemometer at a position that had at least 10 pipe diameters upstream and 4 pipe diameters downstream from the point of measurement. Pressure is measured with a digital manometer. Specifications and accuracy values for the instruments are provided in Table 7.3.

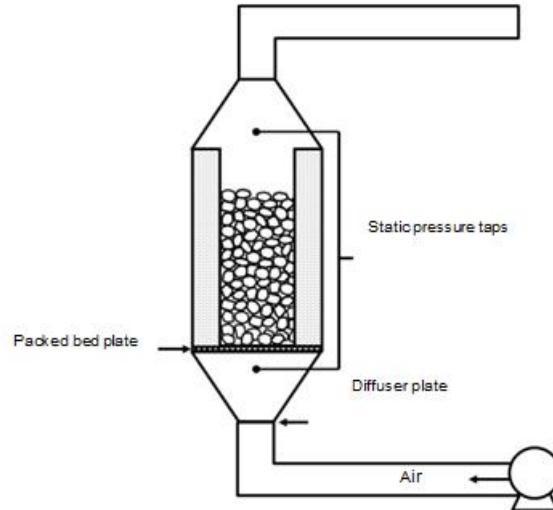


Figure 7.11 Schematic of the packed bed system

Table 7.3 System components

Instrument	Description	Accuracy
Hot wire anemometer	0.15-30 m/s range	± 3% reading
Digital manometer	0-1 in. w.c.(0 – 249.1 Pa) range	± 0.5% F.S./ ± 0.1% F.S. hysteresis
Digital manometer	0-20 in. w.c.(0 – 4.982 Pa) range	± 0.5% F.S./ ± 0.1% F.S. hysteresis
Dayton Blower	¼ hp	-
Dayton Blower	1/30 hp	-
Heavy Duty Blower	7.5 hp / 5.5 kW, 3 phase induction motor	-

To calculate bed porosity, the mass of the pellets and bed volume are used to estimate the bulk density which is then used in the following *Equation* to calculate porosity:

$$\varepsilon = 1 - \frac{\text{Bulk density}}{\text{True density}} \quad (7.13)$$

Porosity is also measured in a separate container with a diameter that is similar to the final bed diameter to verify the voidage. The equivalent diameter of the pellets is obtained by measuring the mass of 35 random samples. The volume of each of the samples is then calculated using the true density, and the average volume of the 35 samples is used to obtain the equivalent particle diameter by volume as defined in *Equation 7.10* with a standard deviation of 0.006426 m. The bed parameters are listed in Table 7.4.



Table 7.4 Bed parameters

Description	Value
Bed voidage	0.51
Equivalent particle diameter	0.04259m
Sphericity	0.495
Solid pellet density	3127kg/m <sup>3</sup>
Tank-to-particle ratio	10.4

The packed bed support plate and the restriction created by the insulation at the exit and entrance of the bed introduce an additional pressure drop. To estimate this value, the pressure drop is measured with an empty bed for different velocities. A third-order polynomial best-fit *Equation* is then used to calculate the additional pressure loss and subtract it from the total pressure drop. In order to test whether there is flow maldistribution due to the inlet geometry, velocity is measured at various points in the cross section of the first five to ten centimeters of the bed with a vane anemometer and found to be acceptable.

### 7.2.2.3 Experimental test results: pressure drop

Tests are conducted for particle Reynolds numbers between  $353 \leq Re_p \leq 5206$ . The particle Reynolds number is calculated by using the equivalent particle diameter by volume,  $D_v$ . The results of the pressure measurements as a function of air mass flux are provided in Figure 7.12. An error propagation uncertainty analysis is conducted and the pressure gradient  $\left(\frac{\Delta P}{L}\right)$  uncertainties are included in the Figure. The air mass flux (kg/m<sup>2</sup>s) uncertainty ranged from 3.1% to 3.8% and is not included in order to maintain clarity within the plot.

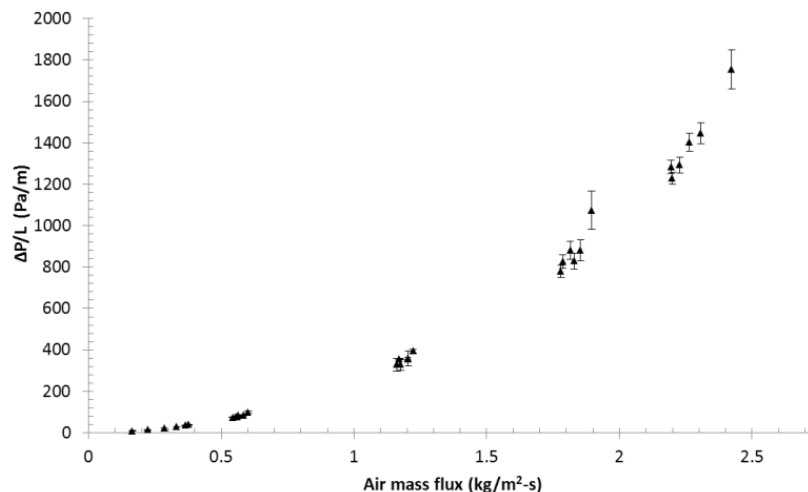


Figure 7.12 Measured pressure gradient versus air mass flux

Since the particle sphericity is difficult to calculate with irregular shaped solids, it is deduced from Ergun's Correlation, *Equation 7.11*, by calculating the root mean square deviation between measured and predicted pressure drop for different sphericity values. This is repeated with Singh *et al.*'s *Equation* using data that fell in the particle Reynolds

number range that has been used to develop the correlation, *i.e.* between  $1047 \leq Re_p \leq 2674$ . The same sphericity value of 0.495 is obtained using both correlations. Figure 7.13 demonstrates the measured pressure drop of the packed bed versus particle Reynolds number. Measured values are plotted with Ergun's original Equation, Equation 7.1, and the Equation presented in Einfeld and Schnitzlein, Equation 7.5, which accounts for the wall-effect. The Sauter diameter is used in both equations. In calculating Equation 7.5, the coefficients for "all shapes" are used, as defined in Table 7.2. Both correlations are plotted with Singh *et al.*'s equation in Figure 7.13, which uses the equivalent particle diameter by volume.

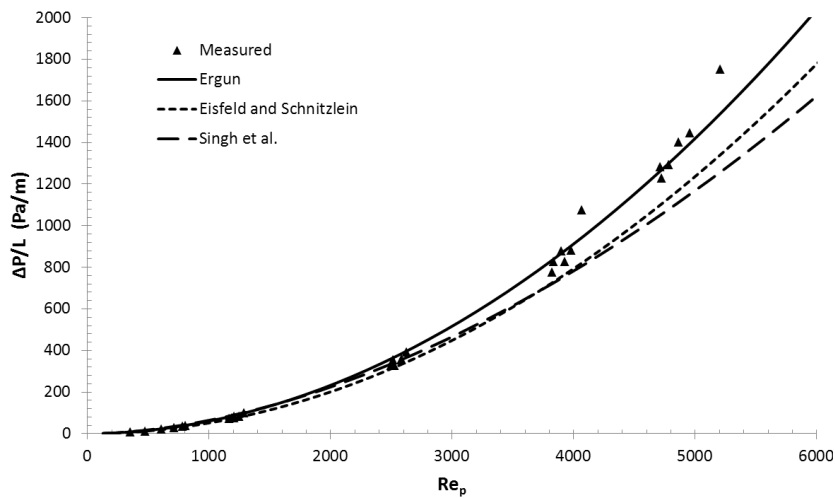


Figure 7.13 Pressure gradient as a function of particle Reynolds number. Shape factor of 0.495 is used in the pressure correlations

Singh *et al.*'s Equation shows a relatively good fit in the Reynolds numbers range of 1166 to 4069, where the difference is between 0 and 18%. The difference between measured and predicted values increases at higher Reynolds numbers (neglecting the 2 outliers), lying between 14 and 20%. At lower Reynolds numbers, *i.e.*  $Re_p < 808$ , the difference is between 14 and 33%. This trend in lower predictability at lower and higher  $Re_p$  is due to the fact that Singh *et al.*'s Equation has a 1.8th power dependence on bed velocity, whereas the measurements show a 2<sup>nd</sup> power dependence ( $r^2 = 0.9986$ ).

The difference between Ergun's Equation and the measured values is between 1% to 14% over the range of  $1166 \leq Re_p \leq 5206$  and 5% to 16% in the lower range of  $353 \leq Re_p \leq 808$ , which is shown in Figure 7.14. Einfeld and Schnitzlein's Equation predicts a lower pressure drop than Ergun's Equation for all Reynolds numbers, even in streamline flow. Since the sphericity effectively reduces the particle diameter, the tank-to-particle ratio increases from 10.4 to 20.9 when the Sauter diameter is used, which, per Einfeld & Schnitzlein, is high enough so that the wall does not have an effect on pressure losses. The measured values are approximately 2% to 14% greater than Einfeld and Schnitzlein's prediction over the entire Reynolds number range. The percent overall average relative absolute error, defined as

$$\frac{1}{n} \sum_{i=1}^n \frac{|x_{i,predicted} - x_{i,measured}|}{x_{i,measured}} \quad (7.14)$$

for the three correlations are provided in Table 7.5.

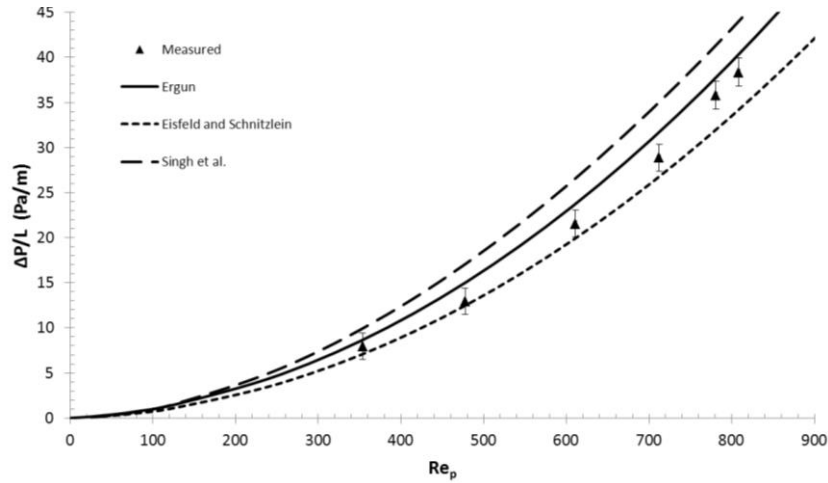


Figure 7.14 Correlation between pressure gradient and particle Reynolds number for lower Reynolds number range. Particle shape factor of 0.495 is considered.

Table 7.5 Percent average relative absolute error (ARAE) for the 3 pressure correlations in which sphericity is considered

Correlation	% ARAE
Ergun	6.9%
Eisfeld and Schnitzlein	10.1%
Singh et al.	14.2%

An attempt is also made to calculate the sphericity using the equivalent particle diameter defined by Li and Ma (2011), however the sphericity that is found with this method did not produce reasonable results in Singh *et al.*'s Equation. Figure 7.15 shows the results of the predictions of the three correlations if the shape factor is determined by the use of Li and Ma's equivalent particle diameter,  $D_{eq}$ . This results consider shape factor value of 0.70. As can be seen in the Figure, Singh *et al.*'s Equation severely underpredicts the pressure drop when the higher shape factor is introduced. The percent average relative absolute error for Ergun's Equation in this instance is 7.6% and for Eisfeld and Schnitzlein is 7.5%. For Singh *et al.*'s correlation it is 43.9%.

Concluding, the purpose of this experimental analysis is to find a pressure drop correlation that can reasonably predict pressure losses in a bed of highly irregular shaped solid pellets. Many correlations are available in the literature and there is little agreement on any universal method that can be used to accurately predict the pressure gradient for non-spherical shapes.

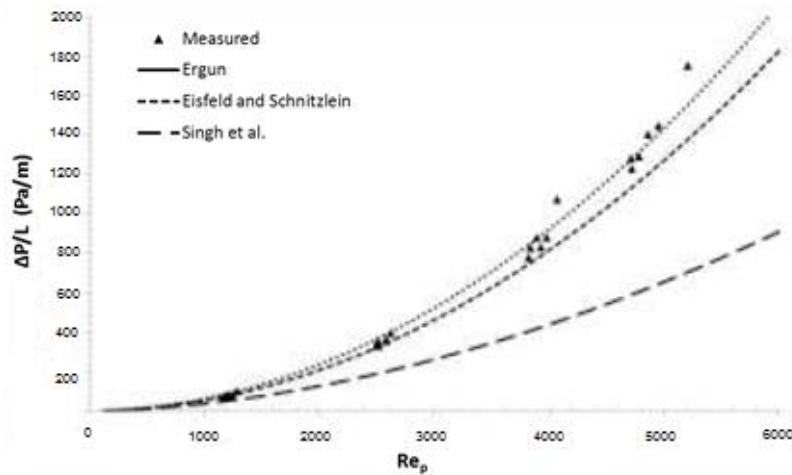


Figure 7.15 Pressure gradient as a function of particle Reynolds number. Shape factor of 0.70 is used in the pressure drop correlations

Concluding, there has even been some dispute in the accuracy of Ergun's correlation for the prediction of spherical particles (Allen *et al.*, 2013). With the many factors that can come into play, it is of no surprise that there is considerable discrepancy between correlations. Key parameters such as inlet and outlet conditions, tank-to-particle ratio, packing method, bed porosity, and particle shape can affect the studies. Hollands and Sullivan (1984) found that by simply washing aggregates of crushed stone and rock, pressure losses decreased by a factor of approximately 2. Correlations are also highly sensitive to slight changes in porosity and particle diameter, which can often be difficult to measure accurately. The equivalent particle diameter by volume,  $D_v$ , is the simplest diameter to determine yet it does not necessarily provide a complete picture of the hydraulic behavior of the bed. The Sauter diameter, which is the product of the sphericity and  $D_v$ , is known to be a more appropriate property, however the sphericity is very difficult to measure for irregular shapes. Therefore, it is back-calculated using Ergun's Equation which shows a similar dependence on the bed velocity as the measured values. The calculated sphericity also produced reasonable predictions from Singh *et al.*'s Equation, which is based on experiments that utilized well-defined shapes so that the sphericity can easily be calculated. The equivalent diameter,  $D_{eq}$ , defined by Li and Ma is also used to determine sphericity but the obtained value do not produce good results with Singh *et al.*'s Equation. Either method alone provided a sphericity that can be used in Ergun's or Eisfeld and Schnitzlein's correlations, however, the physical significance of the smaller shape factor of 0.495 seems to be more reasonable. Since the particles exhibit a shape that is closer to a parallelepiped than a sphere, one would expect the sphericity to be very low. Particle roughness and roundness may also play a role in reducing the shape factor. Their effect is similar to the effect of sphericity in that they change the surface characteristics of the particles, essentially producing smaller channels, which increases inertial resistance within the system (Hollands and Sullivan, 1984). It is difficult to definitively say that the wall does not have an effect on the pressure drop in this instance. Since the tank-to-particle ratio is on the cusp of the limit that was suggested by Eisfeld and Schnitzlein, and there is flexible insulation lining the wall which may reduce

the effects of wall channelling, it is likely that the wall effects are negligible. It is also possible that since the solid particles are randomly placed in the bed and there is little structure both within the bed and at the walls, the effect of wall channelling may not be as severe as compared to a bed packing that is highly structured. Additionally, the tests are conducted in the turbulent regime where, as suggested by Einfeld and Schnitzlein, the wall plays a minor role in pressure losses within the bed. Nevertheless, both Ergun's Equation and Einfeld and Schnitzlein's Equation give comparable results in predicting the measured values during turbulent flow when the calculated shape factor is employed.

### 7.2.3 Preliminary experimental tests: charging and discharging cycles

During the permanence at the Clean Energy Research Center - University of South Florida (Florida - United States) in the 2013, a set of preliminary experimental tests on charging and discharging processes have also been carried out.

Figure 7.16 shows the trend of the central thermocouple temperature in the five thermocouple layers placed inside the packed bed. The hot temperature air flow charges the system with a temperature of about 600°C. During charging process, after 75 minutes 400°C temperature difference between the upper and lower thermocouple rows occur. In addition, Figure 7.17 shows the charging air temperature along the bed height.

The discharging process, performed with a 150°C air flow controlled by the "discharging" electric heater, shows 70°C temperature difference between the upper and lower thermocouple rows after 150 minutes.

Further experimental tests will be carried out in order to better understand the behavior of the developed TES system during charging and discharging process. In particular, the charging and discharging temperature will be properly controlled to simulate the real conditions to be found in the TSP power plant installed by the company Sunborne in India.

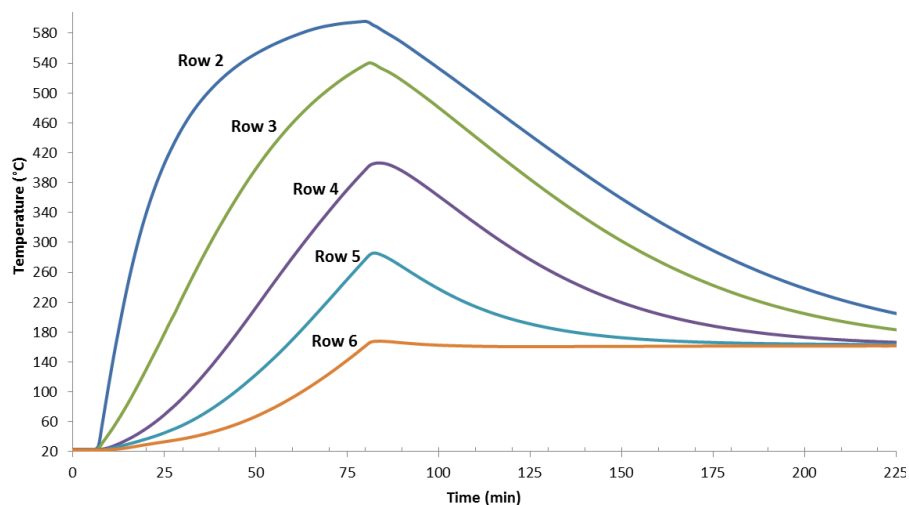


Figure 7.16 Packed bed temperature during charging and discharging mode

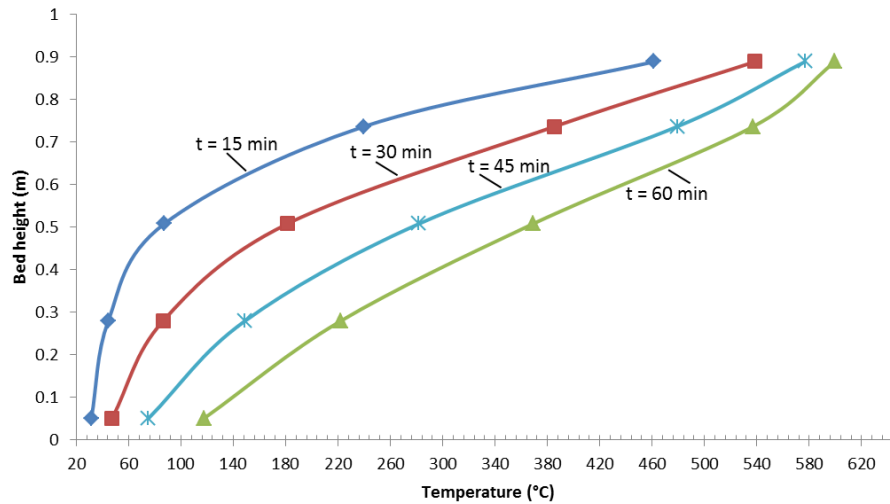


Figure 7.17 Packed bed charging air temperature along bed height

#### 7.2.4 Acknowledgements

This research activity is supported by SunBorne Energy, Inc.

#### References

- Achenbach, E. (1995). Heat and Flow Characteristics of Packed Beds. *Exp Therm Fluid Sci*, 10, 17-27.
- Choi, Y., Kim, S., Kim, D. (2008). A Semi-empirical Correlation for Pressure Drop in Packed Beds of Spherical Particles. *Transp in Porous Med*, 75(2), 133-149.
- Cohen, Y., Metzner, A.B. (1981). Wall effects in laminar flow of fluids through packed beds. *AIChE Journal*, 27(5), 705-715.
- Eisfeld, B., Schnitzlein, K.(2001).The influence of confining walls on the pressure drop in packed beds. *Chem Eng Sci*, 56(14), 4321-4329.
- Ergun, S. (1952). Fluid Flow through Packed Columns. *Chem Eng Prog*, 48(2), 89-94.
- Geldart, D. (1990). Estimation of Basic Particle Properties for Use in Fluid-Particle Process Calculations. *Powder Technol*, 60, 1-13.
- Goswami, D.Y., Kreith, F., Kreider, J. F. (2008). Principles of Solar Engineering, Second Edition. (CRC Press, Ed.).
- Kuravi, S., Trahan, J., Goswami, D. Y., Rahman, M. M., & Stefanakos, E. K. (2013). Thermal energy storage technologies and systems for concentrating solar power plants. *Progress in Energy and Combustion Science*, 39(4), 285–319

- Li, L., Ma, W (2011). Experimental study on the effective particle diameter of a Packed Bed with Non-Spherical Particles. *Transp in Porous Med*, 89: 35-48.
- Meier, A., Winkler, C., Wuillemin, D (1991). Experiment for modelling high temperature rock bed storage. *Sol Energy Mater*, 24(1-4), 255-264.
- Nemec, D., Levec, J. (2005). Flow through packed bed reactors: 1. Single-phase flow. *Chem Eng Sci*, 60, 6947-6957.
- Reichelt, W. (1972). Zur Berechnung des Druckverlustes einphasig durchströmter Kugel- und Zylinderschüttungen. *Chemie-Ingenieur-Technik*, 44, 1068-71.
- Singh, R., Saini, R.P., Saini J.S. (2006). Nusselt number and friction factor correlations for packed bed solar energy storage system having large sized elements of different shapes. *Sol Energy*, 80(7), 760-771.
- Torab, H., Beasley, D.E. (1987). Optimization of a Packed Bed Thermal Energy Storage Unit. *ASME J Sol Energy Eng*, 109, 170-175.
- Trahan, J., Graziani, A., Goswami, D. Y., Stefanakos, E., Jotshi, C., & Goel, N. (2014). Evaluation of Pressure Drop and Particle Sphericity for an Air-rock Bed Thermal Energy Storage System. *Energy Procedia*, 57, 633-642.
- Wadell, H (1935). Volume, Shape, and Roundness of Quartz Particles. *J Geol*, 43(3), 250-280.





## 8. Conclusions

The present Ph.D dissertation presents research activities about the study, design and development of methods and tools for the optimization and enhancement of renewable energy technologies and their effective integration with traditional energy sources powered by fossil fuels and energy storage solutions.

Among the available renewable energy sources (RESs), the focus is on solar, *i.e.* photovoltaic (PV) and concentrated solar power (CSP) plants, and wind power, which recent growth margins show a great potential for a large scale diffusion (See Figure 8.1).

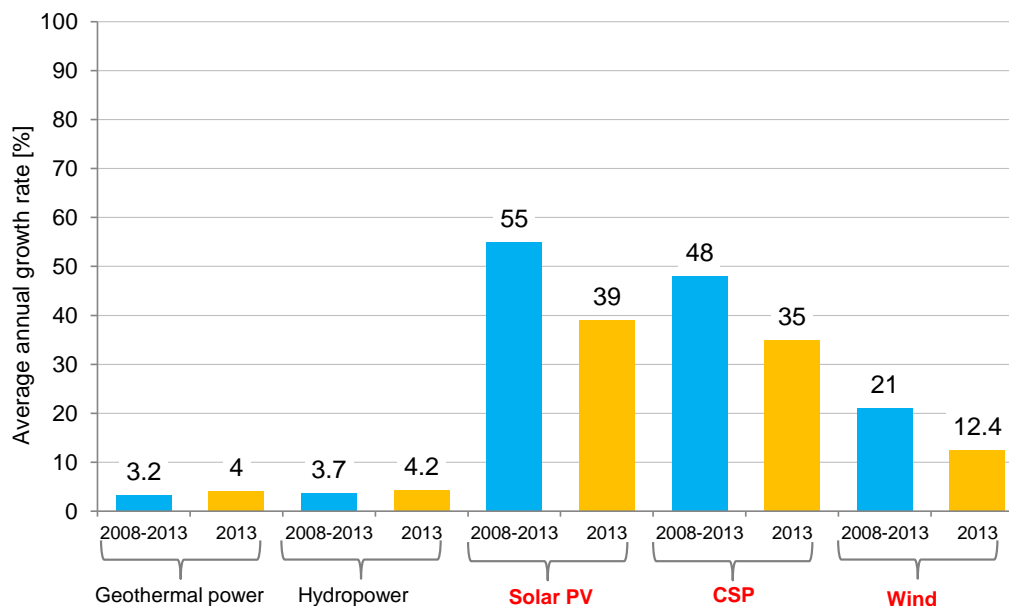


Figure 8.1 Average Annual Growth Rates of RES capacity in the power sector, from 2008 to 2013 (REN, 2014)

The first analysis (*Chapter #2*) deals with the economic feasibility study, through a multi-scenario analysis, of PV plants and small wind turbines (SWTs) in some of the main European Union (EU) countries. Both the investigated RESs are suitable to switch the electricity generation from large centralized facilities to small decentralized energy systems favouring a sustainable development thanks to the environmental impact reduction, the load management benefits and the opportunity to provide electricity to remote areas. The results show that the economic feasibility of PV plants and SWTs were generally still linked to supporting policies in the reference year (2012). However, the cost reduction, due to the industrial development and large scale diffusion, and the increase of the self-consumption rate of the produced energy are favorable conditions to make PV

plants and SWTs economically self-sustainable. The partial or total cut of incentives and uncertainties related to supporting policies within the EU context further emphasizes the concept. The study of the user energy demand profile and the adoption of battery energy storage (BES) systems (presented and described in [Chapter #3](#)) have been identified as effective strategies to increase the energy self-consumption contribution.

Such aspects have led to the development of two analytic models for the techno-economic design of a grid connected and an off-grid hybrid energy systems (HESs) integrating RESs, BES systems and back-up power sources ([Chapter #4](#)). Both the models take into account the hourly energy demand profile determining the energy self-consumption contribution.

The grid connected HES integrates a PV plant and a BES system with the grid used as back-up power source. The model has been applied to design the PV-BES HES for the new buildings of the Engineering and Architecture School at the Bologna University, Italy. The results, referred to the year 2013, show the economic profitability of a PV plant designed to meet the energy demand of the user in a location with medium-high irradiation level ( $\approx 1,700\text{kWh/m}^2\text{year}$ ), and therefore oriented to self-consumption, while the competitiveness of BES systems is connected to the gap between the purchase cost and selling price of electricity from the grid. However, the high BES system costs due to the initial investment and the maintenance activities and the eventual presence of incentives and benefits on the energy sold to the grid can make the investment not particularly attractive.

Thus, the focus has shifted to the techno-economic analysis of off-grid HES meet the energy demand of users in remote areas. In this context, BES systems have a significant role in the operation and management of the system, in addition to the storage of exceeding energy produced by the intermittent and variable RESs. The off-grid HES integrates a PV plant, BES systems and a diesel generator, used as back-up power source. The model is able to design HESs for any installation site and it has been applied to evaluate the optimum configuration of an off-grid HES installed in Yakutsk (Russia), and developed in collaboration with the company Margen S.p.A., to meet the energy demand of a remote village. The results highlight the technical feasibility and the moderate economic profitability of such a system for a context with a medium irradiation level, *i.e.*  $\sim 1,400\text{kWh/m}^2\text{year}$ , and a relatively low fuel cost, *i.e.*  $0.7\text{€/l}$ . The [Chapter 4](#) also includes the technical features of a second HES developed in collaboration with Margen S.p.A. integrating PV plant, SWT, BES system and diesel generators designed to supply a telecommunication system installed in Russia.

In parallel, two experimental activities in the context of solar concentrating technology, a promising and not fully developed technology, have been carried out. The [Chapter 5](#) provides a conceptual background of solar concentration principles and a review of the available technical plant engineering solutions. The [Chapter 6](#) presents a research activity concerning about the design, development and tests of a Fresnel lens pilot-scale solar concentrating prototype for the PV energy distributed generation, through multi-

junction solar cells, and the parallel low temperature heat recovery (micro-cogeneration CPV/T system). The whole research activity is part of the co-financed Mi.S.T.I.Co. project (Micro-systems and innovative technologies for the solar energy cogeneration) - Partners: Bruno Kessler Foundation (Trento, Italy), Universities of Padova, Bologna and Trento. The experimental results have point out the complexity and critical issues of the CPV/T technology, which efficiency depends upon the accurate integration of different expensive components, *i.e.* the solar collectors and receivers, tracking system, etc. Research activities and industrial developments are focused on the efficiency and cost reduction to make such a technology competitive with traditional PV plants and other RESs.

Finally, the *Chapter 7* describes the research activity focused on the development of a low cost storage solution for solar central receiver technology developed during the permanence at the Clean Energy Research Center - University of South Florida (Florida - United States). The system consists of a packed bed of pellets as the storage media and uses air as the heat transfer fluid. This TES system may overcome the intermittent nature of sunlight and increase the capacity factor of solar thermal power plant and it is promising TES concept due to its single tank design and employment of cheap and abundant storage media such as sand and rock. The research activity has focused on the development and implementation of a pilot-scale prototype system adopting iron rocks as the storage media to test its performance and investigate the effectiveness of the system for its future installation in a central receiver CSP plant installed by the company Sunborne in India.

## 8.1 Future developments

Starting from the topics investigated in the present Ph.D. dissertation a set of future developments are encouraged to continue and expand the research on the described models, approaches and strategies. Particularly, the main ideas focus on the techno-economic models developed to design PV plants, SWTs, grid connected and off-grid HESs.

- With reference to the techno-economic design of PV plants and SWTs (*Chapter #2*) further research deals with the application of the proposed analysis to other geographical areas presenting different features, constraints and local conditions. The continuous update of the technical, economic, geographical parameters and country peculiarities with particular reference to the constant monitoring of the national support schemes and the electricity market prices and conditions, is, also, of interest to study new scenarios, perspectives and opportunities of evolution for the PV and SWT renewable energy sector
- Considering the HES analysis, the focus is on the application of the proposed models to other scenarios to compare its performances under different constraints, *i.e.* load profile, energy cost and selling price, fuel cost, *etc.*, and different location features, *i.e.* environmental conditions. A sensitivity analysis of the main parameters affecting the HES profitability is also of interest. The multi-

objective system design is another interesting research path to develop considering economic, environmental and technical performances with the final aim to define the system configuration that contemporary optimize economic evaluation indices, the most widely adopted environmental impact indicators and technical issues, e.g. energy self-consumption rate or the percentage of the met energy demand

- Finally, with reference to the developed PV-SWT-BES-Diesel generator off-grid HES (See *Paragraph 4.5*), further research deals with the development of a multi-objective optimization model able to contemporary optimize economic, environmental and technical indices for a PV-SWT-BES-Diesel generator off-grid HES able to meet both direct current and alternate current loads.



